Development of Bifunctional Catalysts for the Direct Conversion of n-Butane to Isobutene

G.D. Pirngruber

Leden van de promotiecommissie:

Voorzitter/Sekretaris:	Prof. dr. W.E. van der Linden
Promotor:	Prof. dr. J.A. Lercher
Assistent promotor:	dr. K. Seshan
Leden:	Prof. dr. ir. L. Lefferts
	Prof. dr. it. W.P.M. van Swaaij
	Prof. dr. J. Geus
	Prof. dr. A. Bliek
Deskundige:	dr. F.T.B.J. van den Brink

This work was carried out as part of the Innovation Oriented research Program on Catalysis (IOP Katalyse, no. IKA 94023) sponsored by the Netherlands Ministry of Economic Affairs.

ISBN 90 365 13596

DEVELOPMENT OF BIFUNCTIONAL CATALYSTS FOR THE DIRECT CONVERSION OF N-BUTANE TO ISOBUTENE

PROEFSCHRIFT

ter verkrijging van
de graad van doctor aan de Universiteit Twente,
op gezag van de rector magnificus,
Prof. dr. F.A. van Vught,
volgens besluit van het College voor Promoties
in het openbaar te verdedigen
op vrijdag 24 september 1999 te 13:15

door
Gerhard Dieter Pirngruber
geboren op 18 januari 1972
te Oberwart, Oostenrijk

Dit proefschrift is goedgekeurd door de promotor

Prof. dr. J.A. Lercher

en de assistent promotor

dr. K. Seshan.

There is this quality in things, of the right way always seeming the wrong at first. To test our faith.

John Updike, Run Rabbit Run

To my parents and my sister

Acknowledgements

When I arrived in Enschede for the first time in October 1994, for starting my diploma thesis, it was a cold, rainy and misty day. Bad prospects, thus. But the people here and especially the group of Austrians who had moved to the UT with Prof. Lercher gave me a very warm welcome. I could almost feel like at home. So decided that I could not get enough of Enschede and I stayed four years longer in order to do my PhD thesis. I have never regretted that decision. I loved the campus, I met of lot of people from all over the world, I made a lot of good friends. I think that I spent the best years of my life in Twente.
Among all the people with who I became very close here, I especially want to mention my flatmates Eduardo, Laurent and Alberto. I shared a lot of unforgettable moments of happiness with you and, even more important, you gave me a lot of support and comfort when things were going not so well. When I regarded Enschede as "home" in the end, it was thanks to you. Thank you for all that.
Next to my real home, the university was sort of a second home for me. I did not mind that too much. I had very nice colleagues in the lab (it would be a futile effort to name all of them) and made a lot of very good friends there. Of course, I also met a lot of people outside work (again the list would be too long). I spent a very nice time with all of you. I enjoyed the discussions at the friday borrel, the evenings in the city, the skiing trips, parties, dinners, excursions, etc. What intrigued me most was the diversity of our group. We always had people from all over the world, and perhaps just because of that there was a strong feeling of belonging together. I learned a lot from you, I will never forget that experience.
On a more professional basis I want to thank all the staff members of our group who made life a lot easier for me, Cis with all her help in administrative questions, groeps-herder Bert, the doctor for computers, radios, bicycles and other apparatus, Karin, who always found emergency solutions when a gas bottle was needed, Benno and Bert Kamp, who saved me in several cases when my setup did not want to work any more. Thanks a lot for all the help. And I appreciated working with you very much, Olivier, you were not just my student, but a good friend.

I would have missed the nice time here, had Prof. Lercher not offered me the PhD position four years ago. I would like to thank you, Johannes, for the supervision and guidance of the project. You managed very well to push me to edges with your sharp criticism, especially in the end of the writing phase. I am grateful for that (although it made life a lot harder for me). I also want to thank you, Seshan, not only for being my scientific supervisor, but also for your advice in other aspects of life and for the support in difficult times of the project. It was very nice to cooperate with you.
I would also like to thank all the members of my begeleidings-commissie from IOP for all the feedback that they gave me and I am in particular grateful to those, who supported me in the difficult phase when the direction of the project had to be changed.

Last but not least, I want to thank my parents for all the support that they gave me. I know that you were not too happy to see me going to the far away Netherlands, so I am all the more grateful for your patience and understanding.

Table of Contents

Chapter

1

Introduction

Objective and Justification

The objective of this thesis was the development of bifunctional catalysts for the direct conversion of n-butane to isobutene. The research was justified by the exponentially growing demand for MTBE (which is made from isobutene and methanol) in the last 15 years, especially in the US. The growing demand for MTBE was triggered by the Clean Air Act legislation, in which the US government mandated the use of oxygenates as fuel additives. In the meantime, however, the prospective for a future growth in the demand for isobutene has decreased in the US, due to environmental concerns that arose in the past few years. In Europe, on the other hand, the use of MTBE as an octane booster in gasoline has never been as widespread as in the US. In contrast to the US, upcoming gasoline regulations, which will limit the percentage of aromatics in gasoline, are expected to lead to an increase in the demand for MTBE in Europe in the near future. Thus, in spite of the declining demand in the US, there is still a strong incentive for the development of new routes for the production of isobutene, the raw material for MTBE.

Apart from the economic impact, the direct conversion of n-butane to isobutene is a very interesting scientific challenge. Thermodynamics, catalyst and reactor design have to be taken into account. This introductory chapter gives an overview over the industrial processes used for the production of isobutene and discusses their advantages and disadvantages as compared to a one-step process. The possibility of using oxidative dehydrogenation in order to avoid the thermodynamic limitations of "normal" dehydrogenation is also discussed.

Economic importance of isobutene - The MTBE issue

Isobutene is an important intermediate in the petrochemical industry, mainly used for the production of polymers (butyl rubber, polybutene and isoprene) and of MTBE. In 1984 $1.2*10^6$ tons (t) isobutene were used for the production of butyl rubber, polybutene and isoprene, $1.0*10^6$ t for the production of MTBE [1]. Since then the market for MTBE has seen an exponential growth (see Figure 1). In 1998 the world demand for MTBE was estimated to be $1.2*10^7$ t corresponding to an isobutene consumption of $7.8*10^6$ t [2]. MTBE is now – behind ethylene – the second most produced organic chemical in the world.

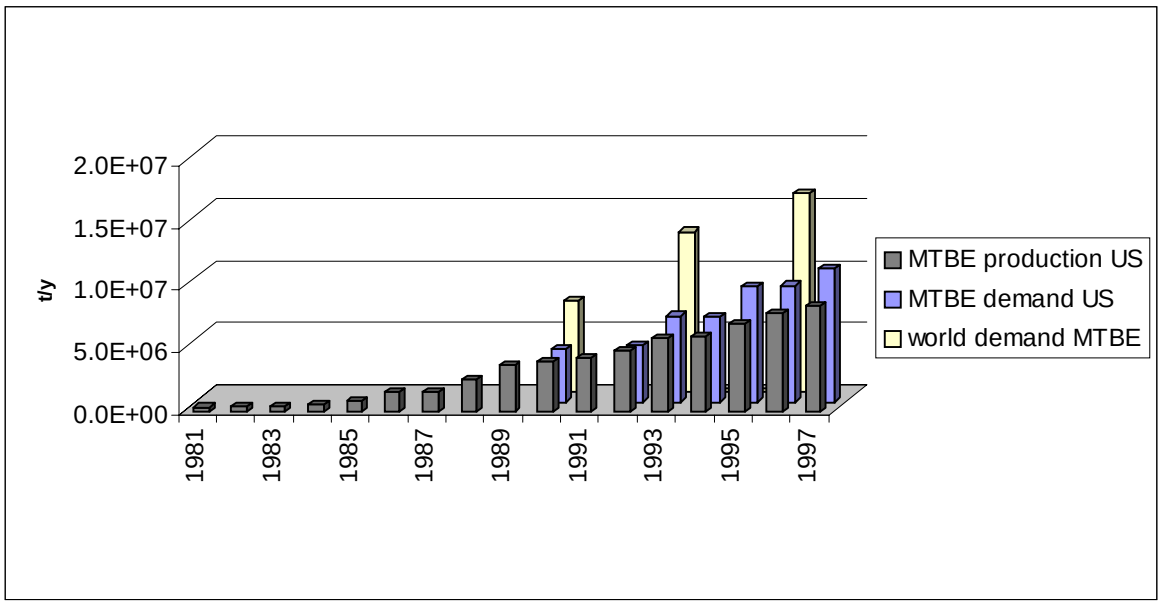

Figure 1 *MTBE production and demand in the US in the last 18 years and world demand for MTBE [3, 4, 5].*

The rising demand for MTBE in the US was caused by an amendment to the Clean Air Act, the so-called reformulated gasoline program. It required fuel oxygenates to be added to gasoline in some metropolitan areas in order to reduce atmospheric concentrations of CO or ozone. The minimum oxygen concentration of the gasoline was set to 2.7 wt%. Mainly ethers and alcohols were found to be suited as oxygen-containing fuel additives (see Table 1). MTBE, however, was the by far the most preferred material because of its (i) high octane number, (ii) its rather low Reid vapor pressure and (iii) its extremely good miscibility with gasoline.

Table 1 *Characteristic properties of oxygenates used as fuel additives*

	MTBE	TAME	ETBE	TBA	Ethanol
Density (kg/dm^3)	0.741	0.770	0.740	0.78	0.789
RON	110	105	112	100	115
Reid vapor pressure (mbar)	550	275	275	650	1240
Oxygen content (%)	18.2	15.7	15.7	21.6	35
vol% necessary for 2.7wt% oxygen in fuel	15.1	17.2	17.2		7.5

In the last years, though, the use of MTBE has come under heavy fire from environmental protection groups. The widespread use has resulted in frequent detection of MTBE in shallow groundwater from urban areas throughout the US [6]. Limited contamination of drinking water has also occurred and is of concern because MTBE is considered a possible human carcinogen by the US Environmental Protection Agency (US EPA). The question of the health damaging effect of MTBE is, however, still under debate. In 1999 the California Department of Health Services issued a maximum contaminant level (MCL) for MTBE of 5 µg/l, based only on taste and odor considerations. A MCL based on health impact is going to be issued later this year. Earlier in 1997 the US EPA had advised a limit of 20 µg/l (also based on taste and odor). In a study in 1993/94 only 3% of the shallow wells sampled in urban areas had concentrations that exceeded this limit. Higher concentrations of MTBE (> 600 µg/l) are only found when leaking underground fuel tanks (LUFTs) are the source of contamination with MTBE [7]. Low concentrations of MTBE (< 3µg/l) are more likely to result from atmospheric sources (MTBE in the air washed out by rain water). There is a high correlation between urban land use, motor vehicle traffic and population density and the frequency of detection and water concentrations of MTBE.

While – as mentioned above – the pollution level with MTBE is still not very high (with the exception of the LUFT sources) the major concern is the ease with which MTBE spreads in the environment. MTBE readily dissolves in water (at 25ºC the solubility is 5 g/l), it is resistant to microbial decomposition and is difficult to remove in water treatment. Therefore fears exist that MTBE contamination may be a progressive problem [7].

While scientifically the question of the environmental behavior of MTBE and its health effects is not settled yet, there has been a growing contra-MTBE movement in the US, fuelled by environmentalist action groups. This lead to an executive order of the California governor in March 1999, declaring the phase-out of MTBE in California before the end of the year

2002. This translates to a loss of $4*10^6$ t/y MTBE consumption [8]. If the phase-out is extended across the US a further $7*10^6$ t/y less MTBE would be needed.

In Europe the situation is quite different. European gasoline regulations do not prescribe the use of oxygenates to meet emission standards. By the year 2000 and 2005, however, the aromatics content of gasoline will have to be reduced to 42% and 35%, respectively. Expecting that MTBE will at least be partly used to replace the aromatics, MTBE producers estimate that this will lead to an additional demand of $1.5*10^6$ t/y MTBE in Europe [9] (in 1998 the MTBE consumption of Europe was $2.4*10^6$ t/y [10]). Environmental problems like in the US are not expected, since the amount blended into gasoline is much smaller than in the US (3 - 4 vol% *vs.* 15 vol%) and the gasoline storage tanks are in a better condition so that leakage problems should not appear [9].

Still, the overall future prospective for the market for MTBE and, thus, also for isobutene is more moderate after the ban in California. One has started to think about alternatives to MTBE. ETBE could be used to replace MTBE, which would keep the demand for isobutene high. Isobutene can also be used in the production of alkylate and isooctane, both of which can substitute MTBE as an octane booster [11]. A respective process has recently been developed by UOP. The Indirect Alkylation (InAlk) process produces high quality alkylate by oligomerization and hydrogenation of an isobutene-rich feed [12].

Apart from its use for fuel additives, there is also a market for pure isobutene as a raw material for polymers, but it is very small. 90% of the total butenes produced are used in fuel applications, the remaining 10% is mainly accounted for by linear butenes as raw materials for, for example, sec-butyl alcohol and butadiene [13].

Industrial processes for the production of isobutene

Isobutene is produced in fluid catalytic and in steam cracking units. Table 2 gives a typical composition of the C_4 fractions obtained in these two units. Isobutene is only a by-product of these processes and the production capacity of isobutene cannot be easily expanded from these sources. Dehydrogenation of butanes is an alternative production route. Butanes are a very attractive raw material because they are readily available on the market, and their supply (from natural gas and from refinery sources) is projected to increase by 40% over the next 15 years [12]. The conversion of butanes to isobutene comprises two separate steps. n-Butane is isomerized, then the isomers are separated by distillation and isobutane is passed on to a dehydrogenation unit, where it is converted to isobutene.

Table 2 *Typical composition (in wt%) of C_4 fractions from FCC and from naphtha steam cracking under medium severity [1].*

Component	FCC	Steam cracking
isobutane	37	2
n-butane	13	6
1-butene	12	14
trans-2-butene	12	5
cis-2-butene	11	4
isobutene	15	26
butadiene	< 0.5	43

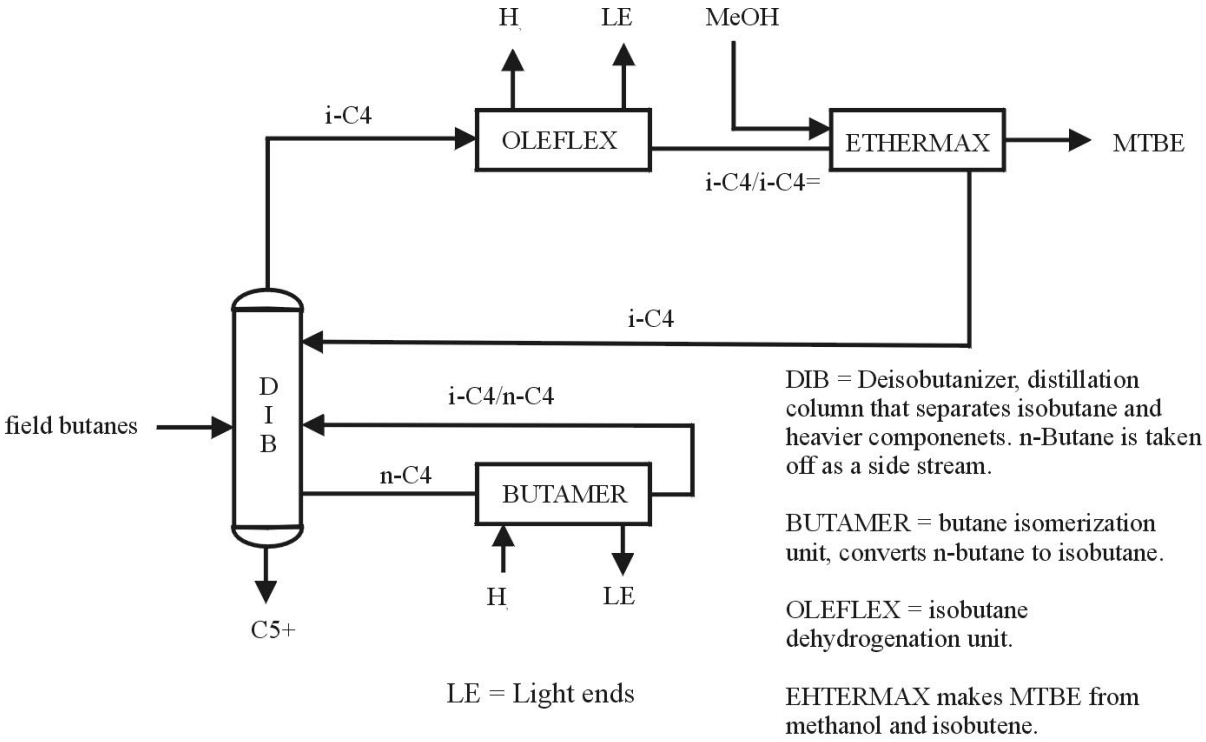

Figure 2 *Scheme of the UOP process for producing MTBE from butane.*

Currently, there are several industrial processes in operation that produce MTBE from an alkane feed. UOP uses a combination of the BUTAMER and the OLFEFLEX process to produce isobutene (and ultimately MTBE) from n-butane. A generalized process scheme is shown in Figure 2. A mixed butane feed is routed to a deisobutanizer column which recovers isobutane as an overhead product. A n-butane sidecut is taken from the column and efficiently isomerized to isobutane in the BUTAMER unit. The BUTAMER process

isomerizes n-butane with a dual-function (metal plus acid sites), chloride-based catalyst in the presence of small amounts of hydrogen. The conversion of n-butane to isobutane is equilibrium limited. The selectivity is excellent (>95%). Only a minor amount of cracking takes place and virtually no heavy by-products are formed. Details of the BUTAMER process are given in [14] and [15].

The isobutane-rich overhead from the deisobutanizer column is routed to the OLEFLEX unit (see Figure 3a) [16, 17], which dehydrogenates isobutane to isobutene at an overall selectivity of about 90%. The amount of coke produced is less than 0.02wt% of the feed processed. Thermodynamic equilibrium conversion is closely approached. Details of the kinetics and catalyst development have been published in [18]. CCR (Continuous Catalyst Regeneration) technology is used for regenerating the catalyst.

The MTBE-unit shown in Figure 2 does not only serve for the production of MTBE. Even if MTBE is not the desired product, the etherification provides a means of separating out isobutene. It is not possible to purify isobutene by classical distillation since the boiling points of isobutene and 1-butene are too close (see Table 3). Isobutene, however, reacts much faster with methanol than the linear isomers and can be selectively removed from the C_4-mixture in this way. The ether-formation is reversible and, if necessary, isobutene and methanol can be recovered from MTBE.

Table 3 *Boiling points of the butene isomers.*

	1-butene	cis-2-butene	trans-2-butene	isobutene
Boiling point (ºC)	-6.26	3.72	0.88	-6.90

An alternative dehydrogenation technology has been developed by Phillips Petroleum Company, the so-called STeam Active Reforming (STAR) [19, 20]. The global process scheme is the same as in Figure 2. The STAR unit (see Figure 3b) replaces the OLEFLEX unit. Table 2 gives a material balance of a STAR unit for a typical isobutane-rich feed [21]. It is operated at around 550 ºC and a pressure of 5 - 15 bar. A minimum of 2 - 3 mol steam/mol of feed is necessary for dilution (low partial pressures of butane favor the dehydrogenation equilibrium). Furthermore steam acts as a source of heat for the endothermic reactions and helps to reduce catalyst deactivation. The catalyst is air regenerated every $7 - 8$ h, so that multiple reactor units are necessary to maintain continuous operation.

Table 4 *Material balance of the STAR process (by weight).*

	Feed	Light gases	Other Products
Hydrogen	-	2.0	-
Carbon oxides	-	2.2	-
C_1-C_3	1.8	2.6	0.5
i-C_4	95.1	1.4	46.1
i-$C_4^=$	-	0.4	43.3
n-C_4	3.1	-	1.5
n-$C_4^=$	-	-	1.4
Heavies (C_5^+)	-	-	0.1
H_2O (consumed)	1.5	-	-

In the Catofin process (licensed by Lummus, originally Houdry Division of Air Products and Chemicals) three reactors are used, one of them processing the hydrocarbon feed, one being regenerated with air, one completing steps of either purging or valve changing (see Figure 3c) [22, 23]. Table 5 shows a typical product yield in the production of MTBE. The process is operated at 550 to 650 ºC and low pressures (0.15 – 1 bar). The endothermic heat of the reaction is primarily supplied by the heat of combustion of the small quantity of coke deposited on the catalyst. The purpose of regeneration is to supply reaction heat rather than to restore a loss in catalytic activity, which is negligible.

Table 5 *Typical product yield of the Catofin process in the production of MTBE.*

Fresh feed, wt%		Products in % of fresh feed	
C_3	4.0	MTBE	110.0
i-C_4	18.0	Fuel	29.3
n-C_4	76.0	Coke and loss	2.4
C_5^+	2.0		

Table 6 sums up the most important data of the three processes described above. Other dehydrogenation technologies are available from Snamprogetti-Yarsintez (FBD) and Linde-BASF [24]. The main differences are in the choices made for supplying heat to reactor and feed-stream and in the systems used for catalyst regeneration (see Figure 3) [25, 26].

Table 6 *Isobutane dehydrogenation processes [27].*

Process	Oleflex	STAR	Catofin
Licensor	UOP	Phillips	Lummus
Temp (ºC)	550	480 – 630	540 – 650
Pressure (bar)	0.35 – 0.7	2.5 – 3.5	0.35 – 0.75
H_2 / HC	3	0 – 2	0
Steam / HC	0	4 (2 – 10)	0
LHSV (h-1)	4	4	0.4 – 2
Conv (%)	~35	40 – 55	65
Sel (%)	91 -93	88 – 92	90
Heat input	interstage heating	furnace	regenerate catalyst
Regeneration	moving bed	cyclic	cyclic
Cycle time	2 – 7 days	7 – 8 h	5 – 15 min
Catalyst	Pt/Sn-Al_2O_3	Pt/Sn/Zn/Al_2O_3	Cr_2O_3/Al_2O_3
Catalyst life	1 – 2 years	1 – 2 years	1.5 – 3 years

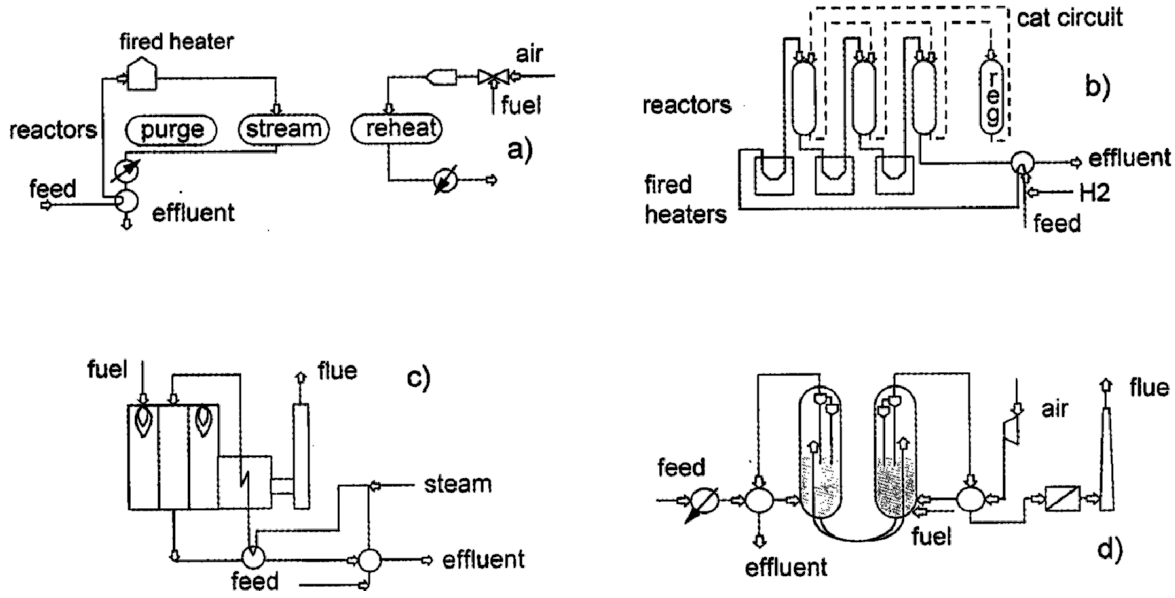

Figure 3 *Types of commercial reactor for alkane dehydrogenation. a) Adiabatic fixed bed (Catofin). b) Adiabatic moving bed (UOP Oleflex). c) Fired fixed bed (Phillips STAR). d) Fluidized bed (FBD).*

Note that all these processes use isobutane as a feed for the dehydrogenation unit. The main

reason is that n-butane can be dehydrogenated to butadiene which (i) enhances catalyst deactivation [25] and (ii) requires an additional hydrogenation unit to take butadiene out of the product stream. Still, one can think of a reversed reaction sequence for the production of isobutene, i.e., first dehydrogenation of n-butane to linear butenes (by one of the processes mentioned above), followed by skeletal isomerization of the linear butenes. Commercial units for butene isomerization are available from Snamprogetti, UOP and Shell/Lyondell.

Thermodynamic considerations

The industrial processes described above contain an isomerization unit for converting n-butane to isobutane and a dehydrogenation unit for converting isobutane to isobutene. Both reactions are thermodynamically limited and the yields that can be obtained depend very much on the reaction conditions (pressure, temperature, dilution with inert gas). Understanding the thermodynamic constraints is therefore essential for the optimization of the process.

Isomerization of n-butane

Figure 4 shows the equilibrium of the reaction n-C_4 ⇌ i-C_4 as a function of temperature. Since the reaction is slightly exothermic (ΔH = -8 kJ/mol) the equilibrium concentration of isobutane decreases with temperature. The number of mols does not change, thus, pressure has no influence on the equilibrium. At 400 ºC (673 K) the equilibrium mol fraction of isobutane is 0.4, which means that the maximum isobutane yield per pass is 40%.

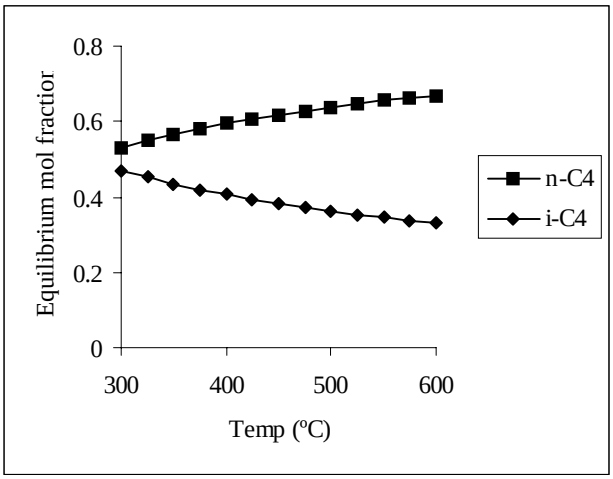

Figure 4 *Thermodynamic equilibrium between n-butane and isobutane as a function of temperature.*

Dehydrogenation of isobutane

The dehydrogenation of isobutane is an endothermic reaction.

$i\text{-}C4 \rightleftharpoons i\text{-}C_4^{=} + H_2$ $\Delta H_{823K} = 122.7$ kJ/mol $\Delta G_{823K} = 27.7$ kJ/mol

Thus, as shown in Figure 5a, the equilibrium mol fraction of isobutene increases with temperature. Increasing the total pressure has a negative influence on the dehydrogenation equilibrium (Figure 5b). The same holds true for increasing the hydrogen/hydrocarbon ratio in the feed. The maximum per pass yield of isobutene is a strong function of all three parameters, temperature, pressure and H_2/isobutane ratio.

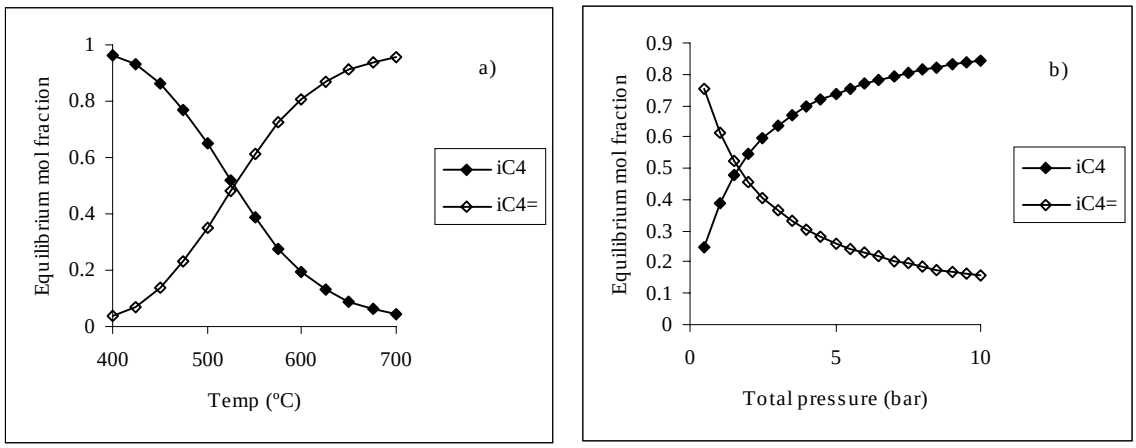

Figure 5 *Thermodynamic equilibrium of isobutene dehydrogenation as a function of (a) temperature and (b) pressure. Input: 0.1 mol isobutane, 0.2 mol H_2, 0.7 mol N_2.*

Dehydrogenation catalysts

In the industrial processes described above two types of dehydrogenation catalysts are being used:

(i) Platinum-based catalysts (UOP Oleflex, Phillips STAR)

(ii) Chromia-based catalysts (Lummus Catofin, Snamprogetti-Yarsintez FBD)

They achieve excellent yields (close to the thermodynamic limits) and selectivities in the dehydrogenation of isobutane, at life-times of more than one year (see Table 6). Differences can be found in the quality of the by-products, the deactivation behavior and the treatment the catalysts require for regeneration. A good deal of catalyst development in the last decades has been devoted to improving activity, selectivity, life-time and ease of regeneration. In choosing between the two catalytic systems, platinum and chromia, platinum catalysts are currently preferred, due to environmental concerns about the use of chromia. Therefore we will limit the following, more detailed discussion to the Pt-based catalysts.

The catalytic properties of Pt are strongly influenced by the support material and the presence of other promoters. The main function of the support is to stabilize the Pt-dispersion during all stages of catalyst treatment. Thermally stabilized, mesoporous alumina (γ-, δ- or τ-Al_2O_3) is often used as support material. Its acidity has to be minimized in order to prolong catalyst life-time and reduce undesired cracking reactions. Hence, alkali metals or rare earth metals are impregnated. In the Phillips STAR process Zn- or Mg-spinels ($ZnAl_2O_4$ or $MgAl_2O_4$) are used instead of Al_2O_3 because of their slight basicity. Sn is added as a promoter. It improves the activity, selectivity and stability of the catalyst. Both, hydrogenolysis and coke formation are suppressed by Sn. The parallel effect on both unwanted side-reactions can be understood from the mechanism of hydrogenolysis. Highly dehydrogenated carbon species are the intermediates of hydrogenolysis [28], but if overdehydrogenated they can be the precursors of coke formation. Thus, the same sites are responsible for hydrogenolysis and coke formation [29] and modification of these sites by Sn affects both reactions.

The beneficial effect of Sn has been explained by electronic [30] and ensemble size [31] effects. When brought into intimate contact with Pt (in a solid solution or an alloy), Sn fills up the holes of the 5d band of Pt [25]. This leads to a decrease in the strength of interaction of hydrocarbon species with Pt, thus, lowering the contribution of both hydrogenolysis [32, 33] and coke formation [34]. The strength of interaction is also related to the ensemble size of the Pt particles. Multiply bonded hydrocarbon species can only be formed on large Pt clusters. Therefore hydrogenolysis and coke formation are enhanced on large Pt ensembles. Alloy formation with Sn, however, reduces the size of the Pt ensembles and suppresses these reactions [31, 35]. Sn also reduces the acidity of the support and stabilizes the surface area of alumina [36].

Table 7 lists a selection of alumina-supported dehydrogenation catalysts described in the patent literature. Since we had learned that the choice of the reaction conditions has a big influence on the thermodynamic equilibrium, also the thermodynamically possible yields are given for comparison. The experimental yields were about 1/3 lower.

Apart from the alumina-supported Pt catalysts, there is also a wealth of (patent) literature describing Pt-catalysts supported on clays or molecular sieves (see Table 8). In a very interesting approach Kerby *et al.* used an alumina-pillared clay (synthetic MICA) as a support. Pt and the promoters were added during the pillaring step. This material achieved excellent yields and selectivities in the dehydrogenation of isobutane even after 10 h on

stream.

Among the molecular sieve-type support all successful materials are either ZSM5 zeolites with low Al-content or silicalites where Group IIa, III or IV metals (Zn, B, In, Ge) were incorporated during the synthesis (AMS-1B is a borosilicate). These materials have a very low concentration of acid sites, confirming that a low acidity is essential for a good catalyst performance. As in the case of alumina-supported catalysts promoters like Zn, Sn (impregnated or incorporated during the synthesis) and Na were found to increase catalyst stability and selectivity.

Table 8 also gives two examples of the dehydrogenation of n-butane. Note that in these cases the catalyst life-time is much shorter and the yields lower than with a feed of isobutane.

Table 7 *Examples of isobutane dehydrogenation catalysts described in the patent literature.*

Catalyst[a]	Feed	Temp (ºC)	SV [b] (h^{-1})	TOS [c] (h)	Conv (%)	Sel (%)	Yield (%)	Max. yield[d] (%)	Ref.
Pt-Sn-ZnO/Al_2O_3	iC_4	560			45	89	40	57	[37]
Ni-Sn-ZnO/Al_2O_3	iC_4	560	300 (G)		44	91	40	57	[38]
0.6Pt/1.3SnO_2-ZnO/Al_2O_3	H_2O/iC_4 = 3.95	577	3.94 (L)	7			47.7	64	[39]
Pt/SnO_2-$ZnAl_2O_4$/$CaAl_2O_4$	H_2O/iC_4 = 3.95	538 – 607		7	40 – 59	89 - 97	39 - 52	49 – 74	[40]
0.7Pt-0.5Sn-3K-0.1Cl-γ-Al_2O_3	H_2/iC_4 = 2	643	5 (L)	20 / 90	44 / 39			62	[41]
Pt/Sn-Al_2O_3				100			>55		[42]

[a] The numbers in front of the elements indicate the weight percentage.

[b] TOS indicates the time on stream at which the yields and selectivities were measured.

[c] (G) indicates GHSV, (L) indicates LHSV.

[d] The maximum possible yield of isobutene is the equilibrium mol fraction determined from thermodynamics.

Table 8 *Examples of dehydrogenation catalysts based on clays or molecular sieves.*

Catalyst[a]	Feed	Temp (ºC)	WHSV (h^{-1})	TOS (h)	Conv (%)	Sel (%)	Yield (%)	Max. yield[b] (%)	Ref.
0.6Pt-0.4Sn-0.5Mg-1.4Na-MICA	H_2/iC_4 = 3 11% iC_4 in Ar	575	1[c]	10	60	94	57	64	[43]
0.43Pt-0.3Ir- 1.03Sn-ZSM5 (56 ppm Al)	iC_4	554	4.8	15			45	55	[44]
0.5Pt-[In]-ZSM5	iC_4			150	36	98	36		[45]
0.5Pt-[1Ge]-silicalite	iC_4	530	25	24	30	99	30	45	[46]
0.5Pt-4Zn-silicate	iC_4	530	5	600	40.7	87.1	35.4	45	[47]
0.5Pt-[Zn]-silicate	iC_4	535	5		33.5	96.6	32.4	47	[47]
0.01Pt-Na-ZSM5 (500 ppm Al, 840 ppm Na)	iC_4 **nC_4**	490 **490**	1.88 **2.9**	18.3 **1**	27.7 **25.6**	84.5 **95.0**	23.4 **23.0**	29.5 **25.2**	[48]
0.3Pt/2.1Na/1.78Zn-AMS-1B/SiO_2	iC_4	540 580	2.9 2.9	145 100	41.3 47.9	92.5 86.7	38.2 41.5	49 65	[49]
0.1Pt-[Zn]-silicate/Al_2O_3	**nC_4**	**538**	**9**	**15**	**29.8**	**76.4**	**22.8**	**41**	[50]

[a] The numbers in front of the elements indicate the wt% in the final material. The []-brackets indicate that the metal was incorporated during the synthesis and not by impregnation.

[b] The maximum possible yield of isobutene (or of linear butenes, when n-butane was the reactant) is the equilibrium mol fraction calculated from thermodynamics.

[c] LHSV

Dehydroisomerization of n-butane

As explained in the previous section, the current processes for the production of isobutene from n-butane are two-step processes with separate isomerization and dehydrogenation units. The reaction conditions and the recovery techniques needed for each of these stages are different and this places an economic penalty on the composite two-stage process. An efficient single-step process would be a very interesting alternative. This is, however, a formidable challenge. First, a single-step process has to cope with the thermodynamic limitations of both the dehydrogenation and the isomerization reaction. Secondly, a catalyst has to be developed that can combine dehydrogenation activity with isomerization activity. For the dehydrogenation a noble metal like Pt can be used. Isomerization is an acid catalyzed reaction. Acidity, however, reduces - as we had learned in the previous section - selectivity and life-time of the dehydrogenation catalyst. Thus, compromises have to be made between the thermodynamic and catalytic requirements of the two reaction steps, dehydrogenation and isomerization.

In the following two sections the thermodynamic constraints of the dehydroisomerization reaction and some catalytic systems described in patent literature are discussed in detail.

Thermodynamic considerations

Dehydroisomerization can be regarded as a combination of two reactions, butane dehydrogenation and butene isomerization. From a thermodynamic point of view the following equilibria have to taken into account.

Dehydrogenation of n-butane to a mixture of linear butenes

$n\text{-}C_4 \rightleftharpoons 1\text{-}C_4^{=} + H_2$	$\Delta H_{823K} = 130.8$ kJ/mol	$\Delta G_{823K} = 38.8$ kJ/mol
$n\text{-}C_4 \rightleftharpoons trans\text{-}2\text{-}C_4^{=} + H_2$	$\Delta H_{823K} = 118.7$ kJ/mol	$\Delta G_{823K} = 33.0$ kJ/mol
$n\text{-}C_4 \rightleftharpoons cis\text{-}2\text{-}C_4^{=} + H_2$	$\Delta H_{823K} = 121.0$ kJ/mol	$\Delta G_{823K} = 35.6$ kJ/mol

Skeletal isomerization of the linear butenes

$1\text{-}C_4^{=} \rightleftharpoons i\text{-}C_4^{=}$	$\Delta H_{823K} = -16.1$ kJ/mol	$\Delta G_{823K} = -9.1$ kJ/mol
$trans\text{-}2\text{-}C_4^{=} \rightleftharpoons i\text{-}C_4^{=}$	$\Delta H_{823K} = -4.0$ kJ/mol	$\Delta G_{823K} = -3.3$ kJ/mol
$cis\text{-}2\text{-}C_4^{=} \rightleftharpoons i\text{-}C_4^{=}$	$\Delta H_{823K} = -6.3$ kJ/mol	$\Delta G_{823K} = -5.8$ kJ/mol

Figure 8 shows the equilibrium distribution of the butene isomers as a function of temperature. The fraction of isobutene decreases with increasing temperature. The endothermic dehydrogenation reaction, on the other hand, is more favored at high

temperatures. The temperature dependence of dehydrogenation is much stronger than that of butene isomerization ($|\Delta H_{dehyd}| >> |\Delta H_{isom}|$). As a result, the overall reaction n-C_4 ⇌ i-$C_4^=$ + H_2 is favored at high temperatures.

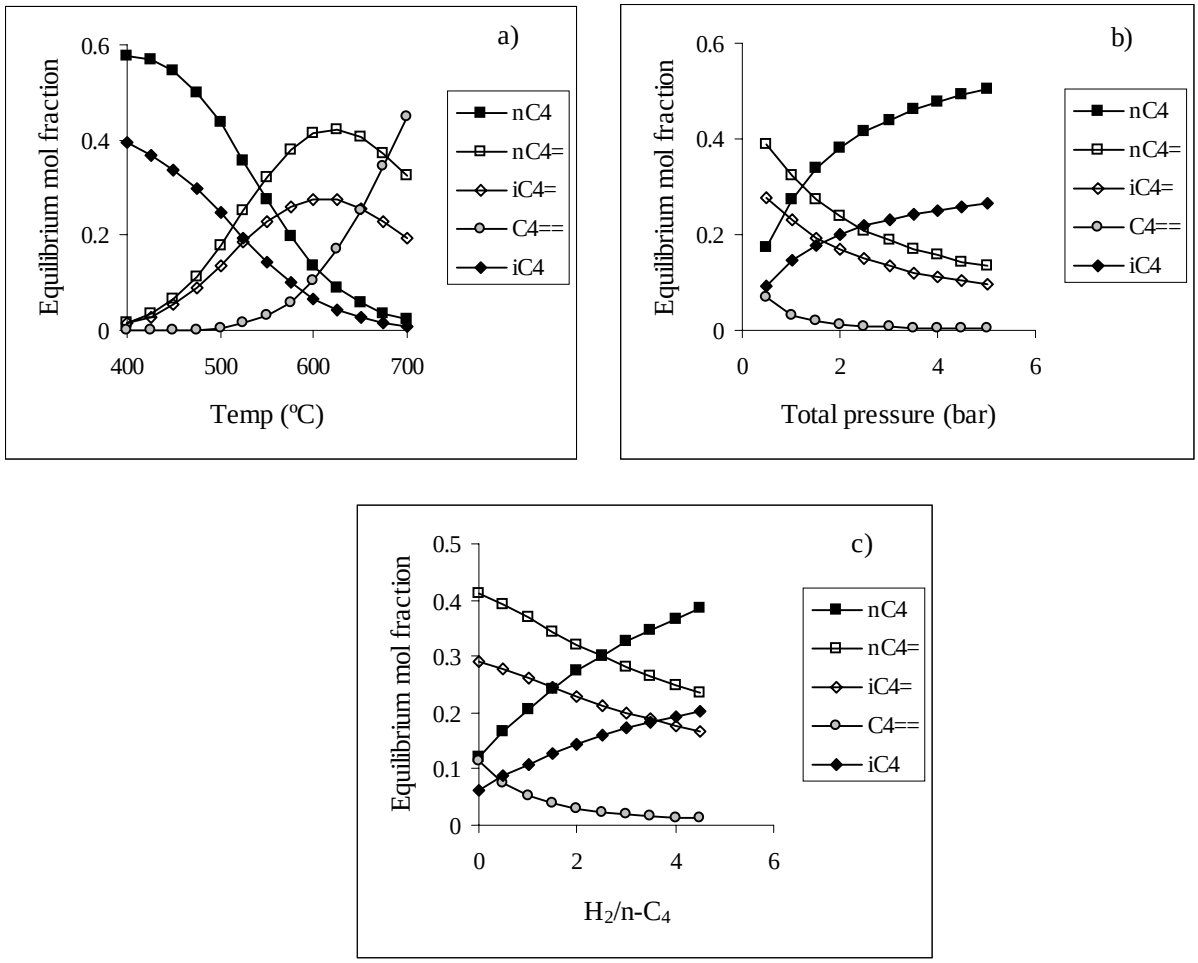

Figure 6 *Thermodynamic equilibrium of n-butane dehydrogenation as a function of (a) temperature, (b) pressure and (c) H_2/n-butane ratio. Input: 0.1 mol n-butane, 0.2 mol H_2, 0.7 mol N_2. In case (c): x mol H_2, 0.9 – x mol N_2.*

Figure 6a, b and c show the C_4 equilibrium distribution as a function of temperature, pressure and H_2/n-butane ratio. Two other products were taken into account in this calculation, i.e., butadiene (formed by dehydrogenation of the linear butenes) and isobutane (formed by hydrogenation of isobutene). The graphs show the following trends. (i) The equilibrium mol fraction of linear butenes and of isobutene increases with temperature till to a maximum at about 625 ºC (~ 900 K). Above 625 ºC the butenes decrease at the expense of an increase in butadiene. (ii) With increasing total pressure and increasing H_2/C_4 ratio the equilibrium mol fractions of linear butenes, isobutene and butadiene decrease, i.e., the dehydrogenation

equilibrium is shifted to the side of the reactants.

Concerning the choice of the operating conditions of a dehydroisomerization reactor we can conclude from the graphs that (i) the temperature window for the reaction is 500-650 ºC (775 – 925 K), (ii) pressure and H_2/C_4 ratio should be as low as possible. Low pressures, however, increase the reactor volume and low H_2/C_4 ratios can be expected to decrease catalyst stability due to a higher rate of coking.

Catalysts for dehydroisomerization

Table 9 gives an overview of patents describing catalysts for the dehydroisomerization of n-butane. The catalyst formulations are rather similar to those given in Table 8.

Already in 1981 a dehydroisomerization process and catalyst were patented by Kolombos *et al.* [51]. They used Ga-catalysts supported on silica, alumina, silicalite or other zeolites (LTL, ERI). Next to isobutene and linear butenes these catalysts also produced a lot of aromatics. The authors concluded that a low aciditiy of the support was crucial for a good performance of the catalyst. Also a process scheme was suggested where the product stream of the dehydroisomerization unit is routed directly (without further separation steps) to a MTBE unit (see Figure 7). The unreacted linear butenes and n-butane are recycled from the MTBE unit to the dehydroisomerization reactor. For the efficiency of the overall process it is very important that the dehydroisomerization catalyst also has the capability to isomerize the linear butenes fed from the recycling stream to isobutene.

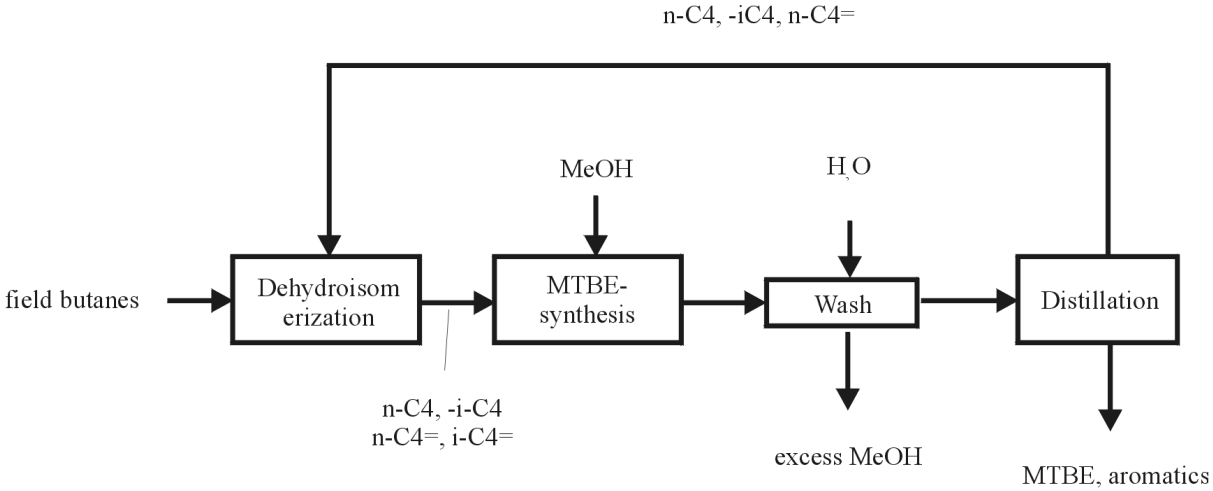

Figure 7 *Scheme of a dehydroisomerization process [51].*

Sikkenga *et al.* [52] used Pt-AMS-1B, a borosilicate, for the dehydroisomerization reaction. Their results demonstrate the effects of temperature and feed composition. The best

conversion and selectivity was achieved at 540 ºC, which was also the highest temperature tested. At low temperatures a lot of isobutane was formed, as predicted by thermodynamics. Adding hydrogen and an inert gas as dilutant strongly reduced the selectivity to cracking reactions and resulted in higher yields of isobutene.

A rather similar catalyst, Pt-[B]-ZSM11, where B was incorporated into the zeolite framework during the synthesis, was used by O'Young *et al*. [53]. Re was added in order to prevent sintering of Pt which is likely to occur at metal loadings above 0.3%. A good catalyst activity could be maintained for a period of about 20 h. Still the Re promoter could not completely prevent catalyst deactivation. The authors also compared the performance of Pt/Re-[B]-ZSM11 with Pt/Re-[B]-ZSM5. The ZSM5-supported catalyst was less active, but more selective and especially more stable. After a stabilization period of less than one hour no deactivation was observed. Note that in all the other references cited in Table 9 no information whatsoever is given about the time on stream behavior of the catalysts.

The highest yields of isobutene were reported by Bellussi *et al*. [54] (although without any information on the stability). They used silylated alumina as a support for Pt and added promoters (Sn, In) in order to improve the activity and selectivity of the catalyst. By adding an isomerization catalyst (silylated alumina or Boralite B, a borosilicate) to the dehydroisomerization catalyst higher yields of isobutene were obtained. A separate bed of the isomerization catalyst (downstream of the dehydroisomerization catalyst) was more effective than mixing the two components. In the latter case the ratio $iC_4^=/C_4^=$ increased only marginally. The results indicate that using a bifunctional catalyst may not be necessary. Good results can also be obtained with a dual bed of two catalyst components.

The authors also gave an economic analysis of the dehydroisomerization process [55] and arrived at the conclusion that above a per pass yield of 13.5% isobutene the one-step dehydroisomerization is economically favorable compared to the two-stage processes described at the beginning of this introduction. The 13.5% value depends, of course, on the market prices of the raw material (n-butane) and the product (MTBE in that case) as well as on the capital investment and is probably not valid any more for the current market situation. Therefore the question of the economic feasibility of dehydroisomerization will be readdressed in the concluding remarks on this thesis.

Table 9 *Selection of patents describing catalysts for the dehydroisomerization of n-butane*

Catalyst	Feed	Temp (ºC)	WHSV (h^{-1})	TOS (h)	Conv (%)	Sel (%)	Yield (%)	Max. yield[a] (%)		Ref.
0.5Pt-1.1Zn-MOR(10)	H_2/nC_4 = 10	550	90	?	48.6	50	6.1	15	11	[56]
Ga-L	nC_4	550		?	55	49	10	24	20	
Ga-SiO_2	nC_4	590			56	39	8	29	25	
0.5Pt-AMS-1B	nC_4	540	8.2	?	45	52	9.3	22	19	[52]
0.5Pt-AMS-1B	H_2/nC_4=0.79 He/nC_4=1.79	540	8.2	?	38	77	10.9	23	19	
0.3Pt/0.3Re-[B]-ZSM11	H_2/nC_4=2 3% steam	567	12.5	21[b]	43	81	10.3	21	16	[53]
0.3Pt/0.3Re-[B]-ZSM5		567	12.5	23[b]	20	82	5.9	21	16	
0.4Pt/0.5Sn/0.4In-SiO_2/γ-Al_2O_3 = Cat I	H_2/nC_4=1 N_2/C_4=2	563	2	?	56	78	11.9	27	22	[54]
Cat I + SiO_2/Al_2O_3 (separate) 1:1		563	2		57	65	13.2	27	22	
Cat I + Boralite B (separate) 2.6:1		552	2		58	65	14.6	25	20	
Cat I + Boralite B (mixed) 2:1		564	2		58	68	12.8	27	22	

[a] The maximum yield of isobutene is the equilibrium mol fraction determined from thermodynamics. In the left column only isobutene and the linear butenes were taken into account, in the right column also isobutane and butadiene.

[b] Yields and conversions were averaged over the whole time on stream.

Oxidative dehydrogenation

The thermodynamic constraints represent an inherent problem of the dehydroisomerization reaction (and also of the two-step dehydrogenation) that cannot be circumvented. The examples in Table 9 show that under realistic conditions (i.e., high pressure, little or no dilutant) the possible per pass yield of isobutene is less than 30%.

By using oxidative dehydrogenation (ODH), however, the thermodynamic limitations of dehydrogenation could be removed. The formation of water makes the ODH-reaction highly exothermic and the thermodynamic equilibrium is completely on the side of the products.

$n\text{-}C_4 + O_2 \rightleftharpoons 1\text{-}C_4^{=} + H_2O \qquad \Delta H_{823K} = -109 \text{ kJ/mol} \qquad \Delta G_{823K} = -189 \text{ kJ/mol}$

But also ODH is not an easy reaction. The butenes are much more reactive species than butane and once formed they can easily react further to butadiene, CO and CO_2. As a result, the selectivity drops with increasing conversion. Consequently, selectivity to butenes is the crucial parameter in catalyst design.

A very nice review of the state of the art in oxidative dehydrogenation is given by Kung [57]. In this review Kung provides a list of the most successful catalysts for the oxidative dehydrogenation of n-butane that have been reported so far (see Table 10). These catalysts are based on V, Mo or Ni with P, Sn, Mg and Ni as promoters. They achieve yields of butene of up to 10%. Note that, along with butene, equal or even higher amounts of butadiene are formed (the only exception is V/SiO_2). The major by-product is in all cases CO_x.

In academic research most of work has been focused on vanadia-based catalysts. In spite of the large amount of research that has been done, some scientific questions still remain open, mainly concerning the mechanism of CO and CO_2 formation. It has not been clearly proven yet whether the reaction is primary (i.e., a direct formation of CO and/or CO_2 from n-butane, as suggested in [58] and [59]) or secondary (i.e. formation from butene [60]) or both (which seems to be most probable). Some authors have suggested the presence of two different catalytic sites, a selective one leading to dehydrogenation and an unselective one leading to combustion [58, 61]. Moreover, it was proposed that gas phase oxygen increases the CO_x formation while lattice oxygen is involved in the selective reaction route leading to butenes [58, 62]. This contradicts to findings that the oxygen/hydrocarbon ratio in the feed has no effect on the selectivity [59, 63]. There is, however, general consensus on the fact that high temperatures [63, 64] and a basic support material [65, 66, 67] enhance the selectivity to dehydrogenation because they weaken the strength of adsorption of butene, thereby reducing

the chance that it reacts further to CO_x. (Some authors [65, 68] report a decrease in selectivity to dehydrogenation with temperature. This is, however, a misinterpretation of the data, which were measured at constant contact time instead of constant conversion.)

Oxidative dehydroisomerization

The examples in Table 10 show that the butene yields of even the best ODH catalyst cannot compete with those achieved in dehydrogenation (see Table 7 and Table 8). But due to the growing market for olefins, interest in ODH is rising and the development of better catalysts can be expected in the near future. With respect to the production of isobutene, it is therefore very interesting to explore whether a combination of oxidative dehydrogenation with isomerization, i.e., oxidative dehydroisomerization (ODHI), is possible.

In principle, three concepts can be thought of:

(i) a simple physical mixture of an ODH with an isomerization catalyst

(ii) a microstructural arrangement of the two components, e.g. an isomerization catalyst coated with small ODH catalyst particles

(iii) a bifunctional catalyst with a metal oxide grafted onto the outer surface of the isomerization catalyst

Scope of the thesis

It was the idea of oxidative dehydroisomerization that had initiated this thesis. In Chapter 3 the potential and limitation of this completely new approach will be discussed. Since the conclusion had to be drawn that oxidative dehydroisomerization is probably not feasible at present, we then turned our attention back to non-oxidative dehydroisomerization. From our knowledge of the patent literature Pt-ZSM5 with a high SiO_2/Al_2O_3 ratio was chosen as a base catalyst. We first tried to understand the effect of the catalyst parameters metal loading and acid site concentration (Chapter 4 and 5), before trying to optimize the yield of isobutene by variation of the reaction conditions (Chapter 6). Pt-ZSM5 gave good yields of up to 15% isobutene, but the rather high selectivity to by-products proved to be a disadvantage of this material. Thus, alternatives were studied and compared with Pt-ZSM5 (Chapter 8 and Chapter 9). The thesis is concluded by general remarks and suggestions for further research.

Table 10 *Performance of catalysts used for the oxidative dehydrogenation of n-butane (adapted from [57]).*

Catalyst	Temp (ºC)	Conv (%)	Sel $C_4^=$ (%)	Sel $C_4^{==}$ (%)	Sel dehyd (%)	Yield $C_4^=$ (%)	Yield dehyd(%)	Ref.
V-Mg-O	500-540	18	36	17	53	6.5	9.5	[60]
		23	32	23	55	7.4	12.7	
	480	40	20	33	53	8.0	21.2	[69]
		31	29	24	53	9.0	16.4	
Ni-Mo-P-O	482	25			75		18.8	[70]
	538	39			72		28.1	
Mg-Ni-Sn-O	482	29	30	21	51	8.7	14.8	
	565	39	19	30	49	7.4	19.1	[71]
Mg-Ni-SO_4	538	36	27	31	58	9.7	20.9	
Ni-P-O	538	42	26	30	60	10.8	25.2	[72]
V-K-SO_4	500	25			72		18	[73]
V/SiO_2	520	15	54	12	66	8.1	9.9	
		16	53	8	61	8.5	9.8	[74]
		25	41	10	51	10.3	12.8	

References:

[1] Obenaus, F., Droste, W., and Neumeister, J., in "Ullmann's encyclopedia of industrial chemistry" (Gerhartz, W., Yamamoto, Y.St., Campbell, F.T., Pfefferkorn, R., and Rounsaville, J.F., Eds.), 5th ed., Vol. A4, p. 483., VCH, Weinheim, 1985-1986.

[2] Energy Security Analysis, Inc., "Supply and cost of alternatives to MTBE in gasoline, Report on the Oxygenate Market: Current Production Capacity, Future Supply Prospects and Costs Estimates", Wakefield, MA , October 1998 (prepared for the California Energy Commission).

[3] Chem. & Eng. News, June 24, 1996, p. 42.

[4] Hydrocarbon Processsing, May 1994, p.66.

[5] Hydrocarbon Processing, December 1996, p. 29.

[6] Squillace, P.J., Zogorski, J.S. Wilber, W.G., and Price, C.V., Environ. Sci. Tech. **30**, 1721, 1996.

[7] Happel, A.M., Beckenbach, E.H., and Halden, R.U., "An Evaluation of MTBE Impacts to California Groundwater Resources", University of California, Berkeley, June 1998 (report submitted to the California State Water Resources Control Board, Underground Storage Tank Program).

[8] European Chemical News, 5-11 April, 1999, p. 4.

[9] European Chemical News, 10-16 May, 1999, p. 23.

[10] European Chemical News, 15-21 March, 1999, p. 16.

[11] European Chemical News, 19-25 April, 1999, p. 16.

[12] Frame, R.R., Stine, L.O, Hammershaimb, H.U., and Muldoon, B.S., Erdöl Erdgas Kohle **114** (7-8), 385 (1998).

[13] Hydrocarbon Processing, Febuary 1999, p. 31.

[14] Rosati, D., in "Handbook of Petroleum Refining Processes", Chemical Process Technology Handbook Series (R.A. Meyer, Ed.), p. 5, Mc Graw-Hill Book Company, New York, 1986.

[15] Frishkorn, G.L., Kuchar, P.J., and Olson, R.K., "Butane Isomerization Technology: Now and for the Future", presented at the AIChE Conference, Denver, Colorado, August 1988.

[16] Pujado, P.R., and Vora, B.V., Hydrocarbon Processing, March 1990, p. 65.

[17] Gregor, J., in "Handbook of Petroleum Refining Processes" (R.A. Meyer, Ed.), 2nd ed., Chapter 5.1., McGraw-Hill Book Company, New York, 1997.

[18] Imai, T., Vora, B.V., and Bricker, J.C. "Development of Dehydrogenation Catalyst and Processes", presented at the International Conference on Recent Developments in Petrochemical and Polymer Technologies, Bangkok, Thailand, December 12-16, 1989.

[19] Schuette, G.F., Brinkmeyer, F.M., and Dunn, R.O., Chim. Oggi, January/Febuary 1994, p. 39.

[20] Dunn, R.O., and Shoemaker, L.W., PTQ, Winter 1998/99, p. 61.

[21] Brinkmeyer, F.M., Rohr, D.F., Olbrich, M.E., and Drehman, L.E., Oil & Gas Journal, March 28,

1983, p. 75.

[22] Hydrocarbon Processing, September 1980, p. 210.

[23] Gussow, S., Spence, D.C., and White, E.A., Oil & Gas Journal, December 8, 1980, p. 96.

[24] Bölt, H., and Zimmermann, H., Erdöl Erdgas Kohle, Febuary 1995, p. 90.

[25] Buonomo, F., Sanfilippo, D., and Trifiro, F., in "Handbook of Heterogeneous Catalysis", (Ertl, G., Knözinger, H., and Weitkamp, J., Eds.), Vol. 5, p. 2140, VHC-Wiley, Weinheim, 1997.

[26] Atkins, M.P., and Evans, G.R., Erdöl Erdgas Kohle, Juni 1995, p. 271.

[27] van den Oosterkamp, P.F., private communication.

[28] Sinfelt, J.H., Adv. Catal. **23**, 91 (1973).

[29] Parera, J.M., and Beltramini, J.N., J. Catal. **112**, 357 (1988).

[30] Burch, R., J. Catal. **71**, 348 (1981).

[31] Cortright, R.D., and Dumesic, J.A., J. Catal. **148**, 771 (1994).

[32] Kemball, C., and Dowden, D.A., in "Catalysis, A Review of the Recent Literature Published up to late 1977", Vol. 2, p.21, The Chemical Society, Burlington House, London, 1977.

[33] Goddard, S.A., Amiridis, D., Rekoske, J.E., Cardona-Martinez, N., and Dumesic, J.A., J. Catal. **117**, 155 (1989).

[34] Bond, G.C., Appl. Catal. A **149**, 1 (1997).

[35] Cortright, R.D., and Dumesic, J.A., Appl. Catal. A **129**, 101 (1995).

[36] Poole, C.P. Jr., and McIver, D.S., Adv. Catal. **17**, 223 (1967).

[37] Yamamoto, S., Asaoka, S., Kobayashi, H., and Nagumo, A., JP Patent 9.070.544 (1997), assigned to Chiyoda Chemical Engineering Construction Co.

[38] Yamamoto, S., Asaoka, S., Kobayashi, H., Nagumo, A., and Okada, Y., JP Patent 9.075.732 (1997), assigned to Chiyoda Chemical Engineering Construction Co.

[39] Olbrich, M.E., McKay, D.L., and Montgomery, D.P., US Patent 4.926.005 (1990), assigned to Phillips Petroleum Co.

[40] Brinkmeyer, F.M., Savage, K.B., Khare, G.P., and Kubicek, D.H., US Patent 5.220.091 (1993), assigned to Phillips Petroleum Co.

[41] Imai, T., and Hung, Chi-W., US Patent 4.438.288 (1984), assigned to UOP Inc.

[42] Kogan, S., Herskowitz, M., Woerde, H.M., and van den Oosterkamp, P.F., DGMK Tagungsberichte **9705**, 117 (1997).

[43] Kerby, M.C., Riley, K.L., Long, F.M., Johnson, J.W., and Brody, J.F., US Patent 5.258.567 (1993), assigned to Exxon Research and Engineering Co.

[44] Dessau, R.M., US Patent 5.122.489 (1992), assigned to Mobil Oil Co.

[45] Indo French Center for the Promotion of Advanced Research, FR Patent 2.724.926 (1996).

[46] Meriaudeau, P., Nascimento, P., Sapaly, G., and Naccache, C., EP Patent 858.834 (1998), assigned to Total Raffinage Distribution S.A.

[47] Barri, S.A.I, and Tahir, R., US Patent 5.208.201 (1991), assigned to The British Petroleum Co.

[48] Kaminsky, M.P., Froment, G.F., and DeHertog, W.J., WO Patent 93/15835 (1993), assigned to Amoco Corp.

[49] Alexander, B.D., Huff, G.A. Jr., and Kaminsky, M.P., WO Patent 96/01239 (1996), assigned to Amoco Corp.

[50] Shum, V.K., US Patent 4.962.266 (1990), assigned to Amoco Corp.

[51] Kolombos, A.J., Telford, C.D., and Young, D., EP Patent 42.252 (1981), assigned to The British Petroleum Company.

[52] Sikkenga, D.L., Nevitt, Th.D., and Jerome, N.F., US Patent 4.433.190 (1984), assigned to Standard Oil Company.

[53] O'Young, Ch.-L., Browne, J.E., Matteo, J.F., Sawicki, R.A., and Hazen, J., US Patent 5.198.597 (1993), assigned to Texaco Inc.

[54] Bellussi, G., Giusti, A., and Zanibelli, L., US Patent 5.335.830 (1994), assigned to Eniricerche SpA, Snamprogetti SpA.

[55] V. Fattore, G. Fornasari, L. Rossi, and L. Zanibelli, in "Proceedings Int. Congress Energy, Environment and Innovation Technology, Caracas, October 1989".

[56] de Agudelo, M.M., Romero, T., Guaregua, J., and Gonzalez, M., US Patent 5.416.052 (1995), assigned to Intevep S.A.

[57] Kung, H.H., Adv. Catal. **40**, 1 (1994).

[58] Pantazaidis, A., Bucholz, S.A., Zanthoff., H.W., Schuurman, Y., and Mirodatos, C., Catal. Today **40**, 207 (1998).

[59] Michaels, J.N., Stern, D.L., and Grasselli, R.K., Catal. Lett. **42**, 135 (1996).

[60] Patel, D., Kung, M.C., and Kung, H.H., in "Proceedings 9th International Congress on Catalysis, Calgary, 1988" (M.J. Philips and M. Ternan, Eds.), Vol.4, p. 1554, Chem. Institute of Canada, Ottawa, 1988.

[61] Kung, H.H., Kundalkar, B., Kung, M.C., and Cheng, W.H., J. Phys. Chem. **84**, 382, 1980.

[62] Sokolovskii, V.D., Catal.Rev.-Sci.Eng. **32**, 1, 1990.

[63] Chaar, M.A., Patel, D., and Kung, H.H., J. Catal. **109**, 463 (1988).

[64] Watling, T.C., Deo, G., Seshan, K., Wachs, I.E., and Lercher, J.A., Catal. Today **28**, 139 (1996).

[65] Concepcion, P., Lopez-Nieto, J.M., and Perez-Pariente, J., Stud. Surf. Sci. Catal. **94**, 681 (1995).

[66] Albonetti, S., Cavani, F., and Trifiro, F., Catal. Rev. **38**, 413 (1996).

[67] Galli, A., Lopez-Nieto, J.M., Dejoz, A., and Vazquez, M.I., Catal. Lett. **34**, 51 (1995).

[68] Centi, F., and Trifiro, F, Appl. Catal. A **143**, 3 (1996).

[69] Chaar, M.A., Patel, D., Kung, M.C., and Kung, H.H., J. Catal **105**, 483 (1987).

[70] Bertus, B.J., US Patent 4.094.819 (1978), assigned to Phillips Petroleum Company.

[71] Bertus, B.J., US Patents 3.886.090 and 3.886.091 (1975), assigned to Phillips Petroleum

Company.

[72] Ripley, D.L., US Patent 4.044.066 (1977), assigned to Phillips Petroleum Company.

[73] Walker, D.W., Hogan, R.J., and Farha, F., US Patent 4.218.343 (1980), assigned to Phillips Petroleum Company.

[74] Owens, L., and Kung, H.H., Prepr. Am Chem. Soc. Div. Pet. Chem. **37**, 1194 (1992).

Chapter

2

Experimental

Abstract

This chapter describes the experimental methods used for the preparation, characterization and kinetic testing of the catalysts, throughout this thesis. The physico-chemical methods described are hydrogen-chemisorption, IR spectroscopy, and HREM (High Resolution Electron Microscopy).

Kinetic setup

Figure 1 shows a schematic drawing of the setup used for catalyst testing. Two separate gas streams were used. Stream 1 was the stream of the reactant gases. Up to four gases could be mixed by a corresponding set of mass flow controllers. Stream 2 was the stream used for pretreatment, purging, regeneration, etc. of the catalyst. Two four-port valves before and after the reactor were used to direct stream 1 and stream 2 to reactor/bypass and sampling-system/vent.

The catalysts were pressed, crushed and sieved to obtain particle sizes in the range of 300 to 500 µm. 10 to 100 mg of the catalyst were mixed with about 60 mg quartz and filled into quartz tube with an inner diameter of 4 mm. The catalyst bed had a typical length of 5 to 15 mm and was supported on both sides by quartz wool. The oven temperature was controlled *via* a thermocouple placed on the outside of the reactor. Two additional thermocouples were placed on top and on bottom of the catalyst bed to measure the actual temperature.

The catalyst was pretreated (oxidized, reduced, degassed, etc.) in stream 2. In the meantime the feed mixture (stream 1) was flowed via the by-pass line. After stabilization for at least 30 min the feed composition was analyzed via the GC sampling system (*vide infra*). The reaction was started by switching V1 from position {stream 1-bypass, stream 2-reactor} to position {stream 1-reactor, stream 2-bypass}. In the first minutes on stream the reactor effluent was stored in sample loops of the two (one for each injection port, see Figure 2) 16-position valves, for post-run GC analysis. After 10 to 30 min, the reactor effluent was analyzed on-line, without making use of the storage loops.

The analysis system is shown in Figure 2. Two parallel injection ports were used. One injection port was connected to an Al_2O_3 PLOT column (530 µm inner diameter, 50 m length) for separating the hydrocarbons in the range C_1 to C_8. A FID was used for detection of the hydrocarbons. The second injection port was connected to a combination of a Hayesep C (6 feet length, 80/100 mesh) with a MS5Å column (4 feet length). The column system was equipped with a 6-port valve allowing to backflush the Haysep column and an 8-port valve, allowing to by-pass the MS5Å column. Since CO_2 and water do not elute from the MS5Å column, the by-pass was necessary in order to be able to separate all the light gases (H_2, O_2, N_2, CO, CO_2, CH_4) as well as water in one run (during the oxidative dehydrogenation experiments). H_2,

N_2 and O_2 were first eluted via the Haysep C and the MS5Å column in series, then the MS5Å column was by-passed for eluting CO_2. After switching back to the MS5Å column, the other light gases were eluted (CO, CH_4, etc.). Finally the MS5Å column was by-passed again for the analysis of water. A TCD was used for detection of the light gases. The response factors of the various compounds were determined by means of reference gases. The FID was not calibrated in absolute terms. It was only used for the determination of the relative concentration of hydrocarbons.

The TCD was only calibrated for on line analysis. Therefore, a determination of absolute concentrations (and, thus, a determination of the carbon balance) was not possible when using the storage loops.

Hydrocarbon conversions and yields were calculated on a carbon basis, using the FID areas A_i and the corresponding response factors rf_i (equation 1). In oxidative dehydrogenation, methane was added as internal standard to the feed. It could be detected in both TCD and FID and allowed relating the amount of CO and CO_2 measured in the TCD to the amount of the other hydrocarbons measured by FID.

$$\text{Conversion} = [\ 1 - A_{n\text{-}C4} * rf_{n\text{-}C4} / \sum (A_i * rf_i)\ ] * 100\ \%$$

$$\text{Yield}_i = A_i * rf_i\ / \sum (A_i * rf_i) * 100\ \%$$

A_i ... area of the FID peak of compound i

rf_i ... response factor (mol carbon/unit area) of compound i (rf_i ~ 1 for most hydrocarbons)

Preparation of the Pt-catalysts

The Pt-zeolites used for dehydroisomerization were prepared by aqueous ion exchange. A highly diluted solution of $Pt(NH_3)_4(OH)_2$ (0.1 - 0.2 mg Pt/ml) and ammonia (concentration approximately 2%) was added dropwise to a suspension of the zeolite (which was usually in the ammonium form) in water (10 ml H_2O/g zeolite) over a period of several hours. The addition of ammonia to the solution slows down the ion exchange reaction and is supposed to give a better dispersion of the Pt-complex over the zeolite pores [1, 2]. The suspension was stirred for 20 h at room temperature. The final pH was typically between 8 and 9. After filtration the filter cake was washed twice with doubly distilled water. The sample was dried, slowly

heated in flowing air to 723 K (0.5 K/min) and kept at this temperature for 2 h to decompose the Pt complex. After cooling down to ambient temperature the calcination tube was flushed with nitrogen. Finally, the sample was reduced in flowing H_2 for 2 h at 773 K (5 K/min) [3].

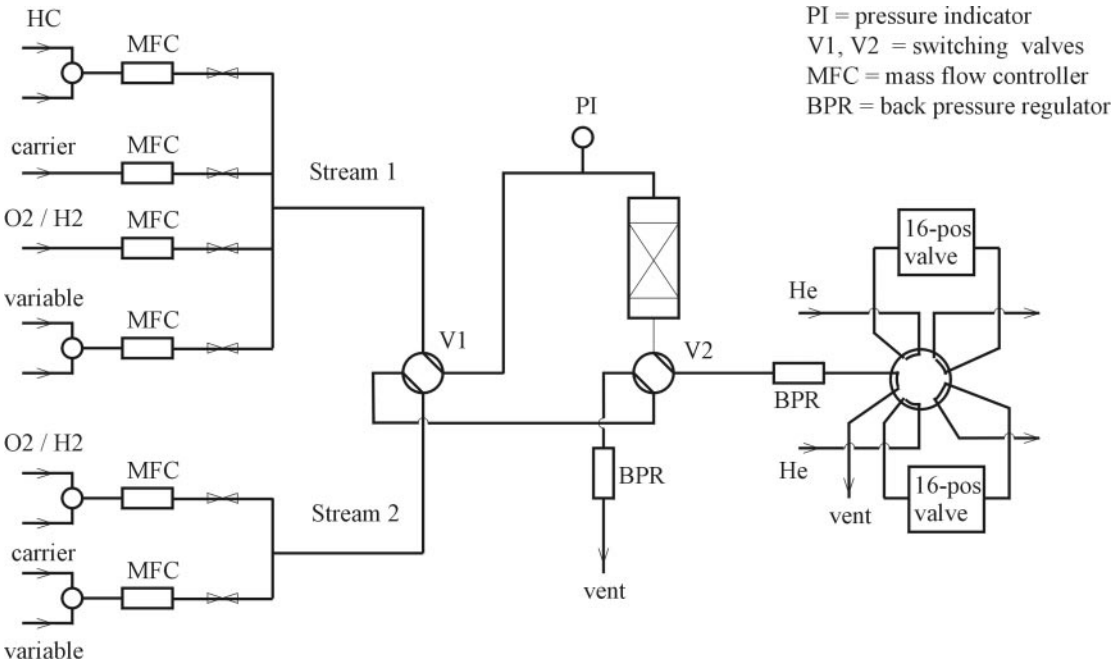

Figure 1 *Schematic drawing of the setup used for catalyst testing.*

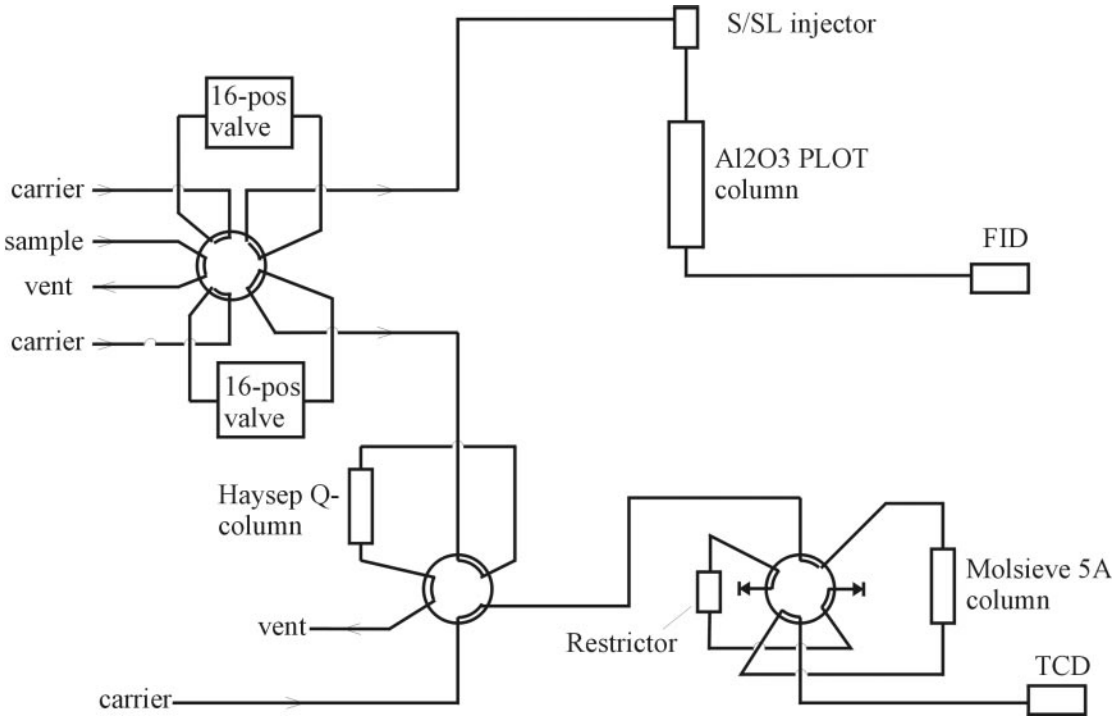

Figure 2 *GC analysis system.*

Hydrogen chemisorption

Hydrogen chemisorption was used to determine the metal dispersion of the Pt catalysts. About 1 g of the sample was reduced for 1 h at 823 K in H_2. After reduction the sample was degassed at 823 K for 1 h in vacuum (10^{-5} mbar). The rather high temperature of 823 K was chosen for reduction and degassing because the dehydroisomerization reaction was also performed at high temperatures (830 K, see Chapter 4). After degassing, the sample was cooled to room temperature and the hydrogen adsorption isotherm was measured by dosing decreasing amounts of H_2 (in the range of 500 to 50 mbar) to the sample. The hydrogen chemisorption capacity was calculated by extrapolation of the hydrogen uptake to zero pressure. A more detailed description of the apparatus can be found in ref. [4].

High resolution electron microsocopy (HREM)

High Resolution Electron Microscopy (HREM) was applied to study the size and location of the Pt particles. The measurements were perfomed in the National Center for HREM, Delft, on a Phillips CM 30 T electron microscope with a LaB_6 filament as the source of electrons operated at 300 kV. The reduced Pt-catalysts (reduced according to the procedure described above) were mounted on a microgrid carbon polymer supported on a copper grid by placing a few droplets of a suspension of ground sample in ethanol on the grid, followed by drying at ambient conditions. Images of several areas of the sample were measured in order to get a representative picture of the Pt distribution.

IR spectroscopy

IR experiments were performed in a flow system connected to a CSTR reactor (internal volume 1.5 cm^3), which was equipped on two sides with CaF_2 windows for allowing the IR beam to pass through the sample [5, 6]. The samples were pressed into self-supporting disks (2-3 mg) and placed into a cylindrical oven, which could be mounted on the IR reactor. The IR spectra were measured in the transmission/absorption mode, using a Nicolet SXB20 spectrometer (resolution 4 cm^{-1}). The intensities of two bands at 1975 cm^{-1} and 1865 cm^{-1}, attributed to the

overtones of zeolite lattice vibrations, were taken as a measure of the thickness of the sample and used for normalization of the spectra.

Acknowledgements

The HREM measurements represent an invaluable contribution to this thesis. I would like to thank P. Kooyman, from the National Center for HREM, Delft, for performing and analyzing the HREM photos.

References

[1] Che, M., and Bennett, C.O., Adv. Catal. **36**, 55 (1989).

[2] Le Page, J.-F., Cosyns, J., Courty, P., Freund, E., Franck, J.-P., Jacquin, Y., Juguin, B., Marcilly, C., Martino, G., Miquel, J., Montarnal, R., Sugier, A., and van Landeghem, H., "Applied Heterogeneous Catalysis", p. 113. Editions Technip, Paris, 1978.

[3] van den Broek, A.C.M. , van Grondelle, J., and van Santen, R.A., J. Catal. **167**, 417 (1997).

[4] Englisch, M., PhD Thesis, University of Twente, Enschede, The Netherlands, 1996.

[5] Mirth, G., Eder, F., and Lercher, J.A., Appl. Spectroscopy **48**, 194 (1994).

[6] Veefkind, V., PhD Thesis, University of Twente, Enschede, The Netherlands, 1998.

Chapter 3

The oxidative dehydroisomerization of n-butane to isobutene

Abstract

The oxidative dehydroisomerization of n-butane to isobutene was studied over physical mixtures of a supported vanadia-niobia mixed oxide with the zeolites ZSM5, FER and MCM36. The zeolites converted a fraction of 10 to 30% of the butenes formed on the vanadia-niobia catalyst to isobutene. The rate of isobutene formation decreased very rapidly, however, due to the presence of butadiene in the reaction mixture. The deactivation was accelerated by the fact that zeolites themselves have some oxidative dehydrogenation activity and transformed butene to butadiene in the presence of oxygen. Only ZSM5 showed a fairly stable activity and selectivity due to its two-dimensional pore-structure which is least sensitive to deactivation. In dehydroisomerization experiments over Pt-ZSM5 in the presence of H_2, the butene isomerization activity was perfectly stable. This was attributed to (i) the presence of H_2 and Pt and (ii) the higher ratio of butene to butadiene in the reaction mixture compared to oxidative dehydroisomerization.

Introduction

In dehydroisomerization of n-butane to isobutene, the yield of isobutene that can be achieved will always be severely limited by thermodynamics. The use of oxygen ($n\text{-}C_4H_{10} + O_2 \rightleftharpoons C_4H_8 + H_2O$), however, removes the thermodynamic constraints of the dehydrogenation step, because the formation of water makes the reaction highly exothermic. As a result, oxidative dehydroisomerization can in principle be carried out at lower temperatures, at which butene isomerization is thermodynamically more favored. Hybrid catalysts containing vanadia species (for oxidative dehydrogenation) grafted on the surface of zeolite particles (for isomerization of the butenes) could be used for such a one-step oxidative dehydrogenation. In an attempt to simulate the properties of these hybrid catalysts we used physical mixtures of supported vanadia catalysts and zeolites. Mixed oxides of vanadia with niobia [1] have been successfully applied for oxidative dehydrogenation of alkanes. In the present study the V-Nb-O mixed oxide was supported on Al_2O_3 and SiO_2. The idea behind this was to mimic the grafting procedure on a zeolite surface. The support properties of Al_2O_3 and SiO_2 are closer to those of zeolites than of the more basic MgO, which – from the point of selectivity in ODH – would be the better support material than Al_2O_3 and SiO_2 (see Chapter 1).

The catalytic properties of these physical mixtures were compared with those of zeolite supported Pt catalysts for dehydroisomerization, in the presence of hydrogen.

Experimental

Catalyst preparation

Three methods for preparing supported V-Nb-O catalysts were compared, (i) wet co-impregnation, using an oxalic acid solution of hydrated niobia and ammoniumvanadate [1], (ii) stepwise wet impregnation of first niobia and then vanadia, (iii) grafting of metal complexes. The grafting procedure was performed similar to a method described by Deo *et al*. [2]. 5.1 g Al_2O_3 C (Degussa, SA = 100 m^2/g) was dried at 373 K under vacuum and then transferred to the glove box. A solution of 165 µl $VO(O\text{-}iC_3H_7)_3$ and 490 µl $Nb(OEt)_5$ in 10 ml dry toluene (Molsieve 4Å) was added dropwise to the alumina powder under constant mixing. About 10 ml toluene were added at the end to reach the incipient wetness point. The powder was left to dry in the glove box for three days, then dried under vacuum for 1 h. Finally it was heated in a flow of air with 2.5 K/min to 400 K and kept there for 3 h, then the temperature was raised to 900 K (2.5 K/min) and kept there for 8 h. The final material

(abbreviation AlVNb) contained 1.1% V_2O_5 and 4.8% Nb_2O_5, as determined by XRF. The surface area was unchanged 100 m^2/g.

In order to check the homogeneity of the vanadia and niobia distribution on the surface of the support, the elemental composition was analyzed by small-area EDAX scans (see ref. [3] for a detailed description of the apparatus). The materials prepared by wet impregnation showed a large scatter of the vanadia and niobia content. Only with the grafting procedure, a rather homogeneous distribution of the two metal oxides could be achieved. Therefore the grafting procedure was selected as the standard preparation method.

Several other catalysts, using Al_2O_3 C or Aerosil SiO_2 (Degussa, 180 m^2/g) with varying vanadia and niobia loadings were prepared by this method. The acidity of the samples was characterized by temperature programmed desorption of pyridine.

MCM36 was prepared according to the method described in ref. [4]. FER was received from TOSOH Inc. (sample code HSZ-720KOA), ZSM5 from ZEOLYST (sample code CBV10002). The characteristics of the materials are summarized in Table 1.

Table 1 *Characteristics of the zeolites used.*

	SiO_2/Al_2O_3[a]	Al (mmol/g)[a]	acid sites (mmol/g)[b]
ZSM5	480	0.07	0.02
FER	17	1.79	2.05
MCM36	23	1.37	n.d.

[a] determined by XRF

[b] determined by temperature programmed desorption of ammonia

For preparing the physical mixtures between zeolite and oxidation catalyst, the two components were mixed, thoroughly ground, pressed into a pellet and then crushed to particles between 300 and 500 µm.

Catalytic testing

10 to 60mg catalyst were filled into quartz reactor of 4 mm inner diameter, supported on both sides by glass wool. The catalyst was activated for 1 h at 825 K in 25 ml/min pure Ar or in a mixture of O_2/Ar (20/80) or H_2/Ar (20/80), depending on whether O_2 (H_2) was part of the feed during the reaction. After activation of the catalyst the reactor was cooled down to the reaction temperature. The reaction was started by switching the inlet stream from Ar to the

feed mixture. Three types of experiments were performed, (i) oxidative dehydrogenation (dehydroisomerization) with a standard feed of 7% n-butane and 14% O_2 in Ar, (ii) butene isomerization with a standard feed of 4.5% 1-butene in Ar, (iii) dehydroisomerization with a standard feed of 10% n-butane and 20% H_2 in Ar.

Also the influence of butadiene on the isomerization of butene was studied. In these experiments the catalyst was first subjected to a feed of 4.5% 1-butene in Ar for 3 h. After these 3 h the reactor was purged with Ar (at reaction temperature) for 1.5 h whereupon the feed was finally switched to a mixture of 1-butene and butadiene.

Reactions were usually followed for at least 2.5 h. In the first minutes the reactor effluent was stored in sample loops for later analysis. In later stages of the reaction, when high time resolution was less important, the reactor effluent was analyzed on line (see Chapter 2). Calculations of yields and selectivities (in %) were done on a basis of mol carbon in the reactants and products.

Calculation of the pseudo first order rate constant of butene isomerization

In order to be able to compare the butene isomerization activity of the catalysts in different types of experiments (i.e., butene isomerization, oxidative dehydroisomerization, dehydroisomerization in the presence of H_2) the pseudo first order rate constant of the reaction (k_{isom}) was calculated using the formula

$$k_{mA} = -\frac{1}{ST} \cdot \frac{K}{K+1} \cdot \ln\left[1 - x - \frac{x}{K}\right] \qquad \text{(see General Appendix A)}$$

where $ST = m_{cat}/(dV_{total}/dt)$, $x = [i\text{-}C_4^{=}]/\sum[C_4^{=}]$, $K = [i\text{-}C_4^{=}]_{eq}/[n\text{-}C_4^{=}]_{eq} = 0.75$ (at 775 K).

In deriving the above equation it was assumed that (i) the reaction is first order in butene, (ii) the double bond isomerization of linear butenes is fast and always in equilibrium (which is confirmed by the experimental results). The rate constant is calculated from the ratio of isobutene to the sum of butenes. The influence of other (by-)products is not taken into account. This allows to calculate k_{isom} even in reactions where butene isomerization is only a secondary reaction step as is the case in (oxidative) dehydroisomerization. Moreover, since first order in butene is assumed, k_{isom} only depends on the space time, but not on the concentration of butenes in the reaction mixture which facilitates the comparison between different types of experiments.

Results and Discussion

Oxidative dehydrogenation of n-butane over supported V-Nb-O catalysts

The silica and alumina support are slightly acidic. Since acidity of the support decreases the selectivity in oxidative dehydrogenation [5, 6, 7] the intention of the preparation procedure was to cover the support surface completely with a homogeneous overlayer of vandia and niobia. The vanadia and niobia loadings required to achieve such a theoretical monolayer coverage were calculated assuming a surface area of 11 $Å^2$ per $VO_{2.5}$ unit and of 15 $Å^2$ per $NbO_{2.5}$ unit [8]. The EDAX measurements of the samples prepared by wet impregnation showed, however, a large scatter of the local vanadia and niobia concentrations, indicating that a homogeneous distribution of the metal oxides on the support surface could not be achieved by that preparation method. The grafting procedure, on the other hand, gave a rather homogeneous distribution of vanadia and niobia (scatter in the EDAX measurements was about 10%). But in IR spectra of the calcined samples surface OH groups could still be detected, indicating that also in these cases a full coverage of the surface was not achieved.

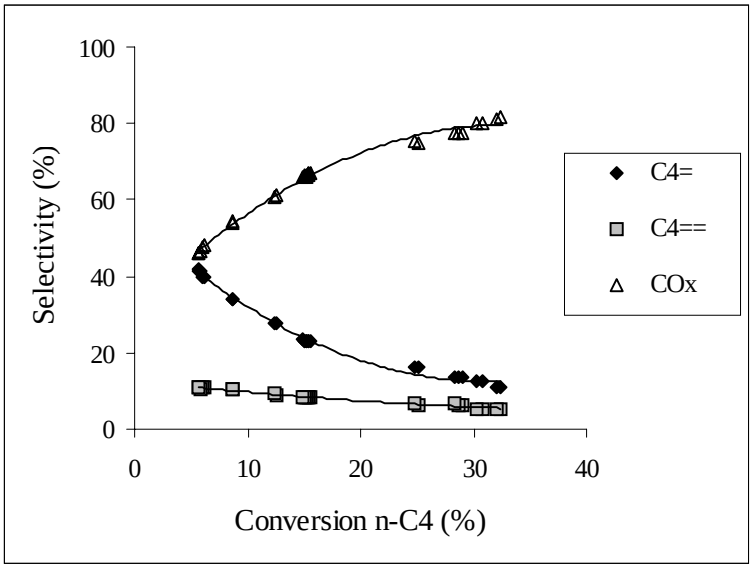

Figure 1 *Selectivity of AlVNb in the oxidative dehydrogenation of n-butane. 775 K, 1 bar, 7% n-butane, 14% O_2.*

Due to their more homogeneous dispersion, only the materials prepared by the grafting procedure were used for the kinetic testing. Four main products were found in the oxidative conversion of n-butane, i.e., CO, CO_2, butenes and butadiene. Apart from theses four products only small amounts of cracking products like propene could be found. Figure 1 shows the selectivity pattern of one selected catalyst (AlVNb, 94% Al_2O_3, 1.6% V_2O_5, 4.8% Nb_2O_5). All the other materials tested gave essentially the same selectivity pattern in the oxidative dehydrogenation of n-butane. With increasing conversion the selectivity to butenes

decreased sharply and the selectivity to CO_x increased. Above 5% conversion CO_x was the major product. The initial selectivity (at zero conversion) to butenes was extrapolated to be between 80 and 100%, the initial selectivity to butadiene and CO_x between 0 and 10%, showing that butenes were the primary products, while CO_x was a secondary product (perhaps with a small primary contribution).

Lowering the reaction temperature to 675 K lead to a decrease in selectivity to dehydrogenation products (butenes and butadiene) at the expense of more total combustion. Increasing the C_4/O_2 ratio from 0.5 to 2 had no influence on the selectivity to total combustion *vs.* dehydrogenation. Also the activity did not change significantly indicating that the order of oxygen was close to zero. Only the ratio of CO to CO_2 slightly decreased with increasing O_2-content in the feed. Similar effect of temperature on hydrocarbon/oxygen ratio were also found by Chaar *et al*. in the oxidative dehydrogenation of propane over V-Mg-O catlaysts [9]. The rates of butene and butadiene formation over AlVNb at 775 K were $1*10^{-7}$ and $1.2*10^{-8}$ mol/s·g·mbar, respectively (extrapolated to zero conversion, 1 bar, feed 7% n-butane, 14% O_2).

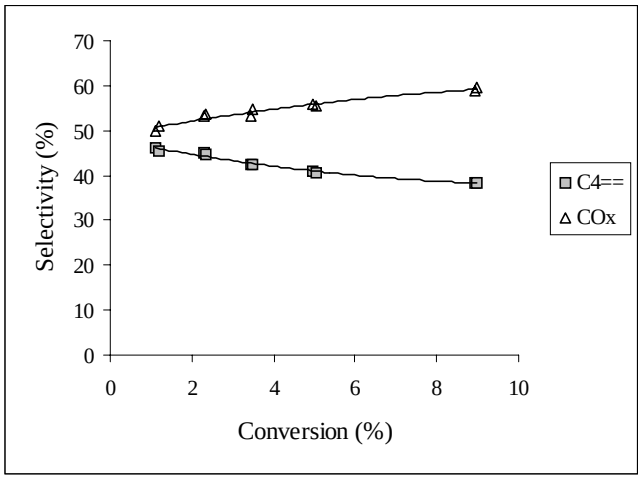

Figure 2 *Selectivity of AlVNb in the oxidative dehydrogenation of 1-butene. 675 K, 1 bar, 5% 1-butene, 10% O_2.*

Starting from 1-butene as a reactant, both butadiene and CO_x were primary products. Butadiene was a stable product in the reaction of 1-butene. Only a small fraction was transformed to CO_x at higher conversions (see Figure 2). As expected, the overall reactivity of 1-butene was much higher than that of n-butane. At 675 K, the rate of conversion was a factor of 7 higher, at 775 K a factor of about 30 (at the higher temperature a reliable rate of 1-butene conversion could not be determined).

It is interesting to note that also hydrogen was found among the products in the oxidative dehydrogenation of n-butane (even at oxygen conversions below 100%). The rate of hydrogen formation was about 25% smaller than the rate of butene plus two times the rate of

butadiene formation. That means that only a small fraction (about 25%) of the hydrogen formed by dehydrogenation was actually oxidized to water.

Oxidative dehydroisomerization over physical mixtures of supported V-Nb-O and zeolite

The AlVNb catalyst described above was used as a base case for the experiments with physical mixtures of oxidation and isomerization catalyst. With respect to the isomerization catalyst, FER, ZSM5 and MCM36 were selected. FER is known for its high selectivity for skeletal isomerization of butene [10]. ZSM5 is less selective, but very stable [11]. MCM36, on the other hand, showed a very high activity in skeletal isomerization of butene. The performance of the catalysts in butene isomerization is compared in Table 2.

Mixtures of AlVNb with each of the three zeolites were tested for the oxidative conversion of n-butane. A ratio of AlVNb/zeolite = 2/1was chosen in order to match the relative activity of the two components. CO_x and butenes were the major products of the physical mixtures. Under identical reaction conditions, they gave a higher yield of CO_x than pure AlVNb (see Table 3). The largest difference was found for AlVNb/MCM36. The yield of butene, on the other hand, was constant for AlVNb and its mixtures with ZSM5 and FER, but lower for the mixture with MCM36.

Table 2 *Skeletal isomerization of 1-butene. 775 K, 1 bar, WHSV = 75 h^{-1}, ST = 5200 sg/m^3. Feed 4.5% 1-butene 100 min time on stream.*

	Yield i-C4= (%)	k_{isom} (m^3/sg)[a]	Selectivity (%)
ZSM5	6.5	$3.4*10^{-5}$	85.4
FER	14.8	$9.2*10^{-5}$	93.1
MCM36	27.8	$2.4*10^{-4}$	84.9

[a] k_{isom} = pseudo first order rate constant of butene isomerization

The higher combustion activity of the physical mixtures could be attributed to two factors, (i) a higher retention of butene in the catalyst bed, thus, increasing the chance of total combustion by the vanadia catalyst, (ii) a combustion activity of the zeolites themselves. Control experiments showed that the latter was the case. When n-butane was converted over ZSM5, FER and MCM36 in the presence of oxygen, all three materials showed some activity for the formation of CO_x (see Table 3). The activity for combustion increased in the order ZSM5 < FER < MCM36 (note that ZSM5 which has the lowest acid site concentration also

had the lowest activity for combustion). The CO_x formation of MCM36 was even comparable with that of AlVNb.

The high activity of MCM36 also explains the low yield of butene obtained with AlVNb/MCM36. MCM36 consumed more butene by oxidation to CO_x than it additionally produced by dehydrogenating n-butane.

Table 3 *Rates of product formation in the oxidative conversion of n-butane over ZSM5, FER and MCM36. 7% n-butane, 14% O_2. 775 K, 1 bar, WHSV = 14 h^{-1}, ST = 45000 sg/m^3. 100 min on stream.*

Rate	ZSM5		FER		MCM36
(10^{-9} mol/sgmbar)	without O_2	with O_2	without O_2	with O_2	with O_2
$C_4^=$	0.5	3.9	4.6	1.4	13
$C_4^{==}$	0.3	0.3	0.0	0.5	1.3
CO_x	0.0	17	0.0	42	93
Conversion (%)	0.14	1.17	2.9	2.4	4.2

Table 4 *Ratio of isobutene to the sum of butenes after 1 and 100 min time on stream in the oxidative conversion of n-butane over AlVNb and its physical mixtures with zeolites. 7% n-butane, 14% O_2. 775 K, 1 bar, $WHSV_{zeolite}$ = 14 h^{-1}, $ST_{zeolite}$ = 45000 sg/m^3.*

	Conversion	Yield CO_x	Yield $C_4^=$	i-$C_4^=$/$\sum C_4^=$	
Time on stream	100 min	100 min	100 min	1 min	100 min
AlVNb	18.1%	12.4%	4.0%	1%	1%
AlVNb/ZSM5	29.5%	22.8%	3.9%	11%	8%
AlVNb/FER	22.5%	16.5%	3.8%	15%	2%
AlVNb/MCM36	32.0%	27.3%	2.8%	28%	4%

Table 4 shows that the physical mixtures of AlVNb and zeolites were able to produce isobutene directly from n-butane. While only 1% of the butenes formed was isomerized to isobutene over AlVNb, the initial isomer fraction (after 1 min on stream) was 28% for AlVNb/MCM36. As expected, the isomer fraction (i-$C_4^=$/$\sum C_4^=$) increased in the order ZSM5 < FER < MCM36, the order of butene isomerization activity of the three zeolites. However, in the case of AlVNb/FER and AlVNb/MCM36 a very rapid decrease of this isomerization

activity was observed (see Figure 3). Also the formation of the cracking products ethene and propene deactivated, while the formation of butadiene increased to a steady state level.

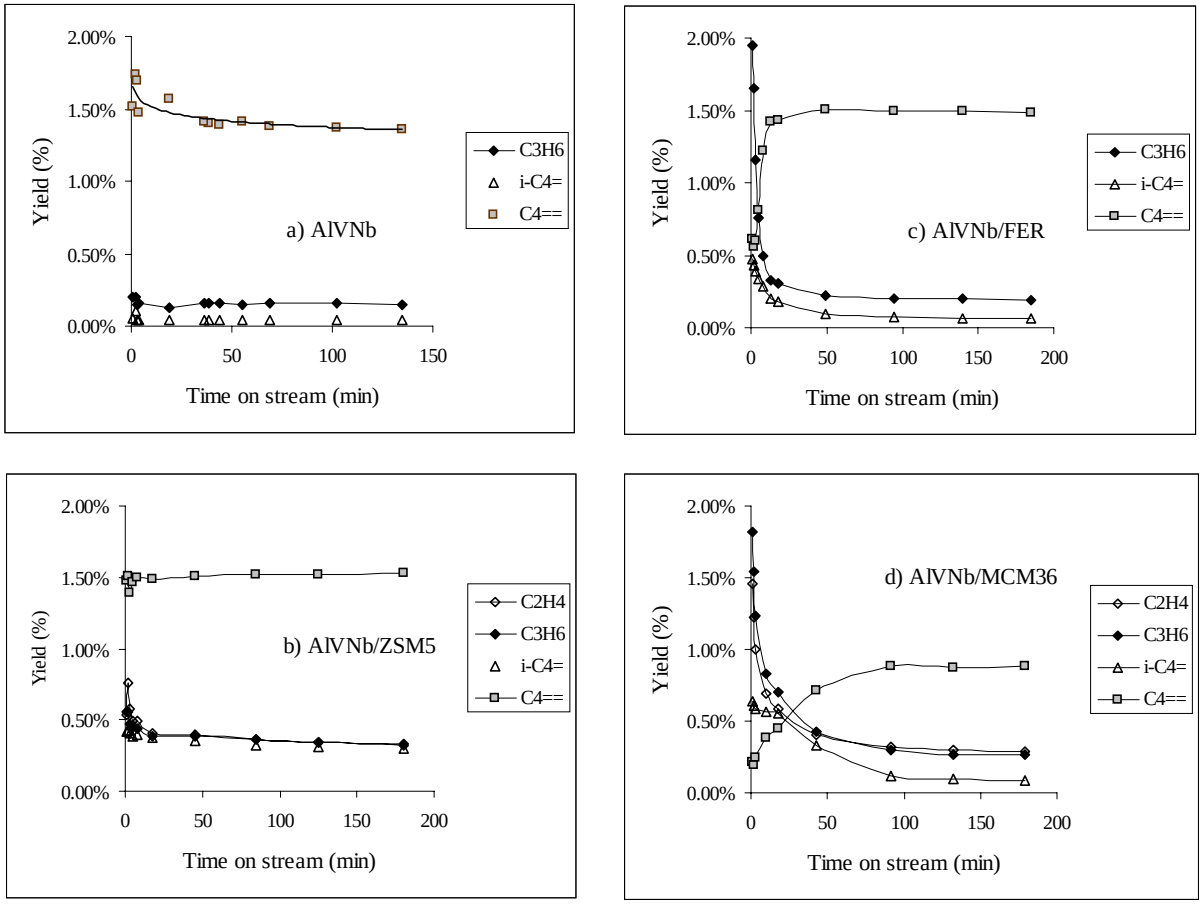

Figure 3 *Oxidative dehydrogenation of n-butane over AlVNb and physical mixtures of AlVNb and zeolite (in a ratio of 2/1). Yield of isobutene, butadiene and cracking products. 775 K, 1 bar, 7% n-butane, 14% O_2, $WHSV_{AlVNb}$ = 7h^{-1}, ST_{AlVNb} = 90000 sg/m^3.*

This gradual increase of the butadiene formation to its steady state level was not observed for pure AlVNb. Over this catalyst the formation of butadiene was fairly stable with time on stream (see Figure 3). This indicates that, in the case of the physical mixtures, butadiene formed on AlVNb was irreversibly adsorbed on the zeolites FER and MCM36, leading to gradual poisoning of the zeolite activity for isomerization and cracking. After filling or blocking the pores of FER and MCM36 a stable butadiene level was obtained, but very little isobutene was formed. AlVNb/ZSM5, on the other hand, showed only a minor initial deactivation. Subsequently, a rather stable production of isobutene was observed.

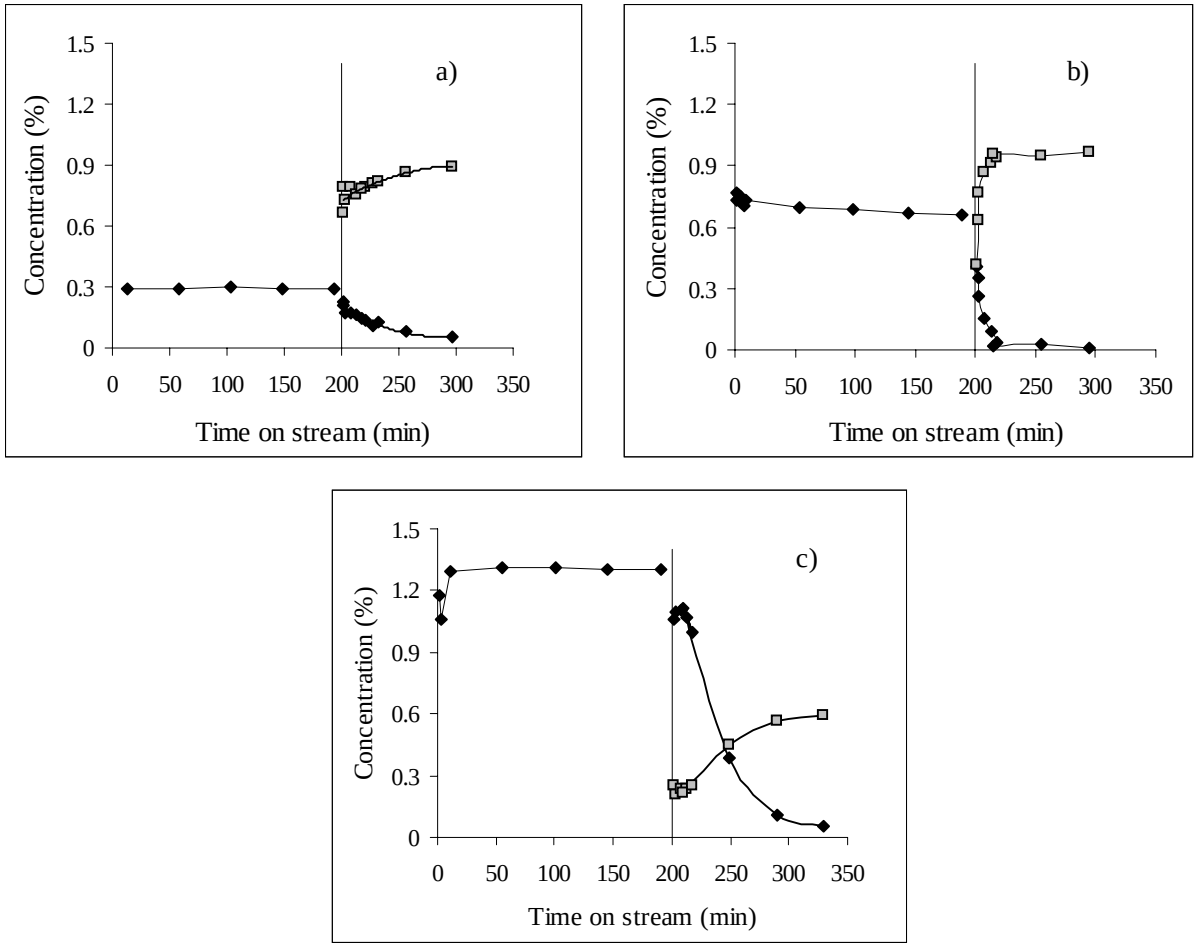

Figure 4 *Effect of butadiene on butene isomerization. (a) ZSM5, (b) FER, (c) MCM36. The beginning of butadiene addition was arbitrarily set to 200min in the Figure. In reality the catalyst was purged for 90 min in between (see experimental section). Shown are the concentrations of isobutene (diamonds) and butadiene (triangles) in the reactor effluent. 775 K, 1 bar, 4.5% 1-butene, 1% butadiene (0.65% in the case of MCM36). $WHSV_{C4=}$ = 75 h^{-1}. ST = 5200 sg/m^3.*

In order to establish that the observed decrease of isomerization activity was caused by irreversible adsorption of butadiene the influence of butadiene on the skeletal isomerization of 1-butene was studied. ZSM5, FER and MCM36 were first treated with a feed of 4.5% 1-butene in Ar for 3 h, then they were subjected to a mixture of 4.5% 1-butene and 1% butadiene in Ar. The ratio of 4.5 to 1 was chosen because it is close to the ratio of butene to butadiene obtained in the oxidative dehydrogenation experiments. Figure 3 compiles the results. For all three catalysts a deactivation of isomerization was observed under the influence of butadiene. The deactivation was almost instantaneous for FER and more gradual for ZSM5 and MCM36. The deactivation was paralleled by a build up of butadiene in the

reactor effluent. Thus, we concluded that butadiene was responsible for poisoning the zeolite in the oxidative dehydroisomerization experiments with the physical mixtures.

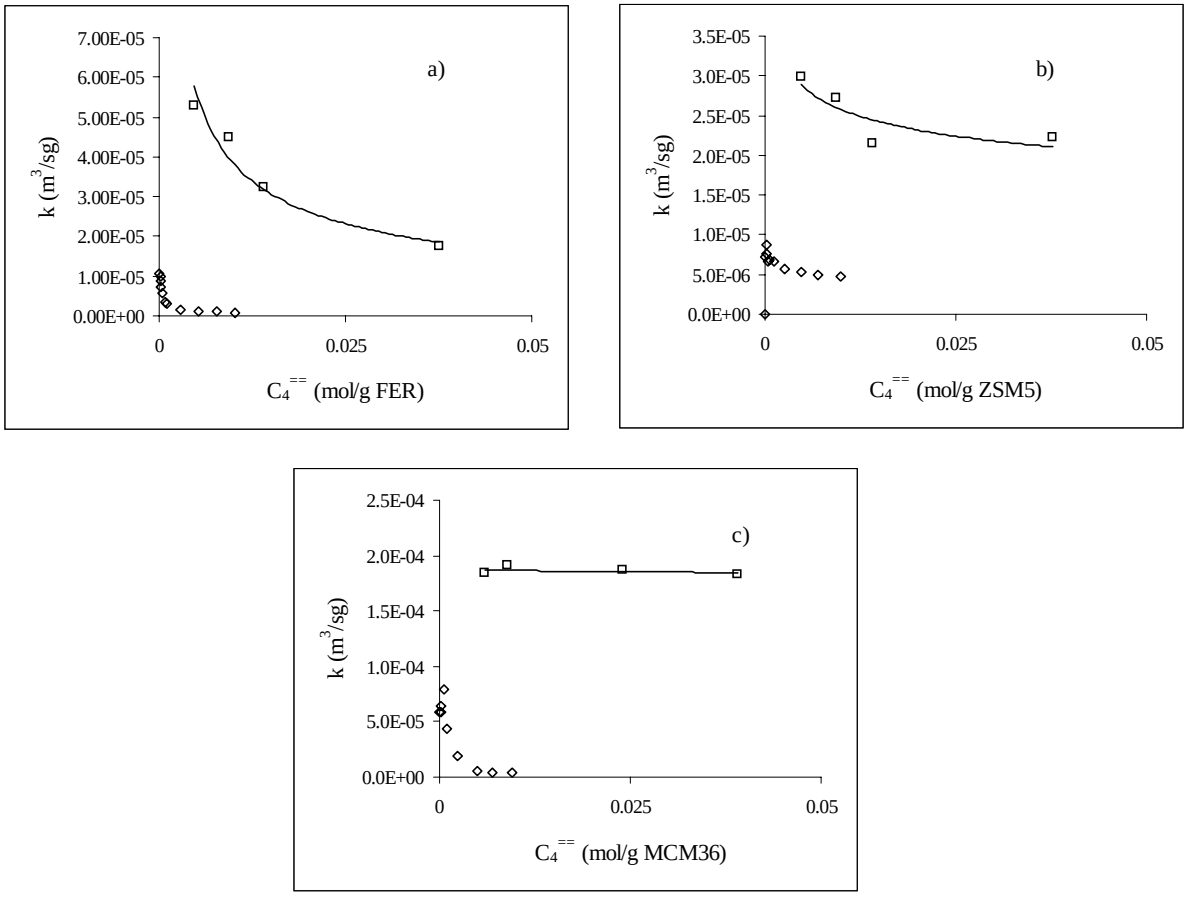

Figure 5 *(a) ZSM5 (b) FER (c) MCM36. Squares: Deactivation of isomerization under the influence of butadiene in the feed (conditions as in Figure 4). Diamonds: Deactivation of isomerization during dehydroisomerization over physical mixtures of AlVNb and zeolite (in a ratio of 2/1, conditions as in Figure 3).*

In order to make a quantitative comparison between the two types of experiments, oxidative dehydroisomerization (ODHI) and butene isomerization in the presence of butadiene, k_{isom}, the first order rate constant of butene isomerization, was calculated from the ratio of isobutene to the sum of butenes for both types of experiments (see experimental section). Furthermore, the two experiments were normalized by the cumulative amount of butadiene passing through the catalyst bed. This quantity was calculated from (i) the butadiene feed rate (in mol/sg) multiplied by the time on stream (in case of butene isomerization in the presence of butadiene), (ii) the amount of butadiene produced by pure AlVNb under the same experimental conditions (in case of ODHI with the physical mixtures). The decrease of k_{isom}

during an experiment was then plotted as a function of this cumulative amount butadiene that the zeolite encountered (see Figure 5), giving a representation of the rate of deactivation per mol of butadiene exposed.

The plots in Figure 5 reveal two effects: (i) The pseudo first order rate constant of butene isomerization in the experiments with the physical mixtures was lower indicating that the zeolite was not efficiently used. (ii) The deactivating effect of butadiene was much higher for the physical mixtures.

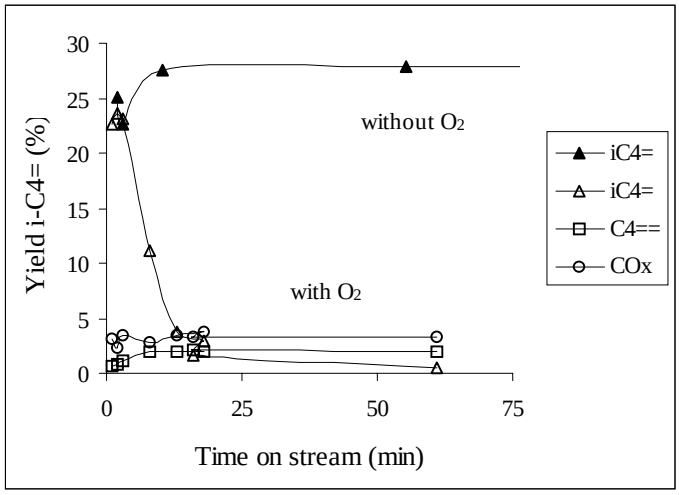

Figure 6 *Yield of isobutene, butadiene and CO_x in the (oxidative) conversion of butene over MCM36. 775 K, 1.2 bar, 4.5% 1-butene. Open symbols: 9% O_2. Full symbols: 0% O_2.*

ZSM5 was an exception. Here a gradual deactivation was observed in both types of experiments. The faster deactivation of FER and MCM36 in the physical mixtures with AlVNb was surprising. Other experiments had shown that the deactivating effect of butadiene decreased with decreasing concentration [12]. The concentration of butadiene in ODHI was, however, much lower than in the butene/butadiene co-feeding experiments. This leaves the presence of oxygen as a possible reason for the enhanced deactivation in ODHI. In order to probe this, butene was converted over MCM36 in the presence of oxygen. The results are shown in Figure 6. The yield of isobutene decreased very rapidly and small amounts of butadiene and CO_x were formed. Again, the concentration of butadiene built up with time on stream from close to zero to a steady state level. We normalized the deactivation to the cumulative amount of butadiene in the reactor effluent. The deactivation per butadiene released was much higher than the deactivation per butadiene fed in the butene/butadiene co-feeding experiments (see Figure 7).

These findings suggested that due to the oxidative dehydrogenation activity of MCM36 butadiene-like species were formed from butene in the presence of oxygen. They polymerize without leaving the catalyst surface and lead to a rapid poisoning of the catalyst, while little butadiene is detected in the gas phase.

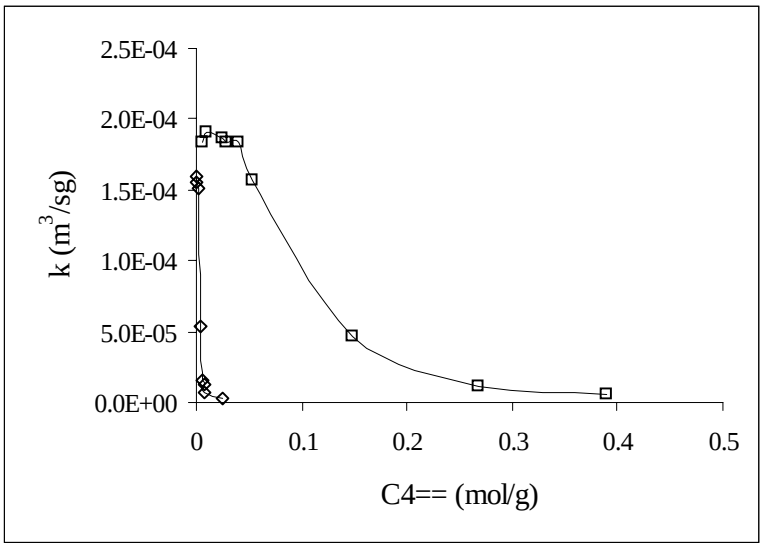

Figure 7 *Decrease of the rate constant of butene isomerization as a function of the cumulative amount of butadiene fed or formed. Squares: Butadiene was cofed. Diamonds: Butadiene was formed because oxygen was fed.*

The same was assumed to happen in the case of FER, causing the much more rapid deactivation of this catalyst in the oxidative dehydroisomerization experiments. ZSM5, on the hand, had a much lower activity for oxidation/oxidative dehydrogenation than FER and MCM36 (see Table 4). Thus, the presence of oxygen did not enhance the polymerization of butene to the same extent as FER and MCM36, leading to a fairly good stability of the catalyst also in the oxidative dehydroisomerization experiments.

Dehydroisomerization of n-butane over Pt-ZSM5

Finally, let us compare the results discussed above with those obtained in the dehydroisomerization of n-butane over Pt-ZSM5 catalyst [13], in the presence of hydrogen in the feed. Also in these experiments significant amounts of butadiene were formed over the Pt catalyst. Here, however, the rate of deactivation ($-dk_{isom}/dn_{C4==}$) was much lower than expected from the butene/butadiene co-feeding experiments. This was attributed to two factors [12]: (i) The presence of hydrogen (in combination with Pt) slows down the deactivation caused by butadiene. (ii) The deactivation rate decreases with decreasing butadiene concentration and with increasing ratio butene/butadiene. The butadiene concentration in reaction mixture of dehydroisomerization was only about 0.05%, the ratio of butene to butadiene on the order of 50, compared to a concentration of 1% and a ratio of 4.5

in the butene/butadiene co-feeding experiments.

Conclusions

The results discussed here have important implications for the feasibility of the concept of dehydroisomerization. First of all, it was shown that the oxidation catalyst used (AlVNb) had a very low efficiency in burning hydrogen. Thus, the thermodynamic limitations of dehydrogenation are not really removed. It follows that the activity of the oxidation catalyst for the conversion of hydrogen to water is an important criterion for the design of an oxidative dehydrogenation catalyst.

With respect to the combination of oxidative dehydrogenation with butene isomerization, deactivation due to butadiene was found to be the main problem. The fact that zeolites seem to transform butenes to coke in the presence of oxygen severs the problem of deactivation. Only the combination of oxidation catalyst with ZSM5 gave a fairly stable yield of isobutene. The superior stability was attributed to the low sensitivity of the ZSM5 pore system to poisoning by coke [14] and to a low activity for oxidative dehydrogenation, which avoids the above-mentioned transformation of butenes via butadiene into polymeric coke species. These two properties are general selection criteria for zeolites to be used for oxidative dehydroisomerization. While at present the yields of isobutene that could be achieved were very poor, the development of a oxidative dehydrogenation catalyst with a high selectivity to butenes and a low selectivity to butadiene in combination with a ZSM5-like material could lead to a successful application of the concept of oxidative dehydroisomerization.

At present, however, standard dehydroisomerization over Pt-ZSM5 catalyst gives by far better results [6]. The astonishing stability of butene isomerization in these system in spite of the presence of butadiene in the reaction mixture is attributed to the low ratio of butadiene to butenes in the reaction mixture (about 1:50) and to the presence of hydrogen and Pt which slow down the build-up of polymeric coke species.

Acknowledgements

I would like to thank Y.J. He for the synthesis of MCM36 and a lot of helpful information on the properties of this material. H.W. Jonk is acknowledged for his skilful assistance in the preparation and characterization of the supported vanadia catalysts.

References

[1] Smits, R.H.H., Seshan, K., Leemreize, H., Ross, J.R.H., Catal. Today **16**, 513 (1993).

[2] Deo, G., and Wachs, I.E., J. Catal. **146**, 323 (1994).

[3] Nivarthy, G.S., He, Y., Seshan, K., and Lercher, J.A., J. Catal. **176**, 192 (1998).

[4] He, Y.J., Nivarthy, G.S., Eder, F., Seshan, K., and Lercher, J.A., Micropor. Mesopor. Mat. **25**, 207 (1998).

[5] Concepcion, P., Lopez-Nieto, J.M., and Perez-Pariente, J., Stud. Surf. Sci. Catal. **94**, 681 (1995).

[6] Albonetti, S., Cavani, F., and Trifiro, F., Catal. Rev. **38**, 413 (1996).

[7] Galli, A., Lopez-Nieto, J.M., Dejoz, A., and Vazquez, M.I., Catal. Lett. **34**, 51 (1995).

[8] Watling, T.C., Deo, G., Seshan, K., Wachs, I.E., and Lercher, J.A., Catal. Today **28**, 139 (1996).

[9] Chaar, M.A., Patel, D., and Kung, H.H., J. Catal. **109**, 463 (1988).

[10] Mooiweer, H.H., de Jong, K.P., Kraushaar-Czarnetzki, B., Stork, W.H.J., and Krutzen, B.C.H., Stud. Surf. Sci. Catal. **84**, 2327 (1994).

[11] Houzvicka, J., Hansildaar, S., and Ponec, V., J. Catal. **167**, 273 (1997).

[12] Chapter 7 of this thesis.

[13] Chapter 4 and 5 of this thesis.

[14] Guisnet, M., and Magnoux, P., Appl. Catal. **54**, 1 (1989).

Chapter

4

The dehydroisomerization of n-butane over Pt-ZSM5 – Effect of metal loading and acid site concentration

Abstract

The dehydroisomerization of n-butane to isobutene over Pt ZSM5 catalysts with a high Si/Al ratio was studied. The catalytic activity increases with increasing metal loading. Butenes formed *via* dehydrogenation over the metallic particles are converted to isobutene over the Brønsted acid sites. The molar fraction of isobutene (in all butenes), which can be taken as a measure for the isomerization activity, increases in parallel with the acid site concentration, but is independent of the metal loading. The highest yields of isobutene achieved at 830 K, 1.8 bar and with a feed of 10% n-butane and 20% hydrogen were approximately 12.5%. The thermodynamic limit under these conditions is about 22%.

The inability to reach the thermodynamic limit is caused by consumption of the primarily formed n-butene by secondary side reactions. The major side reactions are oligomerization and cracking of butenes over Brønsted acid sites leading to propene and pentene. Propene that is formed *via* this route is hydrogenated to propane over Pt. Consequently, propane is the dominant byproduct at high conversions. The metal loading has only a minor influence on the selectivity of the catalyst.

Introduction

In the light of the results reported in Chapter 3 it was concluded that the concept of oxidative dehydroisomerization is at present not feasible. The low selectivity of the vanadia based ODH catalysts and the fast deactivation of the zeolites used for isomerization in the presence of oxygen (due to the formation of butadiene and its oligomers) make the route unfavorable compared to the known dehydrogenation processes. Therefore we turned our attention back to the "classical" dehydroisomerization processes, operating at high temperatures and in the presence of hydrogen.

As already mentioned in Chapter 1, two different approaches to dehydroisomerization have been used so far, a dual catalyst bed and a bifunctional catalyst. An example of a dual bed system (Pt impregnated on a silylated alumina carrier with In and Sn as promoters as a dehydrogenation catalysts, followed by a separate bed of Boralite B as an isomerization catalyst) was given by Bellussi *et al.* [1]. Excellent yields of up to 14.6% isobutene were reported, however, without any information on the stability of the catalyst. In a similar approach Nagata *et al*. [2] found good results for a combination of Cr_2O_3/Al_2O_3 with MFI-type metallosilicates with a very high Si/Me ratio of 1000. Recently, the combination of Zn/K-ZSM5 with H-ZSM22 was published [3].

With respect to the bifunctional catalysts mainly zeolite based materials have been explored, e.g., Pt-MOR [4], Ga-LTL[5], Pt-zincosilicate [6]. The highest isobutene yield (10 %) was obtained with a Pt/Re-{B}-ZSM11 catalyst [7].

We decided to choose Pt-ZSM5 with high SiO_2/Al_2O_3 ratios as our base catalyst. Pt-ZSM5 materials with low Al-contents [8, 9] and silicalites, where elements like Ge [10], In [11] and Zn [12] were incorporated in the framework, had been successfully used for the dehydrogenation of isobutane. Moreover, ZSM5 was shown to be an active, selective and stable catalyst in the skeletal isomerization of butene [13]. Last but not least, good results in dehydroisomerization had been achieved with Pt/Re-[B]-ZSM11 [7], which is a similar material as Pt-ZSM5.

It is generally assumed that with a bifunctional catalyst the dehydrogenation over the metal is the first reaction step, followed by isomerization over the Brønsted acid sites. Systematic studies on the influence of catalyst variables, such as the concentration of acidic and metallic sites, on the activity and selectivity of the catalyst have, however, not yet been performed. The aim of the present contribution is to describe the effect of these catalyst parameters on the complex network of reactions during n-butane dehydroisomerization. This should lead to

guidelines for designing the bifunctional dehydroisomerization catalyst.

Experimental

Catalyst preparation and characterization

The parent ZSM5 materials with a SiO_2/Al_2O_3 ratio of 480, 125 and 80 were supplied by ZEOLYST (sample codes CBV10002, CBV15014 and CBV8014, respectively). Pt was incorporated by ion exchange, followed by calcination at 723 K and reduction at 773 K, as described in Chapter 2. Samples with Pt loadings between 0.1 and 1.0% were prepared. The elemental composition of the samples was determined by XRF. Hydrogen chemisorption was applied to measure the metal dispersion, IR spectroscopy to measure the Brønsted acidity of the catalysts. For the IR experiments the samples were activated *in situ* in a flow of He or H_2 (for the metal exchanged samples) at 823 K for 1 h and then cooled down to 573 K, where a spectrum of the catalyst was taken. The number of Brønsted acid sites was estimated by the relative intensity of the ν(OH) band at 3610 cm^{-1}, using CBV8014 as a reference. For this sample the concentration of acid sites had been determined by gravimetry [14] to be 0.400 mmol/g. Since this number was in excellent agreement with the Al-content determined by XRF (0.405 mmol/g) it was concluded that very little extraframework aluminum was present and that all the acid sites were indeed Brønsted acid sites, making the catalyst a suited reference material.

The results of XRF, IR spectroscopy and hydrogen chemisorption are summarized in Table 1. In spite of the high temperatures used for reduction of the samples rather high metal dispersions were measured for all of the samples. In the following text the samples will be denoted "x%Pt-ZSM5(y)" where x is the Pt-loading in wt% and y is the SiO_2/Al_2O_3 ratio.

With 0.3%Pt-ZSM5 sodium ion exchange was performed to neutralize available Brønsted acid sites. For this purpose the sample was stirred at room temperature in a 0.04 M solution of $NaNO_3$ for 24 h (the volume was chosen such as to have an 20-fold excess of sodium ions compared to the number of acid sites). The suspension was filtered and washed with water. The degree of ion exchange was determined by IR spectroscopy.

Table 1 *Physico-chemical characterization of the Pt-ZSM5 samples.*

Sample	SiO_2/Al_2O_3	Al (mmol/g)	H^+ (mmol/g)[a]	% Pt	H/Pt
0.1%Pt-ZSM5(480)	480	0.070	0.021	0.09	>2.0
0.3%Pt-ZSM5(480)	480	0.068	0.023	0.27	1.2
0.5%Pt-ZSM5(480)	480	0.069	0.023	0.46	1.15
0.1%Pt-ZSM5(125)	125	0.257	n.d.	0.09	n.d.
0.3%Pt-ZSM5(125)	125	0.257	n.d.	0.29	n.d.
0.5%Pt-ZSM5(125)	125	0.259	0.194	0.48	0.66
1% Pt-ZSM5(125)	125	0.257	n.d.	0.89	0.72
0.1%Pt-ZSM5(80)	80	0.404	n.d.	0.10	n.d.
0.5%Pt-ZSM5(80)	80	0.404	0.348	0.53	1.2
1% Pt-ZSM5(80)	80	0.409	0.377	1.04	0.74

n.d. not determined

[a] determined from the intensity of the ν(OH) band at 3610cm^{-1}, using ZSM5(80) as a reference

Catalytic testing

For the catalytic tests the samples were pressed, crushed and sieved to obtain particle sizes in the range of 300 to 600 µm. 10 to 100 mg of the catalyst were mixed with about 100 mg quartz and filled into quartz tube with an inner diameter of 4 mm. The catalyst bed had a typical length of 5 to 15 mm and was supported on both sides by quartz wool.

The samples were reduced *in situ* at 830 K for 1 h in a mixture of H_2/Ar (18/82). The oven temperature was controlled via a thermocouple placed on the outside of the reactor. Two additional thermocouples were placed on top and on bottom of the catalyst bed to measure the actual temperature. The difference between these two thermocouples was not higher than 4 K. The reaction was started by switching from H_2/Ar to the feedstream, which was under standard conditions a mixture of 10% n-butane and 20% H_2, rest Ar. The total flow was between 15 and 180 ml/min. The outlet pressure of the reactor was regulated by a back-pressure regulator, usually to 1.8 bar. The pressure drop over the reactor was not higher than 0.1 bar, in most cases much less than that.

The reaction was usually followed for at least 2.5 h. In the first 10 min on stream the reactor effluent was stored in sample loops for later analysis. After 10 min, the reaction products were analyzed by on line gas chromatography (see Chapter 2 for details). Before starting the reaction the feed was analyzed *via* a bypass line. The TCD was used for the determination of the absolute concentrations of H_2 (bypass and reaction) and n-butane (bypass). It was

calibrated by means of reference gas mixtures. The FID was used to determine the relative concentrations of all hydrocarbons during the reaction. Conversion and yields were calculated on a carbon basis, using the FID areas A_i and the corresponding response factors rf_i.

$$\text{Conversion} = [\ 1 - A_{n\text{-}C4} * rf_{n\text{-}C4} / \sum (A_i * rf_i)\ ] * 100\ \% \quad (1a)$$

$$\text{Yield}_i = A_i * rf_i\ / \sum (A_i * rf_i) * 100\ \% \quad (1b)$$

Results

Characterization of Brønsted acidity

For ZSM5(125) the relative intensity of the Brønsted ν(OH) band at 3610 cm^{-1} was in good agreement with the relative Al content (using ZSM5(80) = CBV8014 as a reference, see Table 2) indicating that also here only minor concentrations of extraframework aluminum were present. The large discrepancy for ZSM5(480) may be explained by the large error of both the XRF and the IR measurement at these low Al contents

.

Table 2 *Relative Al-content and the relative intensity of the ν(OH) band at 3610 cm^{-1} for the parent ZSM5 samples*.

SiO_2/Al_2O_3	480	125	80
Al-content	0.173	0.635	1.000
ν (OH)	0.07	0.57	1.00

Table 3 *Relative intensity of the ν(OH) band at 3610cm^{-1} of the parent and the Pt-impregnated ZSM5 samples*.

SiO_2/Al_2O_3	480	125	80
Parent	1.00	1.00	1.00
0.1% Pt	0.73	n.d.	n.d.
0.3% Pt	0.81	n.d.	---
0.5% Pt	0.78	0.84	0.86
1% Pt	---	n.d.	0.93

After Pt ion exchange and reduction the number of Brønsted sites was reduced by 10-20% (see Table 3). The sodium exchanged 0.3%Pt ZSM5(480) had a relative ν(OH) intensity of

0.4, i.e. about 50% of the Brønsted acid sites had been exchanged.

Time on stream behavior in dehydroisomerization of n-butane

Figure 1 shows the conversion and the yield of the main products obtained with 0.1%Pt-ZSM5(480) at two different weight hourly space velocities (WHSV). At a WHSV of 86 h^{-1} butane was almost exclusively (96% selectivity) converted to butene and butadiene (about 0.5% yield). 18% of the butene fraction was isobutene. The catalyst deactivated with time on stream (the activity decreased by about 30% with 2.5 h).

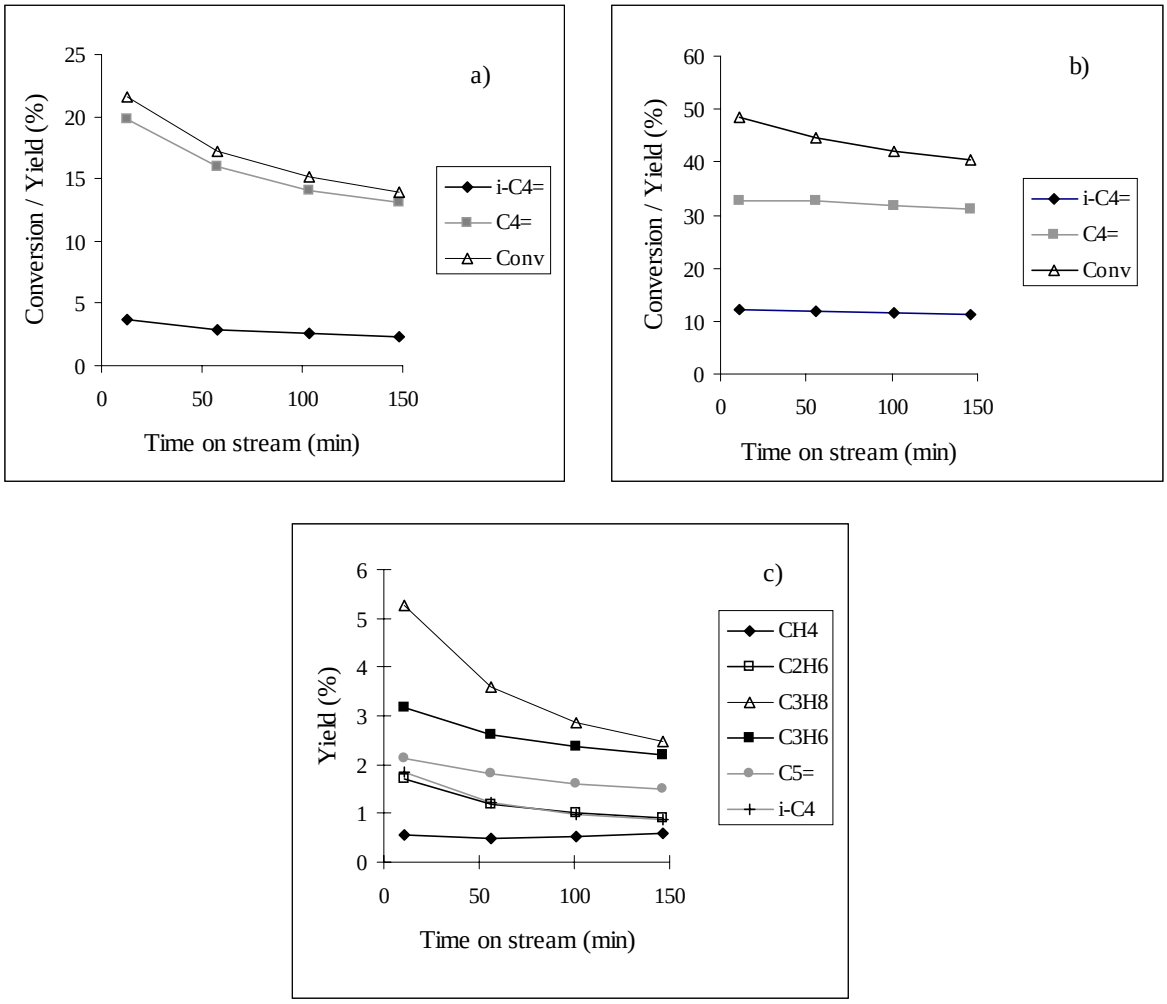

Figure 1 *Conversion and yield of the major products in the dehydroisomerization of n-butane over 0.1%Pt-ZSM5(480). 830 K, 1.8 bar, 10% n-butane, 20% H_2. (a) WHSV = 86 h^{-1}. (b), (c) WHSV = 9.9 h^{-1}.*

At WHSV = 9.5 h^{-1} the catalyst was more stable (Figure 1b). While the conversion slightly decreased with time on stream, the yield of butenes was stable at 32%. 36% of the butenes were isobutene. The selectivity to by-products, however, drastically increased. The main by-

products were propane, propene, ethane methane, pentene and isobutane (in the order of their rates of formation, see Figure 1c). At a WHSV = 86 h^{-1} the order of by-products was propene, methane, ethane and pentene, i.e., the byproduct spectrum shifted in favor of propane and ethane with decreasing WHSV. For both WHSVs, the selectivity to by-products, especially to ethane, propane and isobutane, decreased, as the catalyst deactivated.

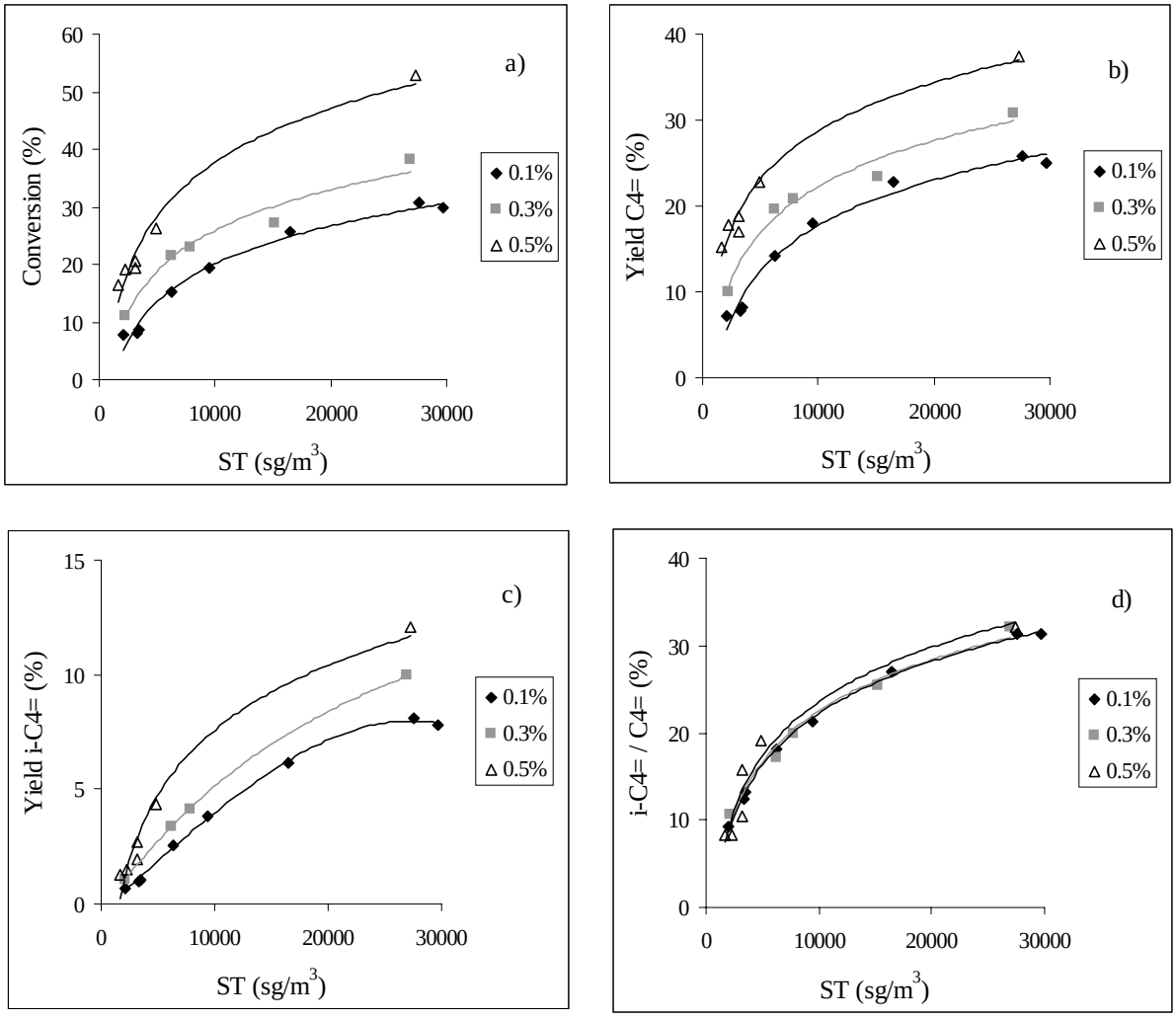

Figure 2 *Catalyst ZSM5(480) (a) Conversion of n-butane, (b) Yield of the sum of butenes ($\sum C_4^=$), (c) Yield of isobutene, (d) Ratio i-$C_4^=/\sum C_4^=$ as a function of space time (ST = $m_{cat}/(dV/dt)$) and metal loading. 830 K, 1.8 bar, 10% n-butane, 20% H_2.*

A similar time on stream behavior was found for all catalysts measured. All of them showed slow deactivation with time on stream (not taking into account the induction period in the first minutes). At high conversions mainly the by-product formation decreased with time on stream and constant yields of total butenes and of isobutene were obtained.

In order to account for the slow deactivation described above, all experiments were compared at two points, (i) at zero time on stream, (ii) after 100 min time on stream, when all catalysts were in a quasi steady state. Since the same trends were observed for both methods of analysis, only the steady state values will be discussed in the following.

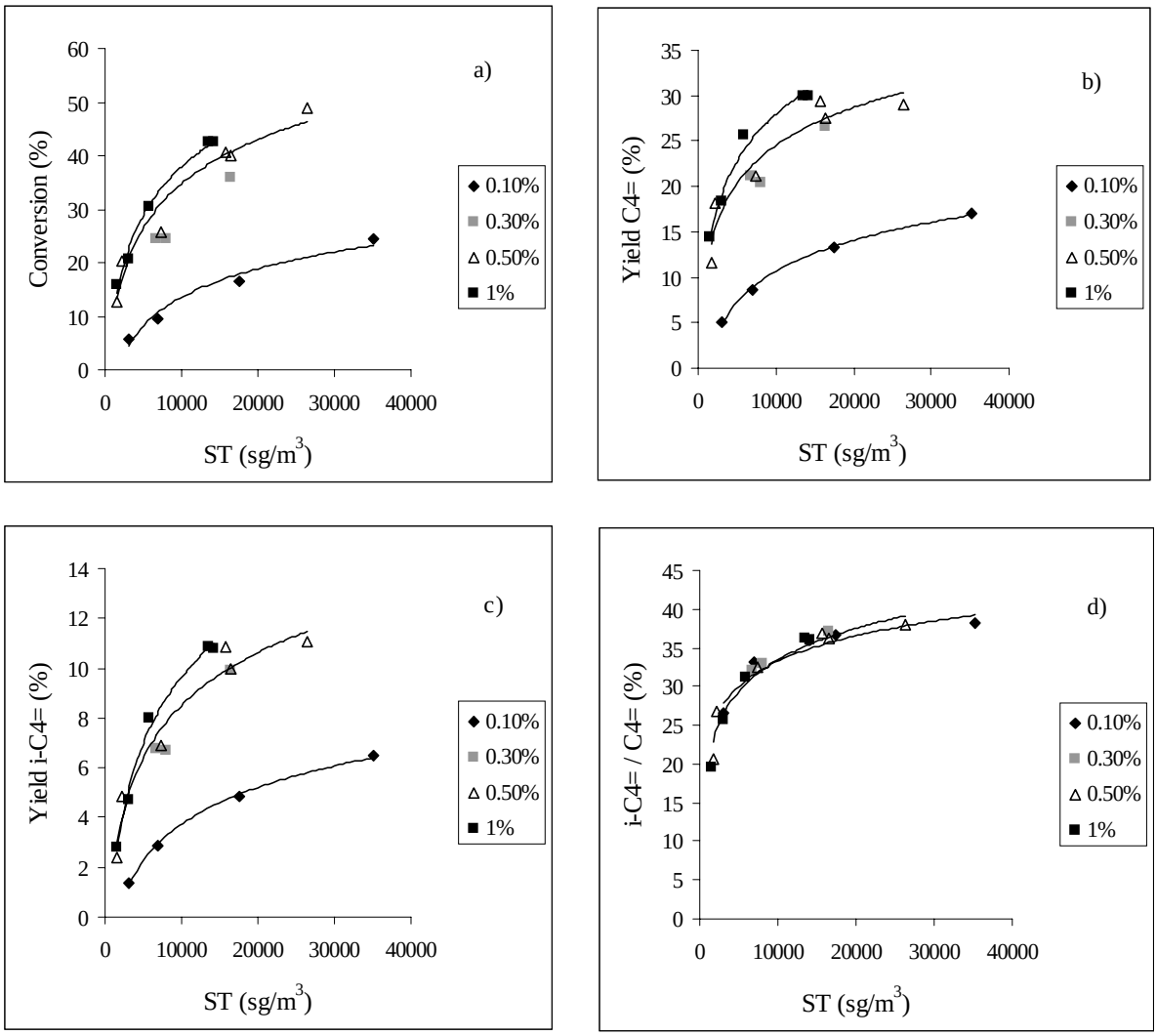

Figure 3 *Catalyst ZSM5(125) (a) Conversion, b) Yield of the sum of butenes ($\sum C_4^=$), (c) Yield of isobutene, (d) Ratio i-$C_4^=$/$\sum C_4^=$ as a function of space time (ST) and metal loading. 830 K, 1.8 bar, 10% n-butane, 20% H_2.*

Activity for dehydrogenation and isomerization

Figure 2 and Figure 3 show the influence of metal loading on n-butane conversion, butene and isobutene yields and the ratio $iC_4^=/\sum C_4^=$ ("isomer fraction") for the two catalysts ZSM5(480) and ZSM5(125), respectively. The conversion, the yield of butenes and the yield

of isobutene increased with metal loading. The small difference in activity between 0.3 and 0.5%Pt-ZSM5(125) was attributed to the rather low dispersion of 0.5%Pt-ZSM5(125). The ratio $iC_4^=/\sum C_4^=$, however, did not vary with metal loading. With increasing space-time it asymptotically approached the thermodynamic equilibrium value of 41%. Note that the material with the higher Brønsted acid site concentration, i.e., ZSM5(125) approached the 41% ratio much faster than ZSM5(480).

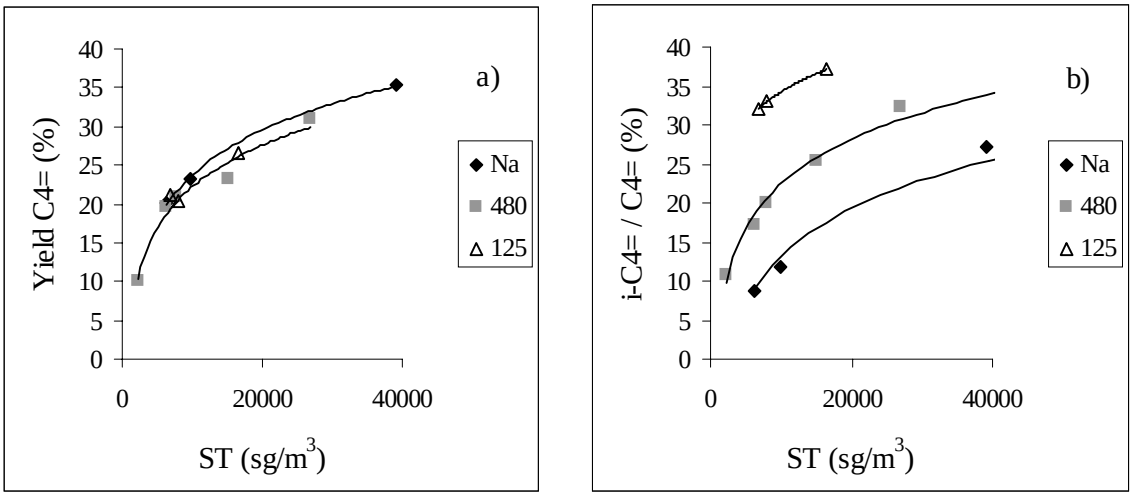

Figure 4 *0.3%Pt-ZSM5. Legend indicates SiO_2/Al_2O_3. Na stands for the Na-exchanged sample. (a) Yield of the sum of butenes ($\sum C_4^=$). (b) Ratio i-$C_4^=/\sum C_4^=$. 1.8 bar, 830 K, 100 min time on stream. Feed 10% n-butane, 20% H_2.*

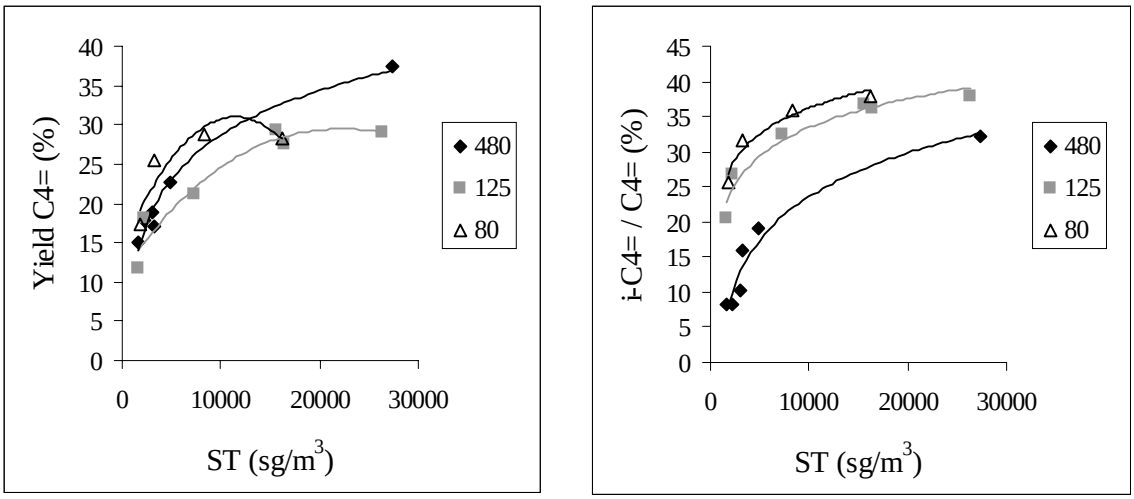

Figure 5 *0.5%Pt-ZSM5. Legend indicates SiO_2/Al_2O_3. (a) Yield of the sum of butenes ($\sum C_4^=$). (b) Ratio i-$C_4^=/\sum C_4^=$. 1.8 bar, 830 K, 100 min time on stream. Feed 10% n-butane, 20% H_2.*

Figure 4 compares the yields of the sum of butenes, i.e., the dehydrogenation activity, and the

isomer fraction for catalysts with a metal loading of 0.3% Pt, but different acid site concentrations. Figure 5 shows the same comparison for catalysts with a metal loading of 0.5% Pt. Both figures show that (at low space times) the yield of butenes did not depend on the acid site concentration. The isomer fraction, however, increased with the acid site concentration.

The effect of conversion on the selectivity

For all catalysts the yields of the sum of all butenes and of isobutene passed through a maximum as a function of conversion (see Figure 6 as an example). At higher conversions the yields decreased at the expense of an increase in by-product formation. Figure 7 gives an example of the selectivity to n-butene, isobutene and to the major by-products as function of conversion. The selectivity to n-butene extrapolated to a value between 90 and 100% at zero conversion, the selectivity to isobutene to a value between 0 and 10%. The initial selectivity to by-products was close to zero. With increasing conversion the selectivity to n-butene decreased, while the selectivity to isobutene and to the by-products increased. Finally, also the selectivity to isobutene decreased at the expense of a sharp increase in the selectivity to propane. Propane dominated the by-product spectrum at high conversions, followed by propene, ethane and isobutane (their order depended on the conversion). The ratios of ethane to ethene, propane to propene and isobutane to isobutene increased with increasing conversion.

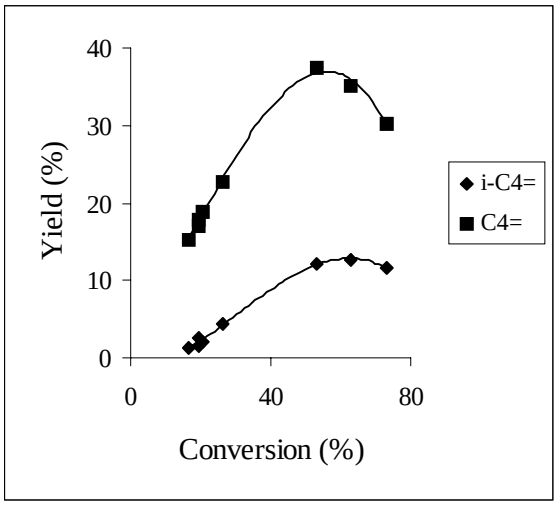

Figure 6 *0.5%Pt-ZSM5(480). Yield of isobutene and the sum of butenes ($\sum C_4^=$). 1.8 bar, 830 K, 100 min time on stream. 10% n-butane, 20% H_2.*

The selectivity was clearly seen to be primarily a function of the ratio between Brønsted acid sites and accessible metal atoms. At a constant acid site concentration, the selectivity to propene decreased and the selectivity to total butenes increased with metal loading. At a constant metal loading, the selectivity to propene increased and the selectivity to total butenes decreased with increasing acid site concentration (see Figure 8). Other variations were too subtle to be described in detail here.

Table 4 *Rates of byproduct formation and rate of dehydrogenation in conversion of n-butane over (Pt)-ZSM5. 830 K, 1.8 bar, 10 % n-butane, 20 % hydrogen, 100 min on stream.*

Rate of formation (10^{-6} mol/s.g)	ZSM5 (480)	0.1% Pt-ZSM5(480)[a]	ZSM5(80)	0.1% Pt-ZSM5(80)[a]
CH_4	0.25	0.9	1.3	2.3
C_2H_6	0.17	0.8	1.2	4.0
C_2H_4	0.19	0.2	1.2	1.3
C_3H_8	0.00	0.4	0.14	4.0
C_3H_6	0.24	1.0	1.2	10
C_4=	0.26	80	1.0	125

[a] extrapolated to zero conversion

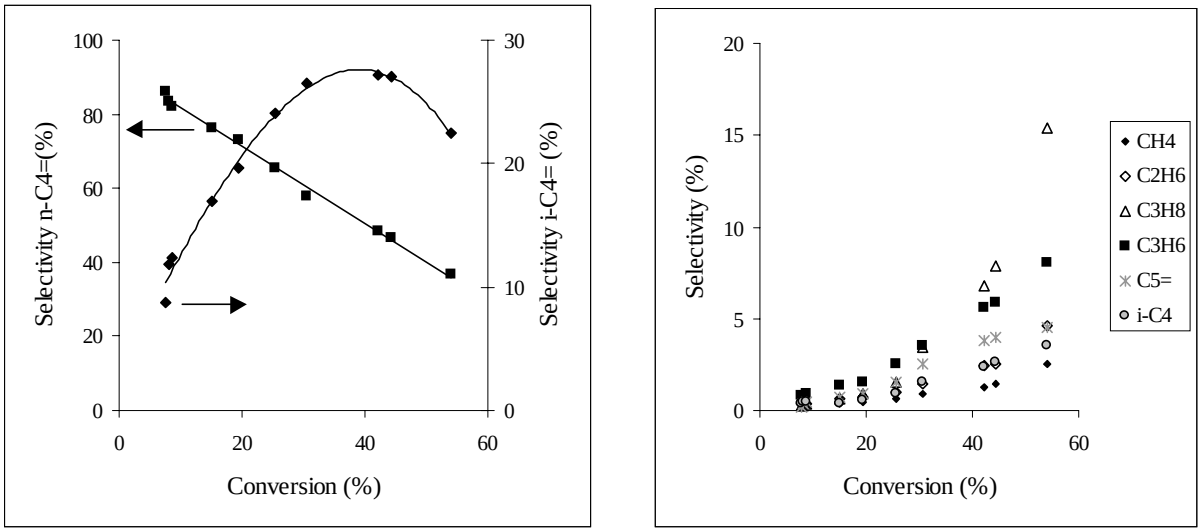

Figure 7 *0.1%Pt-ZSM5(480). Selectivity to the major (by-)products. 1.8 bar, 830 K, 100 min time on stream. 10 % n-butane, 20 % H_2.*

Butane conversion over the parent ZSM5

In order to evaluate the influence the zeolite upon the primary conversion of n-butane the catalytic activity and selectivity of the ZSM5 samples were studied. At WHSV = 10 and 20, under conditions identical to the testing of the bifunctional catalysts, ZSM5(480) gave conversions of only 1.35% and 0.75%, respectively. 0.1%Pt-ZSM5(480) gave conversions of 42% and 31% under the same conditions. The main products of ZSM5(480) were methane, ethane, ethene and propene resulting from (protolytic) cracking of butane according to equations (2) and (3), and butene, formed by acid catalyzed dehydrogenation (4) [15]. Table

4 compares the rates of by-product formation in the absence/presence of Pt for two different SiO_2/Al_2O_3 ratios. Generally, the rate was higher for the metal impregnated samples, even at the lowest metal loading. The difference was largest for propane, ethane and propene and smallest for ethene and methane.

$$n\text{-}C_4H_{10} \rightarrow CH_4 + C_3H_6 \qquad (2)$$

$$n\text{-}C_4H_{10} \rightarrow C_2H_6 + C_2H_4 \qquad (3)$$

$$n\text{-}C_4H_{10} \rightarrow C_4H_8 + H_2 \qquad (4)$$

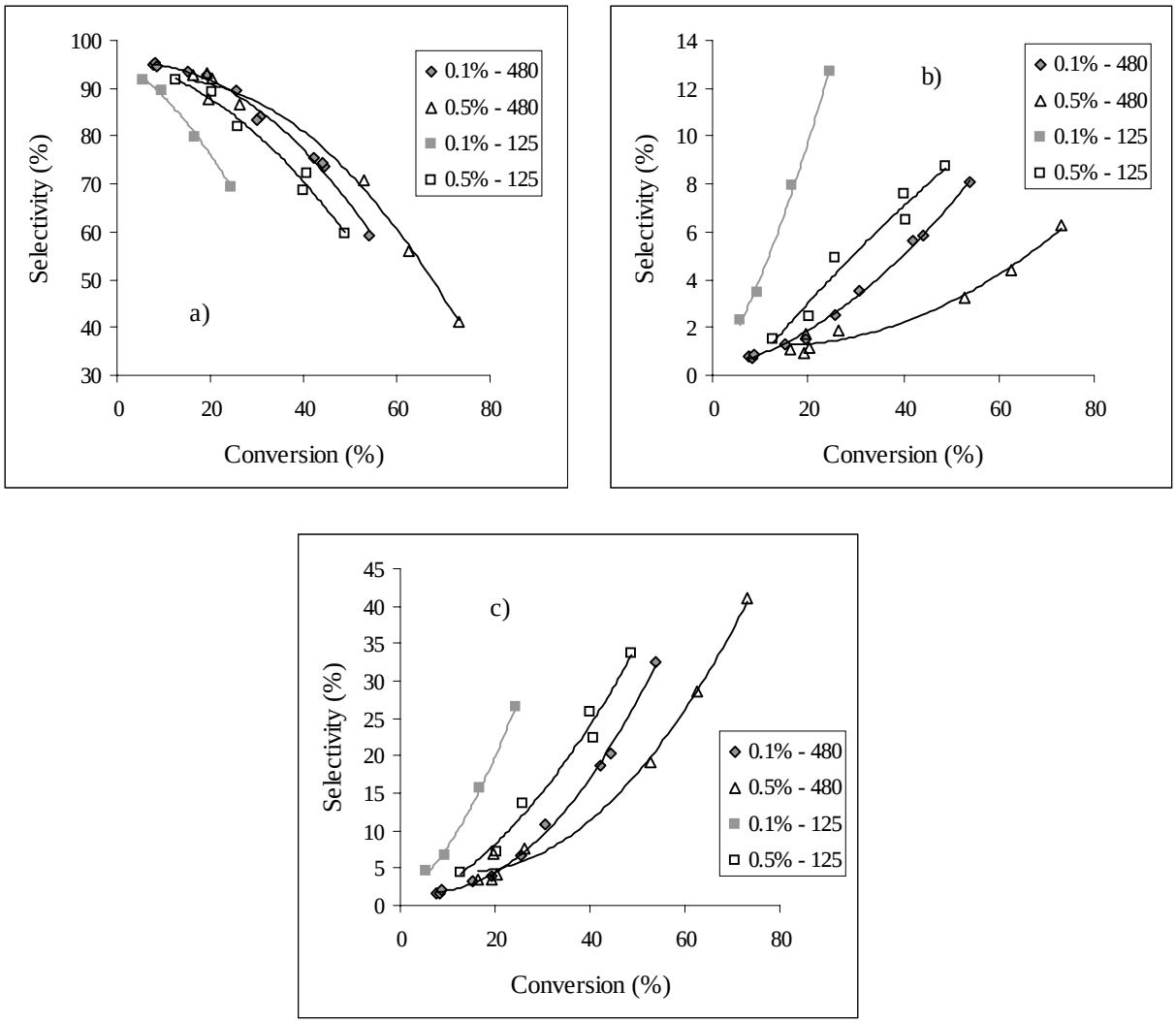

Figure 8 *(a) Selectivity to the sum of butenes ($\sum C_4^=$). (b) Selectivity to propene. (c) Selectivity to the sum of ethane, propane, propene and pentene. 830 K, 1.8 bar, 10% n-butane, 20% H_2, 100 min time on stream.*

Discussion

The bifunctional reaction mechanism

As outlined in the introduction, the formation of isobutene from n-butane over Pt ZSM5 is expected to proceed *via* the classical bifunctional mechanism [16]. The experimental observations fully support this. At short contact times the total conversion and the yield of butene increased with metal loading, but were constant for samples which only differed by the amount of acid sites (Figure 2 to Figure 5) suggesting that both depend only on the metal loading. In accordance with such a model a Pt-free ZSM5 showed hardly any conversion of n-butane. Thus, dehydrogenation of butane to butene is the primary reaction step and proceeds over Pt.

As the selectivity to isobutene extrapolated to a value close to 0% at zero conversion (Figure 7), it is concluded to be a secondary product. The ratio of isobutene to the sum of all butenes (isomer fraction) did not depend on the metal loading, but on the concentration of acid sites (Figure 2 to 5) indicating that the skeletal isomerization takes place over Brønsted acid sites.

The thermodynamics of butane dehydroisomerization

The dehydroisomerization of n-butane involves two equilibrium reactions, i.e., the dehydrogenation of n-butane and the skeletal isomerization of butene.

	$\triangle H_{830K}$	$\triangle G_{830K}$	K	
$n\text{-}C_4H_{10} \rightleftharpoons 1\text{-}C_4H_8 + H_2$	131 kJ/mol	17.4 kJ/mol	0.08	(5)
$1\text{-}C_4H_8 \rightleftharpoons i\text{-}C_4H_8$	-16.1 kJ/mol	-7.4 kJ/mol	2.93	(6)

If residence time of isobutene in the reactor is high enough it can, of course, be rehydrogenated to isobutane. In that case also equilibrium (7) has to be considered.

	$\triangle H_{830K}$	$\triangle G_{830K}$	K	
$i\text{-}C_4H_8 + H_2 \rightleftharpoons i\text{-}C_4H_{10}$	-123 kJ/mol	-5.5 kJ/mol	2.21	(7)

Equations (5) and (6) show that dehydroisomerization is a combination of an endothermic reaction (dehydrogenation) which is favored at high temperatures and a slightly exothermic reaction (butene isomerization) which is favored at low temperatures. Both equilibria limit the possible yield of isobutene. Figure 9 shows the equilibrium concentration of the sum of linear butenes, isobutene and butadiene as a function of temperature. If the other parameters

(pressure and hydrogen to hydrocarbon ratio) are fixed to the values used in the present study, the maximum yield of isobutene is potentially achieved at 900 K. However, at this temperature also large amounts of butadiene are possible to form, which is known to rapidly deactivate acid catalysts. Therefore 830 K was chosen as a reaction temperature. At 830 K reasonable yields of isobutene can be achieved (22%), while the yield of butadiene is limited to less than 2% by thermodynamics.

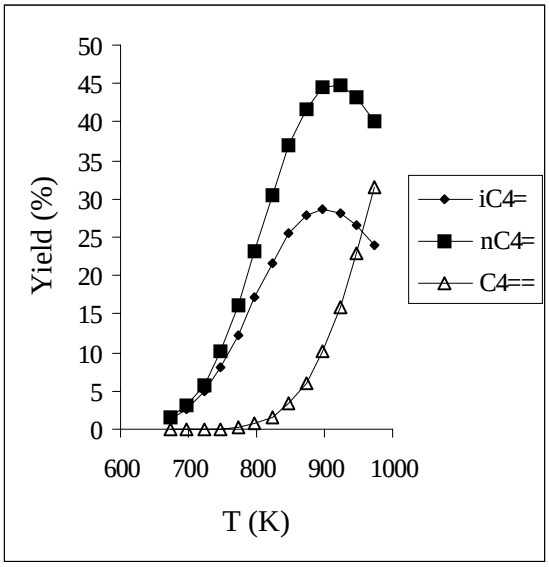

Figure 9 *Dehydrogenation equilibrium as a function of temperature. Pressure set to 1.8 bar. Feed composition 10% n-butane, 20% H_2, 70% N_2. Calculated using HSC Chemistry Version 2.03. Copyright Outokompu Research Oy, Pori, Finland, A. Roine.*

Let us now turn our attention to how the thermodynamic constraints influence the product distribution observed. A direct comparison between thermodynamic calculations and experimental observations has to be done very cautiously, since side reactions are not considered in the calculations. Moreover, the hydrogenation/dehydrogenation equilibria depend on the concentrations of hydrogen and butane/butene, which change in course of the reaction. A comparison between thermodynamic calculations and experimental results is feasible, however, if only the C_4 fraction of the reactor effluent is considered (i.e., the byproduct formation is neglected) and if the hydrogen partial pressure is assumed to be constant at 0.36 bar (the feed value). This is a realistic approximation as the partial pressure of hydrogen additionally produced in the reaction network is marginal compared to the total hydrogen partial pressure. If the hydrogen partial pressure is constant the equilibrium mol fractions are independent of the hydrocarbon concentration.

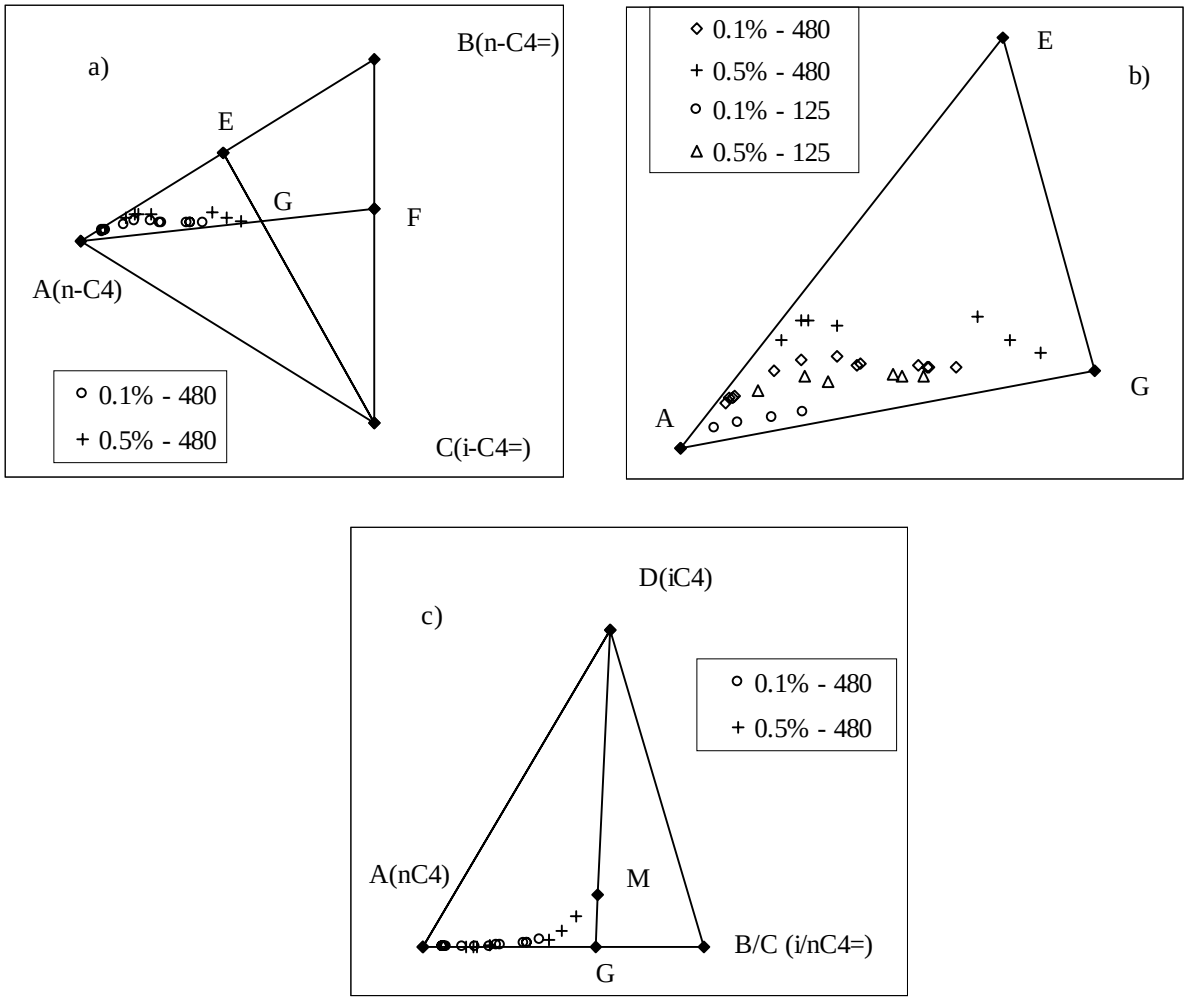

Figure 10 *The n-butane/n-butene/isobutene/isobutane equilibrium tetrahedron. a) Projection of the base triangle. b) Enlargement of the triangle AEG. c) Projection vertical to the base triangle. A ... n-butane, B ... n-butene, C ... isobutene, D ... isobutane, E ... equilibrium between n-butane and n-butene, F... equilibrium between n-butene and isobutene, G... equilibrium between n-butane, n-butene, isobutene, M... equilibrium between all four compounds*

For visualization of how the system approaches the thermodynamic equilibrium between n-butane, n-butene, isobutane and isobutene a tetrahedron can be used (see Figure 10). Every corner of the tetrahedron represents one of the compounds n-C4 (*A*), n-C4= (*B*), i-C4= (*C*) and iC4 (*D*). Every mixture of the four compounds is represented by a point in the tetrahedron. The coordinates of a point *X* with the mol fractions x_A, x_B, x_C and x_D ($\sum x_i = 1$) can be determined from $1 - x_D = (\delta * \mu) / (\mu * \mu)$, where δ is the vector from point *X* to the corner *D* and μ is the normal vector from *D* to the opposite plane of the tetrahedron. The three equations for the three independent mol fractions determine the coordinates of point *X*.

Points E and F on the corresponding edges of the tetrahedron represent the thermodynamic equilibria between n-butane and n-butene and n-butene and isobutene. Assuming that the system first reaches dehydrogenation equilibrium and only then the formation of isobutene starts, the system will follow the line *AEG*. *G* represents the equilibrium between n-butane, n-butene and isobutene.

The reaction data (after 100 min time on stream) illustrated in the graph using the mol fractions of n-butane, n-butene, isobutene and isobutane after normalization to 1 ($\sum x_i = 1$). A series of data points at increasing conversions shows how the system approaches equilibrium for four selected catalysts (see Figure 10). All the data points lie in the corner of the n-butane/n-butene/isobutene equilibrium, which is further evidence that the reaction proceeds *via* dehydrogenation and subsequent isomerization. The enlargement of the triangle *AEG* allows monitoring how the metal loading and acid site concentration affect the pathway of the reaction mixture to thermodynamic equilibrium.

Over 0.5%Pt-ZSM5(480) the reaction mixture first went into the direction of point *E*, the equilibrium point between n-butane and n-butene, before it bent into the direction of *G*. The other extreme behavior was observed with 0.1%Pt-ZSM5(125). The points followed very closely the line AF where butene isomerization is in equilibrium. That means, that over 0.1%Pt-ZSM5(125) butene isomerization was close to equilibrium from the start of the reaction. The higher the ratio of metal to acid sites, the more pronounced was the tendency to reach first the dehydrogenation equilibrium before skeletal isomerization starts. In turn one can state that the higher the concentration of acid sites is, the closer the curves follow first the line of butene isomerization equilibrium. At high conversions the reaction mixture was quite close to the overall equilibrium point *M*, including isobutane. The highest conversion shown here was 73% for 0.5%Pt-ZSM5(480).

Byproduct formation

As side reactions consume a significant fraction of the butenes, it is mandatory to be able to describe and understand these reactions, if the catalyst should be improved. Conceptually, three routes of byproduct formation are conceivable. Their impact will be discussed in the following.

Cracking of butane over Brønsted acid sites

Protolytic cracking of butane over acid sites leads to the formation of methane and propene

and ethane and ethene, respectively [17]. Ethane and propene were formed much faster in the presence of a metal (see Table 4). Thus, we conclude that these products do not originate from cracking of n-butane over the acid sites. The rates of methane and ethene formation, however, were similar in the presence and absence of Pt indicating that they are at least partly formed by acid catalyzed cracking. As even at high conversions methane and ethene are only minor by-products (see Figure 7) it is concluded that the contribution of n-butane cracking to the overall by-product formation is only minor. It increases, however, with decreasing SiO_2/Al_2O_3 ratio.

Hydrogenolysis/isomerization over the metal

In dehydrogenation reactions over non-acidic, supported metal catalysts hydrogenolysis and isomerization are the main side reactions [18] of dehydrogenation. Hydrogenolysis leads to the formation of methane, ethane and propane, metal catalyzed isomerization to the formation of isobutane [19 - 22]. Also here, hydrogenolysis is a primary reaction pathway, which competes with dehydrogenation over the metal. However, the selectivities to possible hydrogenolysis products and to isobutane were very low at zero conversion, less than 1% for 0.1%Pt-ZSM5(480) while the selectivity to butenes was around 95%. 0.5%Pt-ZSM5(480) had a higher initial selectivity to methane, ethane and propane, but still less than 2 % each. This indicates that also hydrogenolysis of butane (like butane cracking) does not significantly contribute to the byproduct formation. The higher rate of methane formation in the presence of Pt (see Table 4), however, indicates that some hydrogenolysis takes place. Its contribution to the by-product spectrum may increase at high conversions, since the competing dehydrogenation reaction is gradually slowed down as it approaches equilibrium [18].

Secondary reactions of butenes

The very low initial selectivity to by-products and the sharp increase at high conversions (Figure 7) indicates that most by-products originate from secondary reactions, i.e., reactions of the butenes formed by dehydrogenation over Pt. Butenes are significantly more reactive than butane. The reaction of butene on acidic zeolites has been extensively studied [23 - 32] and reviewed [33, 34]. The main side reaction competing with skeletal isomerization is di- and oligomerization of the butenes followed by cracking. The main products resulting are propene and pentene, to a smaller extent also ethene and hexene and higher hydrocarbons (see, for example ref. [34]).

Indeed, propene and pentenes were always found as by-products of dehydroisomerization

here. The molar ratio of $C_3^=/C_5^=$ was much higher than one indicating that most of the propene is formed by cracking of larger oligomers than C_8-dimers [20, 35] and/or that pentene cracks further to propene and ethene. The selectivity to propene increased with conversion, as expected for a secondary product. However, at high conversions more propane was formed than propene (see Figure 7). This is tentatively explained by the fact that propene is hydrogenated to propane in the presence of Pt. The thermodynamic equilibrium ratio of propane to propene at reaction conditions was calculated to be around 3. The experimentally observed ratio approached this value with increasing conversion. Thus, we conclude that propane is mainly formed by hydrogenation of propene over Pt.

Similarly, we suggest that isobutane is formed by hydrogenation of isobutene [35] and not by direct isomerization of n-butane over the acid and/or the metal sites and that ethane is formed by hydrogenation of ethene rather than by hydrogenolysis of butane. However, low concentrations of pentanes and hexanes were found in the products. This is due to thermodynamics. The lower the carbon number, the more favorable it is to hydrogenate the alkene in line with the decreasing alkane/alkene ratio in the order $C_2 > C_3 > C_4 > C_5$.

The formation of ethane, propane and isobutane by hydrogenation of the corresponding alkenes was confirmed by the similarity of the by-product pattern when 1-butene was converted over Pt-ZSM5 in the presence of hydrogen [36].

Influence of metal loading and acid site concentration on the selectivity pattern

Up to now dimerization/cracking of butenes over the acid site has been identified as the major route of by-product formation. Moreover, propane and ethane were identified as products of the dimerization/cracking route. Thus, the selectivities to these four products were lumped into a selectivity to secondary cracking, shown in Figure 8c. The Figure shows that the trend in the selectivity pattern follows closely the trend in the ratio between accessible Pt surface atoms and acid sites (see Table 5). The selectivity to secondary cracking decreases in parallel with an increasing ratio of metal to acid sites, the selectivity to dehydrogenation increased.

Catalysts with a high Brønsted acid site concentration approach the isomerization equilibrium quite fast. The marked increase in the selectivity to dimerization/cracking under such conditions (see Figure 11) is explained by the fact that the net rate of further isomerization approaches zero, while the side reactions proceed unlimited. The lower the ratio of metal to acid sites, the lower is the yield of dehydrogenated products at the point when butene isomerization approaches equilibrium (line *AG* in Figure 10), which in turn leads to a drastic

increase in the selectivity to secondary cracking, as shown in Figure 11. Thus, it is concluded that a high ratio of metal to acid sites is beneficial for the selectivity of the catalyst. Note that also the highest yield of isobutene was achieved with 0.5%Pt-ZSM5(480), the catalyst with the highest ratio of metal to acid sites.

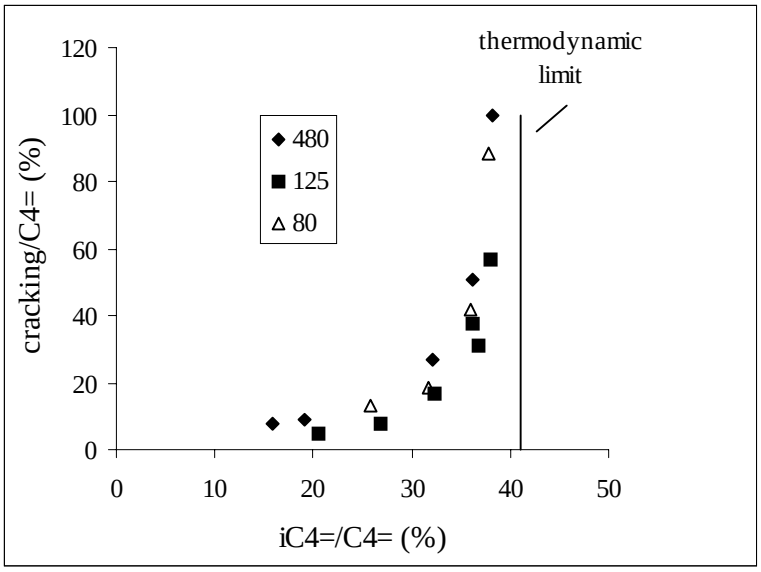

Figure 11 *Ratio of the products of secondary cracking to* $\sum C_4^=$ *vs. the ratio i-*$C_4^=$*/* $\sum C_4^=$*. 0.5%Pt-ZSM5. The legend indicates* SiO_2/Al_2O_3*. 1.8 bar, 830 K, 10% n-butane, 20% hydrogen, 100 min time on stream.*

It should, however, be emphasized that the correlation between the Pt/H^+ ratio and the selectivity is only qualitative. For example, 0.5%Pt-ZSM5(125) had almost the same ratio of Pt/H^+ as 0.1%Pt-ZSM5(480), but still a lower selectivity to dehydrogenation. This is due to the contribution of other side reactions, i.e., hydrogenolysis and protolytic cracking of n-butane. 0.5%Pt-ZSM5(125) has a higher metal loading and a higher acid site concentration than 0.1%Pt-ZSM5(480) leading to a higher contribution of these two reactions and, thus, a lower selectivity.

In addition to these observations we would like to note that the initial values (at zero time on stream) of the selectivity to by-products was higher, but otherwise the same trends were observed as for the steady state values.

Conclusions

The dehydroisomerization of butane proceeds *via* a bifunctional mechanism. n-Butane is dehydrogenated over the metal and is then isomerized over the Brønsted acid sites of the zeolite. The catalytic activity is governed by the metal loading. The concentration of acid sites on the other hand determines how much of the primarily formed n-butene is converted

to isobutene.

The main route of byproduct formation is oligomerization/cracking of the primarily formed butenes. Cracking of the oligomers mainly leads to propene, which in the presence of Pt is hydrogenated to propane (main byproduct at high conversion, see Figure 12). The overall selectivity of the catalyst is governed by the ratio of metal to acid sites. The higher the ratio, the higher is the selectivity to dehydrogenation and the lower the selectivity to secondary cracking. Thus, a high ratio of metal to acid sites is important for successful catalysts.

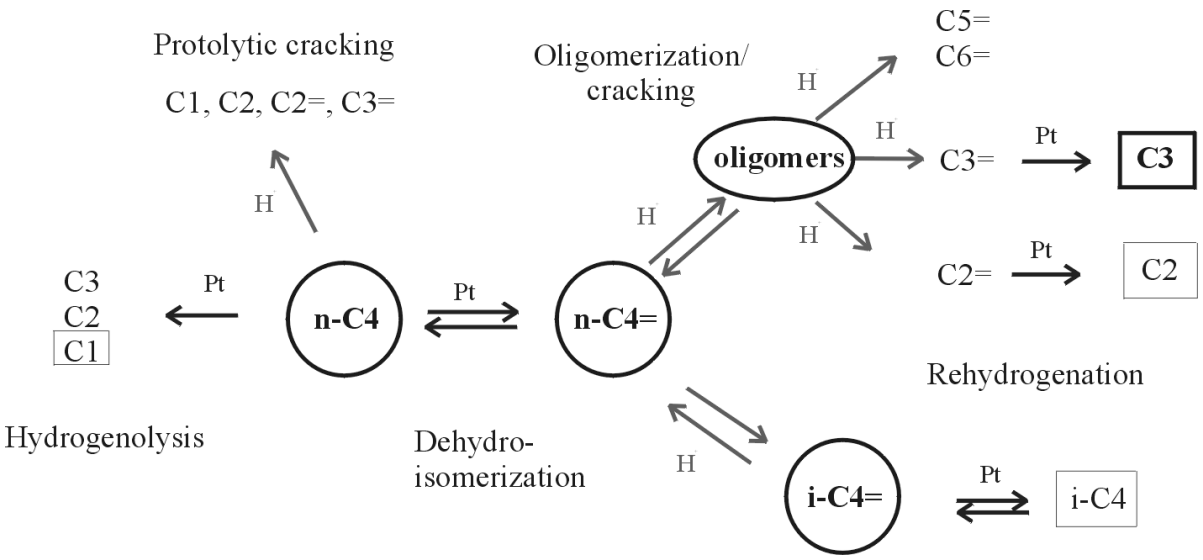

Figure 12 *Scheme of the reaction network of dehydroisomerization of n-butane*

References

[1] Bellussi, G., Giusti, A., and Zanibelli., L., US Patent 5.336.830 (1994), assigned to Eniricerche S.p.A., Snamprogetti S.p.A.

[2] Nagata, H., Iguchi, T., Takiyama, Y., Kishida, M., and Wakabayashi, K., Book of Abstracts 11th Int. Zeolite Conference, Seoul, 1995, p. RP120.

[3] Byggningsbacka, R., Kumar, N., and Lindfors, L.-E., Catalysis Letters **55**, 173 (1998).

[4] de Agudelo, M.M., Romero, T., Guaregua, J., and Gonzalez, M., US Patent 5.416.052 (1995), assigned to Intevep, S.A.

[5] Kolombos, A.J., Telford, C.D., and Young, D., European Patent 42.252 (1981), assigned to The British Petroleum Company Limited.

[6] Shum, V.K., US Patent 4.962.266 (1990), assigned to Amoco Corporation.

[7] O'Young, Ch.-L., Browne, J.E., Matteo, J.F., Sawicki, R.A., and Hazen, J., US Patent 5.198.597

(1993), assigned to Texaco Inc.

[8] Dessau, R.M., US Patent 5.122.489 (1992), assigned to Mobil Oil Co.

[9] Kaminsky, M.P., Froment, G.F., and DeHertog, M.P., World Patent 96/01239 (1996), assigned to Amoco Corp.

[10] Meriaudeau, P., Nascimento, P., Sapaly, G., and Naccache, C., European Patent 858.834 (1998), assigned to Total Raffinage Distribution, S.A.

[11] Indo French Center for the Promotion of Advanced Research, French Patent 2.724.926 (1996).

[12] Barri, S.A.I, and Tahir, R., US Patent 5.208.201, assigned to the British Petroluem Company.

[13] Houzvicka, J., Klik, R., Kubelkova, L., and Ponec, V., Appl. Catal. A **150**, 101 (1997).

[14] Eder, F., PhD Thesis, University of Twente, Enschede, The Netherlands, 1996.

[15] Narbeshuber, T.G., Vinek, H. and Lercher, J.A., J. Catal. 157, 388 (1995).

[16] Weisz, P.B., Adv. Catal. **13**, 137 (1962).

[17] Haag, W.O. and Dessau, R.M., Proceedings 8th International Congress on Catalysis, Vol. II, p. 305. Dechema, Frankfurt am Main, Berlin, 1984.

[18] Corthright, R.D., and Dumesic, J.A., J. Catal. **148**, 771 (1994).

[19] Bond, G.C., and Gelsthorpe, M.R., J. Chem. Soc. Farad. Trans. II **85**, 3767 (1989).

[20] Bond, G.C., and Yide, Xu, J.Chem.Soc. Farad.Trans. I, **80**, 969-980 (1984).

[21] Kempling, J.Ch., and Anderson, R.B., Ind. Eng. Chem. Proc. Res. Devel. **11**, 146 (1972).

[22] Sinfelt, J.H., Adv. Catal. **23**, 91 (1973).

[23] Guisnet, M., Andy, P., Gnep, N.S., Benazzi, E., and Travers, C., J. Catal. **158**, 551 (1996).

[24] Mériaudeau, P., Tuan, V.A., Le, N.H., and Szabo, G., J. Catal. **169**, 397 (1997).

[25] Houzvicka, J., Hansildaar, S., and Ponec, V., J. Catal. **167**, 273 (1997).

[26] Xu, W.-Q., Yin, Y.-G., Suib, L., Edwards, J.C., and O'Young, Ch.-L., J. Phys.Chem. **99**, 9443 (1995).

[27] O'Young, Ch.-L., Pellet, R.J., Casey, D.G., Ugolini, J.R., and Sawicki, R.A., J. Catal. **151**, 467 (1995).

[28] Xu, W.-Q., Yin, Y.-G., Suib, St.L., and O'Young, Ch.-L., J. Catal. **150**, 34 (1994).

[29] Simon, M.W., Suib, St.L., and O'Young, Ch.-L., J. Catal. **147**, 484 (1994).

[30] Byggningsbacka, R., Lindfors, L.E., and Kumar, N., Ind. Eng. Chem. Res. **36**, 2990 (1997).

[31] Mooiweer, H.H., de Jong, K.P., Kraushaar-Czarnetzki, B., Stork, W.H.J., and Krutzen, B.C.H., Stud. Surf. Sci. Catal. **84**, 2327 (1994).

[32] Asensi, M.A., Corma, A., and Martinez, A., J. Catal. **158**, 561 (1996).

[33] Butler, A.C., and Nicolaides, C.P., Catal. Today **18**, 443 (1993).

[34] Houzvicka, J., and Ponec, V., Catal. Rev.-Sci. Eng. **39**, 319 (1997).

[35] Sad, M.R., Querini,C.A., Comelli, R.A., Figoli, N.S., and Parera, J.M., Appl. Catal. A **146**, 131

(1996).

[36] Chapter 5 of this thesis.

Chapter 5

The conversion of 1-butene over Pt-ZSM5

Abstract

The conversion of 1-butene over Pt-ZSM5 was studied in the presence and absence of hydrogen. In the absence of hydrogen, the metal activity was rapidly poisoned and in the steady state the catalyst showed identical properties as the parent ZSM5. In the presence of hydrogen, the formation of new by-products (butadiene, propane, ethane and methane) was observed. The skeletal isomerization of butene was not affected, but the rate of oligomerization/cracking was enhanced. An analysis of the by-product pattern showed that ethane and propane, two major by-products, originated mainly from oligomerization/cracking on the acid sites and not from hydrogenolysis on the metal. The contribution of side reactions on the metal to the overall by-product formation was small. Thus, a tuning of the acid rather than of the metal sites is necessary in order to improve the performance of the bifunctional catalyst.

Introduction

In the preceding chapters we had shown that Pt-ZSM5 is a promising catalyst for the one-step dehydroisomerization of n-butane to isobutene. However, at high conversions side reactions of the primarily formed butenes increased significantly, thereby reducing the selectivity of the catalyst and limiting the yields of isobutene. In order to improve the performance of the dehydroisomerization catalyst it is crucial to understand the exact nature of these side reactions. In Chapter 4 we had concluded that the most important side reaction of butenes is acid catalyzed oligomerization/cracking, leading primarily to the formation of ethene, propene and pentene. Propane and ethane, which are the most abundant by-products at high conversions, were proposed to be formed by hydrogenation of the corresponding alkenes on the metal sites rather than by hydrogenolysis. If this holds true all major by-products originate from oligomerization/cracking reactions of butenes, whereas the contribution of the metal to the overall by-product formation is very small.

Because of the large importance of the above-mentioned side-reactions of the butenes on the selectivity in dehydroisomerization, we wanted to study these reactions in more detail. This was done by converting 1-butene over a series of Pt-ZSM5 catalysts with different metal loadings and acid site concentrations under the conditions used for dehydroisomerization of butane. The aim was to identify the reaction pathways of the conversion of butene over Pt-ZSM5 and to describe the parameters that influence the extent and nature of the side-reactions of the butenes.

Experimental

Catalyst preparation

The parent ZSM5 materials were supplied by ZEOLYST. Pt was incorporated by competitive ion exchange, followed by calcination at 723 K and reduction at 773 K, as described in Chapter 2. The elemental composition of the samples was determined by XRF, the metal dispersion by hydrogen chemisorption, the Brønsted acidity by IR spectroscopy (see Chapter 2 and Chapter 4). The results are summarized in Table 1.

Table 1 *Physico-chemical properties the Pt-ZSM5 samples.*

Sample code	SiO_2/Al_2O_3	H^+ (mmol/g)	Pt-loading (wt%)	H/Pt
0.1%Pt ZSM5(480)	480	0.07	0.09	>2.0
0.5%Pt-ZSM5(480)	480	0.07	0.46	1.2
0.1%Pt-ZSM5(80)	80	0.40	0.10	n.d.

n.d. = not determined

Catalyst testing

For the catalytic tests the samples were pressed, crushed and sieved to obtain a particle size in the range of 300 to 500 μm. 10 to 50 mg of the catalyst were mixed with 50 to 100 mg quartz and filled into a quartz tube with an inner diameter of 4 mm. The catalyst bed had a typical length of 5 to 15 mm and was supported on both sides by quartz wool. The samples were reduced *in situ* at 830 K for at least 1 h in a mixture of H_2/Ar (20/80). 830 K was also the temperature of the reaction. The reaction was started by switching from H_2/Ar to the feed, which was under standard conditions a mixture of 7.5% 1-butene, 0 or 20% H_2, the balance being Ar. The outlet pressure of the reactor was regulated by a back-pressure regulator to 1.8 bar. The pressure drop over the reactor was not more than 0.1 bar.

In order to follow the performance of the catalyst at very short time on stream the reactor effluent was stored in sampling loops for later GC analysis. After 10 min time on stream online GC analysis was employed (see Chapter 2). Conversions and yields were calculated on a carbon basis, using the FID areas and corresponding response factors. Since the double bond isomerization is a very facile reaction and usually reaches equilibrium, cis- and trans-butene were counted as reactants and not as products.

Results

Figures 1a and 1c show the major products in the conversion of 1-butene over 0.1%Pt-ZSM5(480) in the absence of hydrogen. At steady state Pt-ZSM5 showed identical catalytic properties as the parent zeolite. A stable yield of 17% isobutene was obtained. The major by-products were propene and pentene. Traces of ethene, n-butane, isobutane (not shown in Figure 1) and butadiene were also found. In contrast to the parent ZSM5 (which was stable already after 1min when the first data point was taken) the formation

of propene and butadiene decreased at short time on stream with Pt-ZSM5 (see Figure 1c).

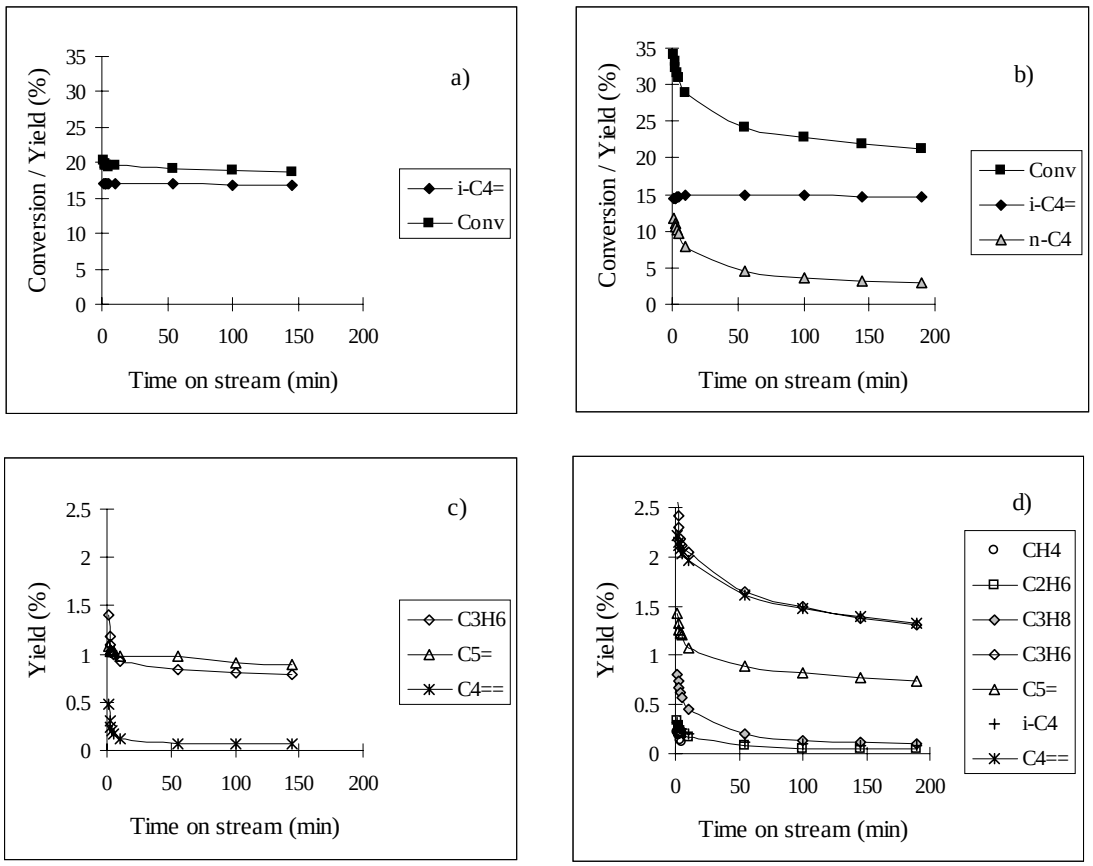

Figure 1 *Butene isomerization over 0.1%Pt-ZSM5(480) in the presence (b, d) and absence (a, c) of H_2. WHSV = 82 h^{-1}. 830 K, 1.8 bar, 7.5% 1-butene, 0 or 20% H_2. Conversion of 1-butene and yield of the major products.*

The comparison of Figures 1a/1b and 1c/1d demonstrates how the product pattern changed when hydrogen was added to the feed. The formation of isobutene was almost unaffected (it decreased from 17% to 16%). The by-product formation, on the other hand, was drastically changed. Not only propene and pentene, but also the saturated by-products n-butane, propane, isobutane, ethane and methane (in this order) were formed. n-Butane was the most abundant by-product, followed by propene and butadiene. The by-product formation deactivated with time on stream for all components.

The higher metal loading of 0.5 wt% Pt lead to a further increase in the formation of n-butane, butadiene, propane, isobutane, ethane and methane (see Table 2). The typical products of butene isomerization, i.e., isobutene, propene and pentene, were affected to a much smaller extent. The rate of isobutene formation slightly decreased. The rate of

propene slightly increased. As observed for 0.1%Pt-ZSM5, the by-product formation deactivated with time on stream, whereas the formation of isobutene did not change.

Figure 2 shows the selectivity over 0.1%Pt-ZSM5(480) as a function of conversion. Isobutene and n-butane were the major primary products with an initial selectivity of 65 and 16%, respectively. Also propene and pentene were primary products (4 and 7% initial selectivity). At conversions above 40%, the selectivity to isobutene decreased sharply, while the formation of especially propane, and to a smaller extent also of propene and pentene increased.

Table 2 *Reaction of 1-butene over Pt-ZSM5(480). WHSV = 82 h^{-1}. 7.5% 1-butene, 0 or 20% H_2. 1.8 bar, 830 K. 100min on stream.*

Pt-content (%)	0.1	0.1	0.5	0.5
H_2 (%)	0	20	0	20
Yield i-$C_4^=$ (%)	16.9	14.9	16.6	11.8
i-$C_4^=/\sum C_4^=$ (%)	17.2	16.2	16.9	15.1
Conversion (%)	18.9	22.7	18.5	33.8
Yield by-products (%)				
CH_4	0.00	0.07	0.00	0.34
C_2H_6	0.00	0.06	0.00	0.39
C_3H_8	0.00	0.14	0.00	0.69
n-C_4	0.11	3.6	0.11	15.8
i-C_4	0.05	0.10	0.04	0.24
C_2H_4	0.08	0.10	0.08	0.12
C_3H_6	0.81	1.5	0.76	1.4
C_5=	0.91	0.82	0.85	0.74
$C_4^{==}$	0.07	1.5	0.09	2.3

Figure 3 shows the influence of acid site concentration on the conversion of butene in the presence of hydrogen. The conversion increased by more than a factor of two and the yield of isobutene rose from 15 to 26 %, when the SiO_2/Al_2O_3 ratio decreased from 480 to 80. The formation of n-butane remained unchanged. The yield of byproducts, however, was also drastically increased, especially the yield of propene which went up by a factor of six. Initially, also large amounts of propane, ethane and isobutane were observed, but

as in the other experiments the formation of the saturated products decreased rather quickly with time on stream.

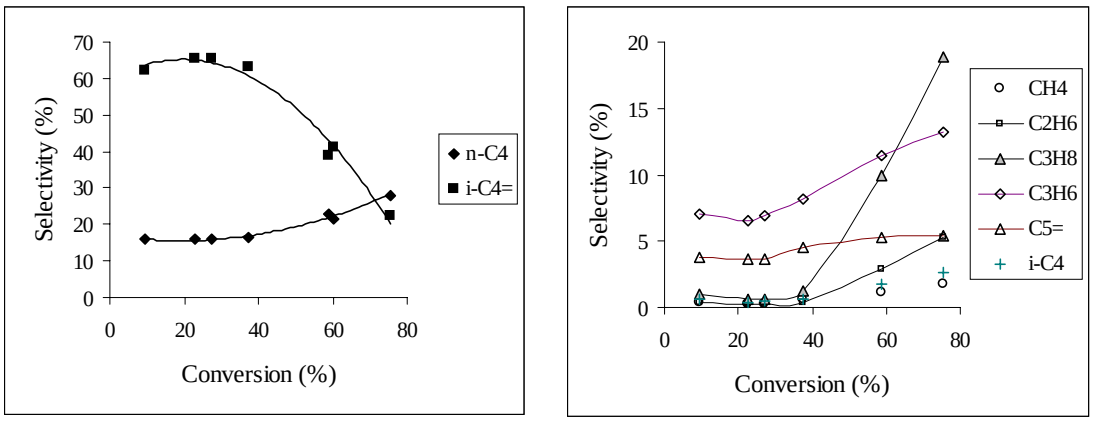

Figure 2 *Selectivity to the major products as a function of 1-butene conversion. 0.1%Pt-ZSM5(480). 830 K, 1.8 bar, 7.5% 1-butene, 20% H_2. 100 min on stream.*

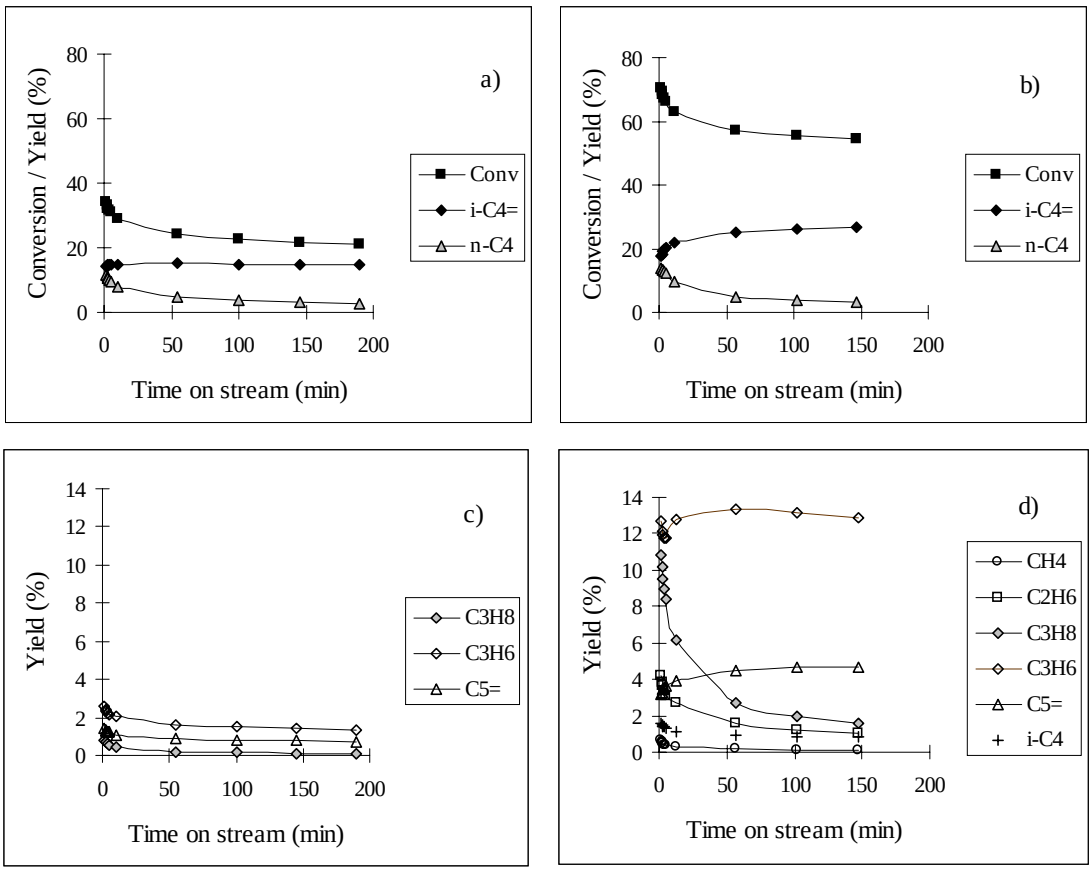

Figure 3 *Butene isomerization over 0.1%Pt-ZSM5 with SiO_2/Al_2O_3 = 480 (a,c) and 80 (b,d). WHSV=82 h^{-1}. 830 K, 1.8 bar, 7.5% 1-butene, 20% H_2. Conversion of 1-butene and yield of the major products.*

Discussion

The formation of (saturated) by-products

In the presence of hydrogen methane, ethane and propane were found as products in the conversion of 1-butene over Pt-ZSM5. Table 3 shows how the yield of methane, ethane and propane depended on the metal loading and the SiO_2/Al_2O_3 ratio. Methane formation increased with the metal content rather than with the concentration of acid sites, the yield of ethane and propane formation on the other hand depended mainly on the concentration of acid sites. The products also showed a different dependence on conversion (see Figure 4). The selectivity to propane and ethane increased drastically above 40% conversion, in parallel with a decrease in selectivity to isobutene (see Figure 2).

Table 3 *Yield of saturated by-products in the reaction of 1-butene over (Pt)-ZSM5. WHSV = 82 h^{-1}. 7.5% 1-butene, 20% H_2. 1.8 bar, 830 K. 100 min on stream.*

SiO_2/Al_2O_3	480	480	80	480
Pt-content (wt%)	0	0.1	0.1	0.5
Conversion (%)	11.7	22.7	55.3	33.8
Yield (%)				
CH_4	0.04	0.07	0.13	0.34
C_2H_6	0.01	0.06	1.22	0.39
C_3H_8	0.00	0.14	1.93	0.69
i-C_4	0.04	0.10	0.84	0.24

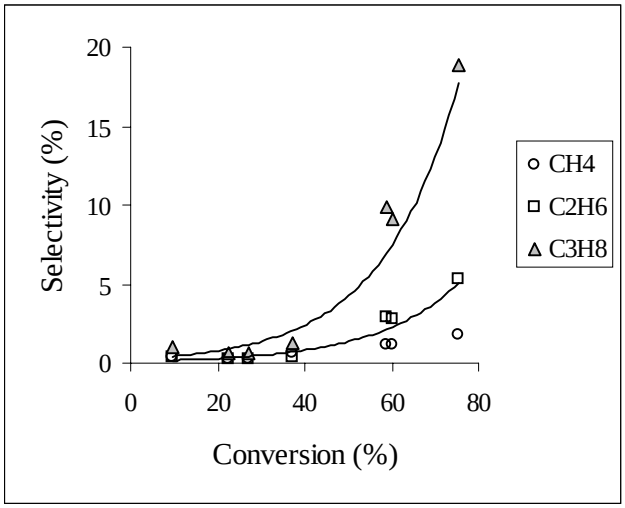

Figure 4 *Selectivity to methane, ethane and propane as a function of conversion. 0.1%Pt-ZSM5(480), 830 K, 1.8 bar, 7.5% 1-butene, 20% H_2. 100 min time on stream.*

The decrease in selectivity to isobutene is connected to the approach to thermodynamic equilibrium. As the ratio $iC_4^=/\sum C_4^=$ approaches its thermodynamic limit, the net rate of isomerization becomes very low. The by-product formation, on the other hand, is unlimited. As a result, the selectivity to by-products increases. Under normal circumstances, *i.e.*, in the absence of hydrogen and Pt, these by-products are propene and pentene [1]. Here, the selectivity to propene and pentene increased only moderately compared to propane and ethane. Also the selectivity to methane remained rather low. Both, the strong dependence on the concentration of acid sites and the strong increase in selectivity with conversion, indicate that ethane and propane actually originate from the oligomerization/cracking route. Methane, on the other hand, is produced by metal catalyzed hydrogenolysis (note the increase of the yield with metal content) as well as by cracking over the acid sites (note the small increase of the yield with acid site concentration).There are two mechanisms by which the formation of ethane and propane via the oligomerization/cracking route can happen. The classical explanation is that the alkenes formed by oligomerization/cracking on the acid sites are hydrogenated on the metal to the corresponding alkanes. It has been suggested, however, that desorption of the alkene from the acid site and diffusion to the metal site may not be necessary [2]. Hydrogen can be spilt over from the metal to the zeolite and assist the desorption of cracking products as saturated species, for example according to reaction (1).

$$Z\text{-}O\text{-}CH(CH_3)_2 + 2H^{\cdot}_{spill} \rightarrow Z\text{-}OH + CH_3\text{-}CH_2\text{-}CH_3 \qquad (1)$$

It is difficult to distinguish between the two routes because the same dependence on metal loading and hydrogen partial pressure is expected for both of them.

Not only the formation of saturated by-products increased in the presence of Pt and hydrogen, but also the rate of propene formation (see Table 2 and Figure 1). We can only give a tentative explanation for this effect. Figure 1c and 1d show that the time-on-stream behavior of propene is closely related to the one of butadiene. When reacting butadiene with ZSM5 at 775 K it oligomerizes and cracks into propene, pentene and ethene as well as higher hydrocarbons (C_5^+) [3]. Thus, the higher propene formation could be due to cracking of butadiene-oligomers. Since the cracking products are richer in hydrogen than butadiene also some carbonaceous deposits have to be formed in order to maintain the hydrogen balance. These deposits deactivate the metal. In the absence of hydrogen the deactivation is fast and after a few minutes on stream Pt-ZSM5 gives the same product pattern as ZSM5. In the presence of hydrogen, however, the deactivation of the metal is

slow. Thus, a significant amount of butadiene is observed even after 100 min on stream, leading to the higher yield of propene by cracking of its oligomers. Note that from a thermodynamic point of view the formation of butadiene should be inhibited in the presence of hydrogen.

The competition between butene isomerization and hydrogenation

Butene isomerization over the acid sites and butene hydrogenation over the metal sites are parallel, competing reactions. When the metal loading was increased, the relative importance of hydrogenation increased. When the acid site concentration was increased, the relative importance of butene isomerization and butene cracking increased (see Figure 2). Like in dehydroisomerization (see Chapter 4), the ratio of metal to acid sites changed the way the reaction mixture approached the thermodynamic equilibrium between n-butene, isobutene and n-butane. This is depicted in Figure 5. In the absence of hydrogen n-butane did not form and the composition of the reaction mixture moved along the line from n-butene to the equilibrium point between n- and isobutene (point F). Over 0.1% Pt-ZSM5(480) the reaction mixture approached the overall equilibrium point G along a curve following first the line of butene isomerization, only then turning into the direction of hydrogenated products (line FG). Over 0.5%Pt-ZSM5(480), the reaction mixture approached the overall equilibrium point G more directly, i.e., hydrogenation was more dominating. The opposite was observed for 0.1%Pt-ZSM5(80). With this catalyst isomerization dominated.

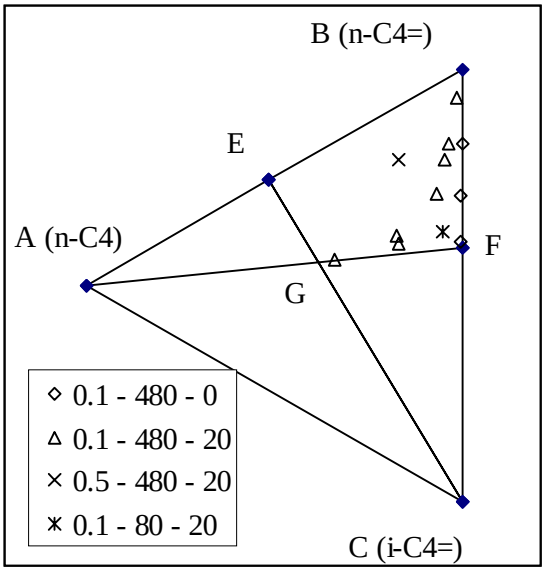

Figure 5 *The n-butane/n-butene/isobutene/isobutane equilibrium tetrahedron. A ... n-butane, B ... n-butene, C ... isobutene, E ... equilibrium between n-butane and n-butene, F... equilibrium between n-butene and isobutene, G... equilibrium between n-butane, n-butene, isobutene. Legend: Metal loading – SiO_2/Al_2O_3 - $\%H_2$ in feed.*

Conclusions

From the results discussed above we can propose a reaction network for the conversion of 1-butene over Pt-ZSM5 as shown in Figure 6. Four parallel reactions take place, (i) isomerization to isobutene (the desired reaction), (ii) oligomerization/cracking of butenes leading to the formation of propene and pentene, (iii) hydrogenation of 1-butene to n-butane as well as dehydrogenation to butadiene, (iv) hydrogenolysis. Ethane and propane are not mainly formed by hydrogenolysis, but via the oligomerization/cracking route. Propane, propene and pentene are the major by-products at high conversions. Thus, even in the presence of Pt and hydrogen, the acid sites are the main source of by-product formation. This conclusion had also been drawn in Chapter 4.

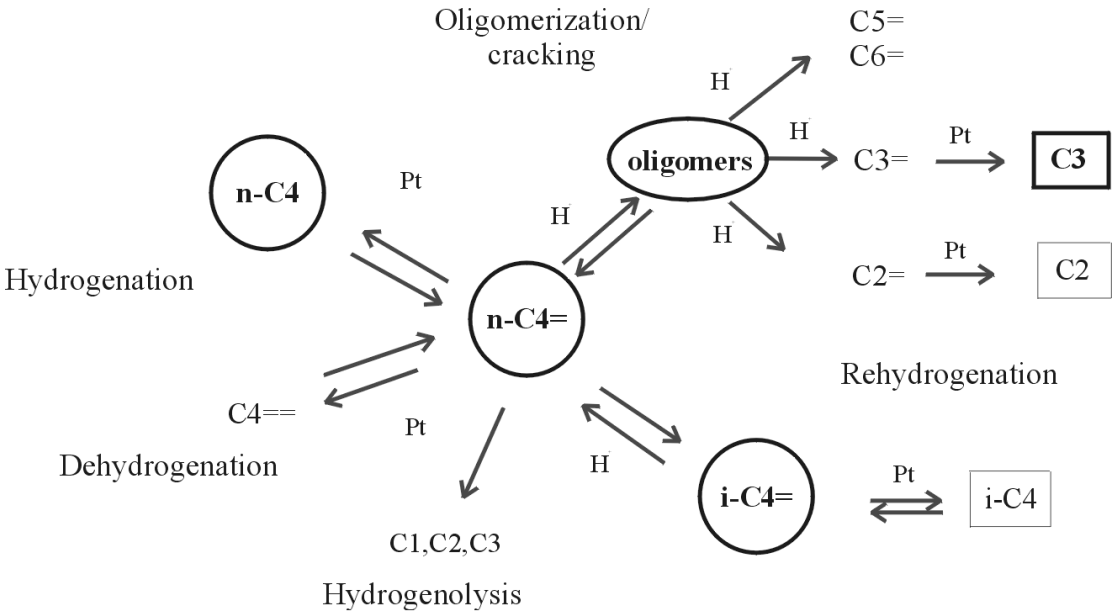

Figure 6 *Scheme of the reaction network in the conversion of n-butene over Pt-ZSM5*

The formation of butadiene (by dehydrogenation of 1-butene on the metal) leads to an enhanced rate of oligomer formation, and as a consequence also to an enhanced rate of propene formation, which is the cracking product of the oligomers. In the oligomerization process also coke deposits are formed which lead to a deactivation of the metal, but not of the acid sites. The isomerization activity is not significantly affected.

With respect to catalyst design the results confirm that the high cracking activity of ZSM5 is the bottleneck for the application of ZSM5 in dehydrogenation reactions. Synergetic effects between metal and acid sites in the by-product formation exist only

indirectly, via hydrogenation of cracking products and enhanced oligomer-formation from butadiene.

References

[1] Houzvicka, J., and Ponec, V., Catal. Rev.-Sci. Eng. **39**, 319 (1997).

[2] F. Roessner, U. Roland and T. Braunschweig, J. Chem. Soc. Faraday Trans. **91**, 1539 (1995).

[3] Chapter 7 of this thesis.

Chapter 6

Dehydroisomerization of n-butane over Pt-ZSM5 – Kinetic and thermodynamic aspects

Abstract

A kinetic model is applied to describe the dehydroisomerization of n-butane over Pt-ZSM5. It is compared with experimental data and used to show how a combination of kinetics and thermodynamics affects the obtained yields. High temperatures reduced the selectivity to by-product formation by oligomerization/cracking of butene. However, the stability of the catalyst decreased. This is attributed to the enhanced formation of butadiene, poisoning metal and acid sites. Lowering the pressure reduced the selectivity to by-products and the thermodynamic constraints and was, thus, favorable for dehydroisomerization. The H_2/n-butane ratio mainly affected the selectivity to hydrogenolysis, which increased with hydrogen partial pressure, while catalyst stability did not improve significantly. An optimum with respect to selectivity and stability was found for a H_2/n-butane ratio of 2.

Introduction

In Chapter 4 we had shown that Pt-ZSM5 can be successfully used as a catalyst for the direct conversion of n-butane to isobutene. We had discussed the influence of the catalyst parameters metal loading and acid site concentration and analyzed the reaction network of dehydroisomerization. Here, we want to build on the knowledge from Chapter 4 and optimize the dehydroisomerization of n-butane over Pt-ZSM5 more with respect to the reaction parameters, such as pressure, temperature, etc. The aim was to describe the reaction kinetics and to achieve a further improvement in the yield and selectivity of isobutene.

In Chapter 4 and 5 we had concluded that secondary cracking of butenes (via formation of di- and oligomers) was the major source of by-products in the dehydroisomerization of n-butane over Pt-ZSM5. Oligomerization/cracking of butenes is favored at low temperatures and high pressures [1]. Thus, higher selectivities to isobutene can be expected when the dehydroisomerization of n-butane is carried out at higher temperatures and lower pressures. Moreover, higher temperatures and lower pressures increase the thermodynamically possible yields of n-butenes and of isobutene. In order to establish these effects experimentally, the influence of pressure and temperature on the dehydroisomerization of n-butane was studied.

In addition to pressure and temperature, the hydrogen to hydrocarbon ratio is an important parameter of the reaction. Hydrogen is added to the feed in order to maintain the stability of the catalyst. From a thermodynamic point of view, addition of hydrogen is not desirable, since it shifts the dehydrogenation equilibrium to the side of the reactant. In addition, hydrogenolysis reactions could possibly be reduced if the hydrogen concentration in the reaction mixture was minimized. A *priori* it is not possible to predict which of these effects dominates in importance. The role of the hydrogen to hydrocarbon ratio with respect to catalyst stability, activity and selectivity to by-products was, therefore, explored.

Experimental

From the Pt-ZSM5 materials described in Chapter 4 0.1%Pt-ZSM5(480) and 0.5%Pt-ZSM5(480) were chosen for the present study, because of their low selectivity to by-

product formation. Two additional ZSM5 samples (SiO_2/Al_2O_3 = 215) with different crystal sizes (1 μm and 4 μm) were received from Exxon. 0.5%Pt was incorporated by ion exchange, followed by calcination at 723 K and reduction at 773 K, as described in Chapter 2. The physico-chemical properties of the samples are summarized in Table 1.

Table 1 *Physico-chemical characterization of the Pt-ZSM5 samples*.

Sample code	SiO_2/Al_2O_3	H^+ (mmol/g)	Pt-loading (wt%)	H/Pt
0.1%Pt ZSM5(480)	480	0.07	0.09	>2.0
0.5%Pt-ZSM5(480)	480	0.07	0.46	1.2
0.5%Pt-ZSM5(1μm)	215	0.15	0.51	1.5
0.5%Pt-ZSM5(4μm)	215	0.15	0.53	1.5

For the catalytic tests the samples were pressed, crushed and sieved to obtain a particle size in the range of 300 to 500 μm. 10 to 50 mg of the catalyst were mixed with 50 to 100 mg quartz and filled into a quartz tube with an inner diameter of 4 mm. The catalyst bed had a typical length of 5 to 15 mm and was supported on both sides by quartz wool.

The samples were reduced *in situ* at 830 K for at least 1 h in a mixture of H_2/Ar (20/80), then cooled to reaction temperature. The reaction was started by switching from H_2/Ar to the feed, which was under standard conditions a mixture of 10% n-butane, 20% H_2, the balance being Ar. Yields of products and the conversion of n-butane were reported on a basis of mol carbon converted.

Since dehydrogenation and isomerization are close to equilibrium at higher conversions, equilibrium effects significantly influenced the measured reaction rates. Therefore, the catalytic activity was expressed in terms of pseudo first order rate constants, which were calculated from a kinetic model assuming first order in the forward and backward reaction steps (see Appendix 1 of this chapter for the details of the calculation). While this model has a limited accuracy in describing the real kinetics, it helped to reduce the dependence of the reaction rates on the level of conversion, thereby facilitating the evaluation of rate constants.

Results

Effect of temperature

Figure 1 shows the effect of temperature on the activity of 0.1 and 0.5%Pt-ZSM5(480). The initial conversion increased with temperature. On the other hand, the catalyst deactivated faster at higher temperatures.

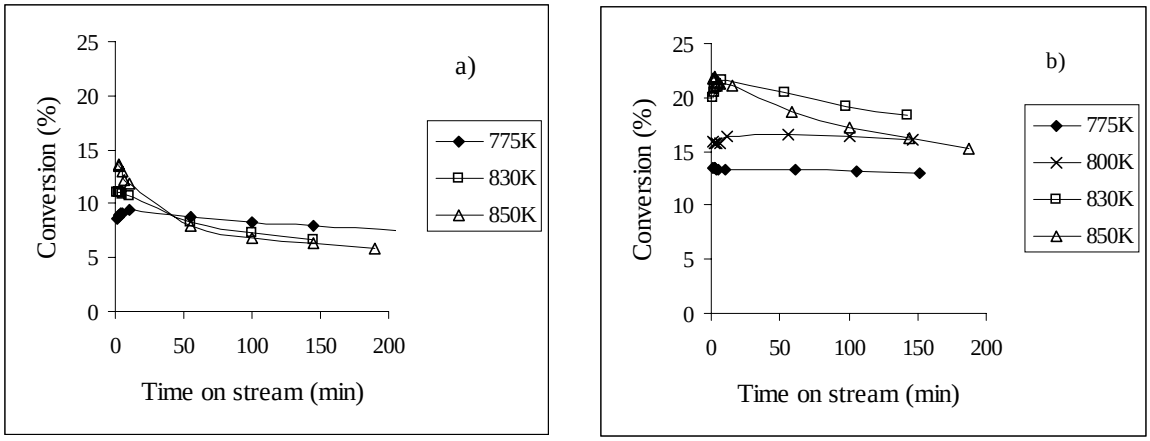

Figure 1 Conversion of n-butane as a function of temperature. WHSV = 260 h^{-1}, 1.8 bar, 10% n-butane, 20% H_2. a) 0.1%Pt-ZSM5(480) b) 0.5%Pt-ZSM5(480).

We calculated the activation energy of dehydrogenation from the initial rates of butene formation, at a constant conversion level of 15%. This was the lowest conversion at which a comparison of all catalysts and temperature was possible. Values of 50 kJ/mol and 85 kJ/mol were obtained for 0.1 and 0.5%Pt-ZSM5(480), respectively. At 15% conversion, however, equilibrium effects already play a role. In order to correct for these effects, the activation energy was determined from the temperature dependence of the rate constant of dehydrogenation (k_1), which was calculated from the initial conversion[1], using the method described in the Appendix 1. Figure 2 shows the respective Arrhenius plots for both catalysts. The equilibrium correction lowered the activation energies to 25 kJ/mol and 40 kJ/mol for 0.1 and 0.5%Pt-ZSM5(480), respectively. The scatter of the data was very large, however, and the error margin of the activation energy was estimated to be 10 kJ/mol.

[1] A small increase of conversion, which was sometimes observed in the first minutes on stream, was attributed to transient phenomena and not taken into account in the extrapolation of the initial conversion.

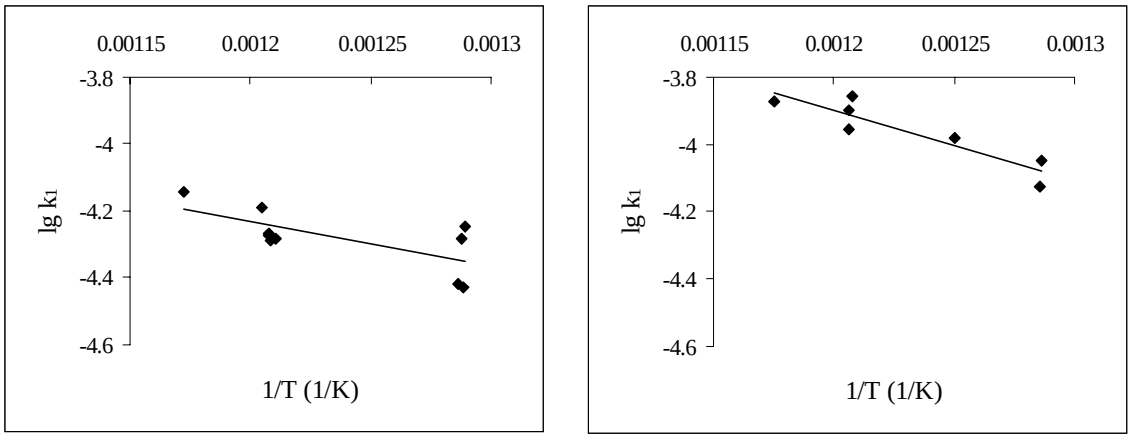

Figure 2 *Arrhenius plot of the pseudo first order rate constant of dehydrogenation (k_1). k_1 was calculated by the method described in Appendix 1, using the initial conversion of n-butane (at zero time on stream). a) 0.1%Pt-ZSM5(480) b) 0.5%Pt-ZSM5(480).*

The temperature dependence of 0.5%Pt-ZSM5 was, however, significantly stronger than that of 0.1%Pt-ZSM5. This was also reflected in the steady state yield of the sum of butenes ($\sum C_4^=$) achieved at higher space times. From 775 K to 830 K it increased by a factor of 2 for 0.5%Pt-ZSM5(480), but only by a factor of 1.5 for 0.1%Pt-ZSM5(480) (see Table 2).

Table 2 *Steady state yields and conversions at a constant WHSV = 20 h^{-1} (ST = 30000 sg/m^3). 1.8 bar, 10% n-butane, 20% H_2. 100 min time on stream. Yields and conversion in mol% carbon.*

	0.1%Pt-ZSM5(480)		0.5%Pt-ZSM5(480)	
	775 K	830 K	775 K	830 K
Yield $iC_4^=$	5.1	8.1	5.0	12.1
Yield $C_4^=$	18.2	25.8	19.1	37.5
Conversion	22.6	30.6	31.0	52.9
$iC_4^=/C_4^=$	28.1	31.4	25.9	32.2

The effect of temperature on the selectivities is shown in Table 3.

Table 3 *Effect of temperature on the steady state selectivities (in mol% carbon). 1.8 bar, 10% n-butane, 20% H_2, 100 min time on stream.*

	0.1%Pt-ZSM5(480) Conversion = 22.5%		0.5%Pt-ZSM5(480) Conversion = 31%	
	775 K	830 K	775 K	830 K
CH_4	0.7	0.6	3.2	1.7
iC_4	5.9	0.9	13.0	2.0
$iC_4^=$	22.6	22.6	16.0	19.0
$C_4^=$	80.4	91.1	61.6	82.0
Sec. cracking[a]	10.8	5.3	20.1	12.0

[a] counted as the sum of ethane, propane, propene and pentene.

As expected, the selectivity to secondary cracking (i.e., to oligomerization/cracking of the butenes) decreased with temperature, while the selectivity to dehydrogenation increased. Moreover, the selectivity to isobutane decreased drastically from 775 to 830 K.

Effect of pressure

Table 4 shows the conversion, the rate of dehydrogenation and the calculated pseudo first order rate constant of dehydrogenation as a function of pressure. (The lower pressure limit was given by the pressure drop at high flow rates.)

The conversion and the rate of dehydrogenation were practically independent of pressure at 775 K and increased slightly at 830 K. As already mentioned above, a comparison of the reaction rates may be misleading because of the pressure dependence of the dehydrogenation equilibrium. Therefore, also the pseudo first order rate constants k_1 of dehydrogenation are given in Table 4. They decreased with increasing pressure.

Table 4 *Conversion of n-butane, rate of dehydrogenation ($\sum C_4^=$) and pseudo first order rate constant of dehydrogenation (k_1), calculated from the initial conversion.*

	0.1%Pt-ZSM5(480)			0.5%Pt-ZSM5(480)		
	Conv (%)	rate (10^{-5}mol/sg)	k_1 (10^{-5} m^3/sg)	Conv (%)	rate (10^{-5}mol/sg)	k_1 (10^{-5} m^3/sg)
775 K, WHSV = 170 h^{-1}						
1.25bar	9.2	7.2	4.5	15.5	12	9.4
1.8bar	9.7	7.7	3.8	14.8	12	7.5
830 K, WHSV = 260 h^{-1}						
1.4 bar	8.8	11	6.1	17.9	21	16.8
1.8 bar	11.0	12	5.3	21.5	24	12.8

For practical applications, the effect of pressure at high conversions is more relevant than the variations at low conversions. Table 5 compiles some activity data at WHSV = 20 h^{-1}. In the case of 0.1%Pt-ZSM5(480), pressure had only a minor effect on the steady state activity. In the case of 0.5%Pt-ZSM5(480), however, a *higher* conversion of n-butane and a higher yield of butenes were obtained at a *lower* pressure.

Table 5 *Effect of pressure on the activity. WHSV = 20 h^{-1}, 100 min time on stream, 775 K, 10% n-butane, 20% H_2. Yields and conversion in mol% carbon.*

	0.1%Pt-ZSM5(480)		0.5%Pt-ZSM5(480)	
	1.0 bar[a]	1.8 bar	1.0 bar[a]	1.8 bar
Yield $iC_4^=$ (%)	5.0	5.1	5.4	5.0
Yield $C_4^=$	20	18.2	27	19.1
Conversion (%)	22	22.6	35	31.0
$iC_4^=/C_4^=$ (%)	25	28.1	25	25.9

[a] values were interpolated

With respect to the selectivity, reducing the pressure from 1.8 to 1.0 bar caused the expected increase in selectivity to dehydrogenation and a decrease in selectivity to secondary cracking. The selectivity to isobutane also decreased drastically.

Effect of hydrogen/hydrocarbon ratio

Figure 3 shows the conversion of n-butane as a function of time on stream for three different H_2/n-butane ratios (WHSV = 170 h^{-1}). For the H_2/n-butane ratios of 3.6, 2.0, and 1.1, deactivation rates $-dk_1/dt$ of $(1.0\pm0.4)*10^{-9}$ $m^3s^{-2}g^{-1}$, $1.0*10^{-9}$ $m^3s^{-2}g^{-1}$ and $(1.3\pm0.1)*10^{-9}m^3s^{-2}g^{-1}$ were calculated (from the decrease of activity between 50 and 150 min time on stream). Thus, the deactivation rate decreased only marginally with increasing H_2/n-butane ratio.

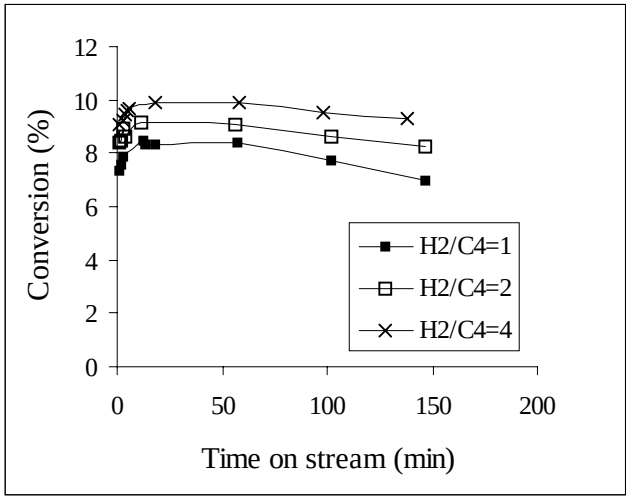

Figure 3 *Conversion of n-butane as a function of H_2/n-butane ratio. WHSV = 170 h^{-1}, 775 K, 1.25 bar, 10% n-butane, 20% H_2. 0.1%Pt-ZSM5(480).*

The H_2/n-butane ratio also had a non-negligible effect on the conversion. It increased with hydrogen partial pressure. A plot of $\ln(k_1)$ *vs.* $\ln(p_{H2})$ yielded an order of approximately 0.4 in hydrogen. At higher contact times, however, the H_2/n-butane ratio had only a minor effect on the steady-state conversion of n-butane (see Table 6). A small optimum in the yield of the sum of butenes and of isobutene was observed for H_2/n-butane = 2.

Table 6 *Conversion of n-butane and yield of the sum of butenes and of isobutene. WHSV = 12 h^{-1}. 775 K, 1.0 bar, 10% n-butane. 0.1%Pt-ZSM5(480).*

H_2/n-butane	1.1	2.0	3.6
Yield i-$C_4^=$	5.9	6.5	5.8
Yield $C_4^=$	21.0	23.1	20.3
Conversion	23.6	26.3	25.4
i-$C_4^=$/$C_4^=$	27.8	28.3	28.5

An analysis of the by-product pattern showed that higher H_2/n-butane ratios led to an increase in selectivity to methane, ethane (see Figure 4) and isobutane. Also the rates

of methane and ethane formation increased with hydrogen partial pressure (see Figure 5). The intercept of both curves was zero, indicating that the presence of hydrogen is necessary for the formation of these products. Assuming a power rate law $r = r_0 \cdot p_{H2}^{x}$, an order of 1 and 1.6 in hydrogen was obtained for methane and ethane, respectively.

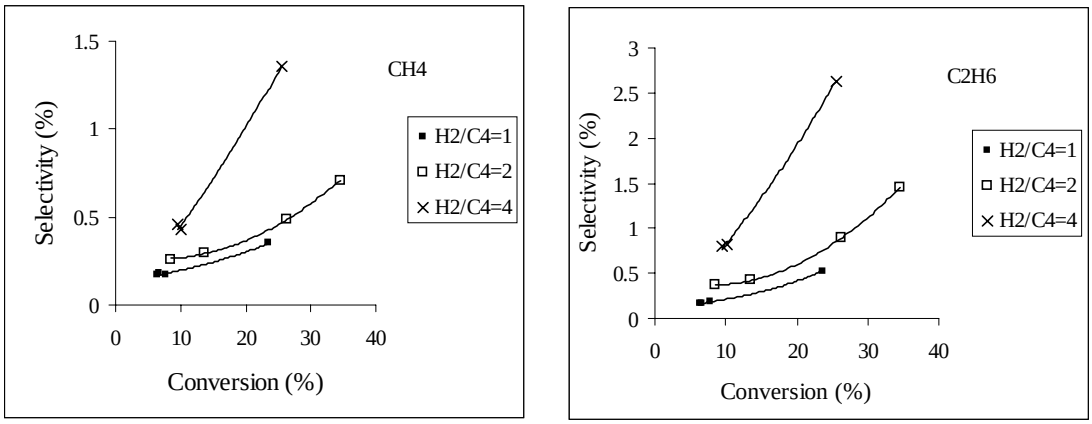

Figure 4 *Selectivity to methane and ethane as a function of H_2/n-butane ratio. 775 K, 1.0 bar, 10% n-butane, 20% H_2. 100 min time on stream. 0.1%Pt-ZSM5(480).*

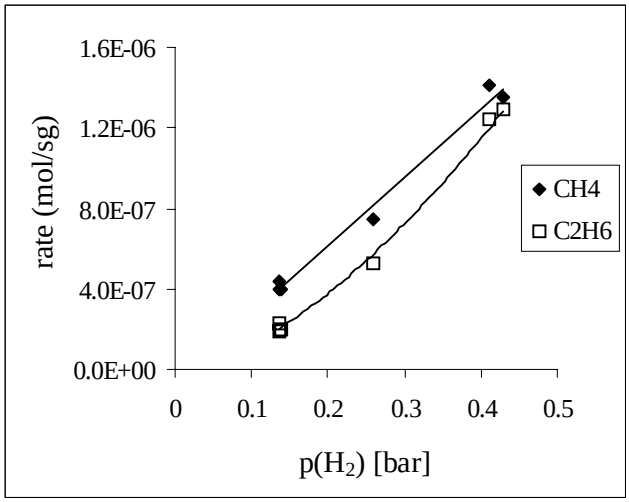

Figure 5 *Rate of methane and ethane formation as a function of hydrogen partial pressure. Conversion 8-10%. WHSV = 170 h^{-1}, 775 K, 1.25 bar, 10% n-butane, 20% H_2. 100 min time on stream. 0.1%Pt-ZSM5(480).*

Diffusional constraints

In order to probe the presence of external diffusion limitations, the flow rate was varied while keeping the space time constant [2]. The difference between these experiments was within the error of measurement (< 10% for the initial conversion, < 2% for the steady state conversion). In order to check the effect of intraparticle diffusion (i.e., within the 300 – 500 µm particles that were pressed from the zeolite powder) also a smaller sieve fraction of 100 – 300 µm particles was tested. The smaller particles tended to give higher conversions (the difference was 0 to 20% for

the initial conversion and 0 to 10% for the steady state conversion). The small increase was rather attributed to the higher pressure drop that was observed with the small particles than to the presence of intraparticle diffusion limitations.

Finally, in order to establish the influence of micropore diffusion (intracrystalline diffusion), the dehydroisomerization of n-butane was performed over 0.5%Pt-ZSM5 catalysts with different crystal sizes (1 µm and 4 µm). Figure 6 shows the respective results. Only marginal differences were observed. The conversion and the yield of the sum of butenes increased slightly with crystal size, the ratio of isobutene to the sum of butenes decreased slightly.

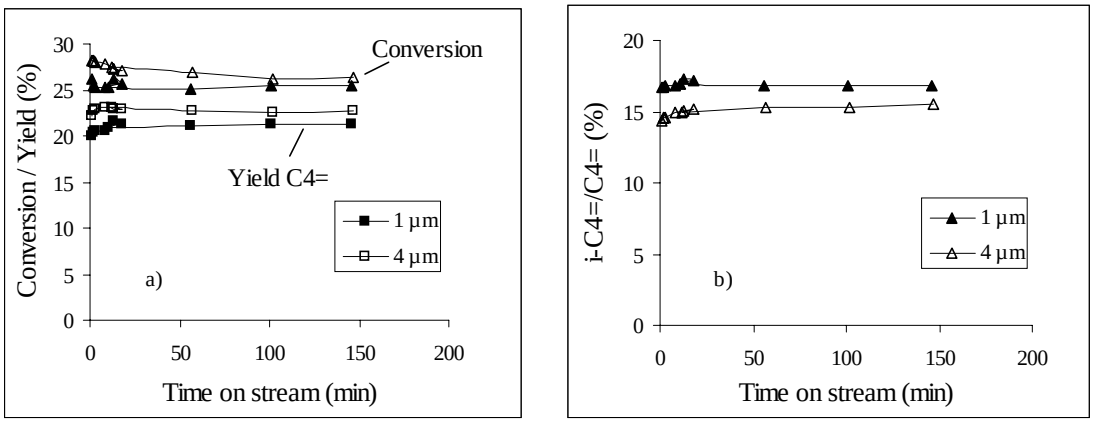

Figure 6 *Dehydroisomerization of n-butane over 0.5%Pt-ZSM5(215) with crystal sizes of 1 (full symbols) and 4 µm (open symbols). a) Conversion of n-butane (△) and yield of the sum of butenes (□). b) Ratio i-$C_4^=$/Σ$C_4^=$. WHSV = 170 h^{-1}, 775 K, 1.2 bar, 10% n-butane, 20% H_2.*

As a control experiment, butene isomerization was performed over the parent ZSM5 materials (without Pt). Also here, an influence of crystal size on the yield of isobutene was not observed.

Discussion

Kinetic model of dehydroisomerization

Dehydroisomerization can be described as a sequence of two reversible reactions.

$$n\text{-}C_4H_{10} \rightleftharpoons n\text{-}C_4H_8 \rightleftharpoons i\text{-}C_4H_8$$

Assuming first order rate equations the kinetics is described by

$$\frac{d[n\text{–}C_4H_{10}]}{dt} = -k_1 \cdot [n\text{–}C_4H_{10}] + k_{-1} \cdot [n\text{–}C_4H_8] \quad (1.)$$

$$\frac{d[n\text{–}C_4H_8]}{dt} = -\frac{d[n\text{–}C_4H_{10}]}{dt} - \frac{d[i\text{–}C_4H_8]}{dt} \quad (2.)$$

$$\frac{d[i\text{–}C_4H_8]}{dt} = k_2 \cdot [n\text{–}C_4H_8] - k_{-2} \cdot [i\text{–}C_4H_8] \quad (3.)$$

k_1 and k_{-1} are the forward and backward rate constants of dehydrogenation. k_2 and k_{-2} are the forward and backward rate constants of butene isomerization. k_1 and k_{-1} and k_2 and k_{-2} are related to each other by the equilibrium constants of dehydrogenation and isomerization (K_1 and K_2), respectively[2].

$$K_1 = [n\text{-}C_4H_8]_{eq} / [n\text{-}C_4H_{10}]_{eq} = k_1 / k_{-1} \quad (4.)$$

$$K_2 = [i\text{-}C_4H_8]_{eq} / [n\text{-}C_4H_8]_{eq} = k_2 / k_{-2} \quad (5.)$$

The analytical solution of this equation system is described by Rodiguin and Rodiguina [3]. The simple model was compared with the presented experimental data. 0.1%Pt-ZSM5(480) was used, since a large amount of experimental data was available for this catalyst. k_1 was estimated from rate data at low conversions (see Table 4). k_2 was determined by measuring the rate of butene isomerization over ZSM5(480). K_1 and K_2 were calculated from thermodynamic data [4]. Figure 7 compares the model calculation with the experimental data. Two main differences were observed. (i) At higher space times the conversion decreased faster than predicted by the model. Obviously, factors, which retard the reaction at higher conversions, were not taken into account in the simple first order kinetics. (ii) The model underestimates the ratio $iC_4^{=}/\sum C_4^{=}$, when the experimentally determined rate constant of butene isomerization is used as k_2.

[2] Since the concentration of H_2 does not vary more than 10% from its feed level (see Chapter 4), *$[H_2]$* was assumed to be approximately constant and its value included in K_1.

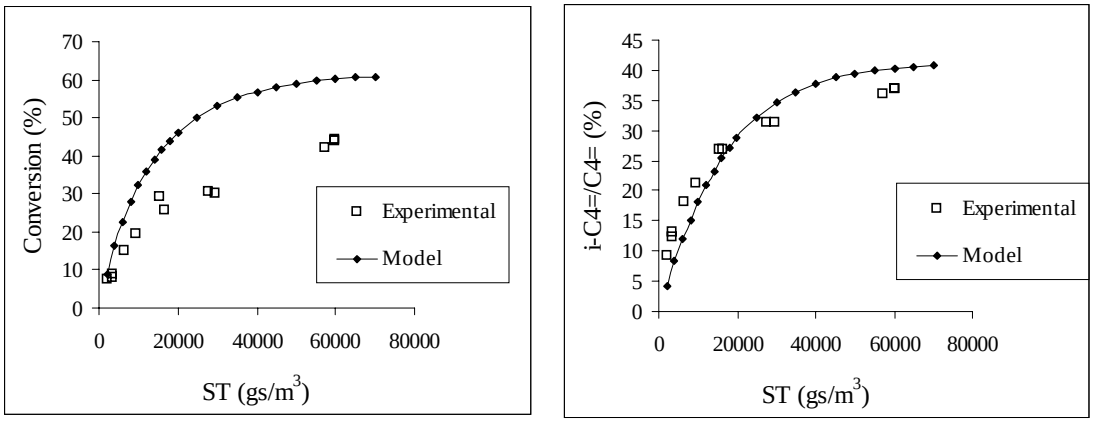

Figure 7 *Comparison of experimental data with a first order kinetic model. Experimental data: 0.1%Pt-ZSM5(480). 830 K, 1.8 bar, 10% n-butane, 20% H_2. 100 min on stream. Model parameters: $k_1 = 5*10^{-5}$ m^3/sg. $k_2 = 4.5*10^{-5}$ m^3/sg. $K_1 = 0.94$, $K_2 = 0.71$.*

In order to get a better description of the experimental data a more detailed kinetic model was developed. The following sequence of elementary steps was assumed [5 - 9] (M represents an adsorption site on the metal).

$2\ M + n\text{-}C_4H_{10}\ (g) \rightleftharpoons M\text{-}C_4H_9 + M\text{-}H$ (1)

$M\text{-}C_4H_9 + 2M \rightleftharpoons M_2\text{-}C_4H_8 + M\text{-}H$ (2)

$M_2\text{-}C_4H_8 \rightleftharpoons 2M + n\text{-}C_4H_8\ (g)$ (3)

$2\ M\text{-}H \rightleftharpoons 2M + H_2\ (g)$ (4)

Also the formation of butadiene via more highly dehydrogenated surface species was included in the model.

$M_2\text{-}C_4H_8 + 4\ M \rightleftharpoons M_4\text{-}C_4H_6 + 2\ M\text{-}H$ (5)

$M_4\text{-}C_4H_6 \rightleftharpoons C_4H_6 + 4\ M$ (6)

Hydrogen/deuterium exchange experiments [8, 10] suggested that step (1), the dissociative abstraction of the first hydrogen, is rate determining. Steps (2) - (6) can then assumed to be in quasi-equilibrium, which yields the following equations for the rates and surface coverages.

$$
\begin{aligned}
r &= \kappa_1 \cdot \Theta_*^{\,2} \cdot [n\text{–}C_4H_{10}] - \kappa_{-1} \cdot \Theta_{C4H9} \cdot \Theta_H \\
\kappa_2 \cdot \Theta_{C4H9} \cdot \Theta_*^{\,2} &= \kappa_{-2} \cdot \Theta_{C4H8} \cdot \Theta_H \\
\kappa_3 \cdot \Theta_{C4H8} &= \kappa_{-3} \cdot \Theta_*^{\,2} \cdot [n\text{–}C_4H_8] \\
\kappa_4 \cdot \Theta_H^{\,2} &= \kappa_{-4} \cdot \Theta_*^{\,2} \cdot [H_2] \\
\kappa_5 \cdot \Theta_{C4H8} \cdot \Theta_*^{\,4} &= \kappa_{-5} \cdot \Theta_{C4H6} \cdot \Theta_H^{\,2} \\
\kappa_6 \cdot \Theta_{C4H6} &= \kappa_{-6} \cdot [C_4H_6] \cdot \Theta_*^{\,4}
\end{aligned}
\qquad (6.)
$$

Θ_* represents the free fraction of the metal surface, Θ_H the fraction of Pt covered by H, Θ_{C4H9} the fraction covered by C_4H_9, Θ_{C4H8} the fraction covered by the olefin precursor C_4H_8, etc. IR studies (at temperature below 300 K) have indicated that butenes are adsorbed on Pt as π-bonded species, di-σ-bonded species and tri-σ-bonded alkylidyne species [11, 12], the latter two prevailing at higher temperature [12]. Natal-Santiago *et al.* have suggested the presence of even more highly dehydrogenated species in the adsorption of isobutene on Pt (1,1,1,2-tetra-σ and 1,1,1,3-tetra-σ) [13]. For the sake of simplicity we assumed the olefin to be adsorbed as a di-σ species, i.e., occupying two Pt sites, while all more highly dehydrogenated species are tetra-σ-adsorbed and lead to the formation of butadiene. Above set of equations (6.) gives the following expression for the reaction rate [8, 9].

$$
r = \kappa_1 \cdot \Theta_*^{\,2} \cdot [C_4H_{10}] \cdot \left[1 - \frac{1}{K_{eq}} \cdot \frac{[n\text{–}C_4H_8] \cdot [H_2]}{[n\text{–}C_4H_{10}]} \right] \qquad (7.)
$$

K_{eq} is the equilibrium constant of the overall reaction. The fraction of free sites (Θ_*) can be calculated from the site balance $\Theta_* + \Theta_{C4H9} + 2\Theta_{C4H8} + 4\Theta_{C4H6} + \Theta_H = 1$. In a detailed kinetic analysis of isobutane dehydrogenation on Pt/Sn-SiO_2, Cortright *et al.* showed that the fractional coverage of the butyl species (C_4H_9) is very low (less than 10^{-5}) [8]. Thus, Θ_{C4H9} can be neglected. Likewise, the adsorption of hydrogen is weak compared to the adsorption of the alkene. In microcalorimetric studies an initial heat of sorption of more than 200 kJ/mol was measured for the adsorption of isobutene on Pt-SiO_2 [13] and for cis-2-butene on Pt-NaY [14], compared to only 100 kJ/mol for hydrogen. Our own experiments showed a positive order in hydrogen, while a negative order would be expected if the surface coverage of hydrogen was high. Thus, we concluded that M_2-C_4H_8 and M_4-C_4H_6 were the dominating surface species, while

Θ_H was neglected.[3] With these assumptions the site balance reduced to $4\Theta_{C4H6} + 2\Theta_{C4H8} + \Theta_* = 1$, i.e.,

$$4K_{C4H6}\,[C_4H_6]\,\Theta_*^4 + 2K_{C4H8}\,[C_4H_8]\,\Theta_*^2 + \Theta_* = 1 \qquad (8.),$$

where $K_{C4H8} = \kappa_{-3}/\kappa_3$ is the adsorption constant of n-butene on the metal and $K_{C4H6} = \kappa_{-6}/\kappa_6$ the adsorption constant of butadiene on the metal. Note that since steps (3) to (6) were assumed to be in quasi-equilibrium the concentrations of butene and butadiene are tied to each other by

$$[C_4H_6] = \frac{K_5 \cdot K_{C4H8}}{K_{H2} \cdot K_{C4H6}} \cdot \frac{[C_4H_8]}{[H_2]} \qquad (9.),$$

where K_5 is the equilibrium constant of step (5) and K_{H2} the adsorption constant of H_2. This is in agreement with the experimental observation that a constant ratio of butadiene to the sum of butenes was found for a certain set of reaction conditions.

Equation (8.) was numerically solved and the solution substituted in equation (7.). For describing dehydroisomerization, equation (7.) was combined with (2.) and (3.). Note that at low coverages ($\Theta_* \sim 1$) equation (7.) reduces to (1.). Under these conditions the refined and the original model are equivalent. Readsorption of isobutene on the metal was accounted for by using the sum of all butenes in the term $[C_4H_8]$ in equation (8.) instead of only the linear butenes.

With $k_1 = 5*10^{-5}$ m^3/sg, $k_2 = 8*10^{-5}$ m^3/sg, $R\cdot T\cdot K_{C4H8} = 10$ bar^{-1}, $R\cdot T\cdot K_{C4H6} = 400$ bar^{-1} and $[C_4H_6]/[C_4H_8] = 0.027$ (the average ratio found in the experiments) a good fit of the experimental values was obtained (see Figure 8). k_2 had to be chosen higher than $4.5*10^{-5}$ m^3/sg (experimentally measured for butene isomerization) in order to obtain a good fit of the isomer fraction at low space times. At high space times the model overestimated the isomer fraction. This is due to increasing contribution of oligomerization/cracking reactions, which were not taken into account in the model.

[3] Note that most kinetic studies, in which negative orders in hydrogen were found, were performed at low conversions and high hydrogen partial pressures. Under these conditions hydrogen is the dominating surface species in spite of its lower heat of sorption. At high conversions and low H_2/hydrocarbon ratios, however, the coverage changes in favor of the alkene, as confirmed by calculations using above-mentioned heats of sorption and thermodynamic data for the sorbed state given in ref. [9].

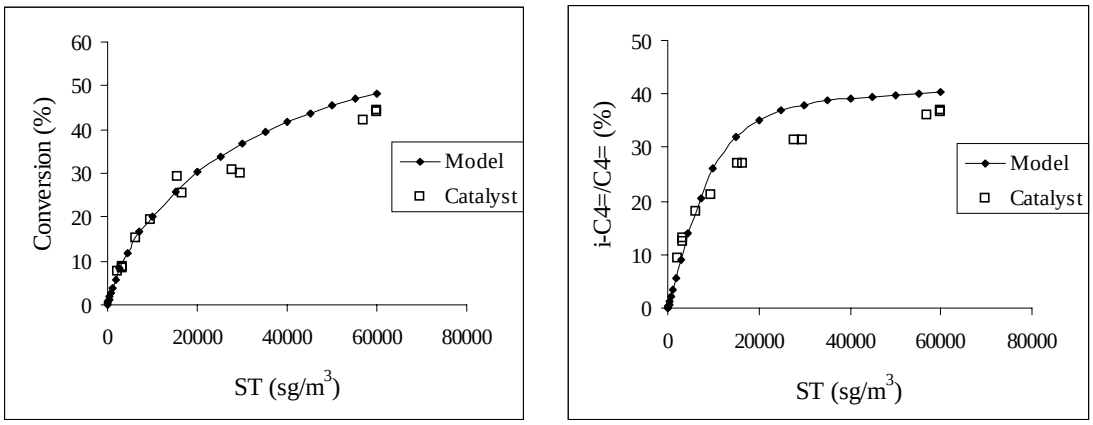

Figure 8 *Comparison of experimental data with the refined kinetic model. Experimental data: 0.1%Pt-ZSM5(480). 830 K, 1.8 bar, 10% n-butane, 20% H_2. 100 min on stream. Model parameters: $k_1 = 5*10^{-5}$ m^3/sg. $k_2 = 8*10^{-5}$ m^3/sg. $R{\cdot}T{\cdot}K_{C4H8} = 10$ bar^{-1}. $R{\cdot}T{\cdot}K_{C4H6} = 400$ bar^{-1}. $K_1 = 0.94$, $K_2 = 0.71$, $[C_4H_6]/[C_4H_8] = 0.027$.*

The effect of temperature and pressure

The effect of temperature and pressure on dehydroisomerization is threefold, (i) on the selectivity to by-products, especially oligomerization/cracking of butenes, (ii) on the thermodynamic constraints and (iii) on the kinetics. With respect to selectivity, the catalysts showed the expected trend. The contribution of butene oligomerization/cracking decreased with increasing temperature and decreasing pressure, as predicted in ref. [1]. Thus, we want to focus the discussion on the question of thermodynamics and kinetics.

Figure 9 shows how the thermodynamically possible yields of isobutene and of n-butene change with temperature and pressure. The maximum yield of isobutene (keeping the pressure constant at 1.8 bar) can be obtained at 900 K. But thermodynamics also predicts a sharp increase in butadiene formation above 830 K. This is not desirable, since butadiene is known to be responsible for catalyst deactivation [6].

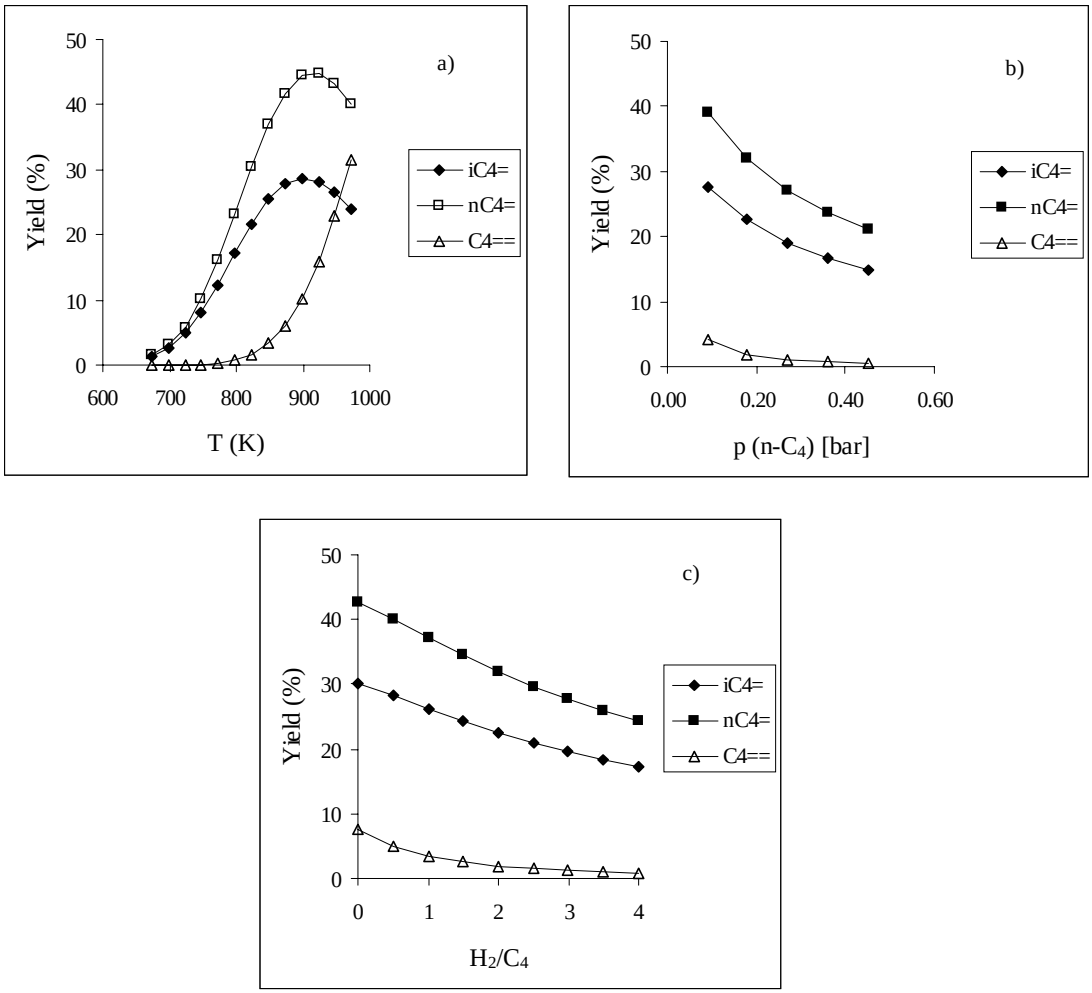

Figure 9 *(a) Dehydrogenation equilibrium as a function of temperature. 1.8 bar, 10% n-butane, 20% H_2, 70% N_2. (b) Dehydrogenation equilibrium as a function of butane partial pressure. 1.8 bar, H_2/n-butane = 2, 830 K. (c) Dehydrogenation equilibrium as a function of H_2/n-butane. 1.8 bar, 10% n-butane, 830 K.*

The thermodynamically predicted increase in butadiene formation with temperature was experimentally confirmed (see Table 7). The steady state yield of butadiene increased with temperature. In parallel, the deactivation rate of both reaction steps, dehydrogenation and isomerization, increased. This indicates that the enhanced butadiene formation is in fact responsible for the poisoning of metal and acid sites at high temperatures. We, therefore, conclude that 830 K is a good compromise with respect to the reaction temperature. While thermodynamic and selectivity aspects would advise the use of even higher temperatures, the actual steady state conversions

are not improved by raising the temperature above 830 K (see Figure 1), because the catalysts deactivate faster.

Table 7 *Steady state yields of butadiene (in mol% carbon) and deactivation rates of dehydrogenation and isomerization as a function of temperature. 1.8 bar, WHSV=260 h^{-1}. 10% n-butane, 20% H_2. 0.1 and 0.5%Pt ZSM5 (480).*

	Temp (K)	Yield $C_4^{==}$ (%)	dk_1/dt [a] ($10^{-9}m^3s^{-2}g^{-1}$)	dk_2/dt [a] ($10^{-9}m^3s^{-2}g^{-1}$)
0.1%Pt	775	0.07	1.1	-0.08
	830	0.18	1.5	-0.07
	850	0.28	1.7	0.45
0.5%Pt	775	0.09	0.7	-0.02
	800	0.18	0.9	0.18
	830	0.39	2.9	0.37
	850	0.54	3.3	0.47

[a] calculated from the decrease in k_1 (dehydrogenation) and k_2 (isomerization) between 50 and 150 min on stream.

In order to discuss the effect of pressure on the kinetics and thermodynamics of dehydroisomerization on Pt-ZSM5, we used the kinetic model described in the previous section. Figure 10 compares the calculated and the measured conversions at 775 K for pressures of 1.0 and 1.8 bar, with 0.5%Pt-ZSM5(480) as a catalyst. In model and experiment the conversion at high space times *decreased* with *increasing* pressure. This decrease was mainly caused by the less favorable thermodynamics at the higher pressure. At 1.8 bar thermodynamic equilibrium does not allow conversions higher than 32%. Due to side reactions the actual conversion can be higher. But since most of the side reactions are secondary reactions of butenes (see Chapter 4 and 5), the overall conversion is still very much governed by the dehydrogenation rate and, thus, subjected to thermodynamic constraints.

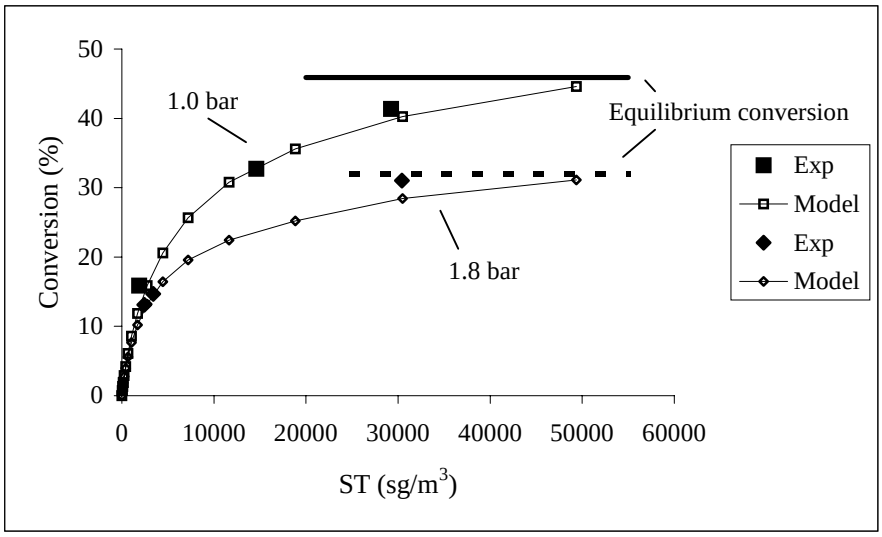

Figure 10 *Comparison of experimental data (full symbols) with the refined kinetic model (open symbols). Experimental data: 0.5%Pt-ZSM5(480). 775 K, 10% n-butane, 20% H_2. 100 min on stream. Model parameters: $k_1 = 1.5*10^{-4}$ m^3/sg (estimated from Table 4), $k_2 = 3.3*10^{-5}$ m^3/sg (measured for butene isomerization under these conditions), $R{\cdot}T{\cdot}K_{C4H8} = 20$ bar^{-1}, $R{\cdot}T{\cdot}K_{C4H6} = 1600$ bar^{-1}. Squares: 1.0 bar. Diamonds: 1.8 bar.*

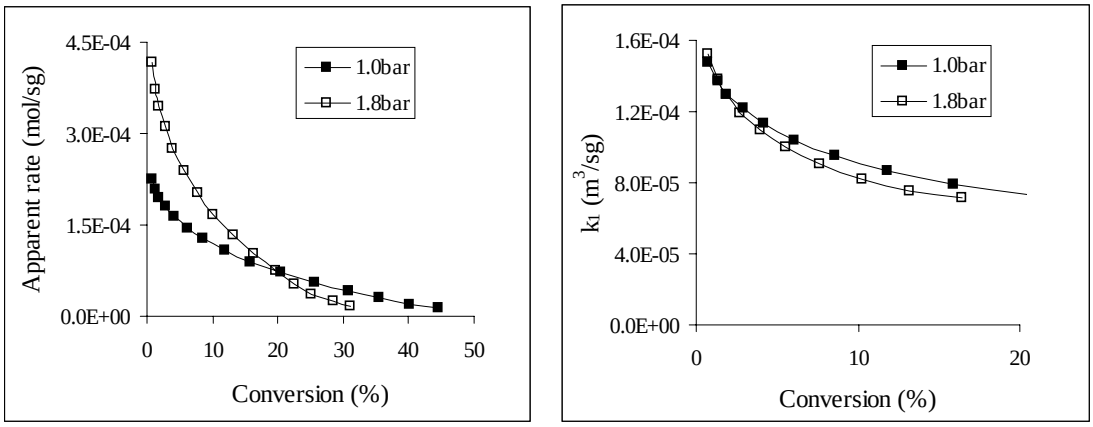

Figure 11 *(a) Apparent reaction rate and (b) pseudo first order rate constant of dehydrogenation, as calculated by the model. Model parameters: $k_1 = 1.5*10^{-4}$ m^3/sg. $k_2 = 3.3*10^{-5}$ m^3/sg. $R{\cdot}T{\cdot}K_{C4H8} = 20$ bar^{-1}. $R{\cdot}T{\cdot}K_{C4H6} = 1600$ bar^{-1}.*

Figure 11a shows how the apparent reaction rate ($r = x / ST \cdot [n\text{-}C_4H_{10}]$, x = conversion) depends on conversion, in the picture of the kinetic model. Initially (at zero conversion), the apparent reaction rate is higher at 1.8 bar than at 1.0 bar, because the reaction is first order in n-butane. With increasing conversion the fraction of free metal sites decreases and the contribution of the backward reaction increases

(see equation (7.)). Both effects are more pronounced at higher pressures. As a result, the apparent reaction rate at 1.8 bar becomes lower than at 1.0 bar above a certain level of conversion (see Figure 11a).

Figure 11a also shows that the apparent reaction rate depends strongly on the conversion, which makes the extrapolation of initial reaction rates (at zero conversion) from the experimental data extremely difficult. The contribution of the backward reaction to this decrease of the apparent rate, i.e. the contribution of the term $1 - [C_4H_8][H_2]/(K_{eq}[n\text{-}C_4H_{10}])$ in equation (7.), can be corrected for by calculating the pseudo first order rate constant k_1, according the method described in Appendix 1. The remaining decrease of k_1 with conversion (see Figure 11b) is caused by the inhibiting effect of butene and butadiene sorption on the metal.

Due to the strong dependence of the rate and of the calculated rate constant k_1 on conversion, the reported rate data have to be interpreted very cautiously, i.e., more in terms of trends than of absolute values. Moreover, it is emphasized that we see the kinetic model merely as a tool, which helps us to qualitatively describe the effects of pressure and thermodynamics. A much more detailed kinetic and calorimetric study would be necessary to obtain reliable values of k_1, K_{C4H8}, K_{C4H6}, etc., in the way demonstrated by Cortright *et al.* [8].

We can summarize that increasing pressure increases the intrinsic reaction rate. At higher conversions (above ~50% of the equilibrium conversion) this is overcompensated by the thermodynamic constraints and the inhibiting effect of product adsorption. The selectivity to oligomerization/cracking of butenes and to the formation of isobutane (via hydrogenation of isobutene) increased by increasing the pressure. Thus, the overall conclusion is that high pressures are not favorable for the dehydroisomerization reaction.

Effect of hydrogen to hydrocarbon ratio

The effect of the H_2/n-butane ratio was similar to the effect of pressure. It increases the activity at low conversions, but it also decreases the thermodynamically possible yield of butene (see Figure 9c). At high conversions these two factors nearly compensate each other (see Table 6). More important is how the H_2/n-butane ratio influences the selectivity to hydrogenolysis and the stability of the catalyst. The rate of methane formation depended linearly on the hydrogen partial pressure (Figure 5).

This indicates that methane is almost exclusively formed by hydrogenolysis and that the contribution of protolytic cracking of n-butane on the acid sites to the methane formation is small (see the discussion of routes of by-product formation in Chapter 4). The selectivity to the hydrogenolysis products methane and ethane (ethane can also be formed by hydrogenation of ethene) increased drastically when the H_2/n-butane ratio was raised from 2.0 to 3.6, whereas the stability of the catalyst was not significantly improved. Therefore, we conclude that a H_2/n-butane ratio of 2 is a good compromise between selectivity and stability.

The positive order in hydrogen is at variance with the results of kinetic studies of dehydrogenation over Pt-Al_2O_3 [5, 9, 10, 15] and Pt-Au alloys [16] where a negative order of hydrogen (-0.5) was reported. This could be due to the fact that higher hydrogen/hydrocarbon ratios and lower temperatures were used in these studies, leading to a higher surface coverage of H_2, which inhibits the reaction [9]. However, even in the absence of such an inhibiting effect, the order in hydrogen should not be larger than zero. The positive effect of hydrogen on the reaction rate (at low conversions) that we observed could, however, be related to reduced butadiene formation. The yield of butadiene decreased from 0.17% to 0.10% to 0.07% with increasing H_2/n-butane ratio. Feeding these values into the kinetic model (with $R \cdot T \cdot K_{C4H6} = 1600\ bar^{-1}$) yields an apparent order of 0.25 in hydrogen. The order in hydrogen increased almost linearly with the value of K_{C4H6}. Although it does not give a firm proof, the result of these model calculations supports the idea that the positive order in hydrogen could be indirectly caused by a reduced butadiene formation.

The activation energy

According to rate equation (7.), the activation energy should be the sum of the true energy of activation of step (1), i.e., the dissociation of n-butane, and a term describing the temperature dependence of the fraction of free metal sites (Θ_*).

Using transition state theory, Cortright *et al.* suggested a true activation energy of 60 kJ/mol for step (1) [9], in line with surface science results [17]. For the coverage term a simple expression cannot be given. Qualitatively, the activation energy should increase with the desorption energy of the metal-bonded hydrocarbon [18].

The zeolite can have a two-fold effect on the activation energy. It increases the reactant concentration due to sorption in the pores. Moreover, the product alkene is

not desorbed from the metal into the gas phase, but into the confined space of the zeolite pore. As a result, the desorption energy is reduced by the heat of sorption of the alkene in the zeolite pore, as shown in the energy scheme in Figure 12.

Both above-mentioned factors reduce the apparent activation energy and could be responsible for the different activation energy of 0.1 and 0.5%Pt-ZSM5(480) (25 and 40 kJ/mol, respectively). At the lower metal loading the relative contribution of sorption effects will be bigger, leading to the lower apparent activation energy.

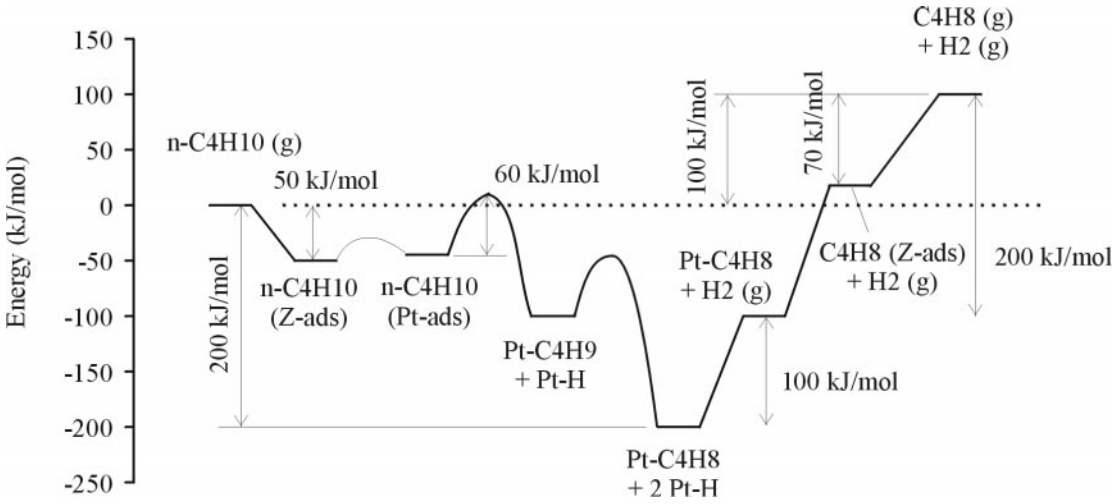

Figure 12 *Energy scheme of n-butane dehydrogenation in Pt-ZSM5. The activation energies and heats of sorption were estimated from literature values (see Appendix 2 for details).*

Conclusions

We have shown that a combination of kinetics, thermodynamics, and sorption is necessary to explain the catalytic results of dehydroisomerization of n-butane. With respect to the optimization of the physical parameters temperature, pressure and H_2/n-butane ratio, the following conclusions can be drawn. (i) High temperatures reduce the selectivity to by-products (oligomerization/cracking of butenes) and the thermodynamic constraints. However, above 830 K, these improvements are overcompensated by a loss in catalyst stability, which is attributed to poisoning by butadiene. (ii) Low pressures reduce the selectivity to by-products and the thermodynamic constraints. (iii) High H_2/n-butane ratios enhance unwanted hydrogenolysis reactions, while catalyst stability is not significantly improved. An optimum with respect to selectivity and stability was found for H_2/n-butane = 2.

Combining these results with those from Chapter 4 we can predict that the best yields of isobutene should be achieved at 830 K, 1 bar, with a H_2/n-butane ratio of 2, using 0.5%Pt-ZSM5(480) as a catalyst. In fact, a stable yield of 14-15% isobutene could be achieved under these conditions (see Figure 13), which is one of the highest yields reported so far (see Table 8).

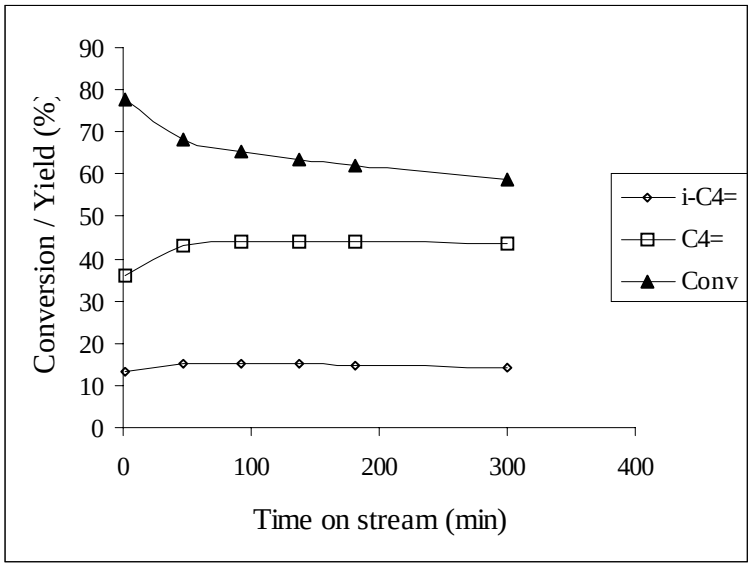

Figure 13 *Conversion of n-butane and yield of the sum of butenes and of isobutene. 0.5%Pt-ZSM5(480). 830 K, 1 bar, 10% n-butane, 20% H_2. WHSV = 10 h^{-1}.*

Acknowledgements

I would like to thank M.J.G. Janssen, from Exxon Chemical International Inc., Basic Chemicals Technology Europe, for supporting this work by supplying us with various ZSM5 samples.

Table 8 *Patents for dehydroisomerization of n-butane.*

Catalyst	Feed	Temp (K)	WHSV (h^{-1})	Conv (%)	TOS (h)	Yield $iC_4^=$ (%)	Max. yield [a] $iC_4^=$ (%)	Ref.
Pt-ZSM5	$H_2/nC_4/Ar$ = 2/1/7	830	10	59	5	14.1	31	this work
Pt/Re-[B]-ZSM11	H_2/nC_4 = 0.8, 3% H_2O	840	12.5	40	21	10	21	[19]
Pt-AMS-1B	$H_2/nC_4/He$ = 0.79/1/1.79	813	8.2	38	?	10.9	23	[20]
Sn/In/Pt-SiO_2/γ-Al_2O_3 + Boralite B	$H_2/nC_4/N_2$ = 1/1/2	825	2	58	?	14.6	25	[21]
Ga-zeolite L	nC_4	823	?	55	?	~10	24	[22]

[a] calculated from thermodynamics.

Appendix 1 – Calculation of the pseudo first order rate constant of dehydrogenation and isomerization

The dehydrogenation of n-butane is an equilibrium reaction. Due to the backward reaction the observed reaction rate is lower than the intrinsic rate. In order to correct for this effect, a simple first order kinetic model was assumed.

$$A \rightleftharpoons B \qquad r = k_1 \cdot [A] - k_{-1} \cdot [B]$$

r is given in mol/sg, k in m^3/sg, the concentration of A and B in mol/m^3. A represents n-butane, B the sum of linear butenes. The integration of this rate equation yields (see General Appendix A)

$$k_1 = \frac{1}{ST} \cdot \frac{K}{1+K} \cdot \ln\left(1 - x - \frac{x}{K}\right) \qquad (10.)$$

where ST = $m_{cat}/(dV_{total}/dt)$, x = conversion, K = equilibrium constant.

Equation (10.) was used to calculate the pseudo first order rate constant of dehydrogenation (k_1) from the experimental conversions. Note that the model assumes that (i) the reaction order of n-butane is 1, (ii) the order in hydrogen is zero and/or its concentration is constant and can be included in k_1. Only the overall equilbrium between n-butane and n-butene is considered. In a rigorous mathematical treatment, the three equilibria with the three linear butenes should be calculated separately. But if we assume that the double bond isomerization is always equilibrated (which is usually the case), the dehydrogenation reaction between can be described by a single equilibrium constant K = ($[\text{cis-2-butene}]_{eq}+[\text{trans-2-butene}]_{eq}+[\text{1-butene}]_{eq}$)/$[\text{n-butane}]_{eq}$.

The formation of isobutene is not taken into account since it does not take place on the metal sites. As a consequence, the correction can only be used at low conversions, i.e., at low values of $[iC_4^=]/\sum[C_4^=]$. Regarding the definition of the conversion x, we decided to use the total conversion of n-butane to all products instead of the conversion to butenes only. The reasoning behind this was that isobutene as well as most of the by-products were formed as secondary products from the linear butenes (see Chapter 4) and should, thus, be included in the conversion. It is clear that this approach will lead to erroneous results if the selectivity to by-products formed by other parallel routes is high.

For the pseudo first order rate constant of butene isomerization (k_2), the same method was applied. Here x was set equal to the ratio of $[iC_4^=]/\sum[C_4^=]$. K was calculated as

$[iC_4^=]_{eq}/\sum[nC_4^=]_{eq}$, the equilibrium concentration of isobutene divided by the sum of the equilibrium concentrations of the linear butenes. As above, this assumes that the linear butenes are already in equilibrium. The side reaction oligomerization/cracking is not taken into account by the model. As a result, the correction can only be applied when the selectivity to oligomerization/cracking is low, i.e., at low values of $[iC_4^=]/\sum[C_4^=]$ (see Chapter 4). The assumption of first order kinetics is correct. It was confirmed by butene isomerization experiments at different partial pressures. This is crucial since butene is a secondary product and its partial pressure strongly depends on the total conversion.

Appendix 2 – The energy diagram of dehydrogenation

The heat of sorption of n-butane in ZSM5(480) was estimated from the measurements of Eder *et al.* [23]. They found a heat of sorption of 58 kJ/mol in H-ZSM5. The contribution of interaction with the acid sites to this value is about 10 kJ/mol. Since the ZSM5 we used had a very low concentration of acid sites and is a more silicalite-like material, we used a heat of sorption of 50 kJ/mol in the scheme. The heat of sorption of the product butenes in ZSM5 was assumed to be 10-20 kJ/mol higher than for the butane [24], i.e., approximately 70 kJ/mol.

The energy of desorption of n-butane from Pt(111) was determined by thermal desorption spectroscopy to be about 45 kJ/mol [25, 26]. This value was taken as an estimation of the energy difference between n-butane in the gas phase and n-butane adsorbed on Pt (the concentration of this species will be practically zero, it either reacts or desorbs).

The activation energy for the dissociation of adsorbed n-butane was estimated from the results of surface science studied [17] and kinetic modeling [9]. The energy of the di-σ-adsorbed state was estimated by the heat of sorption of isobutane on Pt-SiO_2 [13] and the heat of sorption of n-butane on Pt-NaY [14], which were between 200 and 250 kJ/mol. Also the heats of sorption of hydrogen and of butene were taken from these references. Note that with these values the correct reaction enthalpy is obtained ($\Delta H_R \sim 100$ kJ/mol).

References:

[1] Houzvicka, J., Nienhuis, J.G., Hansildaar, S., and Ponec, V., Appl. Catal. A **165**, 443 (1997).

[2] Froment, G.F., Bischoff, K.B., "Chemical Reactor Analysis and Design", 2nd ed., p. 125-160, John Wiley & Sons, New York, 1990.

[3] N.M. Rodiguin, E.N. Rodiguina, "Consecutive Chemical Reactions, Mathematical Analysis and Development", D. van Nostrand Company, Inc., Princeton, New Jersey, 1964.

[4] Roine, A., "HSC Chemistry", Outokumpu Research Oy, Pori, Finland.

[5] Loc, L.K., Gaidai, N.A., Gudkov, B.S., Kostyukovskii, M.M, Kiperman, S.L., Podkletnova, N.M., Kogan, S.B., and Bursian, N.R., Kinet. Catal. **27** (1986), 1190.

[6] F. Buonomo, D. Sanfilippo, and T. Trifiro, "Handbook of Heterogeneous Catalysis", (Ertl, G., Knözinger, H., and Weitkamp, J., Eds.), Vol. 5, p. 2140, VHC-Wiley, Weinheim, 1997.

[7] Cortright, R.D., and Dumesic, J.A., Appl. Catal. **129**, 101 (1995).

[8] Cortright, R.D., Bergene, E., Levin, P., Natal-Santiago, M., and Dumesic, J.A., "11th International Congress on Catalysis, Baltimore, MC", (J.W. Hightower, W.N. Delgass, E. Iglesia, A.T. Bell, Eds.), Vol. 101, p. 1185, Elsevier, New York, 1996.

[9] Cortright, R.D., Levin, P.E., and Dumesic, J.A., Ind. Eng. Chem. Res. **37**, 1717 (1998).

[10] Lok, L.K., Gaidai, N.A., Gudkov, B.S., Kiperman, S.L., and Kogan, S.B., Kinet.Catal. **17**, 1184 (1986).

[11] Cremer, P.S., Su, X., Shen, Y.R., and Somorjai, G., J. Chem. Soc. Faraday Trans. **92**, 4717 (1996).

[12] Shahid, G., and Sheppard, N., Can. J. Chem. **69**, 1812 (1991).

[13] Natal-Santiago, M.A., Podkolzin, S.G., Cortright, R.D., and Dumesic, J.A., Catal. Lett. **45**, 155 (1997).

[14] Meriaudeau, P., Auroux, A., and Viornery, C., Catal. Lett. **41**, 139 (1996).

[15] Loc, L.C., Gaidai, N.A., Kiperman, S.L., and Thoang, H.S., Kinet. Catal. **34**, 451 (1993).

[16] Biloen, P., Dautzenberg, F.M., and Sachtler, W.M.H., J. Catal. **50**, 77 (1977).

[17] Campbell, Ch.T., Sun, Y.-K., Weinberg. W.H., Chem. Phys. Lett. **179**, 53 (1991).

[18] Kaptijn, F., Moulijn, J.A., and van Santen, R.A., in "Catalysis – An Integrated Approach to Homogeneous, Heterogeneous and Industrial Catalysis" (J.A. Moulijn, P.W.N.M. van Leeuwen, R.A. van Santen, Eds.), p. 78, Elsevier, Amsterdam, 1993.

[19] O'Young, Ch.-L., Browne, J.E., Matteo, J.F., Sawicki, R.A., Hazen, J., US Patent 5.198.597 (1993), assigned to Texaco Inc.

[20] Sikkenga, D.L., Nevitt, Th.D., and Jerome, N.F., US Patent 4.433.190 (1984), assigned to Standard Oil Company.

[21] Bellussi, G., Giusti, A., Zanibelli, L., US Patent 5.275.995 (1994), assigned to Eniricerche S.p.A., Snamprogetti S.p.A.

[22] Kolumbus, A.J., Telford, C.D., Young, D., EP Patent 42.252 (1981), assigned to British Petroleum Comp. Ltd.

[23] Eder, F., Stockenhuber, M., and Lercher, J.A., J. Phys. Chem. B **101**, 5414 (1998).

[24] Harflinger, R., Hoppach, D., Quachik, U., and Quitsch, K., Zeolites **3**, 123 (1983).

[25] Salmerson, M., and Somorjai, G.A., J. Phys. Chem. **85**, 3835 (1981).

[26] Xu, Ch., Koel, B.E., and Paffett, M.T., Langmuir **10**, 166 (1994).

Chapter 7

Deactivation of n-butene isomerization by butadiene

Abstract

The deactivation of the 10-membered ring zeolites ZSM5, FER and TON during the skeletal isomerization of butene in the presence of butadiene was studied. The rate of deactivation per butadiene molecule was found to increase with the concentration of butadiene and the contact time. It decreased in the presence of Pt and hydrogen. FER and TON deactivated much faster than ZSM5. This was attributed to two factors. (i) Deactivation of TON occurred by pore-blocking, while direct poisoning of the acid sites by coke-deposits took place on ZSM5. In the case of FER coke was only deposited in the 10-membered ring channels, while the access to the 8-membered ring channels was blocked. (ii) The build-up of carbonaceous deposits on ZSM5 was slower than that of the other zeolites, because ZSM5 had a high activity for cracking oligomeric coke-precursors into smaller fragments that desorbed from the catalyst. While this cracking activity is responsible for the moderate selectivity of ZSM5 for butene isomerization, it is beneficial with respect to the stability against deactivation by butadiene.

Introduction

In oxidative dehydroisomerization of n-butane over physical mixtures of a vanadia catalyst and a zeolite (FER, ZSM5, MCM36) we had observed a very rapid deactivation of the zeolite (see Chapter 3). The effect was partly attributed to the presence of butadiene, which was formed by dehydrogenation of butane (butene) on the vanadia catalyst. The poisoning by butadiene was so severe that it rendered the concept of oxidative dehydroisomerization infeasible.

In non-oxidative dehydroisomerization, Pt-ZSM5 exhibited quite stable activities. Still, it could be shown that also in this case a decrease in the isomerization activity with time on stream was partly related to the formation of butadiene (see Chapter 6). Obviously, the sensitivity to deactivation by butadiene is an important criterion for the choice of the isomerization component in bifunctional dehydroisomerization catalysts. Therefore, we studied in more detail the effect of butadiene on three zeolites that are known to be good butene isomerization catalysts, i.e., ZSM5 [1], TON [2 - 4] and FER [5 - 8]. The motivation was to test the suitability of these materials for dehydroisomerization. Due to the relevance for dehydroisomerization, also the effect of addition of Pt and hydrogen on the deactivation behavior was investigated.

The objective was to identify the mechanism of deactivation by butadiene and the parameters that affect the rate and extent of deactivation. The results form a basis for evaluating the stability of (dehydro-)isomerization catalysts.

Experimental

Catalyst preparation

ZSM5 (SiO_2/Al_2O_3 = 480) was received from ZEOLYST (sample code CBV10002). 0.1 wt% Pt was incorporated by ion exchange with a solution of $Pt(NH_3)_4(OH)_2$, followed by calcination and reduction, according to the procedure described in Chapter 2. The parent ZSM5 was subjected to the same calcination/reduction procedure as Pt-ZSM5, because it was found that the calcination/reduction procedure increased the activity and selectivity of the sample for the skeletal isomerization of butene.

FER with a SiO_2/Al_2O_3 ratio of 90 was provided by Exxon. In order to remove the template the sample was calcined for 2 h at 798 K (temperature increment 1 K/min) in

N_2, then cooled down to 573 K and finally calcined in air at 798 K (temperature increment 1 K/min) for 4 h. Subsequently, the zeolite was ion exchanged three times with 1 M NH_4NO_3 solution, at room temperature. Pt was incorporated as described above.

Mg-TON (SiO_2/Al_2O_3 = 35) was also received from Exxon. The sample was ion exchanged two times with 1 M NH_4NO_3 solution and once with 0.01 M NH_4NO_3 solution (each time for 12 h). The ammonium-exchanged sample was then ion-exchanged with $Pt(NH_3)_4(OH)_2$, calcined and reduced, as above.

The Pt-loading of all three zeolites was 0.1 wt%. In the following text the SiO_2/Al_2O_3 ratio of the samples is given in brackets after the code of the zeolite.

In addition to the three samples mentioned above ZSM5(80) (CBV8014, ZEOLYST), FER(17) (HSZ-720K0A, TOSOH) and TON(72) (received from the TU Vienna) were used as reference materials for the IR measurements in order to study the influence of SiO_2/Al_2O_3 ratio. Table 1 lists the physico-chemical properties of the materials.

Table 1 *Physico-chemical properties of the zeolites.*

Sample	SiO_2/Al_2O_3	Al (mmol/g)	acid sites [a] (mmol/g)	ν(OH) [b] (a.u.)	L/(L+B) [c] (%)
ZSM5(80)	80	0.40	0.40	1.2	10
ZSM5(480)	480	0.07	0.05	0.1	38
FER(17)	17	1.79	1.7	7.7	4
FER(90)	89	0.37	0.45	0.87 ± 0.03	4
TON(35)	35	0.92	0.34	0.7[d]	23
TON(72)	72	0.45	0.26	0.28 ± 0.05	15

[a] Sum of Lewis and Brønsted acid sites, determined by adsorption of pyridine (see Chapter 9).

[b] Intensity of the ν(OH)-band at 3610 cm^{-1} at 473 K.

[c] Ratio of Lewis to Lewis + Brønsted acid sites, determined by adsorption of pyridine (see Chapter 9).

[d] The ν(OH) band has a shoulder at low wavenumbers, the intensity may, therefore, be overestimated.

Catalyst testing

10 to 20 mg of the sample mixed with 60 mg quartz were activated in a stream of 25 ml/min Ar at 830 K for 1 h (10 K/min). Then, the reactor was cooled to 775 K. For Pt-containing samples 5 ml/min H_2 were added to the Ar-stream.

After stabilization of the temperature at 775 K the inlet stream of the reactor was switched from Ar to the feed mixture containing 7.5% 1-butene and optionally 20% H_2, the balance being Ar. In the first 10 min the reactor effluent was collected in storage loops for post-run GC analysis, afterwards the reactor effluent was analyzed directly with time intervals of 45 min.

After 3 h time on stream the inlet stream was switched back to Ar and the reactor was purged for 1.5 h. Then, the reaction was started again, this time with 1% butadiene added to the feed. The activity of the catalyst was followed in the same way as above (using the sample loops for the first minutes on stream, then by on-line GC analysis).

Since the double bond isomerization is a very facile reaction and usually reaches equilibrium, cis- and trans-butene were counted as reactants and not as products in the analysis of the data. Yields were calculated on a carbon basis and related to the amount of 1-butene in the feed, even when butadiene was co-fed. Since butadiene also led to reaction products, the total yield of all products was in that case higher than the conversion of 1-butene.

As the skeletal isomerization of butene is equilibrium limited, an attempt was made to correct the observed overall reaction rates for the backward reaction. The details of this correction are described in the appendix of this chapter.

IR spectroscopy

The zeolites were pressed into self-supporting disks (1 to 3 mg) and placed into a cylindrical oven, which in turn was attached to an IR cell with CaF_2 windows allowing the IR beam to pass through the sample. Reactant gases were passed through the cell by means of 1/16" stainless steal tubing connected to the side of the IR cell. A detailed description of the cell design can be found in ref. [9]. For removing adsorbed ammonia or water, the samples were heated in a stream of He to 773 K and kept there for 1 h. Pre-reduced Pt-containing samples were heated in a mixture of He/H_2 (4/1) instead of pure He.

The adsorption of butadiene was started by switching the reactor inlet to a stream of about 1% butadiene in He (25 ml/min). After 90 min adsorption the reactor inlet was

switched back to the gas mixture used for activation, i.e., He or H_2/He. The sample was purged for 1 h at 773 K, then cooled down to 473 K. The reactive adsorption and desorption of butadiene was followed by IR spectroscopy. At 473 K an additional IR spectrum of the coked sample was taken. At 473 K the bands are sharper and more intense than at 773 K, which facilitated the interpretation of the spectra. In order to quantify the amount of coke formation, the carbon content of the disks was determined by means of a CHNO-analyzer (Carlo-Erba EA1108).

IR spectra were recorded in the transmission mode with a Nicolet SXB20 spectrometer (resolution 4 cm^{-1}). The spectra were normalized to the intensity of the bands at 1980 and 1860 cm^{-1} of the activated zeolite. These bands are attributed to overtones of the lattice vibrations and are an adequate measure of the thickness of the sample disk. The spectrum of the activated zeolite was used as a background for calculating the absorbance during adsorption and desorption of butadiene.

^{13}C-NMR

In order to further characterize the coke formed during reaction with butene/butadiene ^{13}C-NMR spectroscopy was applied. 50 mg of catalyst were treated first with butene for 3 h and then with the mixture of butene/butadiene for 1 h, according to the procedure described above. After stopping the reaction the catalyst was flushed for 1 h at 775 K (the reaction temperature) with a stream of 40 ml/min Ar, in order to remove weakly adsorbed carbon species. Then, the reactor was cooled to room temperature and the catalyst was retrieved.

The solid state ^{13}C-NMR measurements of the coked catalysts were performed on a BRUKER DMX300 spectrometer operating at 75.47 MHz (B_0 = 7.1 T). The spectra were obtained using a 4 mm broad band CP-MAS probe, spinning at 9-10 kHz. Both single pulse excitation proton-decoupled and CP-MAS spectra were taken. A VACP (Variable Amplitude on ^{1}H Cross Polarization) pulse sequence was used for the CP-MAS experiments. The mixing time was 2 ms. The ^{13}C chemical shifts were determined relative to TMS, using adamantane as a secondary standard.

Results

Butene isomerization over (Pt-)ZSM5 in the presence/absence of butadiene

ZSM5 was a very stable catalyst for the conversion of 1-butene. Within the three hours on stream the product pattern did not change significantly. Isobutene was the main product, propene and pentene the major by-products. When hydrogen was added to the feed, the isomerization activity and the selectivity to isobutene slightly decreased.

With Pt-ZSM5 (in the absence of hydrogen) approximately the same butene conversion and the same yield of isobutene were obtained as for the parent material (see Table 2). When hydrogen was added to the feed, Pt acted as a hydrogenation catalyst and large amounts of n-butane were formed. However, also dehydrogenation to butadiene was observed. The isomerization activity was hardly affected by these parallel hydrogenation/dehydrogenation reactions on the metal (compare the values of $iC_4^=/\sum C_4^=$ and of the isomerization rate constant k in Table 2).

Table 2 *Reaction of 1-butene over (Pt-)ZSM5. 775 K, 1 bar, WHSV = 54 h^{-1}. Feed 7.5% 1-butene, 0 or 20% H_2. 100 min on stream.*

Catalyst	ZSM5	Pt-ZSM5	Pt-ZSM5
H_2 (%)	0	0	20
Yield of i-$C_4^=$ (%)	12.8	13.1	10.8
i-$C_4^=/C_4^=$ (%)	13.0	13.3	12.4
Conversion (%)	14.6	15.0	23.7
k (m^3/sg)[a]	$3.5*10^{-5}$	$3.3*10^{-5}$	$3.2*10^{-5}$
Yield by-products (%)			
C_3H_8	0.00	0.00	0.21
C_3H_6	0.90	0.74	1.03
$C_5^=$	0.63	0.91	0.72
n-C_4	0.06	0.05	8.58
$C_4^{==}$	0.04	0.05	1.00

[a] Pseudo first order rate constant of butene isomerization, see appendix.

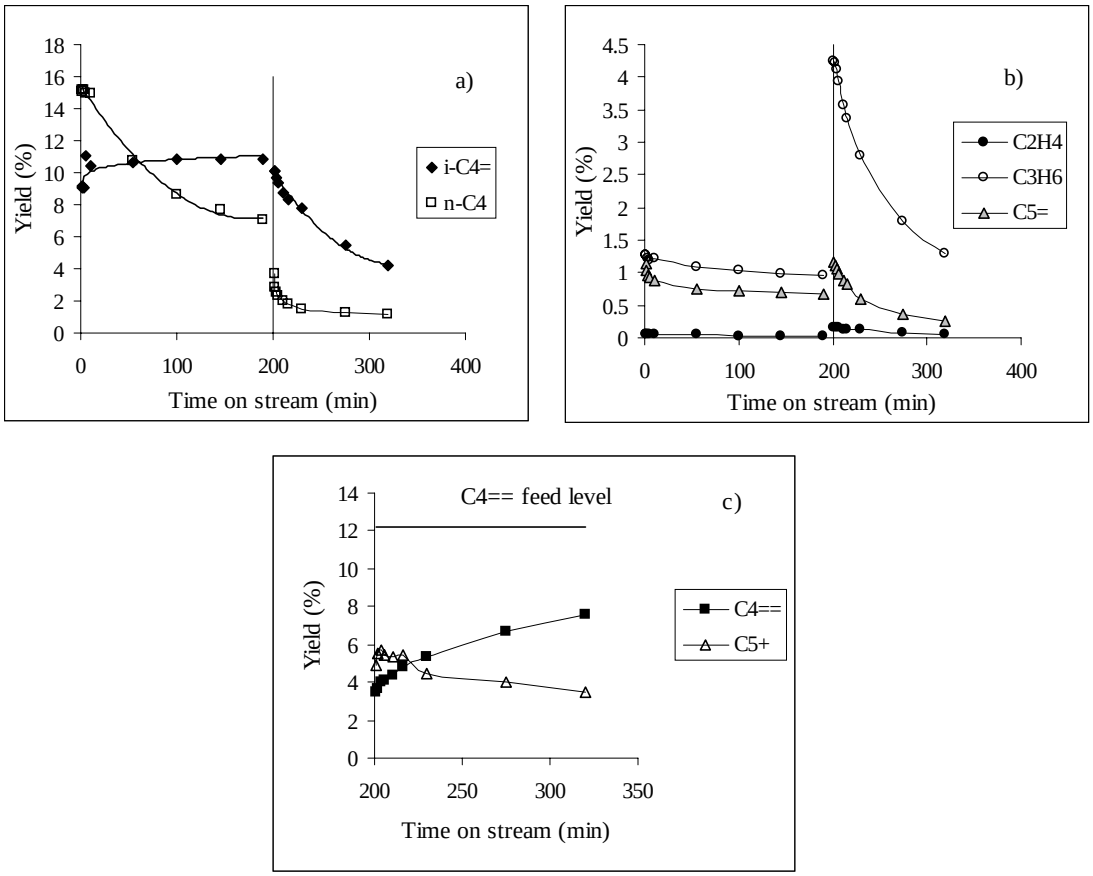

Figure 1 *Pt-ZSM5(480), $WHSV_{C4=}$ = 55 h^{-1}, 775 K, 1.05 bar. Feed 7.5% 1-butene, 20% H_2, 0 or 1% butadiene (The beginning of addition of butadiene was arbitrarily set to 200 min. In reality the catalyst was purged for 90 min in between. See experimental section.) (a) Yield of isobutene and n-butane. (b) Yield of the main by-products. (c) Yield of butadiene and C_5^+.*

Figure 1 shows the effect of butadiene on the conversion of 1-butene over Pt-ZSM5 (in the presence of hydrogen). The formation of both, isobutene and n-butane decreased rapidly in the presence of butadiene. The formation of propene and to a smaller extent also of pentene and ethene, however, was initially enhanced. Moreover, a significant amount of C_5^+ products was formed (see Figure 1c). In the absence of butadiene the yield of these products was lower than 1%.

The initial increase in propene and C_5^+ was followed by a deactivation of all major reaction pathways (isomerization to isobutene, hydrogenation to n-butane and oligomerization/cracking to propene, pentene, C_5^+). At the same time the concentration of butadiene in the reactor effluent slowly increased. It did not reach the feed level within the timeframe of the experiment (see Figure 1c). When the contact

time was increased by a factor of 2 (by doubling the catalyst mass), the build-up of butadiene in the reactor effluent was slower and more propene and C_5^+ was produced. The carbon balance between 15 and 120 min on stream was between 93 and 97%. No clear trends could be observed as a function of time on stream, presence or absence of hydrogen and Pt, or WHSV.

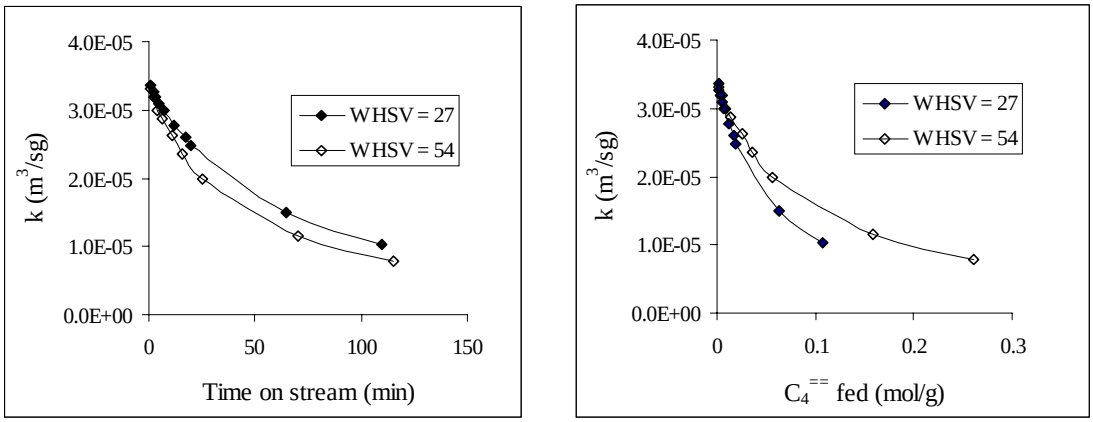

Figure 2 *Pseudo first order rate constant of butene isomerization (a) as a function of time on stream, (b) as a function of the cumulative amount of butadiene fed. Pt-ZSM5(480), 775 K, 1.05 bar. Feed 7.5% 1-butene, 1% butadiene.*

For a quantitative analysis of the data it is better to look at the rate constant of isomerization instead of the yield of isobutene. Figure 2a shows the decrease of the rate constant under influence of butadiene at two different space velocities. The slope (-dk/dt) was bigger at the higher space velocity, because more butadiene was being fed per gram of catalyst. In order to normalize for this effect, the rate constant of butene isomerization was plotted against the cumulative amount of butadiene fed (calculated from the butadiene flow rate in mol/sg multiplied by the time on stream) in Figure 2b. The slope of this curve ($dk/dn_{C4==}$) shows the decrease of the rate constant per mol butadiene fed. ($-dk/dn_{C4==}$) increased with *decreasing* WHSV. In other words, the deactivating effect of one mol butadiene was smaller at the lower contact time (the higher WHSV). Adding hydrogen to the feed also slowed down the rate of deactivation (see Figure 3).

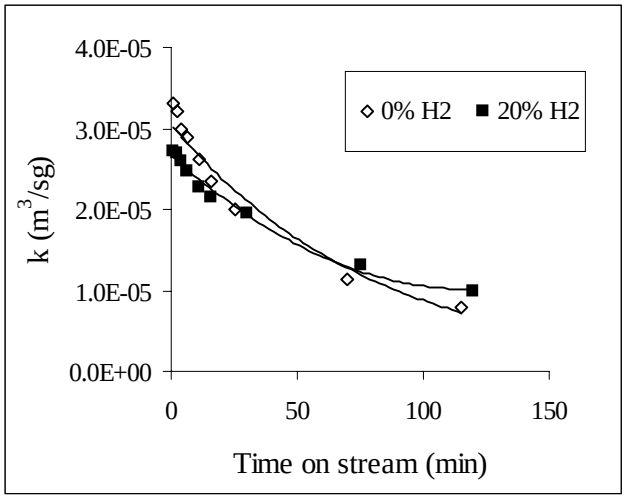

Figure 3 *Pseudo first order rate constant of butene isomerization as a function of time on stream. Pt-ZSM5(480), $WHSV_{C4=}$ = 55 h^{-1}, 775 K, 1.05 bar. Feed 7.5% 1-butene, 1% butadiene, 0 or 20% H_2.*

Table 3 compiles the rates of deactivation calculated from the initial slope of the curves k *vs.* t and k *vs*. $n_{C4==}$ for ZSM5 and Pt-ZSM5, in the presence and absence of H_2.

Table 3 *Rate of deactivation calculated from the slope of the curves k vs. t and k vs. $n_{C4==}$ in the first 30 min. 775 K, 1 bar. Feed 7.5% 1-butene, 1% butadiene, 0 or 20% hydrogen, balance Ar.*

Catalyst	$WHSV_{C4=}$ (h^{-1})	$dn_{C4==}/dt$ (mol/sg)	dk/dt (m^3/s^2g)	$dk/dn_{C4==}$ (m^3/smol)
ZSM5	27	$1.56*10^{-5}$	$-4.0*10^{-9}$	$-2.6*10^{-4}$
	54	$3.98*10^{-5}$	$-7.4*10^{-9}$	$-1.9*10^{-4}$
Pt–ZSM5	27	$1.63*10^{-5}$	$-7.3*10^{-9}$	$-4.5*10^{-4}$
	54	$3.77*10^{-5}$	$-9.0*10^{-9}$	$-2.4*10^{-4}$
Pt-ZSM5, H_2	27	$1.74*10^{-5}$	$-4.1*10^{-9}$	$-2.4*10^{-4}$
	54	$3.64*10^{-5}$	$-4.6*10^{-9}$	$-1.3*10^{-4}$

The reactive adsorption of butadiene on ZSM5 was also studied by IR spectroscopy. Only a very weak hydrocarbon uptake was observed when flowing butadiene over ZSM5(480), resulting in a low signal to noise ratio of the IR spectra of the adsorbed species. Therefore, the IR spectra obtained with a more acidic ZSM5 (SiO_2/Al_2O_3 =

80) are shown in Figure 4. One can mainly see the build up of strong absorptions between 1700 and 1300 cm^{-1}. Their intensity increased with time on stream. Qualitatively, however, the spectra did not change with time. The most intense band was at 1580 cm^{-1}. It is typical for (graphitic) coke species on zeolites [10, 11, 12]. Bands of aliphatic (2925 cm^{-1}) and olefinic/aromatic (3055 cm^{-1}) CH stretching vibrations were extremely weak and can hardly be seen in Figure 4. Due to the low intensity of the CH stretching vibrations, we concluded that the coke was rather poor in hydrogen. All the Brønsted acid sites (see the negative band at 3580 cm^{-1}) and most (~80%) of the silanol groups (negative band at 3730 cm^{-1}) were covered.

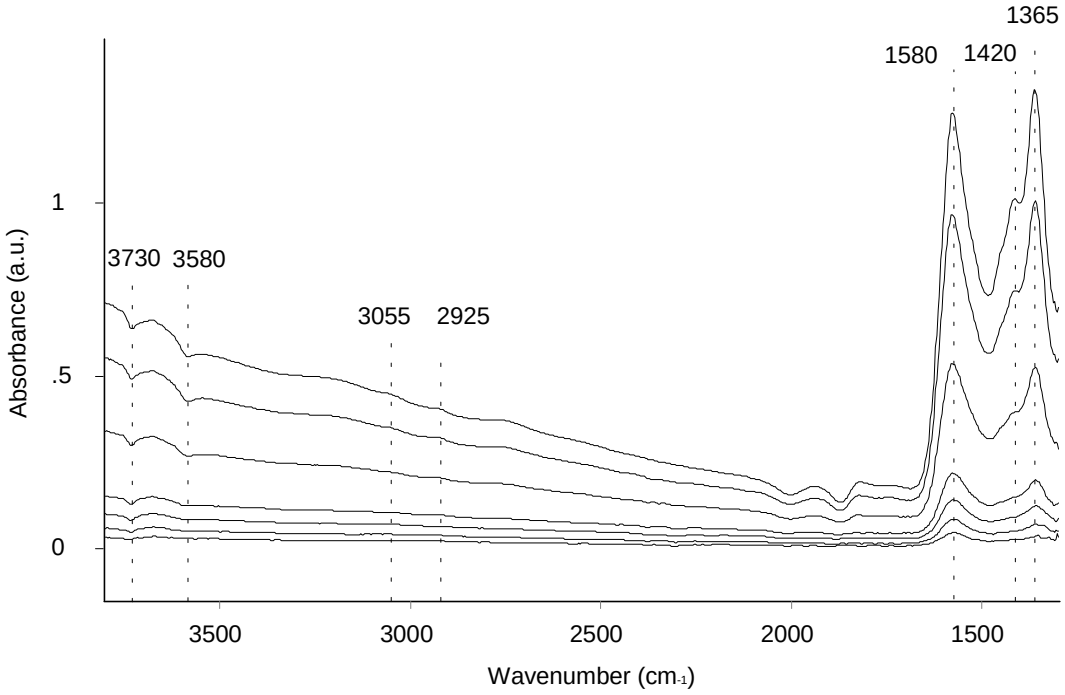

Figure 4 *Reactive adsorption of butadiene on ZSM5(80) at 773 K. Spectra after 3 min, 6 min, 10 min, 15 min, 35 min, 60 min and 105 min (from bottom to top).*

In the reactive adsorption of butadiene on ZSM5(480) we observed qualitatively the same effects. The hydrocarbon uptake of this sample after 1.5 h was, however, 13 times lower than that of ZSM5(80) (see Figure 5). The formation of coke species on the acid sites was irreversible. Flushing for 1 h in a stream of He at 773 K did not lead to any changes in the spectra. Even when 1% Pt was incorporated into ZSM5(80) no desorption was observed upon purging with H_2/He (1/4).

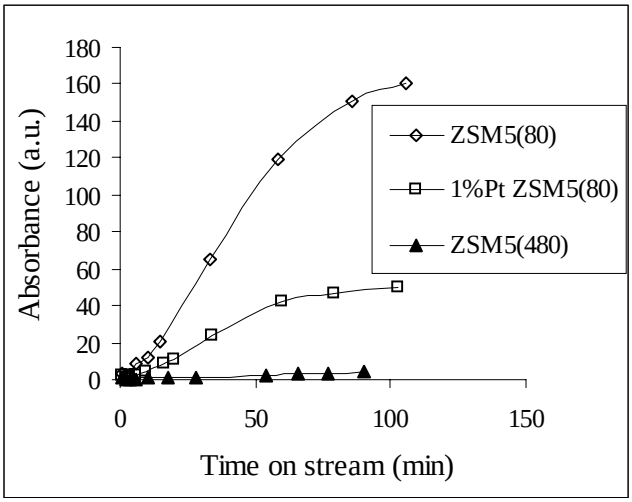

Figure 5 *Reactive adsorption of butadiene on ZSM5(80), 1%Pt-ZSM5(80) and ZSM5(480). Shown is the normalized integral absorbance of the bands between 1670 and 1300 cm^{-1} as a function of time on stream. The relative thickness of the sample disks was 1.17, 0.92 and 1.00, respectively.*

In order to determine whether Brønsted acid sites or silanol groups were the active sites for coke formation, we studied the adsorption of butadiene on Aerosil silica (Degussa, SA = 200 m^2/g). This silica has a high concentration of silanol groups. Adsorption of hydrocarbons was not detected. It was, therefore, concluded that the silanol groups were not active in coke formation under the conditions used.

Butene isomerization over (Pt)-FER in the presence/absence of butadiene

FER was less active and stable than ZSM5, but more selective in the skeletal isomerization of butene (compare the value of k and the selectivity in Table 2 and Table 4). The rates of propene and pentene formation were an order of magnitude lower than for ZSM5. Also the effect of Pt and hydrogen on the catalytic properties of FER differed from the effect on ZSM5. Only small amounts of n-butane were observed, indicating that the hydrogenation activity of Pt in FER was much lower than in ZSM5. Also the formation of butadiene was lower than in the case of Pt-ZSM5 (compare Table 2 and Table 4), but may still be responsible for the faster deactivation of Pt-FER compared to the parent FER (see Figure 6).

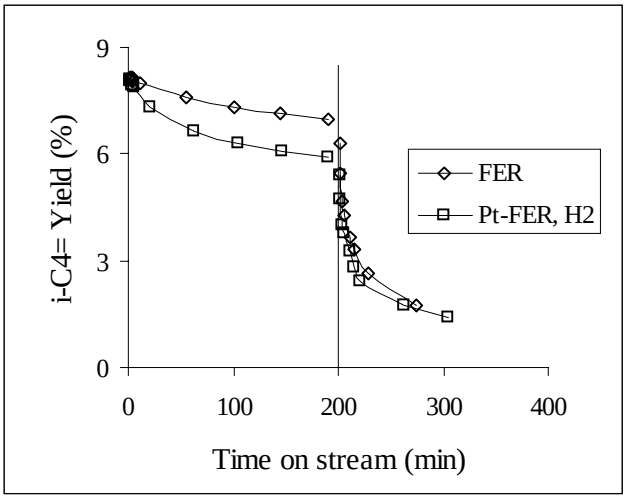

Figure 6 *Deactivation of butene isomerization over (Pt-)FER. 775 K, 1.05 bar, WHSV = 55 h^{-1}. Feed 7.5% 1-butene, 0 or 1% butadiene.*

Table 4 *Reaction of 1-butene over (Pt-)FER and Pt-TON. 775 K, 1 bar, WHSV = 55 h^{-1}. Feed 7.5% 1-butene, 0 or 20% H_2. 100 min on stream.*

Catalyst	FER	Pt-FER	Pt-TON
H_2 (%)	0	20	0
Yield of i-$C_4^=$ (%)	7.3	6.3	16.2
i-$C_4^=$/$C_4^=$ (%)	7.4	6.4	16.6
Conversion (%)	7.8	7.2	18.3
k (m^3/sg)	$1.8*10^{-5}$	$1.4*10^{-5}$	$4.9*10^{-5}$
Yield by-products (%)			
C_3H_6	0.13	0.18	0.81
$C_5^=$	0.15	0.12	0.88
n-C_4	0.01	0.23	0.07
$C_4^{==}$	0.02	0.15	0.08

Upon co-feeding butadiene, qualitatively the same effects were observed as for ZSM5. Initially, the formation of propene and ethene increased, but the formation of these products and the formation of isobutene deactivated very rapidly with time on stream. Especially the initial deactivation was much faster for FER than for ZSM5. Butadiene reached the feed level more quickly. Only traces of C_5^+ products were

found. The presence of Pt and H_2 did not influence the rate of deactivation. The carbon balance was between 96 and 98%.

Table 5 *Rate of deactivation of FER calculated from the initial slope of the curves k vs. t and k vs. $n_{C4==}$ in the first 30 min. 775 K, 1 bar. Feed 7.5% 1-butene, 1% butadiene, 0 or 20% hydrogen, balance Ar.*

$WHSV_{C4=}$ (h^{-1})	ST (sg/m^3)	conc $C_4^{==}$ (%)	$dn_{C4==}/dt$ (mol/sg)	dk/dt (m^3/s^2g)	$dk/dn_{C4==}$ (m^3/smol)
26	9100	1.0	$1.76*10^{-5}$	$-2.2*10^{-8}$	$-1.3*10^{-3}$
54	4800	0.9	$3.18*10^{-5}$	$-2.1*10^{-8}$	$-6.7*10^{-4}$
57	4400	0.4	$1.49*10^{-5}$	$-1.7*10^{-8}$	$-1.1*10^{-3}$

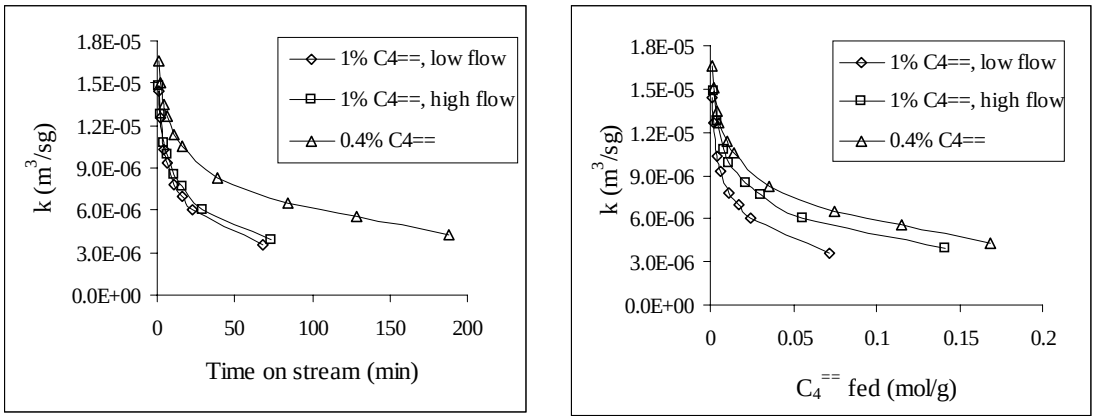

Figure 7 *Pseudo first order rate constant of butene isomerization as a function of (a) time on stream and (b) the cumulative amount of butadiene fed. 775 K, 1.05 bar. Feed 7.5% 1-butene, 0.5 or 1% butadiene. Diamonds: $WHSV_{C4=}$ = 27 h^{-1}, 1% butadiene. Squares: $WHSV_{C4=}$ = 55 h^{-1}, 1% butadiene. Triangles: $WHSV_{C4=}$ = 55 h^{-1}, 0.4% butadiene.*

The effects of butadiene flow rate and concentration on the deactivation of FER are compiled in Table 5 and Figure 7. The rate of deactivation per time (-dk/dt) increased with the concentration of butadiene (compare row 2 and 3 of Table 5). The rate of deactivation per mol of butadiene fed ($-dk/dn_{C4==}$) decreased with the flow rate of butadiene ($dn_{C4==}/dt$) (compare row 1 and 2), but was independent of the concentration (compare row 1 and 3). In other words, ($-dk/dn_{C4==}$) primarily depended on the contact time of butadiene. An increase of ($-dk/dn_{C4==}$) with the contact time had

also been observed for ZSM5 (see Table 3). Note, however, that the values of ($-dk/dn_{C4==}$) are much higher for FER.

When butadiene was adsorbed on FER a very rapid build-up of bands between 1700 and 1300 cm^{-1} was observed by IR spectroscopy. The adsorption reached equilibrium very quickly and was irreversible (desorption in a stream of He for 1 h did not lead to any changes in the spectra). All the Brønsted acid sites seemed to be covered, but due to the low concentration of Brønsted sites a small remaining fraction of the ν(OH) band at 3580 cm^{-1} could have disappeared in the spectral noise. On FER(17) 1/3 of the Brønsted acid sites remained uncovered after adsorption of butadiene which is approximately the fraction of acid sites in the 8-membered ring channels [13]. The integral intensity of the bands between 1670 and 1300 cm^{-1} was 1.6 times higher for this sample than for FER(90). Provided that the Brønsted acid sites are active sites for the coke formation, as in ZSM5, one would expect the coke deposition to increase linearly with acid site concentration. The ratio of Brønsted acid site concentration of the two samples, however, was approximately 4.5 and, thus, much higher than 1.6.

Butene isomerization over Pt-TON in the presence/absence of butadiene

Pt-TON showed a higher activity for butene isomerization than FER and ZSM5. It deactivated with time on stream. Upon co-feeding butadiene, Pt-TON behaved similarly as FER. Only small amounts of C_5^+ products were formed, butadiene built up very fast to its feed concentration and the rate of deactivation was in the same order of magnitude as for FER.

The IR studies of butadiene adsorption on TON, however, revealed a special behavior of the material. The uptake of hydrocarbons was lower than for ZSM5(80), with only 30% of the acid sites covered. Pt-TON and TON showed identical results.

^{13}C-NMR of the coke deposits

ZSM5(80) and FER(17), i.e., the samples with the lowest SiO_2/Al_2O_3 ratio, were chosen for the NMR study. The samples were first reacted in the kinetic setup with 1-butene for 3 h and then for 1 h with the mixture of 1-butene and butadiene, as described in the experimental section. During the 1 h of treatment with the mixture of butene and butadiene, the activity of FER decreased to virtually zero, while that of ZSM5 remained almost unchanged. The hydrocarbon flow was stopped and weakly bound hydrocarbon species were desorbed in a stream of Ar for 1 h before cooling

down to room temperature. A proton-decoupled ^{13}C MAS-NMR spectrum of these samples showed only a very broad, intense band centered around 117 ppm, indicating that the carbonaceous deposits were essentially aromatic and/or olefinic in nature.

In order to improve the spectral resolution, also CPMAS spectra were taken. In CPMAS the signal of ^{13}C attached to ^{1}H is strongly enhanced compared to other carbon atoms [14]. Applying CPMAS lead to a drastic reduction in signal intensity (the number of scans had to be increased by a factor of about 20 to obtain the same signal to noise ratio as in the proton-decoupled experiments), which confirmed that the coke was very poor in hydrogen. The spectra are shown in Figure 8. For FER only one absorption at 130 ppm was found, characteristic for aromatic compounds and/or olefins. On ZSM5 two other absorptions were detected next to the aromatic/olefinic peak, at 88 and 18 ppm. The latter indicated the presence of small amounts of aliphatic carbons, the former was attributed to alkyne species [15].

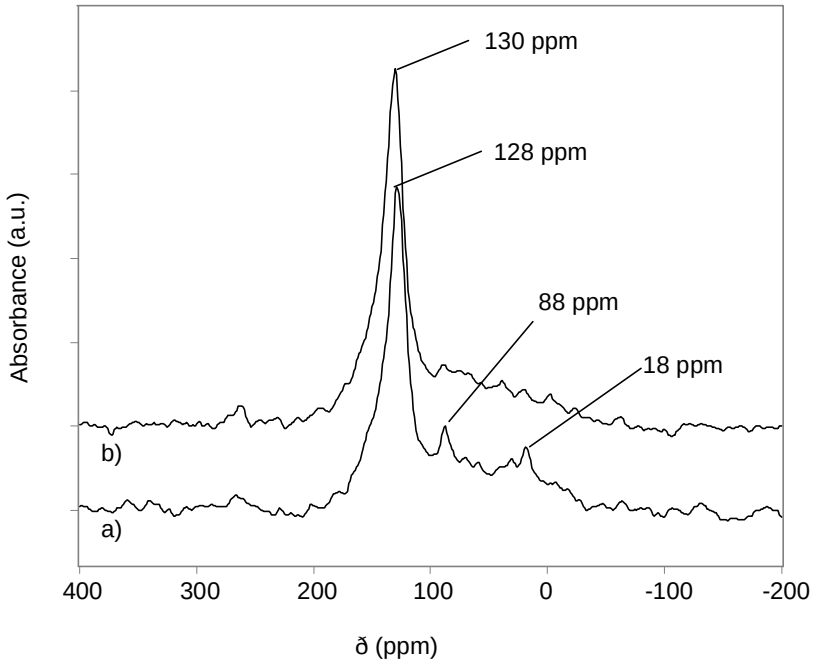

Figure 8 *^{13}C-CPMAS-NMR spectra of a) ZSM5(80) b) FER(19), treated first with butene and then with a mixture of butene/butadiene at 775 K.*

Discussion

Mechanism of deactivation of ZSM5 by butadiene

Butadiene has characteristic IR bands at 1825-1805cm^{-1} and at 1605 and 1585 cm^{-1} (conjugated C=C stretching vibrations) [16]. None of these were observed in the IR

spectra of butadiene in contact with the zeolites. Already the first spectra (taken 30 s after introducing butadiene) showed the same features as those obtained after 1 h. This indicated that at the high reaction temperatures butadiene remained adsorbed on the zeolite only in the form of irreversibly bound species.

The kinetic measurements showed that not only coke, but also cracking products (propene and C_5^+) were formed from butadiene. These products are richer in hydrogen than butadiene, while the coke was very poor in hydrogen (as concluded from IR and NMR measurements), i.e., a disproportionation took place. As the build up of coke proceeded, the formation of all products, even of C_5^+, decreased. After a certain time (which was beyond the time frame of the experiment for ZSM5), the catalyst was completely poisoned and butene and butadiene passed unreacted. Only double bond isomerization of 1-butene still occurred, possibly on weakly acidic sites on the outer surface or on the coke itself.

The higher the contact time of butadiene, the higher was the conversion of butadiene to coke or to cracked products (propene and C_5^+). Consequently, $(-dk/dn_{C4==})$, i.e., the poisoning effect per mol butadiene, was higher at higher contact times.

Comparison of ZSM5, FER and TON

As seen in the result section, the response of FER and TON to co-feeding butadiene was quite different from ZSM5. We focus here on discussing these differences in terms of the pore structure of the materials.

Figure 9 compares the rate of deactivation (at the same contact time) for Pt-ZSM5, FER and Pt-TON. (The kinetic testing had shown that Pt has no influence on the isomerization activity. Thus, FER can be compared with the two other Pt-samples.) Pt-ZSM5 deactivated slower than the two other materials. Assuming that the deactivation is due to a poisoning and/or blocking of active sites (i.e., in the term $k = k_{site} \cdot n_{sites}$, where k_{site} is the rate constant per site and n_{site} the number of sites, only n_{site} changes) one can calculate how many butadiene molecules in the feed are required in order to deactivate one acid site. This number is of the order 2000 for ZSM5, and only about 100 for FER and TON.

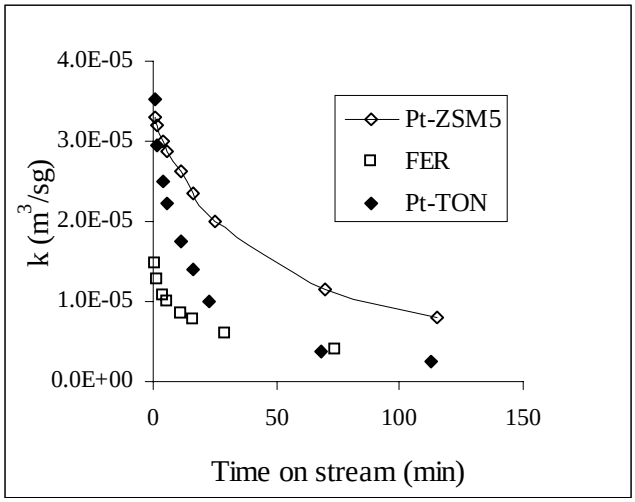

Figure 9 *Pseudo first order rate constant of butene isomerization as a function of time. WHSV = 55 h^{-1}, 775 K, 1.05 bar. Feed 7.5% 1-butene, 1% butadiene.*

In Figure 10 the time on stream behavior of isobutene as well as of propene, C_5^+ and butadiene is shown. On FER and TON the concentration of butadiene in the reactor effluent reached the feed concentration quicker than on ZSM5. The formation of cracking products decreased more rapidly. Table 6 compares the initial rates of propene formation upon co-feeding butadiene. From the difference with the steady state rate of propene formation obtained in butene isomerization, we can see that ZSM5 was three times more active for cracking of butadiene (or its oligomerization products) than FER and TON. Table 6 also compares the yield of propene and C_5^+, based on the butadiene feed. On ZSM5 about 1/3 of the butadiene was converted to propene and C_5^+, for FER it was much less. Especially the yield of C_5^+ was very low on FER.

Table 6 *Rate of propene formation in the absence and presence of butadiene and yield of propene and C_5^+ based on butadiene.*

	FER	TON	ZSM5
C_3H_6 (mol/sg)[a]	$0.4*10^{-6}$	$2.5*10^{-6}$	$2.4*10^{-6}$
C_3H_6 (mol/sg)[b]	$6.4*10^{-6}$	$8.4*10^{-6}$	$19.2*10^{-6}$
Yield C_3H_6 (%)[b, c]	14	11	34
Yield C_5^+ (%)[b, c]	5	21	34

[a] steady state value in butene isomerization

[b] 1min after co-feeding butadiene

[c] based on the conversion of butadiene

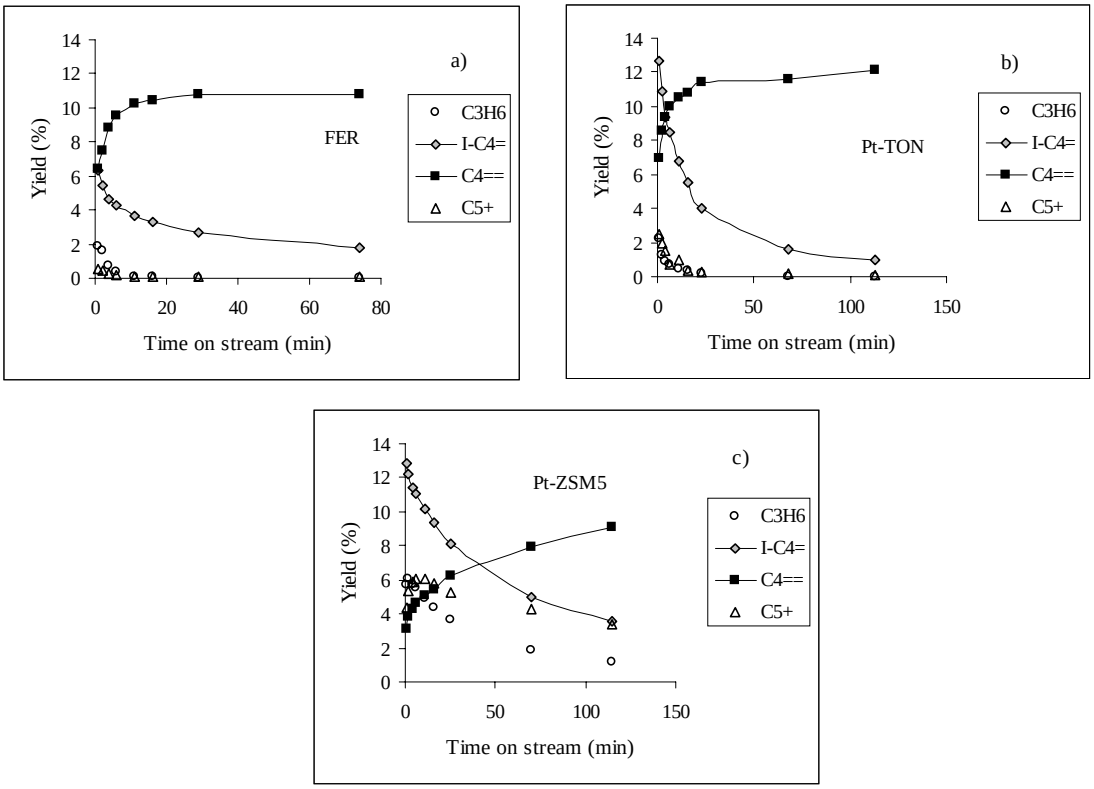

Figure 10 *Time on stream behavior during co-feeding butadiene. a) FER(90). b) Pt-TON(37), c) Pt-ZSM5(480). WHSV = 55 h^{-1}, 775 K, 1.05 bar. Feed 7.5% 1-butene, 1% butadiene.*

The GC-analysis of the reactor effluent gave us no information, however, on the nature and amount of carbonaceous deposits left behind on the catalyst. The accuracy of the carbon balance was insufficient to draw reliable conclusion on the amount of coke deposited as a function of time on stream. Thus, *in situ* IR spectroscopy was applied to characterize the coking process. Figure 11 compares the uptake of hydrocarbon (coke) species as a function of time. The contact time was held approximately constant in these experiments. The graph is analogous to Figure 9. Due to the smaller mass of the IR disks, however, the contact time of butadiene was about a factor of 5 lower than in the kinetic experiments. The uptake values in this graph were calculated from the integral absorbance of the bands between 1670 and 1300 cm^{-1}, using the carbon content at the end of the experiment (determined by CHNO analysis) as a normalization factor. The graph shows that the rate of hydrocarbon uptake (i.e. of coke formation) per butadiene fed decreased in the order FER > TON > ZSM5. The rate of deactivation (-dk/dt) in the kinetic experiments

followed the same order, which clearly showed that coke deposition was responsible for the deactivation.

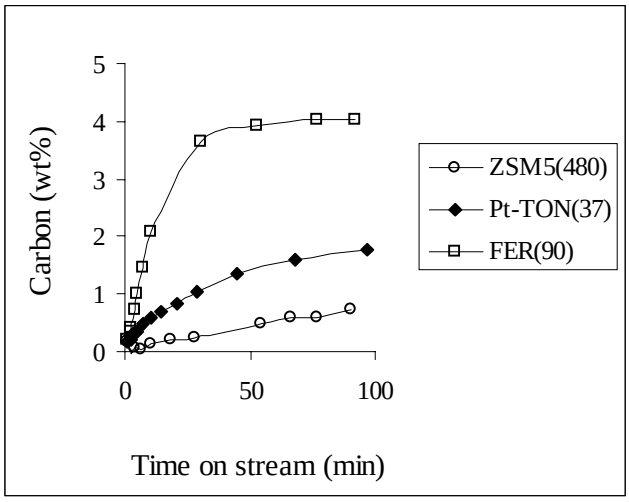

Figure 11 *Build-up of carbonaceous deposits, as measured by IR. The amount of coke was evaluated from the integral intensity of the bands between 1670 and 1300 cm^{-1}, using the carbon content at the end of the experiment (determined by CHNO) as a normalization factor.*

However, different modes of coke formation were operating for ZSM5, FER and TON. Table 7 shows the carbon content of the zeolites and the fraction of Brønsted acid sites and silanol groups covered after adsorption/desorption of butadiene. The build-up of carbonaceous deposits in the samples of similar acid site concentration is shown in Figure 12. In TON very little carbon was deposited and the carbon content after butadiene adsorption/desorption hardly depended on the SiO_2/Al_2O_3 ratio of TON. Only a small fraction of the acid sites, but most of the silanol groups were covered. This indicated that the coke deposition mainly occurred on the outer surface of the material and proceeded only very slowly in the pores of TON, where most of the Brønsted acid sites are located [17]. In a one-dimensional pore system, like that of TON, already a small amount of coke deposited at the entrance of the pores can lead to a fast deactivation by pore blockage [18].

In FER the build-up of carbonaceous deposits was extremely fast and saturation was reached very quickly. Most the acid sites of FER(90) were covered (due to the spectral noise we can only state that the coverage was 75 – 100%). In FER(17) the coke seemed to be deposited only in the 10-membered ring channels. Further access

to the 8-membered ring channels was then blocked. As a result, the amount of coke deposited did not increase linearly with the acid site concentration.

In ZSM5 deactivation occurred by poisoning of the acid sites and the channels were completely filled by carbonaceous deposits.

Table 7 *Concentration of Brønsted acid sites (B) of the parent zeolites. Coverage of Brønsted acid sites and silanol groups, as well as carbon content after reactive adsorption/desorption (1.5 h / 1 h) of butadiene. Contact time was held approximately constant in all the experiments.*

Zeolite	B	Coverage (%) of		Carbon
	(mmol/g)	B	silanol	(wt%)
ZSM5(80)	0.36	100	80	8.9
ZSM5(480)	~0.06	100 (>60)	>80	0.7
FER(17)	1.65	67	0 (<25)	5.3
FER(90)	0.45	100 (>75)	0 (<25)	3.5
TON(35)	0.37	30	75	1.7
TON(72)	0.26	60	80	1.7

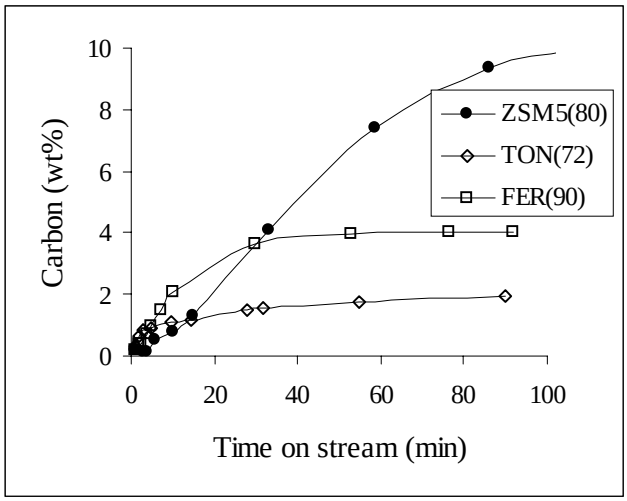

Figure 12 *Build-up of carbonaceous deposits, as measured by IR. The amount of coke was evaluated from the integral intensity of the bands between 1670 and 1300 cm^{-1}, using the carbon content at the end of the experiment (determined by CHNO) as a normalization factor.*

In line with these conclusions the kinetic experiments showed that the relative rate of deactivation (i.e. $-d(k/k_0)/dt$, where k_0 is the rate constant before addition of butadiene) decreased in the order TON > FER > ZSM5 (see Figure 13).

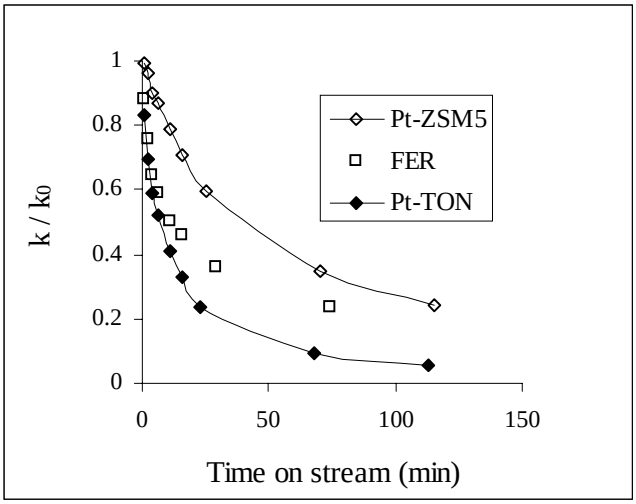

Figure 13 *Relative decrease of the rate constant of butene isomerization as a function of time. k_0 is the rate constant of butene isomerization in the absence of butadiene. k is the actual rate constant during the experiment. WHSV = 55 h^{-1}, 775 K, 1.05 bar. Feed 7.5% 1-butene, 1% butadiene.*

Not only the rate of coke formation differed for the three zeolites, but also the nature of the species which were deposited. The IR spectra measured after reactive adsorption/desorption of butadiene are shown in Figure 14. The most prominent bands of the coke in ZSM5 appeared at 1585, 1370 and 1430 cm^{-1}. The former is attributed to graphitic coke species [10, 11, 12]. The band at 1370 cm^{-1} is usually assigned to CH_3 deformation vibrations [19]. But this contradicts with the fact that only very weak bands for the corresponding CH_3 stretching vibrations could be found. Similarly, the band at 1430 cm^{-1} is usually attributed to the deformation vibrations of CH_2 groups attached to aromatic rings (unsaturation next to a CH_2 group lowers the frequency of its deformation vibration [19]), but again the CH_2 stretching vibrations are comparably weak.

The spectrum of the butadiene coke on ZSM5 is very similar to the spectrum of high temperature coke (650 K) produced by oligomerization of ethene on H-ZSM5 [10] and H-MOR [20]. For the latter it was shown by ^{13}C-NMR that the coke contains mainly olefinic and/or aromatic and only traces of paraffinic carbons. This was confirmed by our own NMR results. Thus, the absorbance at 1370 cm^{-1} should be

related to the graphitic coke species itself rather than to methyl-substituents (the same conclusion was drawn by Ghosh *et al*. in [11]). We therefore tentatively attribute the bands at 1430 cm^{-1} and 1370 cm^{-1} to aromatic ring deformation vibrations, which are shifted to unusually low wavenumbers by coupling to other vibrational modes. The absorption coefficient of aromatic ring vibrations is often much higher than of the corresponding aromatic CH stretching vibrations, so that the absence of intense ν(CH) bands above 3000 cm^{-1} is not surprising.

We want to mention that the intensity of the band at 1370 cm^{-1} was much higher than the one at 1585 cm^{-1}, when butadiene was adsorbed on ZSM5 at 623 K instead of 773 K. It was also very intense in the IR spectrum of coke formed in the MTG process at 693 K on ZSM5 [21]. The fact that its intensity was relatively higher at lower temperatures indicates that the band at 1370 cm^{-1} could be related to less highly condensed aromatic species than the "coke" band at 1585 cm^{-1}.

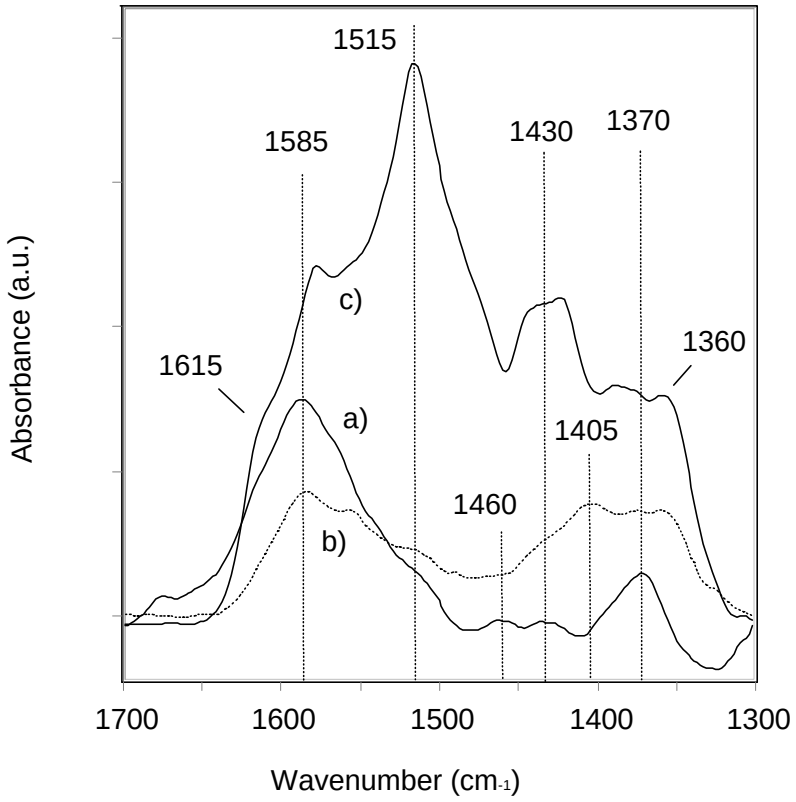

Figure 14 *IR spectra after reactive adsorption of butadiene at 773K. Spectra were measured after cooling to 473K. a) ZSM5(480), x 10. b) TON(37). c) FER(90).*

The spectrum of coke on FER differed qualitatively from ZSM5. The most prominent bands were found at 1515 and 1430 cm^{-1}. Moreover, weaker bands were found at 1580 and 1600 cm^{-1}. These bands are characteristic for substituted aromatic species

[19] (ring vibrations). The fact that the bands at 1580 and 1600 cm^{-1} were rather weak compared to the absorption at 1515 cm^{-1} indicated that para-substituted species dominated. (In para-substituted benzene rings the bands at 1585 and 1600 cm^{-1} are missing for reasons of symmetry. There is no change in the dipol moment for the quadrant stretching mode of the benzene ring which leads to the doublet of bands near 1600 cm^{-1} [19].)

The formation of para-substituted phenyl-species in FER may also explain why the access to the 8-membered ring channels got blocked. Kaskur *et al.* [22] concluded from a XRD and computational study of the adsorption of para-xylene in FER that the molecule is always located in the 10-membered ring channels and not in the 8-membered ring channels. Obviously long, linear aromatic molecules are not flexible enough to enter the 8-membered ring channels and also block the access of other molecules to the small channels.

The band attributed to graphitic coke at 1585 cm^{-1} was less prominent in FER than in ZSM5. This was explained by the fact that the pore system of FER does not easily allow the formation of larger (non-linear) coke-molecules.

In the IR spectrum of coked TON bands at 1585, 1555, 1515, 1405 and 1375 and 1360 cm^{-1} could be distinguished. Compared to ZSM5, the intensity of the bands at 1585 and around 1370 cm^{-1} was less pronounced (relative to the other bands). The spectrum of TON seemed to be a mixture of the bands on FER and ZSM5, indicating that the coke was not as graphitic as on ZSM5, but also did not mainly consist of para-substituted phenyl-species as in FER. The latter conclusion is consistent with the finding that coke was mainly formed on the outer surface of TON where shape-selectivity like in the pores of FER does not exist.

The fact that coke is mainly formed on the outer surface of TON, but in the pores of FER cannot be easily understood from the pore structure of the two materials. The dimensions of the 10-membered ring channels are almost identical (4.2 x 5.4 Å for FER, 4.4 x 5.5 Å for TON). We believe that there are two reasons for the different behavior of the two materials. (i) TON had a much higher concentration of defect sites than FER, as indicated by the higher concentration of silanol groups and of Lewis acid sites, compared to FER. These defect sites could be the active sites for the coke formation on TON, rather than the Brønsted acid sites located in the pores. (ii) FER was very active in the polymerization/cyclization of butadiene. The coke formation propagated very fast in the pores of FER. Such a behavior was not observed

for TON and ZSM5 (which could be related to the higher activity of these materials in cracking of butadiene and its oligomers). Thus, the different behavior of FER and TON could be due to a combination of a higher activity of TON for coke formation on the outer surface (catalyzed by defect sites) and a higher activity of FER for coke formation in the pores (due to the low cracking activity of FER).

Conclusions

The presence of butadiene in the feed leads to a fast deactivation of butene isomerization activity of the zeolites ZSM5, FER and TON. Butadiene is partly cracked to propene, partly converted to higher hydrocarbons (C_5^+), a part passes unreacted and a part remains adsorbed as coke on the catalyst. The rate of deactivation per mol of butadiene increases with contact time. The presence of Pt and hydrogen cannot prevent the deactivation, but it is slowed down, obviously because the build up of unsaturated, polymeric coke species is counteracted by the hydrogenation activity of Pt.

ZSM5 is less sensitive to butadiene than FER and TON. Mainly two factors contribute to the higher stability of ZSM5. (i) Deactivation occurs by actual poisoning of the acid sites and not by pore-blocking like in TON. (ii) The deposition of coke is slowed down, because ZSM5 is very active in cracking oligomeric coke-precursors to propene and C_5^+. In FER, this cracking activity is very low, as a result the build-up of coke occurs much faster. Once aromatic species are formed in FER their diffusion out of the pores is very slow [23] which increases the chance that they oligomerize further. Note that while the high oligomer-cracking activity of ZSM5 is a disadvantage for the selectivity of this material in butene isomerization it actually contributes to the higher stability to deactivation by butadiene. As a result, we can expect that ZSM5 should give a more stable performance when applied for dehydroisomerization at high temperatures than FER and TON.

Acknowledgements

I am very grateful to M.J.G. Janssen, from Exxon Chemical International Inc., Basic Chemicals Technology Europe, and G. Kinger, from the Technical University of Vienna, for supplying the FER and TON samples, which made this work possible. I would like to thank G.H. Nachtegaal (NOW/CW HF-NMR Facility, University of

Nijmegen), who designed and performed the NMR experiments, M. Rep, who contributed to the interpretation of the IR spectra, and especially L. Domokos for his valuable comments on this work.

Appendix – Calculation of the first order rate constant of butene isomerization

The skeletal isomerization of n-butene is an equilibrium reaction. Due to the backward reaction the observed reaction rate is lower than the intrinsic rate. In order to correct for this effect, a simple first order kinetic model was assumed.

$$A \rightleftharpoons B \qquad r = d[B]/dST = k_1 \cdot [A] - k_{-1} \cdot [B] \qquad (1.)$$

The reaction rate r is given in mol/sg_{cat}, the space time $ST = m_{cat}/(dV_{total}/dt)$ in sg_{cat}/m^3, the rate constant k in m^3/sg_{cat}, the concentration of A and B in mol/m^3. A represents the sum of linear butenes, B isobutene. In this approach the three separate equilibria between 1-butene, trans-2-butene, cis-2-butene and isobutene are lumped into one overall equilibrium between n-butene and isobutene with the equilibrium constant $K = [isobutene]_{eq}/([cis\text{-}2\text{-}butene]_{eq}+[trans\text{-}2\text{-}butene]_{eq}+[1\text{-}butene]_{eq})$. This is allowed if the n-butenes are in thermodynamic equilibrium which is usually the case.

The integration of equation (1.) yields

$$k_1 = \frac{1}{ST} \cdot \frac{K}{1+K} \cdot \ln\left(1 - x - \frac{x}{K}\right) \qquad (2.)$$

where $x = [i\text{-}C_4^{=}]/\sum[C_4^{=}]$, K = equilibrium constant.

Equation (2.) was used to calculate the pseudo first order rate constant of dehydrogenation (k_1) from the experimental ratios $[i\text{-}C_4^{=}]/\sum[C_4^{=}]$.

In the derivation of (2.) the assumption was made that both the forward and backward reaction are first order. Our own results indicated that butene isomerization on ZSM5 is indeed first order in butene. For FER Guisnet *et al.* [7] reported orders between 0.5 and 1 for the forward and backward reaction. However, if the reactant concentration does not change too much (i.e. at low conversions), any rate law can be approximated by a (pseudo) first order rate law. Therefore equation (2.) can always be used as an approximation, even if the exact kinetics is not known, provided that the same inlet concentrations are used and the conversion is low.

Note also that the rate constant was calculated from the ratio $[i\text{-}C_4^=]/\sum[C_4^=]$. Secondary or parallel side reactions were not taken into account. At butene selectivities below 80% this may lead to significant errors in the calculated first order rate constant.

References:

[1] Houzvicka, J., Nienhuis, J.G., Hansildaar, S., and Ponec, V., Appl. Catal. A **165**, 443 (1997).

[2] Baeck, S.H., and Lee, W.Y. Appl. Catal. **164** (1997) 291.

[3] Barri, S.A.I., Walker, D.W., and Tahir, R., EP Patent 247.802 (1990), assigned to The British Petroleum Company

[4] R. Byggningsbacka, R., Kumar, N., Lindfors, L.-E., J. Catal. **178**, 611 (1998).

[5] Mooiweer, H.H., de Jong, K.P., Kraushaar-Czarnetzki, B., Stork, W.H.J. and Krutzen, B.C.H., Stud. Surf. Sci. Catal. 84, 2327 (1994).

[6] Grandvallet, P., de Jong, K.P., Mooiweer, H.H., Kortbeek, A.G.T., and Kraushaar-Czarnetzki, B., EP Patent 501.577 (1992), assigned to Shell Internationale Research Maatschappij B.V.

[7] Guisnet, M., Andy, P., Gnep, N.S., Benazzi, E., and Travers, C., J. Catal. **158**, 551 (1996).

[8] Xu, W.-Q., Yin, Y.-G., Suib, St.L. Edwards, J.C., and O'Young, Ch.-L., J. Phys. Chem. 99, 9443 (1995).

[9] Mirth, G., Eder, F., and Lercher, J.A., Appl. Spectroscopy **48**, 194 (1994).

[10] Karge, H.G., and Boldingh, E., Catal. Today **3**, 379 (1988).

[11] Ghosh, A.K., and Kydd, R.A., J. Catal. **100**, 185 (1986).

[12] Blackmond, D.G., Goodwin, J.G., and Lester, J.E., J. Catal. **78**, 34 (1982).

[13] Sarv, P., Wichterlova, B., and Cejka, J., J. Phys. Chem. B **102**, 1372 (1998).

[14] Koenig, J.L, "Spectroscopy of Polymers", American Chemical Society, Washington DC, 1992.

[15] Levy, G.C., and Nelson, G.L., "Carbon-13 Nuclear Magnetic Resonance for Organic Chemists", p.71, Wiley-Interscience, New York, 1972.

[16] Voskoboinikov, T.V., Coq, B., Fajula, F., Brown, R., McDougall, G., and Couturier, J.L., Micropor. Mesopor. Mat. **24**, 89 (1998).

[17] Pieterse, J.A.Z., Reyes-Gonzales, S., Seshan, K., and Lercher, J.A., submitted to J. Am. Chem. Soc.

[18] Guisnet, M., and Magnoux, P., Appl. Catal. **54**, 1 (1989).

[19] Colthup, N.B., Daly, L.H. and Wiberly, S.E., "Introduction to Infrared and Raman Spectroscopy", Academic Press, New York, 1975.

[20] Lange, J.-P., Gutzse, A., Allgeier, J., and Karge, H.G., Appl. Catal. **45** (1988), 345.

[21] Bauer, F., Geidel, E., Geyer, W., and Peuker, Ch., Micropor. and Mesopor. Mat. **29**, 109 (1999).

[22] Kaskur, Z.A., Jones, R.H., Bell, R.G., Catlow, C.R.A., and Thomas, J.M., Mol. Physics **89**, 1345 (1996).

[23] Andy, P., Gnep, N.S., Guisnet, M., Benazzi, E., and Travers, C., J. Catal. **173**, 322 (1998).

Chapter 8

The effect of zeolite pore structure in the dehydroisomerization of n-butane

Abstract

The catalytic properties of Pt-ZSM5, Pt-TON and Pt-FER in dehydroisomerization of n-butane were compared. Pt-ZSM5 gave the highest yield of isobutene and also the lowest selectivity to by-products. Most of by-products of Pt-ZSM5 were formed by oligomerization/cracking of butene, while acid catalyzed cracking and metal catalyzed hydrogenolysis of n-butane played a larger role with Pt-TON and especially with Pt-FER. Butene isomerization and cracking of n-butane are both acid catalyzed. But since the rate of n-butane cracking depends stronger on the concentration of acid sites than the rate of butene isomerization, low acid site concentrations are desirable for dehydroisomerization catalysts. The dehydrogenation activity of the Pt-zeolites is not primarily related to the dispersion of the metal. Pt-FER had the highest dispersion, but the lowest dehydrogenation activity. This was attributed to diffusional constraints in the narrow pores of ferrierite.

Introduction

Pt-ZSM5 is a good catalyst for the dehydroisomerization of n-butane, as shown in Chapters 4 and 6. But its potential for further improvement is limited by the rather high selectivity to oligomerization/cracking of this material. This property is inherent to ZSM5 and related to the fact that the pores of ZSM5 are too large to obtain a high selectivity to butene isomerization [1]. Better results should be achieved by using other microporous materials that have a higher selectivity to butene isomerization *vs.* oligomerization/cracking than ZSM5. Several materials have been successfully used for the skeletal isomerization of butene, e.g., FER [2, 3, 4], TON [5, 6], ZSM-23 [7], SAPO-11 [8], MeAPOs [9], MCM22 [10], etc. From these, the zeolites TON and FER were chosen. For both materials excellent selectivities in butene isomerization have been reported in patent literature [11, 12]. Their framework structures are sufficiently stable for use at the high temperatures employed in the dehydroisomerization reaction.

The objective of the work was to transform the good catalytic performance of FER and TON in butene isomerization to a good catalytic performance of Pt-FER and Pt-TON in dehydroisomerization of n-butane. The respective results are discussed in terms of the effect of zeolite structure, acid site concentration and metal dispersion on the catalytic properties.

Experimental

Catalyst preparation

ZSM5 (SiO_2/Al_2O_3 = 480) was received from ZEOLYST Int. (sample code CBV10002). K-FER with a SiO_2/Al_2O_3 ratio of 17 was provided by TOSOH. In order to obtain the ammonium form, the sample was ion-exchanged three times for 12 h at room temperature with 1M NH_4NO_3 solution. Two FER samples, with SiO_2/Al_2O_3 ratios of 90 and 670, respectively, were provided by Exxon Chemicals Europe. FER(90) was received in the as synthesized form. In order to remove the template, the sample was calcined for 2 h at 798 K (temperature increment 2 K/min) in N_2, then cooled to 573 K and finally calcined in air at 798 K (temperature increment 2 K/min) for 4 h. The template-free zeolite was ion exchanged three times with 1 M NH_4NO_3 solution in the same way as described above. FER(670) was already received in the ammonium form.

Mg-TON (SiO_2/Al_2O_3 = 35) was received from Exxon Chemicals Europe. In order to obtain the ammonium form, the sample was ion exchanged two times with 1 M NH_4NO_3 solution and once with 0.01 M NH_4NO_3 solution (each time for about 12 h). NH_4-TON with a SiO_2/Al_2O_3 of 72 (synthesized according to the procedure described in ref. [13]) was received from the Technical University of Vienna.

Pt was incorporated by slow addition of a dilute aqueous solution of $Pt(NH_3)_4(OH)_2$ (0.1 mg Pt/l) and NH_3 (~2%) to a suspension of the zeolite in doubly distilled water (10 ml H_2O/g zeolite) (see Chapter 2). After stirring for 12 h the sample was filtered and dried. Subsequently, it was calcined at either 523 K or 723 K (temperature increment 0.5 K/min) in air for 2 h and pre-reduced at either 673 K or 773 K (temperature increment 5 K/min) in H_2 for 2 h. Because the catalysts were reduced *in situ* at even higher temperatures (1 h at 823 K) before use in the reaction, the choice of the calcination procedure had no effect on the catalytic behavior.

The samples were characterized by X-ray fluorescence (elemental composition) and pyridine adsorption (concentration of Lewis and Brønsted acid sites) [14]. The results are given in Table 1. In the following text the SiO_2/Al_2O_3 ratio of the samples is indicated in brackets at the end of the name. The morphology of the samples was determined by SEM (see Table 2 and General Appendix B).

Table 1 *Physico-chemical characterization of the samples. SiO_2/Al_2O_3 ratio, Al-, and Pt-content were determined by XRF, the total concentration of acid sites and the ratio of Lewis acid sites (L) to the total number of acid sites (L + B) by adsorption of pyridine (IR).*

Sample	Pt-loading (wt%)	SiO_2/Al_2O_3	Al (mmol/g)	(L + B) (mmol/g)		L/(L+B) (%)	
				parent	Pt	parent	Pt
ZSM5(480)	0.09	480	0.07	n.d.	0.05	n.d.	38
FER(17)	0.10	17	1.79	1.7	1.65	4	7
	0.31	19	1.59	1.7	n.d.	4	n.d.
FER(90)	0.10	89	0.37	0.45	n.d.	4	n.d.
FER(670)	0.10	670	0.05	n.d.	n.d.	n.d.	n.d.
TON(35)	0.11	35	0.92	0.4	0.5	23	26
TON(72)	0.09	72	0.45	0.25	n.d.	17	n.d.

n.d. = not determined

Table 2 *Morphology of the samples, as analyzed by SEM.*

Sample	Morphology
0.1%Pt-ZSM5(480)	spheres, 1-4 µm
0.1%Pt-FER(17)	platelets, length 0.5 –1.5 µm
FER(90)	platelets, 6-10 µm (also some smaller ones, down to 2 µm)
0.1%Pt-FER(670)	platelets, needles, 4 µm
0.1%Pt-TON(35)	needles, length 1-3 µm, plus smaller particles
0.1%Pt-TON(72)	needles, length 1 µm, plus smaller particles (0.1-0.2 µm)

Catalytic testing

The catalysts were mixed with about 60 mg quartz and placed in a quartz reactor of 4 mm inner diameter. Each sample was activated *in situ* in a flow of 25 ml/min H_2/Ar (20/80) at 830 K for 1 h and then cooled to reaction temperature. The reaction was carried out at 775 K and atmospheric pressure. 775 K was chosen as the reaction temperature in order to minimize catalyst deactivation (see Chapter 6). The reaction was started by switching the reactor inlet to a mixture of 10% n-butane, 20% H_2, the balance being Ar. In the first minutes on stream the reactor effluent was stored in sample loops for post-run GC analysis. After 10 min, the reactor effluent was analyzed on-line in intervals of about 45 min, without making use of the storage loops. Yields and selectivities are reported on a basis of mol% carbon converted.

Characterization of Pt

High Resolution Electron Microscopy (HREM) was applied to study the size and location of the Pt particles (see Chapter 2). In addition, two test reaction were used to quantify the amount of Pt on the outer surface and in the pores of the zeolite, (i) the hydrogenation of 2,4,4-trimethyl-1-pentene (244TMPe) and (ii) the hydrogenation of ethene [15]. 244TMPe is too large to enter the pores of 10-ring zeolites [16] and can therefore react only on the outer surface. Ethene, on the other hand, can easily diffuse into the zeolite channels. The hydrogenation rate of ethene and of 244TMPe should, therefore, give a measure of the total concentration of accessible metal sites and of the metal on the external surface, respectively.
For both test reactions, the catalyst was reduced *in situ* at 830 K for 1 h in a combined flow of 5 ml/min H_2 and 20 ml/min Ar at atmospheric pressure. Afterwards the reactor was cooled to 425 K. Then, during 30 minutes, the bed was flushed with approximately 20 ml/min of a mixture containing 20% NH_3 in He. Subsequently, weakly bound NH_3 was desorbed for 2 h

in a stream of 25 ml/min Ar. The purpose of the NH_3 treatment was to deactivate acid sites, which could catalyze unwanted isomerization reactions of 244TMPe. For ethene, the NH_3 treatment was omitted. Finally, the catalyst was cooled to reaction temperature. The reaction was started by switching from Ar to the alkene/H_2 feed. The feed composition for ethene hydrogenation were chosen in analogy to ref. [15], i.e., 3% ethene, 20% H_2, the balance being Ar. The reaction temperature of 273 K was kept constant by an ice bath. The catalyst mass was 10 mg, the total flow 45 ml/min.

For the hydrogenation of 244TMPe, the feed composition was 0.3% 244TMPe, 88% H_2, the balance being Ar. The reaction temperature was 293 K, the catalyst mass 10 mg, the total flow 175 ml/min. Both reactions were carried out at atmospheric pressure.

Pt-SiO_2 (0.1 wt% Pt, Aerosil SiO_2 Degussa, SA = 200 m^2/g), prepared according to the method of Benesi *et al.* [17], was used as a reference for the test reactions. Since the silica support is non-porous [18], all Pt in this material was necessarily located on the outer surface.

Results

Characterization of Pt particle size and accessible Pt

For both, 0.1 and 0.3%Pt-FER(17), only small Pt-particles (0.5-3 nm) were found by high resolution electron microscopy which were distributed throughout the zeolite and most likely located in the zeolite channel system (Figure 1a). For 0.1%Pt-FER(90), on the other hand, mainly intermediate size (3-10 nm) Pt particles were found. Some were located at or at least near to the outer surface, some were located inside the crystal (Figure 1b).

The HREM photos of Pt-TON(35) also showed only small Pt particles (0.5-4 nm). Their location could not be clearly determined from the pictures. Some seemed to be located inside the zeolite channel system, some on the outer surface. In Pt-TON(72) also mainly small particles were found (1- 5 nm). A certain accumulation at the edge of the crystals (see Figure 1c) indicated that a significant fraction was located on the outer surface.

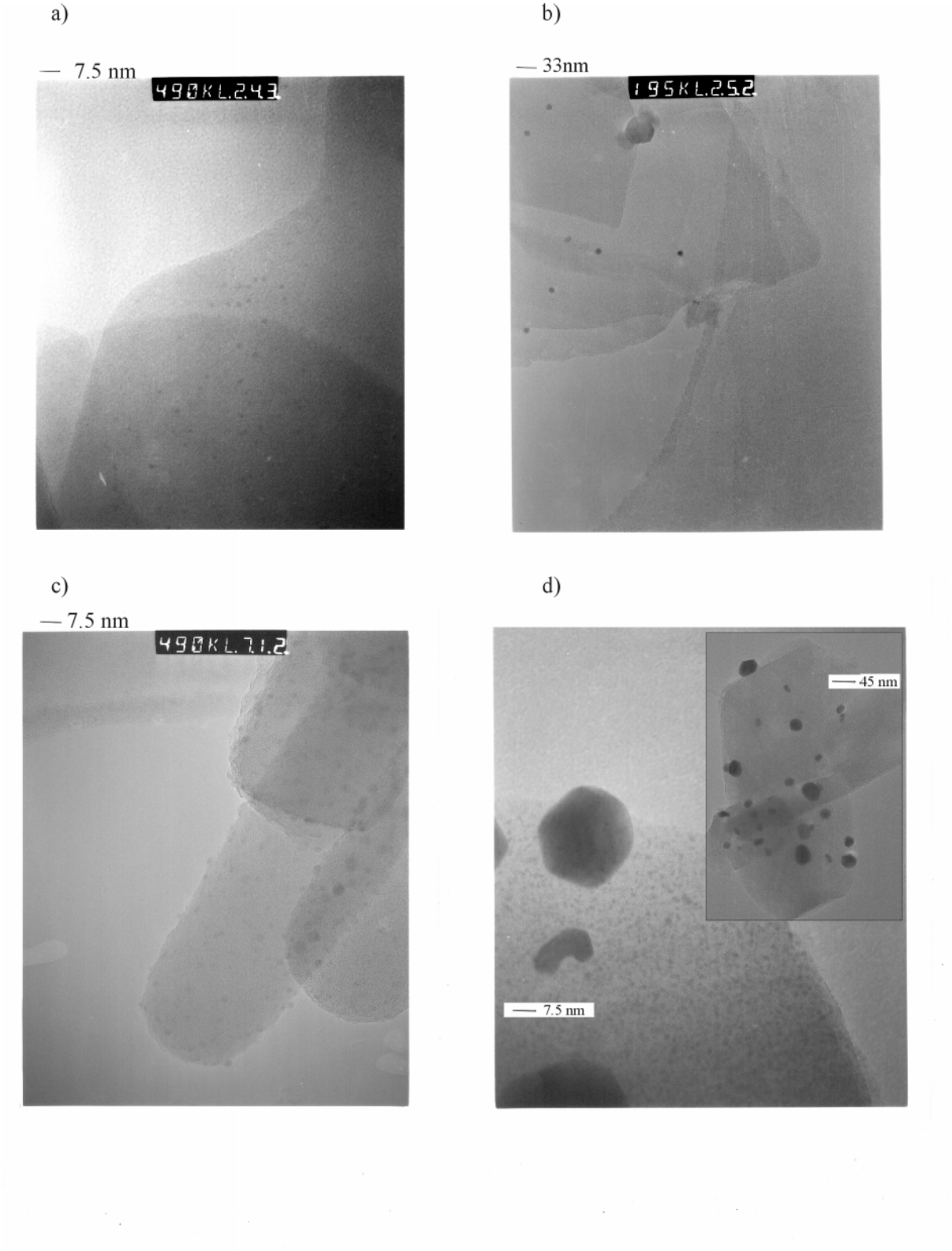

Figure 1 *HREM photos of (a) 0.1%Pt-FER(17) (b) 0.1%Pt-FER(90) (c) 0.1%Pt-TON(72) (d) 0.1%Pt-ZSM5(480).*

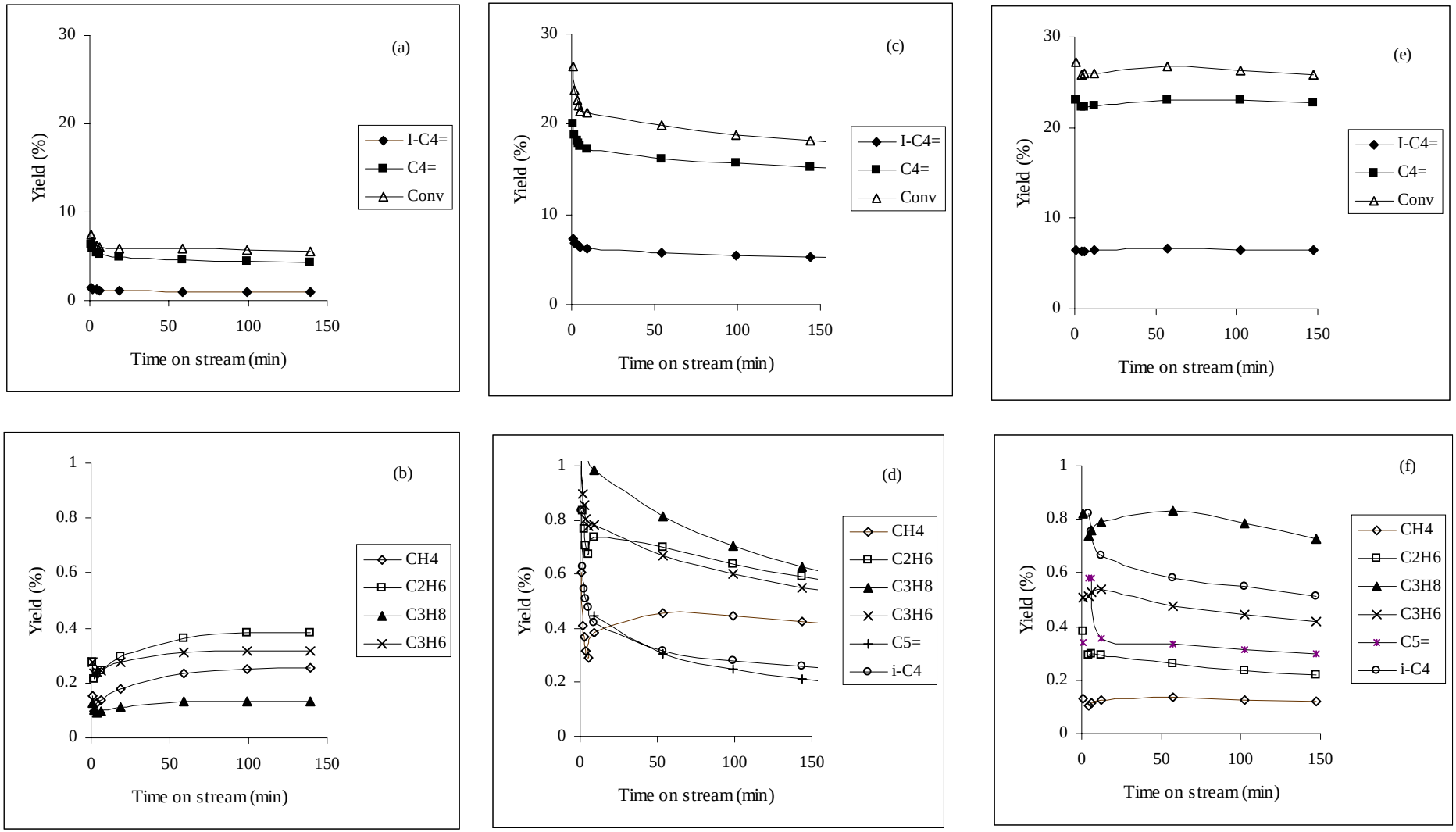

Figure 2 *Time-on-stream behavior in dehydroisomerization. (a, b) 0.1%Pt-FER(90) (c, d) 0.1% Pt-TON(35). (e, f) 0.1% Pt-ZSM5(480). 775 K, 1.0 bar, WHSV = 14 h^{-1}. Feed 10% n-butane, 20% H_2, balance Ar.*

In contrast to the results obtained with FER and TON, the Pt distribution in ZSM5(480) was very inhomogeneous with respect to particle size and location (Figure 1d). Large Pt particles (15-45 nm) were found at the external surface of the zeolite, next to small particles inside the channel system. In some areas an accumulation of Pt on the outer surface was observed, in other areas no Pt particles could be found. Additional EDX analysis also did not show Pt in these areas. Similar results were found for ZSM5(480) with a metal loading of 0.5 wt%.

The general trend observed in the HREM measurements was that the samples with lower SiO_2/Al_2O_3 ratio had smaller Pt particles. This could be related to the higher ion exchange capacity and the resulting better stabilization of Pt ions in these samples.

HREM measures only a small fraction of the sample and gives only qualitative information on the dispersion and location of the metal. Thus, test reactions were employed in an attempt to quantify the amount of accessible Pt located on the outer surface and in the pores of the zeolite. The rate of hydrogenation of 244TMPe, which is too large to enter the pores of 10-ring zeolites [16], should give a measure of the concentration of Pt on the outer surface of the zeolite. Ethene, on the other hand, can diffuse into the zeolite pores. Its hydrogenation rate should, thus, be representative for the total concentration of accessible Pt. Since hydrogenation of alkenes was reported to be a structure insensitive reaction [15, 19, 20], the rate of hydrogenation is directly proportional to the accessible Pt surface area. The hydrogenation activities are reported in Table 3.

Pt-FER(17) had an extraordinarily high activity for the hydrogenation of ethene. In order to check whether this high activity was related to the high acid site concentration of Pt-FER(17) (1.7 mmol/g), we measured two Pt-ZSM5 samples of different acid site concentrations (0.05 and 0.26 mmol/g, respectively). The two ZSM5-samples gave similar activities for the hydrogenation of ethene. This suggests that sorption on the acid sites affects the observed reaction rates if the acid site concentration is very high, but has little effect on samples of lower acid site density. We, therefore, believe that – with the exception of Pt-FER(17) – the ethene hydrogenation rate correctly represents the metal dispersion.

Absolute dispersion values calculated from this data using turn over frequencies given in ref. [15] are in the order of 100% and above. The turn over frequencies in ref. [15] were, however, determined from steady state activities, while we preferred to use initial activities, due to the different deactivation pattern of the various Pt-zeolites used. Therefore, only a comparison of the concentration of accessible Pt was reported here, but not absolute dispersion values.

Table 3 *Initial activity in the hydrogenation of ethene and 2,4,4-trimethylpent-1-ene and the fraction of accessible Pt on the outer surface, as calculated by the ratio of the two rates. The hydrogenation rates r_{C2H4} and r_{TMPe} are given in 10^{-4} mol/s·g·bar. Metal loading 0.1 wt%.*

	Ethene		244TMPe		Accessible Pt
	Yield (%)	r_{C2H4}	Yield (%)	r_{TMPe}	outer surface(%)
Pt-ZSM5(480)	12	3.3	1.9	2.3	20
Pt-ZSM5(125)	11	2.9	n.d.	n.d.	n.d.
Pt-FER(17)	100	>30	0.5	0.6	<1
Pt-FER(90)	20	5.4	2.2	2.5	15
Pt-FER(670)	1	0.4	0.6	0.7	60
Pt-TON(35)	14	4.3	10.9	12.9	90
Pt-TON(72)	14	4.3	1.0	1.4	10
Pt-SiO_2	10 [a]	1.2	3.3	4.0	100

n.d. = not determined

[a] 25 mg catalyst instead of 10 mg

Table 3 shows that the rate of ethene hydrogenation, i.e., the dispersion of the samples, decreased in the order Pt-FER(90) > Pt-TON > Pt-ZSM5 > Pt-SiO_2 >> Pt-FER(670). This trend is generally in line with the results of HREM. Note that for Pt-FER the dispersion strongly increased with the acid site concentration.

Large differences were also found in the rate of hydrogenation of 244TMPe. The catalytic activity decreased in the order Pt-TON(35) > Pt-SiO_2 > Pt-FER(90) ~ Pt-ZSM5(480) > Pt-TON(72) > Pt-FER(670) ~ Pt-FER(17). Note that only the *accessible* Pt sites on the outer surface are measured by this method. If large Pt particles are present on the outer surface of the zeolite, like in the case of Pt-ZSM5(480), the amount of Pt on the outer surface will be high, but the fraction of accessible metal sites low.

If we assume that on the external surface of a material the same number of metal sites is accessible for ethene and for 244TMPe, it is possible to calculate the fraction of Pt sites located on the external surface from the ratio $q = r_{TMPe}/r_{C2H4}$. Pt-SiO_2 can be used as a reference, since the material is non-porous and all metal sites have to be located on the outer surface. The fraction of Pt sites on the external surface of the Pt-zeolites is then calculated from q(Pt-zeolite)/q(Pt-SiO_2). According to this estimation, most of the active Pt in TON(35) and FER(670) was located on the outer surface. For the other samples, i.e., Pt-ZSM5(480),

Pt-TON(72), Pt-FER(90), the fraction was between 10 and 20%. Due to the above-mentioned influence of the high acid site concentration on the ethene hydrogenation rate of Pt-FER(17) it was not possible to give an reliable value for the fraction of accessible Pt on the outer surface of this material. But the very low activity in the hydrogenation of 244TMPe indicated that most Pt was located in the pores.

For the Pt-FER samples the fraction of accessible Pt on the outer surface decreased with increasing acid concentration, showing the stabilizing effect of acid sites on Pt particles in the pores. For Pt-TON, however, just the opposite effect was observed. Pt-TON(35) had most of the active Pt located on the outer surface, Pt-TON(72) only a small fraction. The different behavior could be related to the lower crystallinity of TON(35) compared to TON(72), as indicated by XRD.

Skeletal isomerization of 1-butene

It has been mentioned above that the selectivity of a material in butene isomerization is an important criterion for its suitability in dehydroisomerization. Therefore, the activity and selectivity of the parent zeolites in butene isomerization was studied. The results are compiled in Table 4. The activity in butene isomerization decreased in the order FER(17) > TON(72) ~ TON(35) > ZSM5(480) > FER (90). As expected, FER was the most selective catalyst. It should, therefore, be the most suited dehydroisomerization.

Table 4 *Comparison of activity and selectivity of ZSM5, TON and FER in butene isomerization. 775 K, 1 bar, Feed 7% 1-butene in Ar. 100 min on stream.*

Sample	ST (sg/m^3)	Yield i-$C_4^=$ (%)	k [a] (m^3/sg)	Selectivity i-$C_4^=$ (%)
ZSM5(480)	5200	13.1	$3.3*10^{-5}$	87.1
TON(72)	4650	16.6	$5.3*10^{-5}$	86.8
TON(35)	4500	16.2	$4.9*10^{-5}$	88.6
FER(90)	4850	7.3	$1.4*10^{-5}$	94.3
FER(17) [b]	2400	14.8	$9.2*10^{-5}$	93.1

[a] Pseudo first order rate constant of butene isomerization.

[b] 4.5% 1-butene in the feed instead of 7%.

Dehydroisomerization of n-butane

The samples listed in Table 1 were tested for the dehydroisomerization of n-butane at 775 K. Figure 2 shows as an example the time-on stream behavior of Pt-ZSM5(480), Pt-TON(35) and Pt-FER(90). Several important trends can be seen in Figure 2. (i) The dehydrogenation activity, i.e., the yield of $\sum C_4^=$, increased from Pt-FER(90) to Pt-TON(35) to Pt-ZSM5(480). The same held true for the yield of isobutene. (ii) The dehydrogenation activity was quite stable for all three samples. (iii) The by-product spectrum of the three samples differed. In the case of Pt-FER(90), ethane was the most abundant by-product. With Pt-TON(35), almost equal amounts of propane, ethane and propene were formed. In the case of Pt-ZSM5(480), on the other hand, propane and isobutane dominated the by-product spectrum.

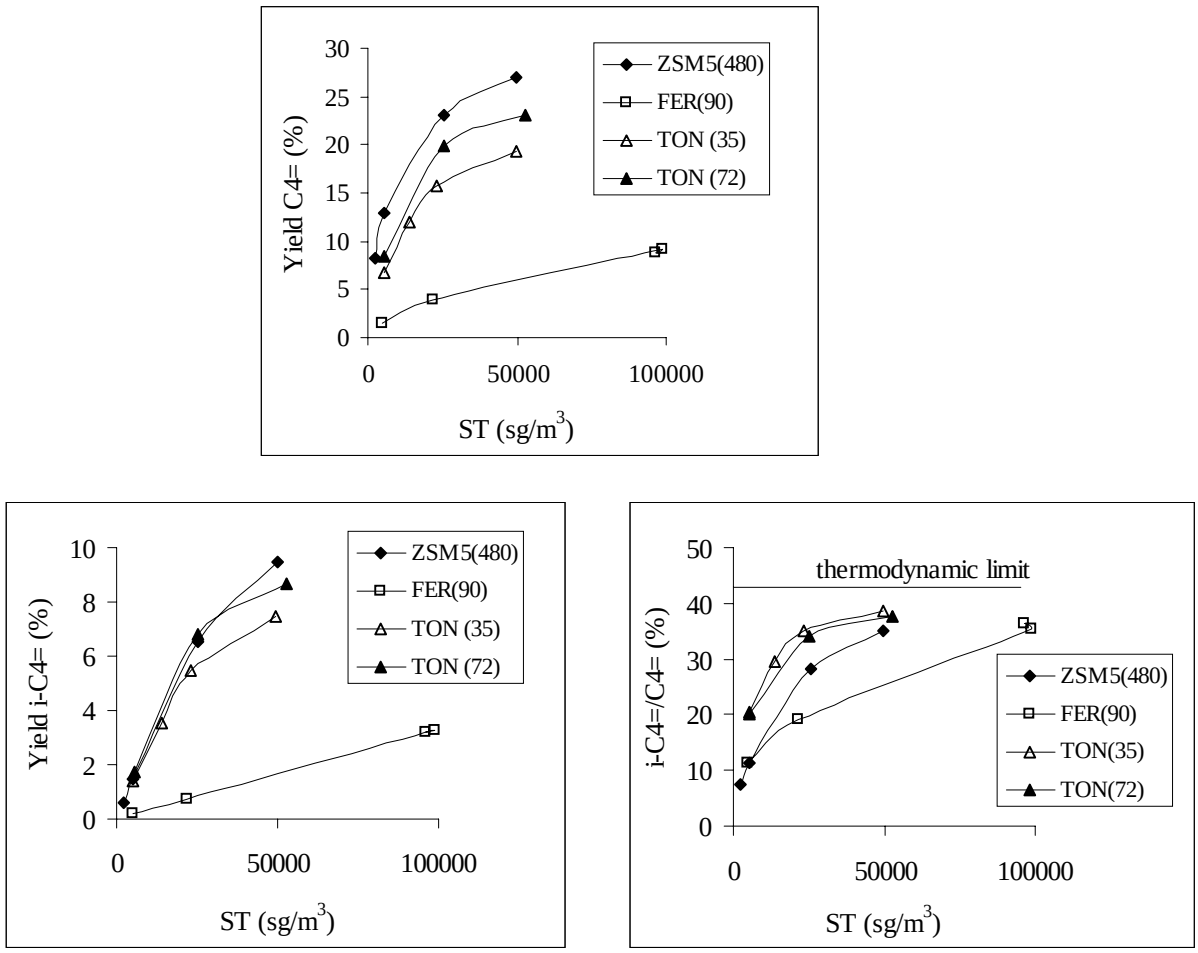

Figure 3 *Yield of (a) $\sum C_4^=$ and (b) i-$C_4^=$. (c) Ratio i-$C_4^=/\sum C_4^=$. All as a function of space time (ST = (dV/dt)/m_{cat}, where (dV/dt) is the total flow in m^3/s at reactor temperature and pressure, and m_{cat} the mass of the catalyst in g). 775 K, 1.0 bar, 100 min on stream. Feed 10% n-butane, 20% H_2. Metal loading of all samples 0.1 wt%.*

Figure 3 shows the steady state (after 100 min time on stream) yields of the sum of butenes and of isobutene, as well as the ratio $iC_4^=/\sum C_4^=$ as a function of space time. As already seen in Figure 2, the dehydrogenation activity (the yield of $\sum C_4^=$) decreased in the order Pt-ZSM5(480) > Pt-TON(72) > Pt-TON(35) > Pt-FER(90). The yield of $\sum C_4^=$ leveled off at higher space times. The leveling off was caused by approaching the dehydrogenation equilibrium (the highest yield of $\sum C_4^=$ in Figure 3 corresponds to about 75% of the equilibrium yield) and by a kinetic inhibition due to adsorption of butenes on the metal sites (see Chapter 6).

The isomerization activity, i.e., the ratio $iC_4^=/\sum C_4^=$, of both Pt-TON samples was higher than that of Pt-ZSM5 and Pt-FER. At low space times Pt-ZSM5 and both Pt-TON samples gave almost the same yield of isobutene. However, as isomerization approached thermodynamic equilibrium (at ST > 25000 sg/m^3), the higher dehydrogenation activity of Pt-ZSM5 led to higher yields of isobutene than with Pt-TON.

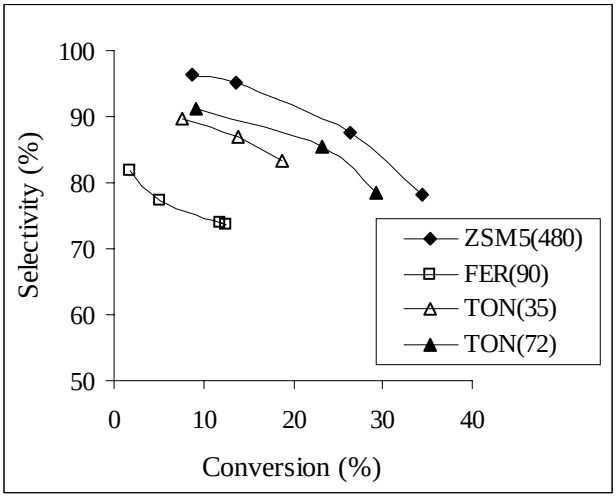

Figure 4 *Selectivity to $\sum C_4^=$ as function of the conversion of n-butane. 775K, 1.0bar, 100 min on stream. Feed 10% n-butane, 20% H_2. Metal loading 0.1 wt%.*

Figure 4 shows the selectivity to dehydrogenation ($\sum C_4^=$) for the four samples. It increased in the order Pt-FER(90) << Pt-TON(35) < Pt-TON(72) < Pt-ZSM5(480). The by-product pattern is analyzed in more detail in Figure 5. The by-products of Pt-ZSM5(480) originated almost exclusively from secondary reactions, as seen from the negligible intercept of the selectivity curves. Pt-FER(90), on the other hand, showed a significant primary contribution of ethane, propene, methane and propane (decreasing in this order). Pentene was not detected,

indicating that oligomerization/cracking of butenes did not play a role in the by-product formation of Pt-FER.

Also in the case of Pt-TON the selectivity curves of methane, ethane and propene had a positive intercept at zero conversion indicating that they were formed by primary reactions. The selectivity to these products was lower than for Pt-FER, but higher than for Pt-ZSM5. In contrast to Pt-FER, formation of pentene was observed and its selectivity increased with conversion. Thus, oligomerization/cracking of butenes contributed to the by-product formation on Pt-TON like in the case of Pt-ZSM5.

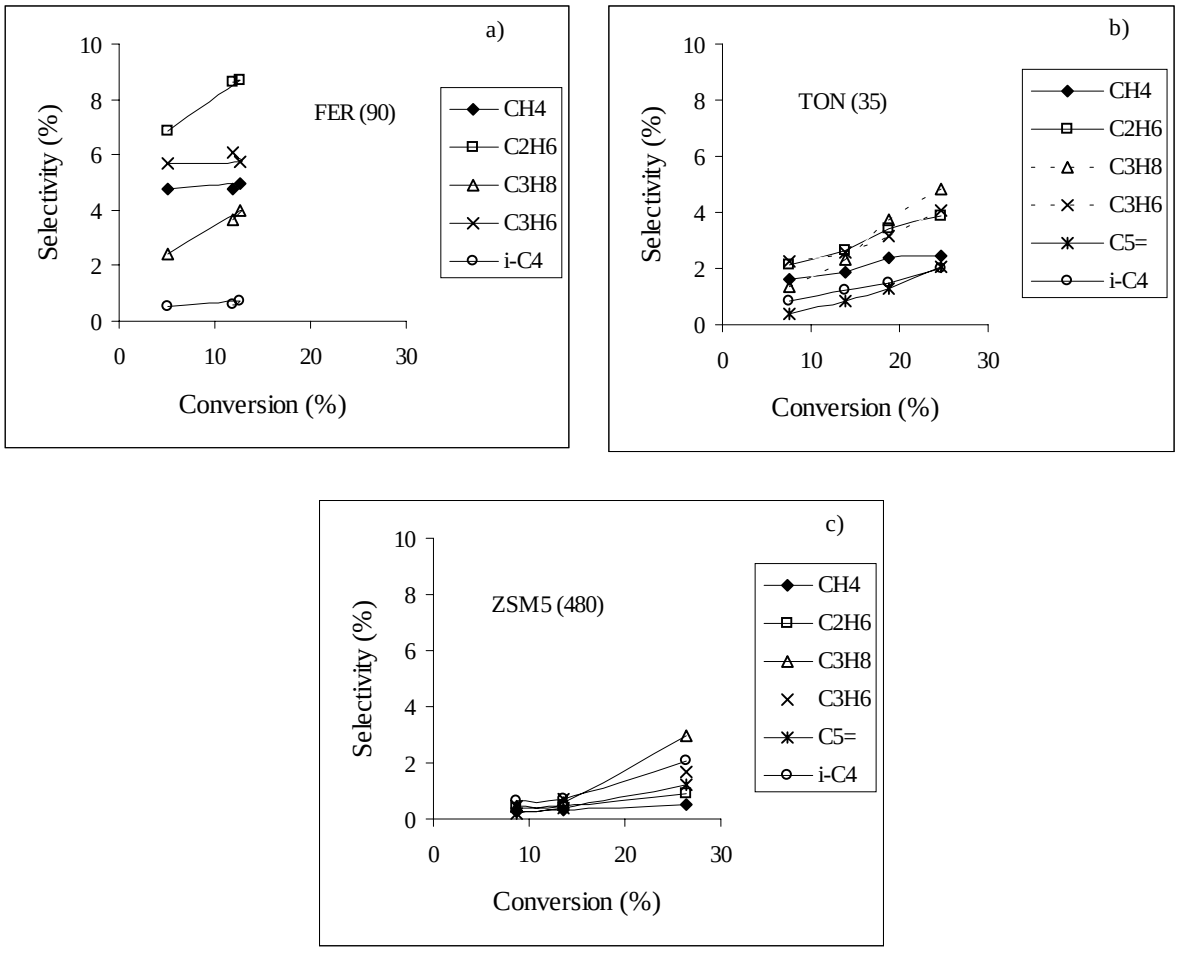

Figure 5 *Selectivity to the major by-products as a function of the conversion of n-butane. (a) Pt-FER(90). (b) Pt-TON(35). (c) Pt-ZSM5(480). 775 K, 1.0 bar, 100 min on stream. Feed 10% n-butane, 20% H_2.*

In order to determine the contribution of protolytic cracking of butane to the byproduct formation, the conversion of n-butane over the parent zeolites was studied (in the absence of Pt). n-Butane was converted to cracking products, according to the reactions (1) and (2), to isobutane (3) and to an equilibrium mixture of butenes (4).

$n\text{-}C_4H_{10} \rightarrow CH_4 + C_3H_6$ (1)

$n\text{-}C_4H_{10} \rightarrow C_2H_6 + C_2H_4$ (2)

$n\text{-}C_4H_{10} \rightarrow i\text{-}C_4H_{10}$ (3)

$n\text{-}C_4H_{10} \rightarrow C_4H_8 + H_2$ (4)

Table 5 *Rate of byproduct formation over the parent zeolites and the Pt-zeolites (0.1 wt% Pt). WHSV = 14 h^{-1} (ST = 25000 m^3/sg), 775 K, 1.0 bar. Feed 10% n-butane, 20% hydrogen, balance Ar. 100 min on stream.*

rate (10^{-7}mol/sg)	ZSM5(480)	Pt-ZSM5(480)	TON(35)	Pt-TON(35)
CH_4	0.50	3.3	1.2	12
C_2H_6	0.25	3.1	1.4	8.9
C_2H_4	0.25	0.15	1.4	0.6
C_3H_8	0.00	6.8	0.0	6.5
C_3H_6	0.50	3.9	1.2	5.6

rate (10^{-7}mol/sg)	FER(90)	Pt-FER(90)	FER(17)	Pt-FER(17)
CH_4	0.60	6.7	11	29
C_2H_6	0.60	5.1	10	26
C_2H_4	0.60	0.76	10	1.4
C_3H_8	0.017	1.2	0.22	2.7
C_3H_6	0.59	2.8	10	8.2

Table 6 *Ratio of the rates of C_1-C_3 (alkane + alkene) formation in the presence and absence of Pt (0.1 wt%). WHSV = 14 h^{-1} (ST = 25000 m^3/sg), 775 K, 1.0 bar. Feed 10% n-butane, 20% hydrogen, balance Ar. 100 min on stream.*

	ZSM5(480)	TON(35)	FER(90)	FER(17)
C_1	6.6	10.0	11.1	2.6
C_2	6.5	3.4	4.9	1.4
C_3	21.4	10.1	6.6	1.1
$\sum nC_n$	14	6.5	6.3	1.4

Table 5 compiles the rates of formation of C_1-C_3 hydrocarbons for the parent and the Pt-zeolites. For the parent zeolites the rates of methane and propane and of ethane and ethene formation matched exactly, as expected from the stoichiometry of reactions (1) and (2). In the case of the Pt-zeolites alkanes and alkenes can be interconverted by hydrogenation/dehydrogenation on the metal (see Chapter 4 and 5). Therefore, it is better to compare the total rate of alkane + alkene formation in the presence and absence of Pt. These values are listed in Table 6. The ratio of the rates shows that in the case of Pt-ZSM5(480) and Pt-TON(35) the by-product formation was significantly higher than for the parent zeolite. From this we could conclude that the contribution of protolytic cracking to the overall by-product formation was small. Also in the case Pt-FER(90) the by-product formation was much higher than for the parent. In contrast to Pt-ZSM5 and Pt-TON, however, the increased by-product formation was due to an increase in protolytic cracking itself, as will be discussed later.

For Pt-FER the effect of SiO_2/Al_2O_3 ratio was studied over a wide range from 17 to 670. Table 7 compares the results obtained with the three samples. With decreasing SiO_2/Al_2O_3 ratio (with increasing acid site concentration) the conversion of n-butane and the ratio $iC_4^=/\sum C_4^=$ increased. The increased conversion was due to an increased by-product formation. The yield of $\sum C_4^=$, however, decreased. For Pt-FER(17) the by-product formation was in the same order of magnitude as for the parent FER(17) (see Table 5 and Table 6). Thus, the contribution of protolytic cracking to the overall by-product formation of Pt-FER(17) was very high.

Figure 6 shows the dependence of the rate of by-product formation on the Al-content of the Pt-FER samples. The rate of methane and ethane formation increased almost linearly with Al-content, as expected if methane and ethane originate from protolytic cracking on the Brønsted acid sites. The rate of C_3 formation, however, did not increase in parallel with the formation of methane, as predicted by the stoichiometry of reaction (1). Thus, a significant part of the methane formation (and probably also the ethane formation, since the curves were parallel) must be due to hydrogenolysis and not to protolytic cracking. Note that the contribution of hydrogenolysis, represented by the difference in the rates of methane and C_3 formation in Figure 6, increased with the acid site concentration of the zeolite.

Table 7 *Yield of major products in the dehydroisomerization of n-butane over Pt-FER. WHSV = 14 h^{-1}. 775 K, 1.0 bar, 100 min on stream. Feed 10% n-butane, 20% H_2.*

SiO_2/Al_2O_3	670	90	17	17
wt% Pt	0.1	0.1	0.1	0.3
CH_4	0.01	0.24	1.06	13.4
C_2H_6	0.01	0.35	1.92	6.4
C_2H_4	0.01	0.05	0.09	0.18
C_3H_8	0.00	0.12	0.30	0.88
C_3H_6	0.02	0.29	0.90	0.40
i-$C_4^=$	0.04	0.75	1.04	0.75
$\sum C_4^=$	4.7	3.9	3.4	1.9
Conversion	4.9	5.1	7.7	25
$iC_4^=/\sum C_4^=$	0.8	19	31	39

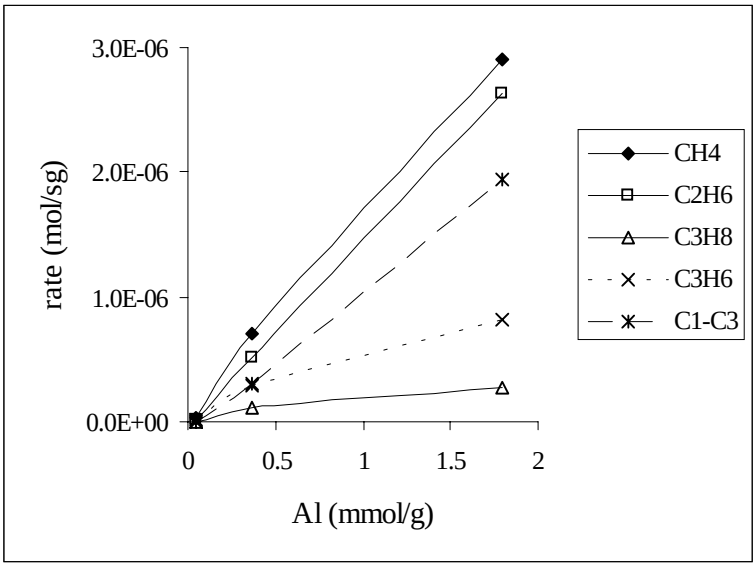

Figure 6 *Rate of by-product formation as a function of the Al-content of Pt-FER. WHSV = 14 h^{-1}, 775 K, 1.0 bar, 100 min on stream. Feed 10% n-butane, 20% H_2.*

Increasing the metal loading of Pt-FER(17) from 0.1 to 0.3 wt% Pt led to a drastic increase in the formation of methane and ethane (see column 4 of Table 7) indicating that mainly hydrogenolysis took place with this sample. The yield of $\sum C_4^=$ was only 1.9%.

Discussion

In the skeletal isomerization of 1-butene FER gave a significantly lower selectivity to by-products than TON and ZSM5. In dehydroisomerization of n-butane, however, the selectivity to by-products (i.e., other products than $C_4^=$) increased in the order Pt-ZSM5(480) < Pt-TON(35) < Pt-FER(90). The by-product pattern of the three catalysts (see Figure 5) showed that on Pt-TON and especially on Pt-FER a large fraction of the by-products was of primary nature, whereas over Pt-ZSM5(480) most of the by-products were formed by secondary reactions. The selectivity to primary by-products (i.e., the selectivity to by-products extrapolated to zero conversion) increased from Pt-ZSM5(480) (< 4%) to Pt-TON(35) (~ 9%) to Pt-FER(90) (~ 17%) (see Figure 4). While oligomerization/cracking of butenes was the only relevant side reaction with Pt-ZSM5(480), its contribution was negligible with Pt-FER(90). Pt-TON(35) was an intermediate case. Both primary and secondary side reactions took place over this catalyst.

We conclude, thus, that suppressing oligomerization/cracking reactions of the butenes is not sufficient for improving the selectivity of a catalyst for dehydroisomerization of n-butane. The other side reactions, protolytic cracking of n-butane on the acid sites and hydrogenolysis of n-butane on the metal sites, have to be taken into account, as well.

The contribution of protolytic cracking of n-butane

Provided that the rate of protolytic cracking is constant in the presence and absence of Pt, protolytic cracking accounted for 9% (on a carbon basis) of the light by-products (C_1-C_3) in the case of Pt-ZSM5(480) and for 15-16% in the case of Pt-TON(35). With Pt-ZSM5(480) and Pt-TON(35), the other light hydrocarbons were formed by hydrogenolysis and oligomerization/cracking. In the case of Pt-FER(90), however, we had concluded from the absence of pentene in the products that oligomerization/cracking did not take place. The increase in the formation of propene (see Table 5) must, therefore, be due to an increase in protolytic cracking in the presence of Pt. We, thus, conclude that most of the light by-products of Pt-FER(90) were formed by protolytic cracking.

For the overall selectivity in dehydroisomerization the relative rates of the two parallel reactions protolytic cracking and dehydrogenation are important. The corresponding rate constants and their ratio are given in Table 8. The ratio k_{dehyd} / k_{crack} was inversely proportional to the selectivity to protolytic cracking, measured by the selectivity to C_3H_6 at

zero conversion[1]. The increase in selectivity to protolytic cracking from Pt-ZSM5 to Pt-TON to Pt-FER was caused by the increase in the rate of cracking *and* the decrease in the rate of hydrogenation in this order.

Table 8 *Pseudo first order rate constants of protolytic cracking (k_{crack}) and dehydrogenation of n-butane (k_{dehyd}) as well as of skeletal isomerization of 1-butene (k_{isom}). The ratio k_{dehyd}/k_{crack} is correlated to the selectivity to protolytic cracking, represented by the selectivity to propene at zero conversion.*

	k_{crack} [a] (10^{-7} m^3/sg)	k_{isom} ($10^{-5}m^3$/sg)	k_{dehyd} [b] (10^{-5} m^3/g)	k_{dehyd} /k_{crack}	Sel. C_3H_6 (%) [c]
(Pt-)ZSM5(480)	0.43	3.3	5.0 ± 0.5	1150	0.1 ± 0.1
(Pt-)TON(72)	0.8	5.3	2.2 ± 0.2	275	1.5 ± 0.1
(Pt-)TON(35)	1.7	4.9	1.8 ± 0.2	105	2.1 ± 0.1
(Pt-)FER(90)	0.74 (4.3[d])	1.4	0.3 ± 0.1	40 (7[d])	5.7 ± 0.3
(Pt-)FER(17)	130	9.2	<0.3	<0.2	~30

[a] k_{crack} was determined from the rate of protolytic cracking over the parent zeolite.

[b] k_{dehyd} was calculated according to the method described in Chapter 6 and extrapolated to zero conversion.

[c] Selectivity was extrapolated to zero conversion.

[d] Since the Pt-FER(90) had a significantly higher activity than the parent (see text), its cracking rate was estimated from $r_{C3} + 0.5r_{C2}$. The value is given in the brackets.

The higher cracking activity of TON and FER compared to ZSM5 was due to the higher acid site concentration of these samples. In dehydroisomerization over Pt-TON and Pt-FER, the initial selectivity to propene at zero conversion decreased with increasing SiO_2/Al_2O_3 ratio, showing that the selectivity to protolytic cracking could be reduced by reducing the acid site concentration. But since butene isomerization is also acid catalyzed, the acid site concentration cannot be reduced beyond a certain limit. Pt-FER(670), for example, had a very low activity for protolytic cracking, but also hardly any activity in butene isomerization. In general a material will be more the suited for dehydroisomerization the higher its activity for

[1] In contrast to the suggestion of Haag *et al.* [21] to use the paraffinic products for analyzing the rate of protolytic cracking we used propene, because the paraffins methane and ethane can also be formed by hydrogenolysis. The contribution of secondary reactions to the formation of propene was eliminated by extrapolation of the selectivity to zero conversion.

butene isomerization is compared to its activity for protolytic cracking. The ratio k_{isom}/k_{crack} decreased in the order ZSM5(480) > TON(72) > TON(35) > FER(90) > FER(17). We can also see from Table 8 that the rate of protolytic cracking depended stronger on the concentration of acid sites than the rate of butene isomerization. Thus, materials with high SiO_2/Al_2O_3 should be more suited for dehydroisomerization.

The contribution of hydrogenolysis

It is difficult to distinguish the contribution of hydrogenolysis from protolytic cracking of n-butane and from oligomerization/cracking of butenes. In the presence of Pt and hydrogen the alkenes formed by cracking can be hydrogenated to the corresponding alkanes. As a result, ethane and propane can be formed via all three reaction routes. But there are possibilities to estimate the contribution of hydrogenolysis. If only protolytic cracking and oligomerization/cracking take place, the molar ratio C_1/C_3 must be ≤ 1 (= 1, if only protolytic cracking takes place, see equation 0, < 1 if C_3 is also formed by oligomerization/cracking). On the other hand, methane is the main product of hydrogenolysis at the high reaction temperatures applied, next to only small amounts of ethane and propane (the selectivity to methane in hydrogenolysis increases with temperature [22]). Hence, we can use the difference in the rate of methane formation and the rate of C_3 formation (propane + propene) as a measure of the hydrogenolysis activity. Especially at low conversions, when the contribution of oligomerization/cracking to the C_3 formation is low, the difference $r_{CH4} - r_{C3}$ should give a good estimate of the rate of hydrogenolysis. This method was already applied in Figure 6.

Table 9 *Rate of hydrogenolysis (estimated by $r_{CH4} - r_{C3}$) and selectivity to hydrogenolysis. Both were extrapolated to zero conversion.*

	rate (10^{-7}mol/sg)	k_{dehyd}/k_{hydr}	Sel. (%)
Pt-ZSM5(480)	n.d.	n.d.	0.1 ± 0.1
Pt-TON(72)	5.7 ± 0.5	60	0.6 ± 0.1
Pt-TON(35)	6.0 ± 0.5	50	0.6 ± 0.1
Pt-FER(90)	3.5 ± 0.3	15	2.5
Pt-FER(17)	20	<2.5	>5

Using this approach, the initial selectivity to hydrogenolysis (extrapolated to zero conversion) and the reaction rate were estimated. The results are shown in Table 9. The rate of hydrogenolysis increased from Pt-FER(90) to Pt-TON (both SiO_2/Al_2O_3 ratios were comparable) to Pt-FER(17). Due to the big relative error margin of the extrapolation no rate could be given for Pt-ZSM5(480). The selectivity to hydrogenolysis, which is determined by the relative rates of dehydrogenation and hydrogenolysis, increased from Pt-ZSM5(480) to Pt-TON (both) to Pt-FER(90) to Pt-FER(17).

The effect of the zeolite on the metal activity

The results discussed so far showed a very peculiar behavior of Pt-FER. In contrast to Pt-ZSM5 and Pt-TON, it had a very low activity for dehydrogenation and a high selectivity to hydrogenolysis, especially in the case of Pt-FER(17). The high selectivity of this material in hydrogenolysis could be related the small size of the metal particles, as observed in HREM. The TOF of hydrogenolysis increases with decreasing particle size [19, 22, 23, 24, 25]. Dehydrogenation is structure insensitive [26] and its TOF is independent of the particle size. Thus, the selectivity to hydrogenolysis is expected to be higher for small Pt particles. Indeed, the highest selectivity to hydrogenolysis was found for the sample with the smallest Pt particles in found by HREM, Pt-FER(17), while Pt-ZSM5(480) had the largest particles and the lowest selectivity to hydrogenolysis. But another effect can play a role, as well. Looking at Table 8 and Table 9 we see a correlation between hydrogenolysis and protolytic cracking. The rates of both reactions are low on Pt-ZSM5(480), average on Pt-TON and high on FER(17). Among the Pt-FER materials we had observed an increase of hydrogenolysis with the Al-content. This could be due to the observed decrease in Pt particle size with increasing Al-content (see the dispersion data in Table 3). But it is also possible that a synergy between the two reactions exists. Alkenes formed by cracking can be preferentially adsorbed on the metal and be responsible for the extensive hydrogenolysis observed for Pt-FER(17) [27].

The large difference in dehydrogenation activity, which decreased from Pt-ZSM5 to Pt-TON to Pt-FER, is more difficult to understand. The HREM measurements indicated that the different dehydrogenation activity was not primarily related to the metal dispersion. Pt-ZSM5(480) exhibited only a moderate dispersion, but the highest dehydrogenation activity, while Pt-FER(90) had a rather high dispersion, but a very low dehydrogenation activity. Interestingly, the differences between Pt-ZSM5, Pt-TON and Pt-FER were much larger than the differences within one zeolite family. For both Pt-TON and all three Pt-FER materials

similar dehydrogenation rates were found. Thus, the different metal activity was more related to the differences in framework structure and morphology of ZSM5, FER and TON than to a variation in the SiO_2/Al_2O_3 ratio. This suggested that the different behavior of the Pt-zeolites could be related to diffusion. ZSM5 has a two-dimensional pore system and diffusion of the reactants and products is easier than in FER and TON, which have a one-dimensional channel system (the channel system of FER is two-dimensional, but most molecules cannot pass the 8-member ring channels). The pores are narrower than those of ZSM5, even more so when Pt particles are present in the channel system. It is, thus, possible that pore diffusion of the reactants and/or products is the rate limiting step in Pt-TON and Pt-FER. The rate of diffusion in Pt-TON and Pt-FER, however, should be quite similar and cannot explain why Pt-TON was about six times more active for dehydrogenation than Pt-FER. This difference was attributed to the morphology of the samples. The crystals of Pt-FER(90) were larger than those of Pt-TON (see Table 2). A lot of small particles were found next to the well-shaped needles in both Pt-TON materials. Thus, on average the length of the pores was shorter in Pt-TON than in Pt-FER, thereby reducing the diffusion path length and the negative effect on the reaction rate. Pt-FER(17), on the other hand, had crystals of comparable size as the two Pt-TON materials. On this sample the low concentration of Pt on the outer surface, as a result of which most of the dehydrogenation has to take place in the pores, in combination with the high acid site density could make product desorption the rate limiting step.

Conclusions

While in the dehydroisomerization of n-butane over Pt-ZSM5(480) the selectivity was almost exclusively determined by the extent of oligomerization/cracking reactions, protolytic cracking and hydrogenolysis had a significant contribution to the by-product spectrum in the case of Pt-TON(35 and 72) and Pt-FER(17 and 90). The selectivity to protolytic cracking was inversely proportional to the ratio k_{dehyd}/k_{crack}. Thus, a high ratio of k_{dehyd}/k_{crack} is an important design parameter for a dehydroisomerization catalyst. The contribution of protolytic cracking can be reduced by increasing the SiO_2/Al_2O_3 ratio. But since butene isomerization is also acid catalyzed, the increase in SiO_2/Al_2O_3 cannot be unlimited and an optimum has to be found. In general, zeolites with a high TOF for butene isomerization and a low TOF for protolytic cracking should be more suited as dehydroisomerization catalysts. Since protolytic cracking shows a stronger dependence on the concentration of acid sites than butene isomerization

materials with low acid site concentrations should give better selectivities in dehydroisomerization.

Surprisingly, the dehydrogenation activity of the Pt-zeolites is not primarily related to the metal dispersion. Pt-ZSM5(480) with a moderate dispersion and a very inhomogeneous distribution of the metal gave the best results, while the opposite was the case for Pt-FER(17), which had a very homogeneous distribution of small particles mainly located in the zeolite pores. The zeolite framework, on the other hand, has a big influence on the dehydrogenation activity, which decreased significantly from Pt-ZSM5 to Pt-TON to Pt-FER. The effect is tentatively attributed to diffusion control. The presence of small metal particles located in the narrow pores of large zeolite crystals is not desirable for dehydroisomerization, since it enhances the diffusional constraints.

Acknowledgements

I am indebted to M.J.G. Janssen, from Exxon Chemical International Inc., Basic Chemicals Technology Europe, and G. Kinger, from the Technical University of Vienna, for supplying the FER and TON samples. I also want to thank P. Kooyman (National Center for HREM, Delft) and O.P.E. Zinck-Stagno (Pt test-reactions) who contributed very much to the work presented here.

References:

[1] O'Young, Ch.-L., Pellet, R., Casey, D., Ugolini, J., and Sawicki, R.A., J. Catal. **151**, 467 (1995).

[2] Mooiweer, H.H., de Jong, K.P., Kraushaar-Czarnetzki, B., Stork, W.H.J. and Krutzen, B.C.H., Stud. Surf. Sci. Catal. **84**, 2327 (1994).

[3] Xu, W.-Q., Yin, Y.-G., Suib, St.L. Edwards, J.C., and O'Young, Ch.-L., J. Phys. Chem. **99**, 9443 (1995).

[4] Guisnet, M., Andy, P., Gnep, N.S., Benazzi, E., and Travers, C., J. Catal. **158**, 551 (1996).

[5] Simon, M.W., Suib, S.L., and O'Young, Ch.-L., J. Catal. **147**, 484 (1994).

[6] Byggningsbacka, R., Lindfors, L.-E., and Kumar, N., Ind. Eng. Chem. Res. **36**, 2990 (1997).

[7] Xu, W.-Q., Yin, Y.-G., Suib, St.L., and O'Young, Ch.-L., J. Catal. **150**, 34 (1994).

[8] Gajda, G.J., US Patent 5.132.484 (1992), assigned to UOP.

[9] Gielgens, L.H., Veenstra, I.H.E., Ponec, V., Haanepen, M.J., and van Hooff, J.H.C., Catal. Lett. **32**, 195 (1995).

[10] Asensi, M.A., Corma, A., and Martinez, A., J. Catal. **158**, 561 (1996).

[11] Grandvallet, P., de Jong, K.P., Mooiweer, H.H., Kortbeek, A.G.T., and Kraushaar-Czarnetzki, B., EP 0.501.577 A1 (1992), assigned to Shell Internationale Research Maatschappij B.V.

[12] Barri, S.A.I., Walker, D.W., and Tahir, R., EP Patent 247.802 (1990), assigned to The British Petroleum Company.

[13] Ernst, S., Weitkamp, J., Martens, J., and Jacobs, P., Appl. Catal. **48**, 137 (1989).

[14] Chapter 9 of this thesis.

[15] Cortright, R.D., Goddard, S.A., Rekoske, J.E., and Dumesic, J.A., J. Catal. **127**, 342 (1991).

[16] Houzvicka, J., Klik, R., Kubelkova, L, and Ponec, V., Catal. Lett. **43**, 7 (1997).

[17] Benesi, H.A., Curtis, R.M., and Studer, H.P., J. Catal. **10**, 328 (1988).

[18] Degussa, Schriftenreihe Pigmente, "Aerosil, Aluminiumoxid C und Titandioxid P25 für Katalysatoren", Nr. 72.

[19] Schlatter, J.C., and Boudart, M., J. Catal. **24**, 482 (1972).

[20] Che, M., and Bennett, C.O., Adv. Catal. **36**, 55 (1989).

[21] Haag, W.O., and Dessau, R.M., Proc. 8th Int. Congress on Catalysis, Berlin, 1984, p. 305.

[22] Bond, G.C., and Gelsthorpe, M.R., J. Chem. Soc. Faraday Trans. I **85**, 3767 (1989).

[23] Bond, G.C., Calhoun, J., and Hooper, A.D., J. Chem. Soc. Faraday Trans. **92**, 5117 (1996).

[24] Rodriguez-Reinoso, F., Rodriguez-Ramos, I, Moreno-Castilla, C., Gruerrero-Ruiz, A., and Lopez-Gonzalez, J.D., J. Catal. **107**, 1 (1987).

[25] Campbell, R.A., Guan, J., and Mady, T.E., Catal. Lett. **27**, 273 (1994).

[26] Biloen, P., Dautzenberg, F.M., and Sachtler, W.M.H., J. Catal. **50**, 77 (1977).

[27] Kemball, C., and Dowden, D.A., "Catalysis", Vol. 2, p. 21, The Chemical Society, Burlington House, London, 1977.

Chapter 9

Direct conversion of n-butane to isobutene over Pt-MCM22

Abstract

MCM22 is a very active and selective catalyst for the skeletal isomerization of butene. At temperatures up to 775 K, Pt-MCM22 gives good results in the dehydroisomerization of n-butane, achieving higher yields of isobutene than Pt-ZSM5. Most notably, the formation of cracking products is low. Alternatively, MCM22 can also be used as isomerization catalyst in combination with Pt-ZSM5 (which then mainly serves as a dehydrogenation catalyst) in order to increase the yield of isobutene in dehydroisomerization. A disadvantage of the MCM22 materials, however, is their moderate stability, especially at higher temperatures. During calcination/reduction of Pt-MCM22 partial dealumination of the framework takes place and results in enhanced deactivation by coking.

Introduction

In the preceding chapter we had compared the performance of Pt-ZSM5, Pt-TON and Pt-FER in dehydroisomerization. Among the three zeolites ZSM5, TON and FER, FER had the highest selectivity in butene isomerization. Therefore, Pt-FER was expected to be a very selective catalyst in dehydroisomerization. However, the opposite was the case. Cracking of n-butane dominated with Pt-FER, while the dehydrogenation activity was very low. The low dehydrogenation activity was attributed to diffusion limitations in the narrow pores of FER. It was concluded that a combination of a one-dimensional channel system (the channel system of FER is practically one-dimensional), large crystal size and a high fraction of Pt in the pores was unfavorable for dehydroisomerization.

Thus, we turned our attention to MCM22. MCM22 is a microporous material with a layered structure [1]. Within the layers is a two-dimensional sinusoidal channel system, accessible through 10-membered ring apertures. Between the layers supercages are formed, defined by 12-membered rings. The cages are accessible through 10-ring apertures. The two channel systems are not connected. The product pattern of MCM22 in the isomerization and hydrocracking of decane, a testreaction for the determination of unknown pore structures [2, 3], was similar to those of 10-membered ring zeolites [4]. The dimensions of the 10-membered ring channel system of MCM22 are quite similar to those of FER. Therefore, MCM22 should, in principle, have the right shape-selective properties for butene isomerzation [5, 6]. Indeed, a successful application of MCM22 for this reaction was reported by Asensi *et al.* [7]. Being suited for butene isomerization, MCM22 was also an interesting material for application in the dehydroisomerization of n-butane. In contrast to FER, the two-dimensionality of the pore-system of MCM22 should facilitate the accessibility of the metal in the pores (like in the case of Pt-ZSM5) and avoid diffusion limitations.

Since the SiO_2/Al_2O_3 ratio has a large influence on the catalytic performance (see the preceding chapters), we tested two MCM22 samples with SiO_2/Al_2O_3 ratios of 25 and 35, respectively, for the dehydroisomerization of n-butane. Even higher SiO_2/Al_2O_3 ratios would be desirable. The synthesis of highly siliceous MCM22 is difficult, however, and often leads to the formation of other crystal phases [8]. Thus, we chose high metal loadings of 0.5-1wt% Pt in order to compensate for the rather high acid site concentration of the MCM22 materials (recall that we had concluded in Chapter 4

that a high ratio of metal to acid sites is beneficial for the selectivity in dehydroisomerization). The objective of the study was to evaluate the catalytic performance of Pt-MCM22 and correlate it with its physico-chemical properties.

Experimental

Catalyst preparation

MCM22 with SiO_2/Al_2O_3 = 35 was received from the University of Stuttgart (ST). It had been prepared according to procedure outlined in ref. [9]. In order to remove the template the sample was calcined in a flow of 70% N_2 and 30% air at 813 K for 15h (ramp rate 2 K/min).

MCM22 with SiO_2/Al_2O_3 = 25 was received from Shell Research and Technology Center Amsterdam (SR). It was prepared following US patent 5.085.762 [10]. After synthesis the sample was dried at 393 K and calcined at 813 K for 10 h (ramp rate 1.67 K/min).

Both samples were ion-exchanged with an aqueous solution of NH_4NO_3 in order to obtain the ammonium form. Pt was incorporated by ion-exchange with a dilute aqueous solution of $Pt(NH_3)_4(OH)_2$ (0.1 mgPt/l) and NH_3 (~2%) (see Chapter 2). After ion-exchange the samples were dried, calcined in air at 723 K for 2 h (ramp rate 0.5 K/min) and reduced in H_2 at 773 K for 2 h (ramp rate 5 K/min). The Pt-loading was varied between 0.5 and 1 wt%.

Characterization

The elemental composition of the samples was determined by XRF. The crystal phase was determined by powder X-ray diffraction, using a Phillips PW3710 in continuous scan mode. In order to quantify the crystallinity of the MCM22 samples, they were mixed in a 1:1 (m/m) ratio with α-Al_2O_3. The relative intensity of the reflections at 2Θ = 10.1º (102) and 2Θ = 26.1º (302), of MCM22, and at 2Θ = 35.25º (104), of α-Al_2O_3, was used for comparison of the samples.

For measuring the Brønsted and Lewis acidity of the materials, adsorption of pyridine was employed. The samples were pressed into self-supporting wafers (2-3 mg) and activated in the IR cell described in Chapter 2 in a stream of 25 ml/min He at 773 K for 30 min. A temperature ramp of 10 K/min was used. Pt-containing samples were –

although pre-reduced as described above - reduced *in situ* in a stream of 20/80 H_2/He. Subsequently, the samples were cooled down to 473 K. At this temperature pyridine was adsorbed by passing a stream of 25 ml/min He, containing 14 mbar pyridine, over the catalyst. The high adsorption temperature was chosen in order to accelerate the diffusion of pyridine. After equilibrium was reached (5-30 min), weakly bound pyridine was desorbed for 1 h in 25 ml/min He. The relative concentration of Lewis and Brønsted acid sites was evaluated from the intensity of the bands at 1540 cm^{-1}, attributed to coordinatively bound pyridine, and at 1455 cm^{-1}, attributed to pyridinium ions [11], after desorption, using the absorption coefficients given by Khabtou *et al.* [12]. The absolute concentration of acid sites was calculated by using a reference material (ZSM5, SiO_2/Al_2O_3 = 80) for which the concentration of acid sites (Brønsted + Lewis) had been determined by TGA (see Chapter 4).

In addition to the pyridine sorption experiments, the amount of tetrahedral and octahedral alumina was determined by solid state ^{27}Al NMR. The experiments were performed on a Chemagnetics Infinity CMX-600 spectrometer operating at 156.33 MHz (B_0 = 14.2 T). The spectra were obtained using a 2.5 mm or 3.2 mm Chemagnetics MAS probe, spinning at 25 kHz. Short-pulse excitations (0.7 μs = 0.056π, ν_{rf} ~ 40 kHz) were used to ensure quantitative excitation of the ^{27}Al resonances [13, 14] with 0.6 or 1.0 s relaxation delays and 100 kHz spectral width. Per measurement 3500-6000 free induction decays were collected. The ^{27}Al chemical shifts were determined relative to a standard of 1M aqueous $Al(NO_3)_3$ solution.

Catalyst testing

The parent MCM22 materials were first tested for their selectivity and activity in butene isomerization. For this purpose 10 mg of sample were mixed with about 60 mg quartz and put into a quartz reactor of 4 mm inner diameter. The sample was activated *in situ* in a flow of 25 ml/min at 830 K for 1 h and then cooled to 775 K. Then, the inlet stream was switched to a mixture of 7% 1-butene in Ar. The butene isomerization over MCM22 was followed for 3 h by GC analysis.

The actual dehydroisomerization experiments were performed similarly. The sample was activated *in situ* in a flow of 25 ml/min H_2/Ar (20/80) at 830 K for 1 h and then cooled to reaction temperature. The reaction was carried out under the same conditions as in Chapter 8, i.e., 775 K and atmospheric pressure (unless otherwise noted). While higher temperatures would be more favorable for dehydrogenation, 775

K was chosen to avoid problems with the structural stability of MCM22 at higher temperatures (the calcination temperature was 813 K). The reaction mixture contained 10% n-butane, 20% hydrogen, balance Ar.

Results

Catalyst characterization

The Pt-content and the SiO_2/Al_2O_3 ratio were determined by XRF (see Table 1). Traces of Fe (<0.03 wt%), Zr (<0.02 wt%) and Ti (<0.01 wt%) were found in all the samples. ν(OH), the intensity of the IR band at 3610 cm^{-1}, and B, the concentration of Brønsted acid sites determined by pyridine sorption, were proportional to each other (within the error of measurement) and decreased with the Al-content of the samples. Approximately 15% of the total acid sites were Lewis sites, for both parent MCM22 materials. The fraction increased slightly for the Pt-samples.

Table 1 *Characterization of the (Pt-)MCM22 materials.*

Sample	%Pt [a]	SiO_2/Al_2O_3 [a]	Al (mmol/g)	ν(OH) [b] (a.u.)	B [b] (mmol/g)
ST	0.00	37.7	0.85	2.4	0.9
	0.55	35.0	0.90	2.1	1.0
SR	0.00	25.1	1.24	3.0	1.2
	0.54	25.5	1.29	2.2 ± 0.3	1.1
	1.10	23.8	1.30	2.3 ± 0.2	1.1

continued

Sample	L/(L+B) [b] (%)	$Al_{oh}/(Al_{oh}+Al_{td})$ [c] (%)	rel. crystallinity (%) [d] (102)	(302)
ST	15	25	100	100
	18	31	95	95
SR	17	15	95	100
	22	26	65	65
	22	29	75	70

determined from [a] XRF, [b] IR, [c] ^{27}Al-NMR, [d] XRD

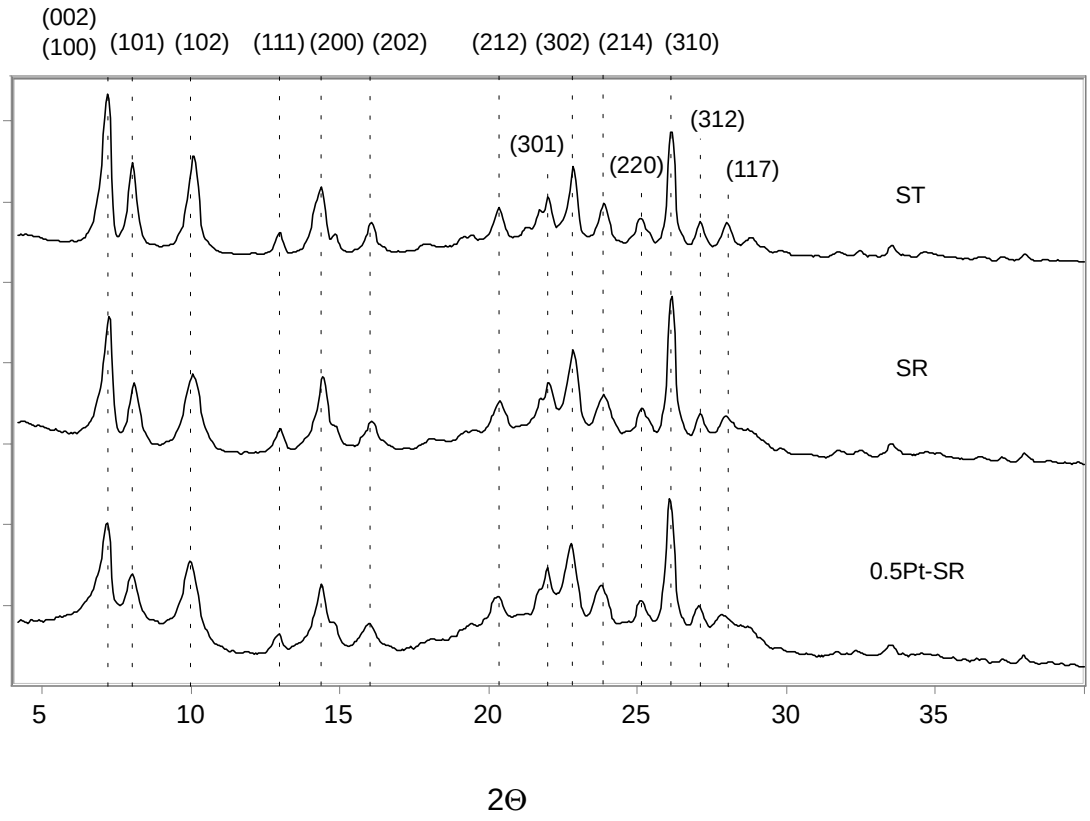

Figure 1 *XRD patterns of (a) MCM22 ST, (b) MCM22 SR, (c) 0.5%Pt-MCM22 SR.*

Figure 1 compares the powder XRD patterns of the parent MCM22s and 0.5%Pt-MCM22 SR. The assignment of the XRD reflections was taken from ref. [15]. The crystallinity of the two parent MCM22 materials was not significantly different (see Table 1). MCM22 ST, however, had a higher fraction of octahedral Al (see the NMR spectra in Figure 2), which is usually related to the presence of extraframework Al [16]. Incorporation of Pt, i.e., ion-exchange, followed by calcination and reduction, did not significantly change the properties of MCM22 ST. In the case of MCM22 SR, however, dealumination took place during the calcination/reduction procedure, as indicated by the increase in octahedral Al. The dealumination also led to a significant decrease in the crystallinity of the sample. A detailed comparison of the XRD patterns of the parent MCM22 and Pt-MCM22 showed that in Pt-MCM22 the intensity of lower indexed reflections (like (100)/(002) and (101)) decreased compared to the higher indexed reflections. This could point to a local destruction of the framework, which affected short range reflections in XRD, while on a larger scale the structure was only slightly perturbed.

The relative concentration of Lewis acid sites measured by pyridine adsorption did not exactly agree with the ratio $Al_{oh}/(Al_{oh}+Al_{td})$. Especially in the case of MCM22 ST the concentration of octahedral Al was higher, indicating that not all the extraframework Al was Lewis acidic.

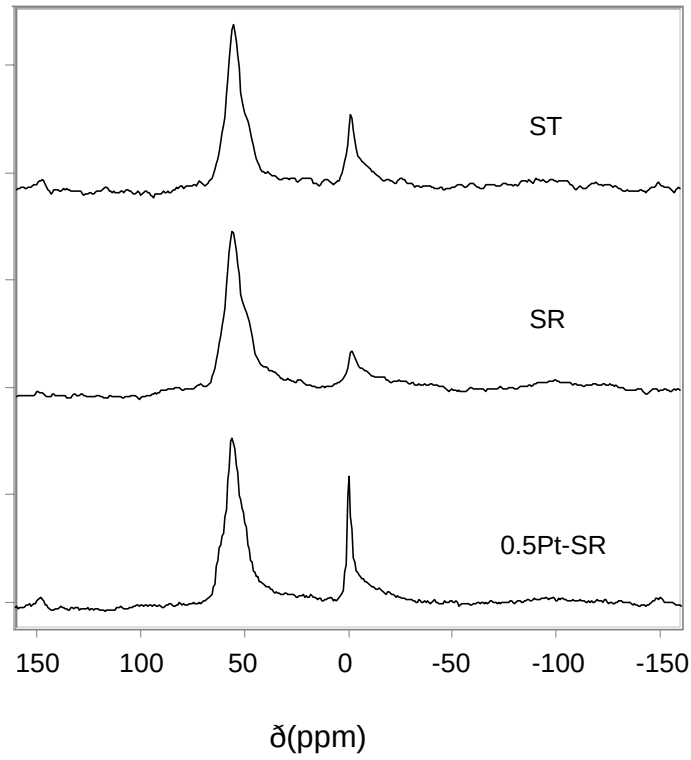

Figure 2 *^{27}Al-MAS-NMR spectra of (a) MCM22 ST, (b) MCM22 SR, (c) 0.5%Pt-MCM22 SR.*

Butene isomerization and butadiene poisoning

Figure 3 compares the performance of the MCM22 materials in the isomerization of 1-butene. For both catalysts the yield of isobutene increased drastically within the first minutes on stream. Simultaneously, the formation of by-products (mainly propene and pentene, in the case of MCM22 SR also n-butane) decreased. After this period, stable yields of isobutene were obtained with MCM22 SR and ST, at excellent selectivity. Table 2 compares the activity and selectivity of the MCM22 materials with those of other isomerization catalysts (ZSM5, TON, FER) (see Chapter 7 and 8). The MCM22 catalysts were an order of magnitude more active and achieved higher yields of isobutene than the other materials at a comparable selectivity.

Table 2 *Comparison of activity and selectivity of different zeolites in butene isomerization. SiO_2/Al_2O_3 ratio of the zeolites is given in brackets. 775K, 1 bar, Feed 7% 1-butene in Ar. 100 min on stream.*

Sample	ST (sg/m^3)	Yield i-$C_4^=$ (%)	k [a] (m^3/sg)	Selectivity i-$C_4^=$ (%)
ZSM5(480)	5200	13.1	$3.3*10^{-5}$	87.1
TON(35)	4500	16.2	$4.9*10^{-5}$	88.6
FER(90)	4850	7.3	$1.4*10^{-5}$	94.3
FER(17) [b]	2400	14.8	$9.2*10^{-5}$	93.1
MCM22 (25) SR [c]	2500	37.0	$>1*10^{-3}$	88.0
MCM22 (38) ST [c]	2250	28.0	$>6*10^{-4}$	92.4

[a] Pseudo first order rate constant of butene isomerization.

[b] 4.5% 1-butene in the feed instead of 7%.

[c] No data were measured at low conversions. As a result, only a lower limit of the rate constant could be given.

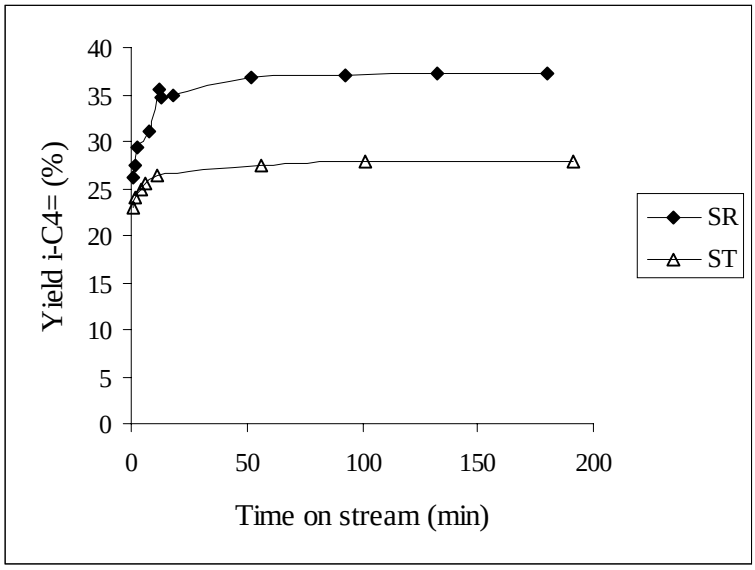

Figure 3 *Isomerization of 1-butene over MCM22. 775 K, 1.2 bar, WHSV = 110 h^{-1}, ST = 2250 sg/m^3. Feed 7% 1-butene in Ar.*

Dehydroisomerization of n-butane

All four Pt-MCM22 materials listed in Table 1 were tested in the dehydroisomerization of n-butane under varying reaction conditions. Figure 4 shows a

typical time-on-stream-behavior of 0.5%Pt-MCM22 ST. Initially, large amounts of methane and propane were formed. The rate of formation of these products decreased very fast. Simultaneously, the yield of the sum of butenes and of isobutene increased. After 20 min the performance of the catalyst was rather stable. The main products were linear butenes, isobutene and isobutane.

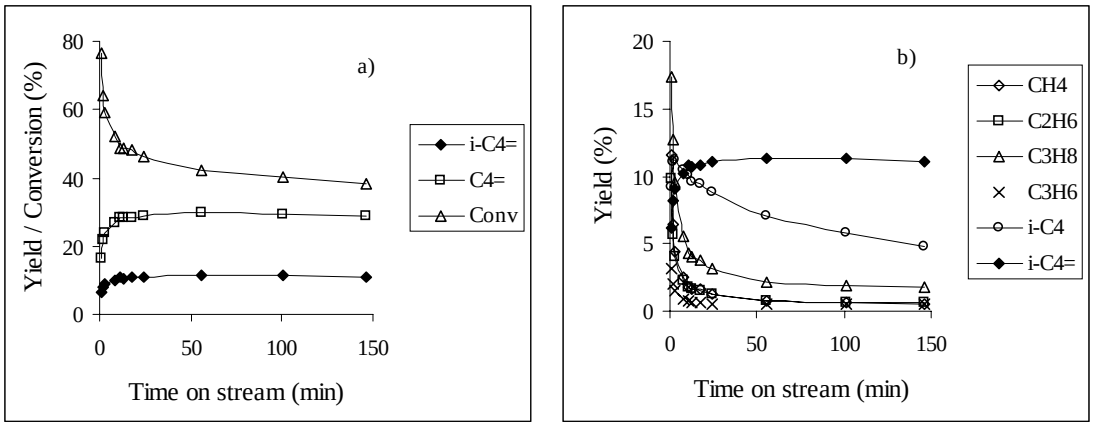

Figure 4 *Dehydroisomerization of n-butane over 0.5%Pt-MCM22 ST. 775 K, 1 bar, WHSV = 23 h^{-1}. Feed 10% n-butane, 20% H_2.*

Figure 5 compares the steady state performance (i.e., after 100 min on stream) of 0.5%Pt-MCM22 and 0.5%Pt-ZSM5(480). The dehydrogenation activity of the two Pt-MCM22 materials, ST and SR, and of Pt-ZSM5 was quite similar. The ratio $iC_4^{=}/\sum C_4^{=}$, however, was much higher in the case of the Pt-MCM22s (see Figure 5c). It came close to the thermodynamic limit at space times above 10000 sg/m^3. As a result of the higher isomerization activity higher yields of isobutene were obtained with Pt-MCM22 than with Pt-ZSM5 at the same contact time.

The by-product patterns of Pt-ZSM5 and Pt-MCM22 were quite different (see Figure 6). For Pt-MCM22 isobutane was the most abundant by-product, as opposed to propane in the case of Pt-ZSM5. The total selectivity to by-products (i.e., all products apart from butenes) was comparable for the two materials.

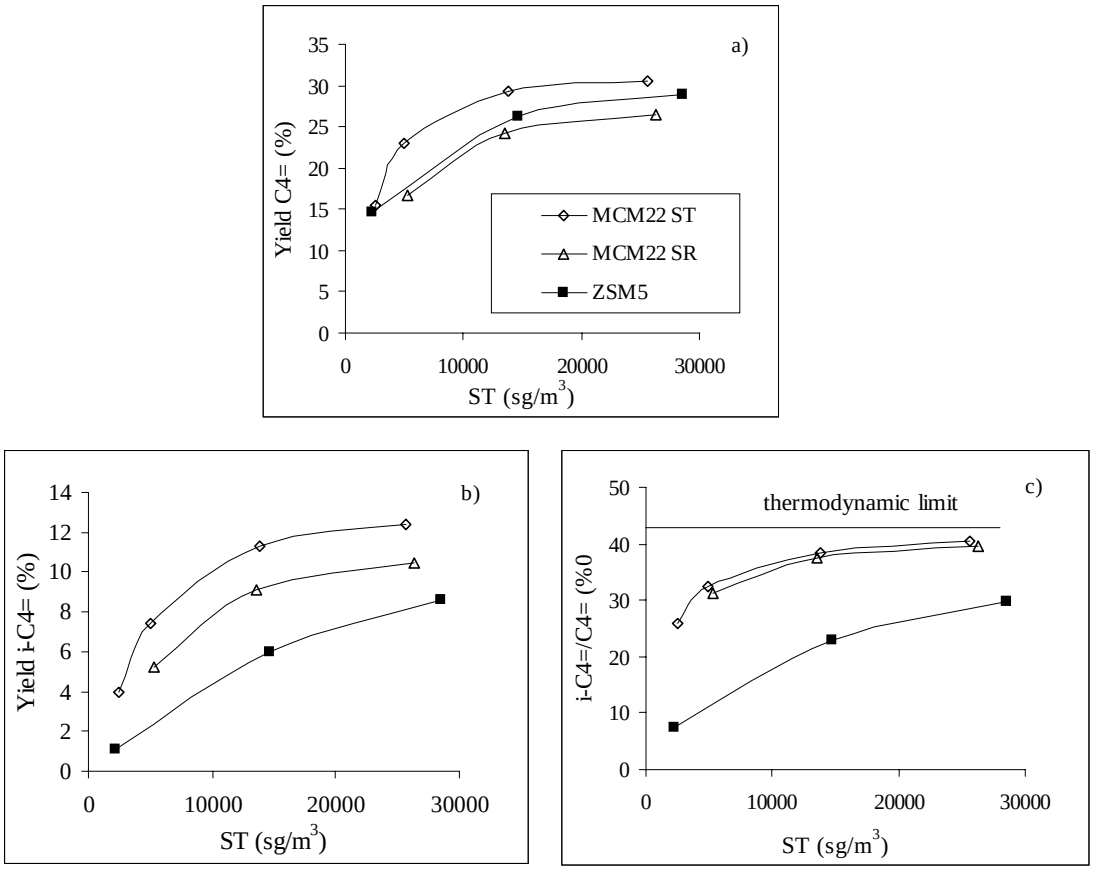

Figure 5 *(a) Yield of $\sum C_4^=$, (b) yield of isobutene, (c) ratio $iC_4^=/\sum C_4^=$ as a function of the space time. 775 K, 1 bar, 100 min on stream. Feed 10% n-butane, 20% H_2. Metal loading of all three catalysts was 0.5% Pt.*

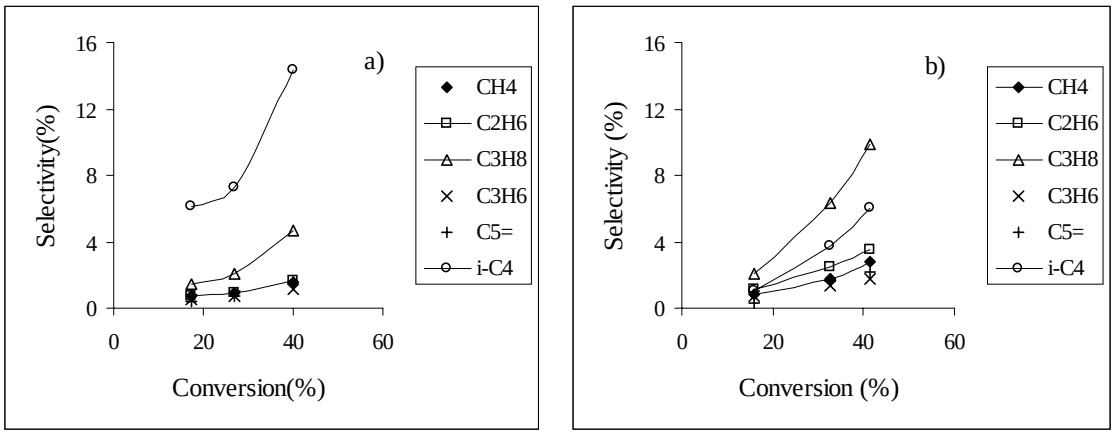

Figure 6 *Selectivity to by-products as a function of the conversion of n-butane. (a) 0.5%Pt MCM22 ST (b) 0.5%Pt-ZSM5(480). 775 K, 1 bar, 100 min on stream.*

The high selectivity to isobutane at low conversions suggested that it could be a primary product formed by direct isomerization of n-butane on the acid sites. In order

to check this hypothesis, the reaction of n-butane over the parent MCM22 ST was performed under the same conditions as used in dehydroisomerization. Table 3 compares the yield of cracking products and the conversion of n-butane. The yield of isobutane was a factor of 40 smaller than in the presence of Pt. The yields of methane and ethane, cracking products of n-butane (n-$C_4H_{10} \rightarrow CH_4 + C_3H_6$, $C_4H_{10} \rightarrow C_2H_6 + C_2H_4$), were a factor of 10 lower. It was, therefore, concluded that (i) isobutane was not formed by isomerization of n-butane on the acid sites, but by hydrogenation of isobutene on Pt, (ii) the contribution of protolytic cracking of n-butane on the acid sites to the overall by-product formation in dehydroisomerization was negligible.

Table 3 *Yield of by-products in the conversion of n-butane over (Pt-)MCM22 ST. 775 K, 1.2 bar, WHSV = 180 h^{-1}. Feed 10% n-butane, 20% H_2. 100 min on stream.*

Yield (%)	MCM22 ST	Pt-MCM22 ST
CH_4	0.009	0.12
C_2H_6	0.014	0.13
C_2H_4	0.014	0.01
C_3H_8	0.000	0.26
C_3H_6	0.025	0.09
i-C_4	0.027	1.08
$\sum C_4^=$	0.041	15.5
Conversion	0.13	17.4

Figure 7 compares the stability of Pt-MCM22 and Pt-ZSM5 during dehydroisomerization under identical reaction conditions. While the dehydrogenation activity of Pt-ZSM5 was stable, deactivation was observed for both Pt-MCM22 materials. It was much stronger for Pt-MCM22 SR than for ST. Increasing the metal loading of to 1% did not improve the stability of Pt-MCM22 SR.

Under the conditions shown in Figure 7, the ratio $iC_4^=/\sum C_4^=$ was stable for all three catalysts. At higher WHSVs, however, also a decrease of the isomerization activity of the Pt-MCM22s was observed with time on stream. The rate of deactivation was higher with Pt-MCM22 SR than with Pt-MCM22 ST.

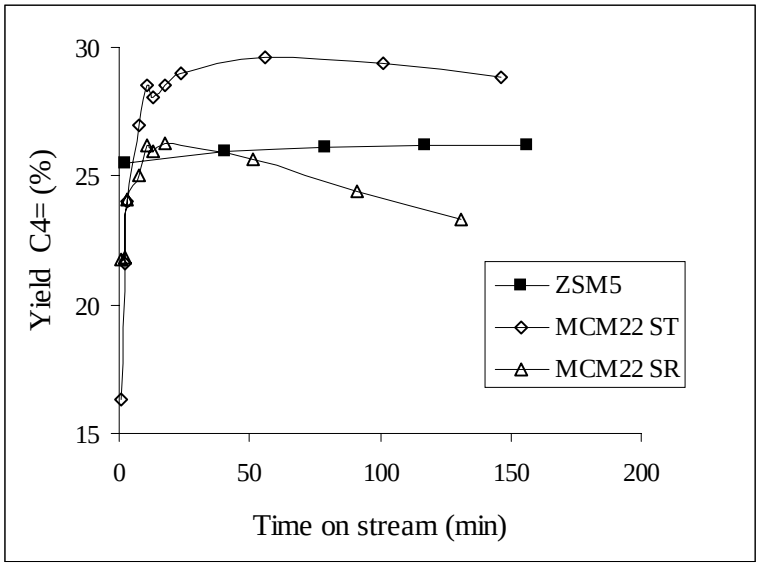

Figure 7 *Stability of dehydrogenation for Pt-MCM22 ST, Pt-MCM22 SR and Pt-ZSM5(480). Metal loading 0.5% for all three catalysts. 775 K, 1 bar, WHSV = 25 h^{-1}, Feed 10% n-butane, 20% H_2.*

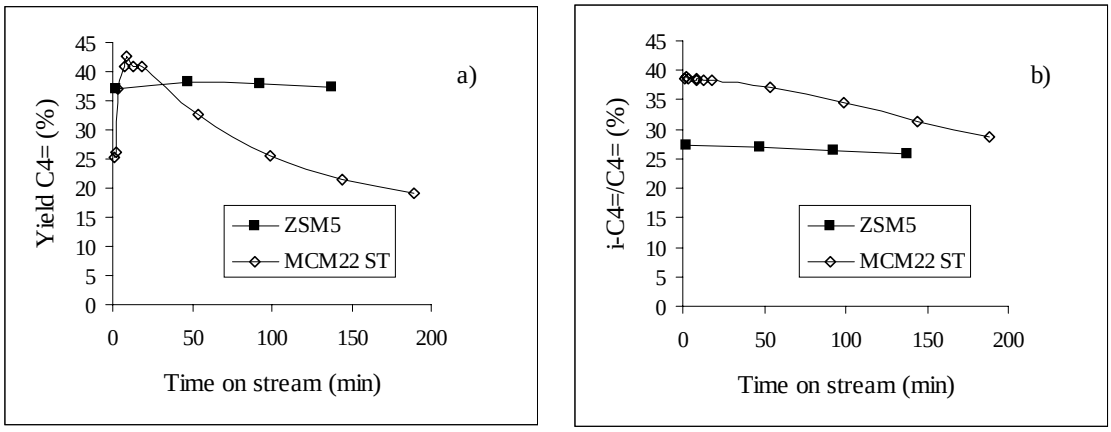

Figure 8 *Stability of (a) dehydrogenation and (b) isomerization for 0.5%Pt-MCM22 ST and 0.5%Pt-ZSM5(480). 825 K, 1 bar, WHSV = 20 h^{-1}, Feed 10% n-butane, 20% H_2.*

The dehydroisomerization reaction over Pt-MCM22 ST also performed at 825 K where dehydrogenation is thermodynamically more favored than at 775 K. Under these conditions Pt-MCM22 ST achieved an initial yield of more than 16% isobutene. But the dehydrogenation activity decayed much faster than at 775 K (see Figure 8), while Pt-ZSM5 was still stable.

Dehydroisomerization over a staged bed of Pt-ZSM5 and MCM22

Pt-ZSM5 had a high stability in dehydroisomerization (see Chapter 5), but only a moderate selectivity. The results presented so far suggest an opposite behavior for Pt-MCM22. MCM22 was a very active and selective catalyst in butene isomerization, but the stability of Pt-MCM22 in dehydroisomerization was at best moderate, especially at higher temperatures (see Figure 8). In trying to combine the stability of Pt-ZSM5 with the high isomerization activity of MCM22 staged bed experiments were performed, with a layer of Pt-ZSM5 upstream of a layer of MCM22 SR (the most active isomerization catalyst). 805 K was chosen as reaction temperature in order to stay below the calcination temperature of MCM22 (813 K). Figure 9 compares the results of two-component catalysts with that of Pt-ZSM5 and Pt-MCM22.

Due to low activity of MCM22 in cracking of n-butane the additional bed of MCM22 SR did not lead to a higher n-butane conversion compared to Pt-ZSM5. Only the butenes formed on Pt-ZSM5 underwent secondary transformation over MCM22, i.e., cracking, mainly to ethene and propene, and isomerization. Because of the cracking reactions, the yield of $\sum C_4^=$ decreased slightly from Pt-ZSM5 to the 3/1 and 2/1 mixture with MCM22 SR. The yield of isobutene, on the other hand, increased significantly from 8 to 12.5% upon adding MCM22 SR (see Table 4). Note that increasing the MCM22 content in the staged bed from 25 to 33 wt% did not lead to a further increase in the yield of isobutene, but only in the yield of cracking products.

A yield of 12.5% isobutene could also be obtained with Pt-ZSM5, when the contact time was doubled (see Table 4). But in that case the selectivity to isobutene was significantly lower than with the staged bed (23.5% compared to 30% for the staged bed).

Pt-MCM22 ST obtained initially the highest yield of isobutene (14%). But, as at 825 K, the dehydrogenation activity decayed very fast, while the staged bed was stable.

Table 4 *Dehydroisomerization of n-butane over Pt-MCM22 ST, Pt-ZSM5 and a staged bed of Pt-ZSM5/MCM22 SR. 805 K, 1.0 bar, 200 min on stream. Feed 10% n-butane, 20% H_2, balance Ar.*

	Pt-MCM22 ST	Pt-ZSM5		Pt-ZSM5 / MCM22 3/1	Pt-ZSM5 / MCM22 2/1
WHSV (h^{-1})	25	25	12.5	25	25
Yield ∑C4= (%)	25.0	34.6	38.0	32.4	30.5
Yield i-C4= (%)	9.0	8.1	11.8	12.4	12.0
i-C4=/∑C4=	35.5	23.5	31.0	38.5	40.1
Sel. ∑C4= (%)	86	84	76	78	76
Sel. i-C4=	30	23.5	20	30	30

Discussion

As butene isomerization approaches thermodynamic equilibrium, the selectivity of ZSM5 to oligomerization/cracking products (mainly propene and pentene) increases exponentially (see Chapter 5 and ref. [17]). The increase in oligomerization/cracking limits the yield of isobutene that can be achieved with Pt-ZSM5 in dehydroisomerization.

MCM22, on the other hand, reached $iC_4^=/\sum C_4^=$ ratios of up to 39% in the skeletal isomerization of 1-butene, i.e., close to the thermodynamic limit of 43%, while maintaining a high selectivity of around 90%. At similar ratios of $iC_4^=/\sum C_4^=$ the selectivity of ZSM5 to butene isomerization was only 60%. It is, therefore, to be expected that Pt-MCM22 should suffer much less from loss in selectivity by oligomerization/cracking reactions in the dehydroisomerization of n-butane. This was fully confirmed by the present findings. Pt-MCM22 and Pt-ZSM5 achieved comparable yields of $\sum C_4^=$. But the yield of isobutene was higher for Pt-MCM22, due to the higher isomerization activity of MCM22. Very little cracking products were observed even at high conversions. The main by-product of Pt-MCM22 was isobutane, formed by hydrogenation of isobutene on the metal, as opposed to propane in the case of Pt-ZSM5, which is formed by oligomerization/cracking and subsequent hydrogenation.

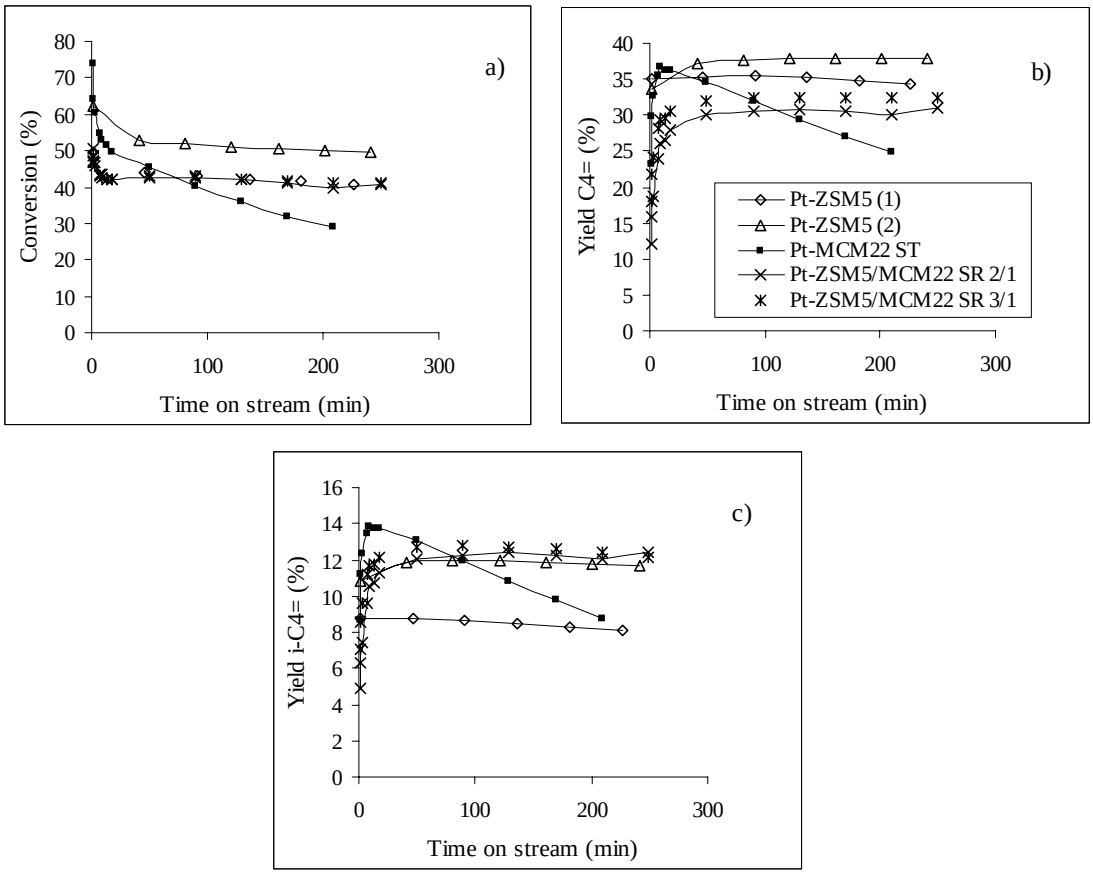

Figure 9 *Dehydroisomerization of n-butane over Pt-MCM22 ST, Pt-ZSM5 and a staged bed Pt-ZSM5/MCM22 SR (m/m = 3/1 and 2/1). Metal loading of all catalysts 0.5% Pt. (a) Conversion of n-butane. (b) Yield of* $\sum C_4^=$*. (c) Yield of isobutene. 805 K, 1.0bar, WHSV = 25* h^{-1} *(12.5* h^{-1} *for Pt-ZSM5(2)). Feed 10% n-butane, 20%* H_2*.*

In explaining the catalytic properties of (Pt-)MCM22, two questions have to be addressed. (i) Why is the intrinsic selectivity of MCM22 to isomerization *vs.* oligomerization/cracking higher than for ZSM5? (ii) What are the reasons for the different behavior of Pt-MCM22 as compared to Pt-FER, which is also a very selective catalyst for butene isomerization?

Let us first turn to the high activity and selectivity of MCM22 in butene isomerization. Table 5 compares the channel dimensions of MCM22, ZSM5, FER and TON. In the case of ZSM5 it is usually argued that the moderate selectivity of this material in butene isomerization is due to its too large pores [18]. Especially, the cavities formed at the intersections of straight and sinusoidal channels are large enough to form larger molecules, which subsequently crack unselectively. In the light of these arguments, the high selectivity of MCM22 is surprising, since the inter-layer

pore system of MCM22 contains even larger cavities (diameter 18 Å). MCM22 was, however, only selective in steady state (see Figure 3). Initially, the by-product formation was very high. It is, thus, possible that the inter-layer channel system with the large cages was rapidly deactivated in the initial stages of the reactions. Subsequently, the reaction took only place in the intra-layer channel system. The dimensions of this channel system are smaller than in the case of ZSM5 and comparable to FER, explaining the high selectivity to butene isomerization. Moreover, the pore system of MCM22 is two-dimensional, which facilitates diffusion of the molecules, and could be responsible for higher activity of MCM22 compared to FER and TON (see Table 2)[1].

Table 5 *Channel dimension of MCM22, ZSM5, FER and TON [19]. " ⇔ " indicates that the channels are connected, " | " that they are not.*

Zeolite	Channel dimensions (Å)	Diameter cavity (Å)
MCM22	10MR 5.5 x 4.0 (2-dim) | 10MR 5.5 x 4.0 (2-dim)	- | 18
ZSM5	{10MR 5.3 x 5.6 ⇔ 10MR 5.1 x 5.5}(3-dim)	8-9
FER	10MR 4.2 x 5.4 (1-dim) ⇔ 8MR 3.5 x 4.8 (1-dim)	6-7
TON	10MR 4.4 x 5.5 (1-dim)	-

The higher dehydrogenation activity of Pt-ZSM5 and Pt-MCM22 compared to Pt-FER was attributed to diffusion limitations in the case of Pt-FER, as extensively discussed in the previous chapter. In the case of Pt-FER most of the Pt was present in the form of small particles in the zeolite pores. Due to the large zeolite crystals (6-10 µm) diffusion pathways were long. As a result, access to the metal was constrained. SEM photographs of MCM22 showed that the dimensions of the MCM22-layers were rather small (0.5-1 µm). Moreover, the two-dimensionality of the pore system facilitates diffusion. Therefore, access to the metal was not hindered and a high dehydrogenation activity was obtained, like in the case of Pt-ZSM5.

[1] Also FER has a two-dimensional pore systems, but the openings of the 8-ring pores are so small that diffusion is very slow.

Apart from activity and selectivity, however, also the stability is a very important quality of a catalyst. In this respect the performance of Pt-MCM22 was only moderate. Deactivation was always observed. The rate of deactivation increased with increasing temperatures. Pt-MCM22 SR deactivated faster than Pt-MCM22 ST, with respect to dehydrogenation (see Figure 7) and isomerization. In the skeletal isomerization of butene, on the contrary, MCM22 ST and SR gave both stable performances (Figure 3). The observed deactivation in the dehydroisomerization reaction was, therefore, attributed to structural changes caused during calcination/reduction of Pt-MCM22. The concentration of octahedral Al in MCM22 SR increased significantly upon incorporation of Pt (see Table 1), indicating that the framework was dealuminated. XRD showed a concomitant loss in crystallinity. The framework structure of MCM22 ST was less affected during the calcination/reduction of Pt. Pt-MCM22 ST maintained a rather stable isomerization and dehydrogenation activity, while Pt-MCM22 SR did not. This suggested that the deactivation was strongly related to the crystallinity of the samples. Enhanced deactivation of dealuminated samples was also observed in the skeletal isomerization of n-butene over ferrierites modified by steaming [20] and for dealuminated TON [21].

In order to avoid the problems with the stability of Pt-MCM22 at high temperatures, the use of the parent MCM22 as an additional isomerization catalyst in combination with Pt-ZSM5 is a very interesting alternative. In such a staged bed Pt-ZSM5 should mainly act as a dehydrogenation catalyst, while the ratio $iC_4^{=}/\sum C_4^{=}$ should be kept low in order to avoid extensive by-product formation. The MCM22 content must be chosen high enough to bring the ratio $iC_4^{=}/\sum C_4^{=}$ close to thermodynamic equilibrium. A too high MCM22-content, however, will lead to unnecessary cracking reactions of butene and lower the selectivity (see Table 4).
Similar yields of isobutene as with the staged bed could also be achieved with Pt-ZSM5, but only at significantly higher contact times and, hence, a lower selectivity to isobutene.

Conclusions

MCM22 is a very active and selective catalyst for butene isomerization at high temperatures. The high selectivity and activity is attributed to the shape-selective properties of the 10-membered ring channels in the layers, whose dimensions are

similar to those of FER, and to the two-dimensionality of the pore system of MCM22 which facilitates diffusion.

The good catalytic properties of MCM22 in butene isomerization can be successfully made use of in the dehydroisomerization of n-butane over Pt-MCM22. Due to the higher activity and selectivity of MCM22 in butene isomerization compared to ZSM5, Pt-MCM22 gives higher yields of isobutene than Pt-ZSM5 and less oligomerization/cracking products. The contribution of the other possible side reaction, protolytic cracking of n-butane on the acid sites and hydrogenolysis on the metal, is negligible.

The deactivation of the dehydrogenation and isomerization activity of Pt-MCM22 during dehydroisomerization is attributed to defects created in the material. The good catalytic properties of MCM22 can only be maintained when the framework remains intact during calcination/reduction of Pt-MCM22. The observed differences between Pt-MCM22 SR and ST were mainly related to the different deactivation behavior, i.e., the different crystallinity, of these samples. The SiO_2/Al_2O_3 ratio, on the other hand, had only a minor influence of the performance, at least within the reported range of variation (25 to 35).

As an alternative to a bifunctional Pt-MCM22, the parent MCM22 can also be used as a pure isomerization catalyst in combination with Pt-ZSM5 in order to increase the yield of isobutene in dehydroisomerization, in analogy to the staged bed approach of Bellussi *et al.* [22]. The two-component catalyst has a significant advantage over Pt-ZSM5 with respect to selectivity and activity in isobutene formation and does not suffer from deactivation, like Pt-MCM22.

Acknowledgements

I am very much indebted to Prof. Weitkamp, from the University of Stuttgart, and to Dr. Nowak, from Shell Research and Technology Center Amsterdam, for supplying the MCM22 samples. NMR experiments were performed at the NOW/CW HF-NMR Facility (NSR Center, University of Nijmegen). I would like to thank G.H. Nachtegaal for skillfully designing and performing the NMR experiments, O.P.E. Zinck-Stagno for his help in preparing the Pt-MCM22 samples and H. Koster for carrying out the XRD-measurements.

References

[1] Leonowicz, M.E., Lawton, J.A., Lawton, S.A., and Rubin, M.K., Science **264**, 1910 (1994).

[2] Martens, J.A., Tielen, M., Jacobs, P.A., and Weitkamp, J., Zeolites **4**, 98 (1984).

[3] Martens, J.A., and Jacobs, P.A., Zeolites **6**, 334 (1986).

[4] Souverijns, W., Verrelst, W., Vanbutsele, G., Martens, J.A., and Jacobs, P.A., J. Chem. Soc., Chem. Comm. 1671 (1994).

[5] Thomas, J.M., Sci. Am. **April** 112 (1992).

[6] Houzvicka, J., Hansildaar, S., and Ponec, V., J. Catal. **167**, 273 (1997).

[7] Asensi, M.A., Corma, A., and Martinez, A., J. Catal. **158**, 561 (1996).

[8] Corma, A., Corell, C., and Perez-Pariente, J., Zeolites **15**, 2 (1995).

[9] Hunger, M., Ernst, St., and Weitkamp, J., Zeolites **15**, 188 (1995).

[10] Abril, R.P.L., Bowes, E., Green, G.J., Marler, D.O., Sihabi, D.S., and Sacha, R.F., US Patent 5.085.762 (1992), assigned to Mobil.

[11] Ward, J.W., J. Catal. **9**, 225 (1967); **11**, 271 (1968).

[12] Khabtou, S., Chevreau, T., and Lavalley, J.C., Micropor. Mat. **3**, 133 (1994).

[13] Samoson, A., and Lippmaa, E., Chem. Phys. Lett. **100**, 205 (1983).

[14] Samoson, A., and Lippmaa, E., Phys. Rev. B **28**, 6567 (1983).

[15] Lawton, St.L., Fung, A.S., Kennedy, G.J., Alemany, L.B., Chang, C.D., Hatzikos, G.H., Lissy, D.N., Rubin, M.K., Timken, H.K.C., Steuernagel, S., and Woessner, D.E., J. Phys. Chem. **100**, 3788 (1996).

[16] Engelhardt, G., in "Introduction to Zeolite Science and Practice" (H. van Bekkum, E.M. Flanigen, J.C. Jansen, Eds.), p. 285, Elsevier, Amsterdam, 1991.

[17] Houzvicka, J., Nienhuis, J.G., and Ponec, V., Appl. Catal. A **174**, 207 (1998).

[18] O'Young, Ch.-L., Pellet, R., Casey, D., Ugolini, J., Sawicki, R.A., J. Catal. **151**, 467 (1995).

[19] Meier, W.M., Olson, D.H., and Baerlocher, Ch., Atlas of Zeolite Structure Types (4^{th} ed.), 1996, Butterworth-Heinemann, Stoneham, USA.

[20] Xu, W.-Q., Yin, Y.-G., Suib, St.L., Edwards, J.C., and O'Young, Ch.-L., J. Catal. **163**, 232 (1996).

[21] Baeck, S.H., and Lee, W.Y., Appl. Catal. A **168**, 171 (1998).

[22] Bellussi, G., Giusti, A., Zanibelli, L, US Patent 5.336.803 (1994), assigned to Eniricerche SpA, Snamprogetti SpA.

Chapter 10

Summary/Samenvatting

Summary

The research presented here was largely motivated by the exponential growth in the market for MTBE in the last 15 years, especially in the US, which asked for new routes for producing the MTBE-raw material isobutene. The direct, one-step conversion from butanes, which are available in abundant supply from natural gas reserves and refinery sources, is a very attractive method for making isobutene. It could replace or be used in addition to the current two-step processes, which have separate isomerization and dehydrogenation units.

Dehydroisomerization of n-butane to isobutene is a very challenging reaction. Since dehydrogenation is highly endothermic, it has to be carried out at high temperatures. High temperatures are, however, unfavorable for the isomerization equilibrium. As a result, the yield of isobutene is always limited by thermodynamics. Oxidative dehydrogenation offers a possibility to circumvent the thermodynamic constraints, because the formation of water makes the reaction exothermic. Therefore, the concept of oxidative dehydroisomerization was explored by using physical mixtures of an oxidative dehydrogenation catalyst (supported vanadia-niobia mixed oxides) with an isomerization catalyst (10 membered-ring zeolites, like FER, ZSM5, MCM36). These physical mixtures were able to produce small yields of isobutene from n-butane.

However, a strong decrease of the isomerization activity of the zeolite was observed with time on stream. The deactivation was caused by butadiene, which was formed over the oxidative dehydrogenation catalyst. The presence of oxygen in the reaction mixtures accelerated the acid catalyzed transformation of butadiene to coke, thereby enhancing the deactivation of the zeolite. Due to the severeness of deactivation and the fact that the formation of butadiene cannot be avoided with oxidative dehydrogenation catalysts, the concept of oxidative dehydroisomerization did not seem feasible. Hence, we turned our attention to catalytic systems for non-oxidative dehydroisomerization. Due to the absence of oxygen and the higher ratio of butene to butadiene obtained in non-oxidative dehydrogenation, deactivation by butadiene could be expected to be less severe in that case.

Pt-zeolites were the materials of choice for non-oxidative dehydroisomerization. Pt is the most commonly used metal for dehydrogenation reactions and zeolites are the most selective and stable materials for butene isomerization. Motivated by similar examples in patent literature, we started using Pt-ZSM5 and studied the influence of metal loading, acid site concentration and reaction conditions (pressure, temperature, H_2/n-butane ratio). Pt-ZSM5 catalysts with high metal loading and low acid site concentration gave the highest yield of isobutene and the lowest by-product formation. This was attributed to the fact that most of the by-products of Pt-ZSM5 were formed by acid catalyzed oligomerization/cracking of butenes. The selectivity to oligomerization/cracking increased drastically, as the ratio $iC_4^{=}/\sum C_4^{=}$ approached thermodynamic equilibrium. Materials with a high metal loading and a low acid site concentration allowed to approach dehydrogenation equilibrium, while $iC_4^{=}/\sum C_4^{=}$ was still far from equilibrium and, thus, the by-product formation low. Materials with high acid site concentration, on the other hand, approached isomerization equilibrium fast and, as a result, by-product formation increased while the yield of $\sum C_4^{=}$ was still low.

With respect to the reaction temperature an optimum was found at 830 K. At lower temperatures, high yields of isobutene could not be achieved due to the thermodynamic constraints of dehydrogenation. At higher temperatures, the stability of the catalysts deteriorated due to increased butadiene formation. Low pressures helped to reduce the selectivity to oligomerization/cracking and were also favorable with respect to thermodynamics. Addition of hydrogen to the feed was necessary in

order to maintain a stable activity of the catalyst. However, increasing the H_2/n-butane ratio above 2 led to a drastic increase in hydrogenolysis reactions.

From these results we concluded that the optimum conditions for dehydroisomerization of n-butane should be obtained using 0.5%Pt-ZSM5 (SiO_2/Al_2O_3 = 480) at 830 K, 1 bar and H_2/n-butane = 2. In fact a stable yield of 14-15% isobutene could be obtained under these conditions, which is among the highest yields reported in patent literature.

The potential for further improvement of Pt-ZSM5 is limited by the rather high selectivity to oligomerization/cracking of this material. This property is inherent to ZSM5 and related to the fact that the pores of ZSM5 are too large to obtain a high selectivity to butene isomerization. Better results should be achieved by using other microporous materials that have a higher selectivity to butene isomerization *vs.* oligomerization/cracking than ZSM5. Hence, the catalytic performance of Pt-TON and Pt-FER in dehydroisomerization was studied and compared with Pt-ZSM5. Pt-ZSM5 had, however, a higher dehydrogenation activity and, in contrast to the expectations, also a higher selectivity than Pt-TON and Pt-FER. The lower selectivity of Pt-TON and Pt-FER was caused by a higher contribution of hydrogenolysis and cracking of n-butane to the by-product formation. With Pt-ZSM5, these two side reactions were only of minor importance.

More important, however, was the different dehydrogenation activity of Pt-ZSM5 and Pt-TON and Pt-FER. Since Pt-ZSM5 had a moderate Pt-dispersion and a rather inhomogeneous distribution of Pt in the zeolite, but a high dehydrogenation activity, while the opposite was the case for Pt-FER, the different activity was not primarily related to the metal dispersion. It was rather due to diffusional limitations in the narrow, one-dimensional pores of Pt-TON and Pt-FER. The diffusional constraints were especially severe, when the zeolite crystals were large and, thus, the diffusion pathways long. Note that with Pt-ZSM5, where the channel system is two-dimensional and diffusion fast, no influence of crystal size on the catalytic performance was found.

MCM22 is a 10-membered ring with a high activity and selectivity in butene isomerization. It has a two-dimensional pore system like ZSM5 and should thus be a very suited material for dehydroisomerization. In fact, Pt-MCM22 achieved very better yields and selectivities than Pt-ZSM5 up to temperatures of 775 K. At higher

temperatures, however, the dehydrogenation activity of Pt-MCM22 decayed rather rapidly with time on stream.

In trying to combine the good stability of Pt-ZSM5 with the high isomerization activity and selectivity of MCM22, a staged bed of Pt-ZSM5 and MCM22 was used for dehydroisomerization. Here, Pt-ZSM5 mainly acted as a dehydrogenation catalyst, while the ratio $iC_4^=/\sum C_4^=$ was kept low in order to avoid extensive by-product formation. The MCM22 content was chosen high enough to bring the ratio $iC_4^=/\sum C_4^=$ close to thermodynamic equilibrium. This two-component catalyst gave an improved performance with respect to activity and selectivity, compared to Pt-ZSM5.

We can conclude that various parameters are important for the performance of a dehydroisomerization catalyst, which can be summed up in the following catalyst design criteria:

- The metal loading of the dehydroisomerization catalyst should be high in order to increase the dehydrogenation activity. There is however an optimum (about 0.5 wt% Pt), above which dehydrogenation activity does not increase significantly while selectivity is lost due to an increase in hydrogenolysis.
- The acid site concentration should be as low as possible in order to avoid cracking reactions. A certain acid site concentration is necessary, however, for butene isomerization. A good dehydroisomerization catalyst should have a high TOF for butene isomerization and a low TOF for cracking of n-butane.
- The zeolite pore geometry has to suppress the formation of larger oligomers from butene, which can subsequently crack into smaller fragments. In this respect, FER and MCM22 are very suited materials, while ZSM5 has a rather high selectivity to oligomerization/cracking.
- In order to avoid internal diffusion limitations, the zeolite should have a two-dimensional pore-system (like MCM22 and ZSM5) and/or small crystals (TON *vs.* FER).
- A homogenous distribution of the metal in the pores of the zeolite seems to be counterproductive and enhance hydrogenolysis rather than dehydrogenation.

Since acid site concentration, metal dispersion and zeolite crystal size can often not be varied independent of each other, it is difficult to separate the influence of these parameters. A more detailed study, in which only the crystal size is of FER and TON

is varied, while acid site concentration, metal dispersion, etc. are kept constant, would be necessary to get more insight into the effect of diffusion in the one-dimensional pore systems. Moreover, methods should be developed to prepare Pt-zeolites with a tailored metal distribution, containing Pt either mainly in the pores or on the outer surface, having mainly intermediate size (3 – 10 nm) or very small particles (< 2 nm), etc. This would give a better understanding of the chemistry on the outer surface and in the pores of the zeolite and enable an optimization of the metal function with respect to location and dispersion. Prerequisite for such a study is the improvement of tools for characterization of Pt-zeolites with low metal loadings, by spectroscopic methods and test reactions.

Another important issue that has not been dealt with in depth in this work is the question of catalyst deactivation, due to sintering, coke formation, etc. Further studies in this field will be especially important to improve the stability of Pt-MCM22, which is – due to its very high activity and selectivity – the most promising catalyst for dehydroisomerization.

The ultimate goal of this project was to lay the basis for a dehydroisomerization process that can compete with the current two-step processes for making isobutene. A preliminary economic evaluation showed that the size of the recycle streams (H_2, dilutant, n-butenes) is probably the bottleneck for the feasibility of one-step dehydroisomerization. In to reduce the recycle volumes and, thus, the size of the reactor and the separation sections, the process should be operated without dilutant and with as little hydrogen as possible. Industrial dehydroisomerization catalysts have to prove to be selective and stable under these more severe conditions.

Samenvatting

De sterk groeiende vraag naar MTBE, veroorzaakt door het verplichte gebruik van zuurstofverbindingen (vooral MTBE) in brandstof in de VS (Clean Air Act), gaf aanstoot tot onderzoek naar nieuwe routes om isobuteen (de uitgangsstof voor MTBE) te produceren. Een heel attraktieve route is de direkte omzetting van butaan, dat in aard- en raffinaderijgas in ruime hoeveelheden beschikbaar is, naar isobuteen in een stap (in tegenstelling tot de huidige twee-staps processen).

Dehydroisomerisatie van n-butaan naar isobuteen is een lastige reaktie. Omdat dehydrogenering endotherm is, moet de reaktie bij hoge temperaturen worden uitgevoerd. Hoge temperaturen zijn echter nadelig voor de isomerisatie-stap. Oxidative dehydrogenering biedt een mogelijkheid deze thermodynamische limiteringen te omzeilen, omdat de vorming van water de reaktie exotherm maakt. Daarom hebben we ons onderzoek eerst op de oxidatieve dehydroisomerisatie van n-butaan gericht ($n\text{-}C_4H_{10} + O_2 \rightleftharpoons i\text{-}C_4H_8 + H_2O$). Met fysische mengsels van een oxidatieve-dehydrogenerings-katalysator (gedragen vanadia-niobia-mengoxides) en een isomerisatie-katalysator (10-ring zeolieten, b.v., FER, ZSM5, MCM36) konden we kleine hoeveelheden isobuteen produceren. Er trad echter een snelle afname van de isomerisatie-aktiviteit met de tijd op. De deaktivering werd veroorzaakt door butadieen dat over de oxidatieve-dehydrogenerings-katalysator gevormd werd. De aanwezigheid van zuurstof in het reaktiemengsel versnelde de deaktivering door de omzetting van butadiene naar coke op de zure plaatsen van de zeoliet te katalyseren. Omdat de vorming van butadieen over de oxidatieve-dehydrogenerings-katalysator uit principe niet kan worden voorkomen, leek het concept van oxidatieve dehydroisomerisatie niet haalbaar. We gingen daarom verder met onderzoek naar katalysatoren voor niet-oxidatieve dehydroisomerisatie. Wegens de afwezigheid van zuurstof en de lagere verhouding van butadieen tot buteen in niet-oxidatieve dehydrogenering, konden we voor deze reaktie minder problemen met deaktivering verwachten.

Pt-zeolieten zijn geschikte materialen voor de niet-oxidatieve dehydroisomerisatie. Pt is het meest gebruikte metaal voor dehydrogenerings-reakties en zeoliten zijn de meest stabiele en selektieve katalysatoren voor buteen-isomerisatie. Na aanleiding van voorbeelden uit de octrooi-literatuur, kozen we voor Pt-ZSM5 als base-case katalysator en bestudeerden de invloed van metaal-belading, concentratie aan zure plaatsen en de reaktie-condities (druk, temperatuur, H_2/n-butaan verhouding). Pt-ZSM5 materialen met hoge metaal-belading en lage concentratie aan zure plaatsen leverden de hoogste opbrengst van isobuteen op en de laagste selektiviteit naar bijprodukten. Dit werd toegeschreven aan het feit dat de meeste bijprodukten van Pt-ZSM5 door oligomeriseren/kraken van buteen worden gevormd. De selektiviteit naar oligomeriseren/kraken neemt drastisch toe als de verhouding $iC_4^{=}/\sum C_4^{=}$ thermodynamisch evenwicht benadert. Materialen met een hoge metaal-belading en

een lage concentratie aan zure plaatsen komen dicht bij het dehydrogenerings-evenwicht, terwijl $iC_4^=/\sum C_4^=$ nog ver van het thermodynamisch evenwicht is. De bijprodukt-vorming blijft dus laag. Anderzijds, materialen met een hoge concentratie aan zure plaatsen anderzijds benaderen het isomerisatie-evenwicht veel sneller. De bijprodukt-vorming wordt hoog en de opbrengst van buteen is dan nog steeds laag.

De optimale reaktietemperatuur was 830 K. Bij lagere temperaturen kon om thermodynamische redenen geen hoge opbrengst van isobuteen worden bereikt. Bij hogere temperaturen nam de stabiliteit van de katalysator-aktiviteit af, als consequentie van deaktivering door butadieen. Lage drukken helpen om oligomeriseren/kraken te onderdrukken en zijn ook thermodynamisch gunstig. Het toevoegen van waterstof aan de feed was nodig om een stabiele aktiviteit te garanderen. Echter boven een H_2/n-butaan verhouding van twee namen hydrogenolyse reakties sterk toe.

Bij gebruik van de beste condities (830 K, 1 bar, H_2/n-butaan = 2) en de beste Pt-ZSM5 katalysator (0.5 wt% Pt, SiO_2/Al_2O_3 = 480) konden we een stabiele opbrengst van 14-15% isobuteen bereiken, vergelijkbaar met de beste resultaten uit de octrooi-literatuur.

Het potentiaal voor een verdere verbetering van Pt-ZSM5 is gelimiteerd door de hoge selektiviteit van ZSM5 naar oligomeriseren/kraken. Deze eigenschap van ZSM5 wordt toegeschreven aan de iets te grote poriëen van de zeoliet die de vorming van oligomeren niet kunnen onderdrukken. Betere resultaten kunnen worden verwacht met materialen als TON en FER die een hogere selektiviteit naar buteen isomerisatie t.o.v. oligomeriseren/kraken hebben. In de dehydroisomerisatie van n-butaan bleek Pt-ZSM5 echter een hogere aktiviteit en, in tegenstelling tot de verwachtingen, ook een hogere selektiviteit te hebben dan Pt-TON en Pt-FER. De lagere selektiviteit van Pt-TON en Pt-FER werd veroorzaakt door een hogere bijdrage van hydrogenolyse en kraken van n-butaan tot de bijprodukt-vorming. Bij Pt-ZSM5 was de bijdrage van deze reakties verwaarloosbaar klein.

Opmerkelijk was vooral het verschil in dehydrogenerings-aktiviteit tussen Pt-ZSM5, Pt-TON en Pt-FER. Aangezien Pt-ZSM5 een slechts bescheiden dispersie, een vrij inhomogene verdeling van Pt in de zeoliet en toch een hoge dehydrogenerings-aktiviteit had, terwijl het tegendeel voor Pt-FER het geval was, hangt het verschil in aktiviteit blijkbaar niet samen met de Pt-dispersie. De lage aktiviteit van Pt-FER en Pt-TON werd verklaard door diffusie-limitering in de nauwe, een-dimensionale

poriëen. Porie-diffusie heeft vooral invloed op de reaktie, als de zeoliet-kristallen groot en de diffusie-wegen lang zijn, zoals bij Pt-FER. Bij Pt-ZSM5, waar het porie-systeem twee-dimensionaal en diffusie snel is, had de kristalgrootte geen effekt.
MCM22 is een 10-ring zeoliet met een hoge aktiviteit en selektiviteit voor buteen isomerisatie. MCM22 heeft een twee-dimensionaal porie-systeem, zoals ZSM5, en zou daarom geschikt moeten zijn voor dehydroisomerisatie. Inderdaad bereikt Pt-MCM22 een hogere aktiviteit en selektiviteit naar iosbuteen dan Pt-ZSM5, bij temperaturen tot 775 K. Bij hogere temperaturen treedt echter een snelle afname van de dehydrogenerings-aktiviteit op.
In een poging de hoge stabiliteit van Pt-ZSM5 en de hoge isomerisatie-aktiviteit en –selectiviteit van MCM22 te kombineren hebben we een dubbel bed van Pt-ZSM5 en MCM22 voor dehydroisomerisatie gebruikt. Pt-ZSM5 heeft daarin vooral de rol van een dehydrogenerings-katalysator, terwijl de verhouding $iC_4^{=}/\sum C_4^{=}$ laag blijft om een extensieve bijprodukt-vorming te voorkomen. De MCM22-gehalte in het dubbel bed werd hoog genoeg gekozen, om $iC_4^{=}/\sum C_4^{=}$ dicht bij het thermodynamisch evenwicht te brengen. Deze twee-komponenten katalysator vertoonde een hogere aktiviteit een selektiviteit naar isobuteen dan Pt-ZSM5.

We kunnen samenvatten dat tal van faktoren invloed hebben op de katalytische eigenschappen van dehydroisomerisatie-katalysatoren. De volgende algemene kriteria voor katalysator-ontwerp hebben we kunnen afleiden:

- Een hoge metaal-belading is gunstig, omdet ze een hogere dehydrogenerings-aktiviteit leidt. Boven een metaal-belading van 0.5 wt% Pt echter stijgt de dehydrogenerings-aktiviteit nauwelijks, terwijl hydrogenolyse toeneemt.
- De concentratie aan zure plaatsen moet zo laag mogelijk zijn, om kraak-reakties te voorkomen. Een minimum aan zure plaatsen is echter nodig voor buteen isomerisatie. Een goede dehydroisomerisatie katalysator heeft een hoge TOF voor buteen isomerisatie en een lage TOF voor het kraken van butaan.
- De geometrie van de zeoliet porie moet dusdanig zijn om de vorming van oligomeren, die daarna kunnen kraken, te voorkomen.
- Twee-dimensionale porie-systemen zijn beter geschikt dan een-dimensionale porie-systemen, omdat diffusie gemakkelijker verloopt.

- Een homogene verdeling van kleine metaal-deeltjes in de porie is niet wenselijk en bevordert hydrogenolyse in plaats van dehydrogenering.

Aangezien de concentratie van zure plaatsen, de Pt-dispersie and de zeoliet-kristalgrootte vaak niet onafhankelijk van elkaar zijn, is het moeilijk de invloed van deze drie parameters exakt te onderscheiden. Een gedetailleerdere studie, waarin b.v. alleen maar de kristalgrootte van Pt-TON en Pt-FER gevarieerd wordt, terwijl de concentratie van zure plaatsen en de metaal-dispersie konstant blijven, zou een beter inzicht van de effekt van porie-diffusie in een-dimensionale zeoliten geven. Bovendien zouden er method moeten worden ontwikkeld om Pt-zeolieten met goed gedefineerde metaal-verdeling te bereiden, b.v. met Pt alleen in de pories of alleen aan het buitenoppervlak, met vooral grote of vooral kleine partikelen, enz. Dit zou meer informatie geven over de chemie in de porie en aan het buitenoppervlak en een optimalisatie van de metaal-verdeling (qua lokatie en dispersie) mogelijk maken. Voorwaarde voor een dergelijke studie is de beschikbaarheid van methodes om Pt-zeoliten met lage beladingen te karakteriseren, door middel van spektroskopische methoden en/of testreakties.
Een ander punt, dat hier niet uitgebreid behandeld was, is de kwestie van deaktivering door sinteren, coke vorming, enz. Verdere studies op dat gebied zijn noodzakelijk om de katalytische stabiliteit van Pt-MCM22 te verbeteren. Pt-MCM22 is, wegens zijn hoge aktiviteit een selektiviteit, de meestbelovende dehydroisomerisatie katalysator.

De uiteindelijke doelstelling van het projekt was een basis te leggen voor een dehydroisomerisatie-proces die kan concurreren met de huidige twee-staps processen. Een voorlopige proces-evaluatie heeft laten zien dat het recycle-volume (H_2, inertgas, n-buteen) het knelpunt van het een-staps proces is. Om het recycle-volume te verkleinen (en dus ook het volume van de reaktor en van de scheidings-sektie), zou het proces zonder gebruik van inert-gas moeten opereren. Veelbelovende katalysatoren moeten daarom onder dergelijke condities worden getest.

General Appendix A - Calculation of the first order rate constant of a reversible reaction

The outlet concentration of a plug flow reactor is related to the inlet concentration of the reactant by the same equation as in a batch reactor with the same residence time τ. For an equilibrium reaction between A and B, assuming first order for both forward and backward reaction

$$A \rightharpoonup B \qquad r = k_A * [A]$$

$$B \rightharpoonup A \qquad r = k_B * [B]$$

the following equation gives the outlet concentration of A ($[A]_0$ is the inlet concentration of A):

$$[A] = \frac{k_B + k_A \cdot e^{-(k_A + k_B)\cdot\tau}}{k_A + k_B} \cdot [A]_0 \qquad (1)$$

In equilibrium $d[B]/dt = 0$, from which we can define an equilibrium constant K:

$$k_A*[A]_{eq} = k_B*[B]_{eq} \qquad \Rightarrow \qquad k_A/k_B = [B]_{eq}/[A]_{eq} =: K$$

Equation (1) rearranges to

$$k_A = -\frac{K}{K+1} \cdot \frac{1}{\tau} \cdot \ln\left[1 - x - \frac{x}{K}\right] \qquad (2)$$

where x is the conversion: $x = ([A]_0 - [A]) / [A]_0$

$[A]$ is experssed in concentration in mol/m^3, the rate mol m^{-3} s^{-1}, k_A in s^{-1}.

For our purposes it is more convenient to express the rate per catalyst mass instead of reactor volume.

$k_A = m_{cat} / V_R * k_{mA}$

$k_A * \tau = k_A * V_R / (dV/dt) = = m_{cat} / V_R * k_{mA} * V_R / (dV/dt) = k_{mA} * m_{cat} / (dV/dt)$

The last term $m_{cat} / (dV/dt)$ is defined as the space time ST [g s m^{-3}].

Combining this with equation 2 gives ([k_{mA}] = m^3 s^{-1} g^{-1})

$$k_{mA} = -\frac{1}{ST} \cdot \frac{K}{K+1} \cdot \ln\left[1 - x - \frac{x}{K}\right] \qquad (3)$$

The intrinsic reaction rate is then

$$r = k_{mA} * [A]_0 = k_{mA} * p_{A0} / (R * T) \qquad (4)$$

Butene isomerization is a special case because we have to deal with equilibrium between four compounds instead of two.

$$A_1 \rightleftharpoons B$$
$$A_2 \rightleftharpoons B$$
$$A_3 \rightleftharpoons B$$

$$d[B]/dt = k_{A1}*[A_1] - k_{B1}*[B] + k_{A2}*[A_2] - k_{B2}*[B] + k_{A3}*[A_3] - k_{B3}*[B]$$

A_i represent the three linear isomers, B represents isobutene.
Double bond isomerization is much faster than skeletal isomerization. Thus, one can assume that the linear isomers are equilibrated very fast and the inlet stream can be treated as an equilibrium mixture of the three linear butenes (instead of 1-butene).

$$[A_2] = K_{21} * [A_1] \qquad [A_3] = K_{31} * [A_1]$$
$$[A] = \sum [A_i] = (1 + K_{21} + K_{31}) * [A_1]$$

We then get $d[B]/dt = k_A * [A] - k_B * [B]$, with $k_A := (k_{A1} + k_{A2} * K_{21} + k_{A3} * K_{31}) / (1 + K_{21} + K_{31})$ and $k_B := k_{B1} + k_{B2} + k_{B3}$, i.e., butene isomerization can be treated like a single equilibrium between n-butene and isobutene.

General Appendix B – SEM photographs of the (Pt-)zeolites

Figure 1 *SEM photographs of (a) 0.1%Pt-FER(670), (b) FER(90), (c) 0.1%Pt-FER(17).*

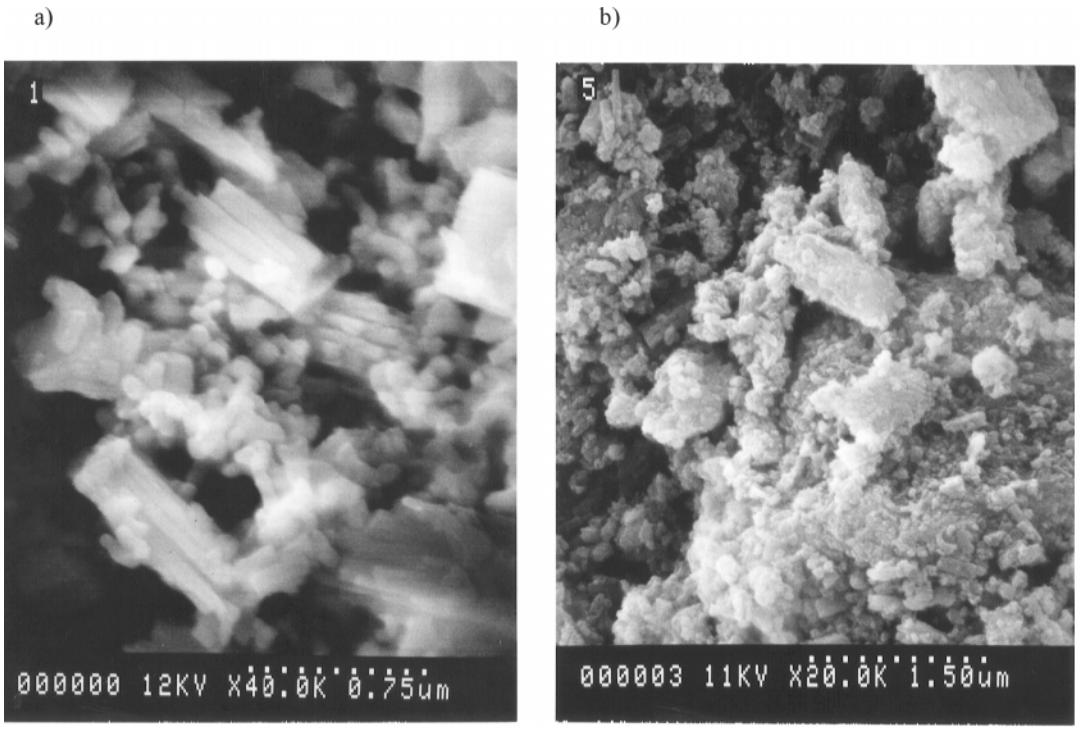

Figure 2 *SEM photographs of (a) 0.1%Pt-TON(72), (b) 0.1%Pt-TON(35).*

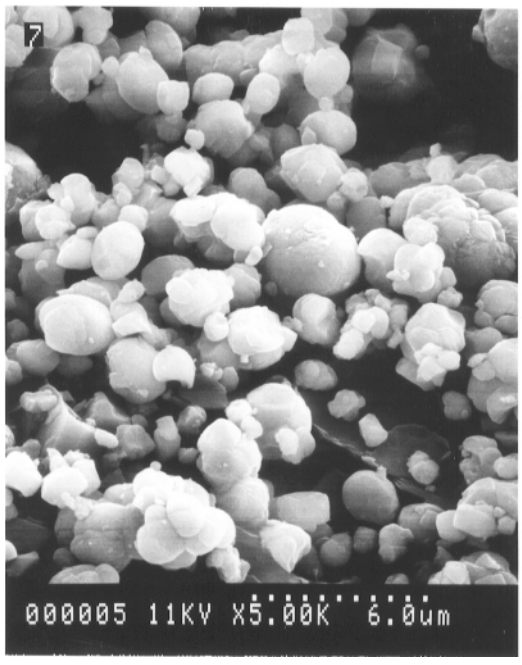

Figure 3 *SEM photograph of 0.1%Pt-ZSM5(480).*

a)

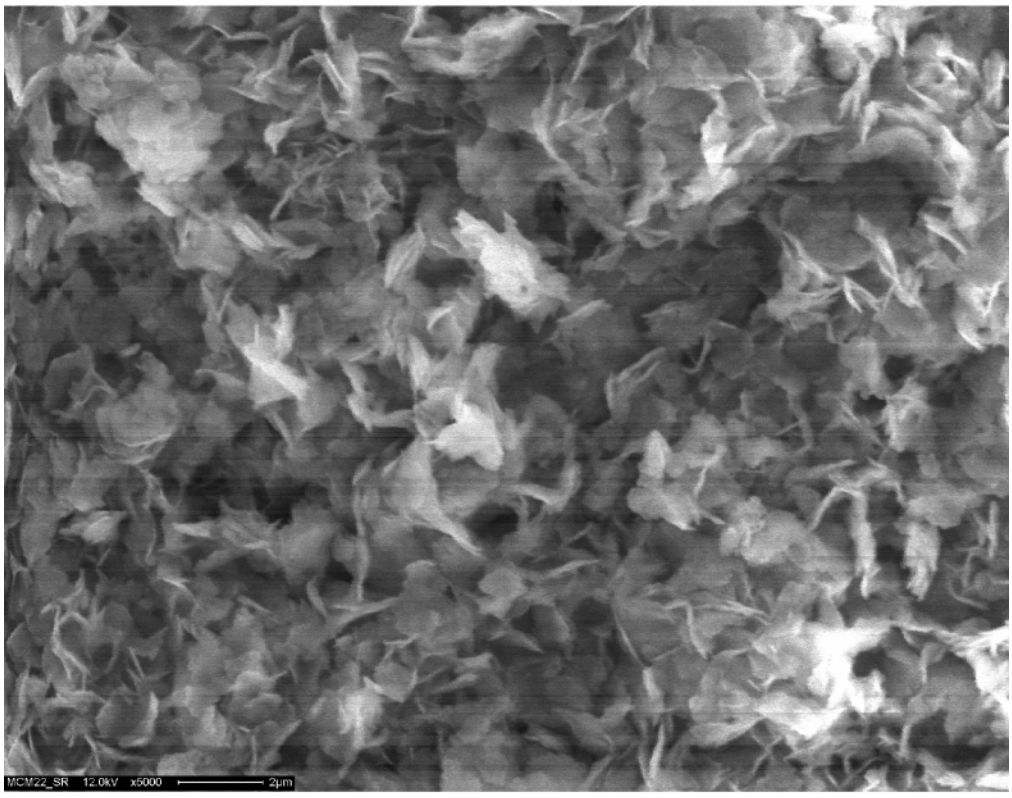

b)

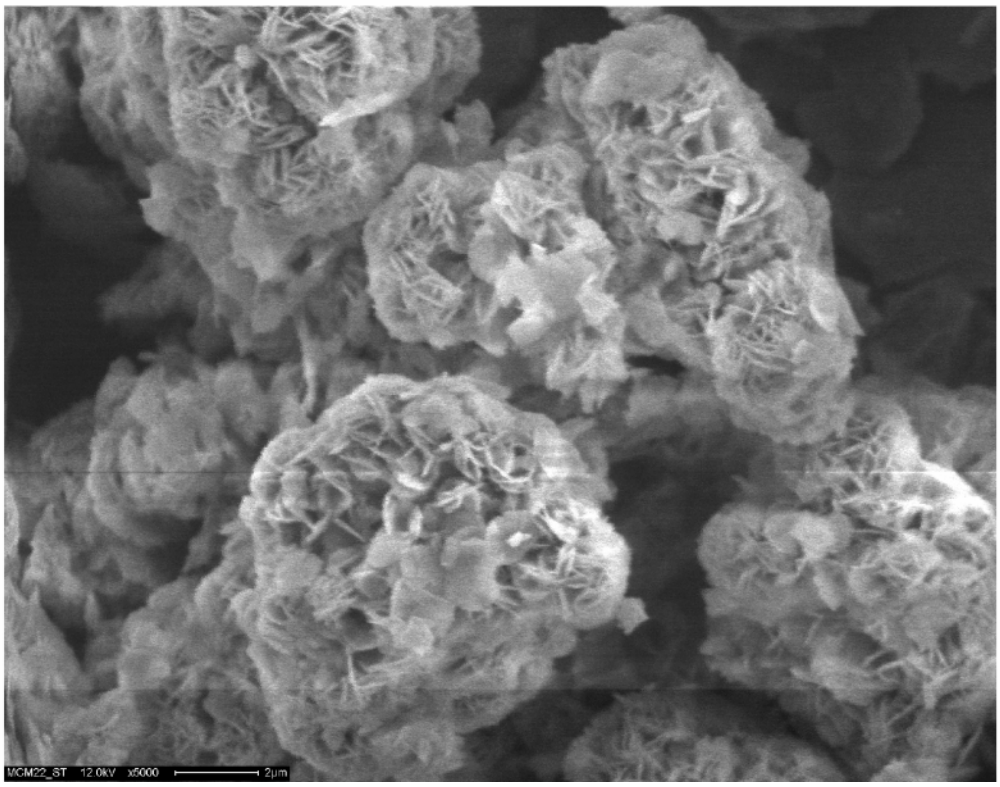

Figure 4 *SEM photographs of (a) MCM22 SR, (b) MCM22 ST.*

Curriculum Vitae

Gerhard Pirngruber was born on the 18th of January 1972 in Oberwart, Austria. From 1982 to 1990 he attended the Gymnasium Oberschützen (scientific branch), from which he graduated with distinction in June 1990. Following his interest for chemistry, he inscribed for studying Technical Chemistry at the TU Wien, with specialization in Physical and Analytical Chemistry. His diploma work on the sorption and catalytic conversion of ethanolamine on mordenites (an IR-spectroscopic study) was performed in an exchange-program at the University of Twente, The Netherlands, under the supervision of Prof. H. Vinek (TU Wien) and Prof. J.A. Lercher (UT) (1994/95). The diploma thesis was awarded a price from the Austrian Chemical Society.

After graduation at the TU Wien in June 1995 (with distinction), Gerhard Pirngruber started working as a PhD student with Prof. J.A. Lercher at the University of Twente. The results of his research on the development of bifunctional catalysts for the direct conversion of n-butane to isobutene are described in this thesis.